Tampere University

JANNE KOIVISTO

Development and Characterization of Gellan Gum Based Hydrogels for Soft Tissue Engineering Applications

JANNE KOIVISTO

Development and Characterization of Gellan Gum Based Hydrogels for Soft Tissue Engineering Applications

ACADEMIC DISSERTATION
Tampere University, Faculty of Medicine and Health Technology
Finland

Responsible supervisor or/and Custos	Prof. Minna Kellomäki, Dr. Tech. Tampere University Finland	
Supervisor(s)	Prof. Minna Kellomäki, Dr. Tech. Tampere University Finland	Prof. Katriina Aalto-Setälä, M.D., PhD. Tampere University Finland
Pre-examiner(s)	Prof. Sandra Van Vlierberghe, PhD. Ghent University and Vrije Universiteit Brussels Belgium	Prof. Anna Finne Wistrand, PhD. KTH Royal Institute of Technology Sweden
Opponent	Senior Research Fellow, Principal Investigator Eileen Gentleman, PhD. King's College London United Kingdom	

The originality of this thesis has been checked using the Turnitin OriginalityCheck service.

Cover design: Roihu Inc.

Älykäs selviää tilanteista, joihin viisas ei joudu.

Abstract

The aim of tissue engineering (TE) is the production of live and functional tissues by combining a biomaterial scaffold, living cells, and a relevant bioactive stimulus. The engineering of soft tissues, such as brain and heart, requires a scaffold material that represents the natural tissue, meaning that it needs to be soft, elastic, flexible, and possibly strain hardening. Additionally, a scaffold material must allow the diffusion of nutrients and the penetration of migrating cells inside the microstructure. Furthermore, the scaffold must provide the encapsulated cells with enough attachment sites to ensure the cells can function in their natural way.

Hydrogels are promising scaffold candidates for soft tissue engineering applications. They are crosslinked, hydrophilic polymer networks with a high water content in the structure. Hydrogels can be produced from a large variety of natural or synthetic polymers by implementing a variety of physical and chemical crosslinking strategies. Here, hydrogels based on the polysaccharide gellan gum are studied in a conclusive manner from both the materials science and biological perspective. The gelation process and chemistry of modified hydrogel-forming biopolymers are characterized. The mechanical properties of the hydrogels as well as their microstructure and the effects of different functionalization strategies on these characteristics are studied in detail. Novel imaging methods are applied for the analysis of hydrogel microstructure. Similarly, the mechanical properties of the hydrogels are studied using methods that have never before been applied to gels in hydrated form. Then, the newly developed hydrogel formulations are used with human cells for the soft tissue engineering of the two most vital and poorly regenerating organs of the human body – the central nervous system and the heart.

The developed gellan gum-based hydrogels have biomimicking mechanical properties with adjustable stiffness corresponding to either brain or heart muscle tissue, depending on the exact composition used. The elasticity of the hydrogel network enables the spontaneous beating of human induced pluripotent stem cell-derived cardiomyocytes in three-dimensional culture. The polymer network creating the hydrogels is loose enough so that the cells can grow inside and that nutrients and waste products of cell metabolism can also be transported in and out of the hydrogel. The functionalization of gellan gum with extracellular matrix proteins, such as laminin and collagen-derived gelatin, enhances the cytocompatibility, growth, and elongation of cells cultured in the novel three-dimensional microenvironments.

Tiivistelmä

Kudosteknologia tähtää elävän ja toimivan kudoksen tuottamiseen yhdistelemällä biomateriaalitukirakennetta, eläviä soluja ja sopivia bioaktiivisuutta stimuloivia ärsykkeitä. Pehmytkudoksen kudosteknologia vaatii tukirakenteen, joka vastaa aitoa kudosta, tarkoittaen että sen pitää olla pehmeä, elastinen, joustava ja mahdollisesti muokkauslujittuva. Tukirakenteen materiaalin pitää sallia ravinteiden diffuusio lävitseen ja solujen migraatio mikrorakenteen sisällä. Lisäksi tukirakenteen pitää tarjota soluille riittävästi kiinnittymiskohtia, jotta solut voivat toimia niille luontaisella tavalla.

Hydrogeelit ovat lupaava materiaaliryhmä tukirakenteiksi pehmytkudoksen kudosteknologisiin sovelluksiin. Ne ovat ristisilloittuneita, hydrofiilisiä polymeeriverkkoja, joiden rakenne sisältää paljon vettä. Niitä voi valmistaa monista eri luonnon- tai synteettisistä polymeereistä käyttäen useita eri fysikaalisia ja kemiallisia ristisilloitusmenetelmiä. Tässä työssä polysakkaridiin nimeltä gellaanikumi pohjautuvia hydrogeelejä on tutkittu perusteellisesti sekä materiaalitekniseltä että biologiselta kannalta. Geeliytymisprosessi ja hydrogeelejä muodostavien biopolymeerien kemia on karakterisoitu. Hydrogeelien mekaanisia ominaisuuksia, kuten myös niiden mikrorakennetta, sekä eri funktionalisointistrategioiden vaikutusta perusominaisuuksiin, on tutkittu yksityiskohtaisesti. Uusia kuvantamismenetelmiä on sovellettu hydrogeelien mikrorakenteen analysointiin. Samoin mekaanisessa testauksessa on sovellettu menetelmiä, joita ei ole aiemmin käytetty märille geeleille. Analyysien pohjalta kehitettyjä hydrogeelikoostumuksia on käytetty sovelluksissa yhdessä ihmissolujen kanssa, tavoitteena pehmytkudoksen kudosteknologia, keskittyen kahteen elintärkeään mutta huonosti uusiutuvaan ihmiskehon kudokseen, eli keskushermostoon ja sydämeen.

Kehitetyt gellaanikumipohjaiset hydrogeelit ovat biomimikoivia eli vastaavat mekaanisilta ominaisuuksiltaan, ja säädettävissä olevalta jäykkyydeltään, joko aivo- tai sydänlihaskudosta, riippuen tarkasta geelikoostumuksesta. Hydrogeelin verkkorakenteen elastisuus sallii ihmisen uudelleenohjelmoiduista kantasoluista erilaistettujen sydänlihassolujen spontaanin sykkeen kolmiulotteisessa viljelmässä. Polymeeriverkko on riittävän väljä, jotta solut voivat kasvaa sen sisään ja jotta ravinteet ja solumetabolian jätteet pääsevät kulkeutumaan sen läpi. Gellaanikumin funktionalisointi soluväliaineen proteiineilla, kuten laminiinilla ja kollageenistä johdetulla gelatiinilla, parantaa soluyhteensopivuutta, kasvua ja levittymistä, kun soluja kasvatetaan näissä uusissa kolmiulotteisissa ympäristöissä.

Acknowledgements

Table of contents

List of abbreviations

2D	Two-dimensional
3D	Three-dimensional
3D-DIC	Three-dimensional digital image correlation
AI	Artificial intelligence
ACNT2	α-actinin
ASTM	American Society for Testing and Materials
BDNF	Brain-derived neurotrophic factor
bFGF	Basic fibroblast growth factor
Ca-AM	Calcein acetoxymethyl
CaCl$_2$	Calcium chloride
CiPA	Comprehensive in Vitro Proarrhythmia Assay
CNS	Central nervous system
CPVT	Catecholaminergic polymorphic ventricular tachycardia
DAPI	4',6-diamidino-2-phenylindole
DIC	Digital image correlation
DMSO	Dimethyl sulfoxide
DMEM/F-12	Dulbecco's Modified Eagle Medium/Ham's Nutrient Mixture F-12
ECM	Extracellular matrix

EDC	1-ethyl-3-[3-(dimethylamino)-propyl]–carbodi-imide
EHT	Engineered heart tissue
EtHD-1	Ethydium Homodimer-1
FBS	Fetal bovine serum
FBP	Filtered back projection algorithm
FITC	Fluorescein isothiocyanate
FRAP	Fluorescence recovery after photobleaching
FTIR	Fourier-transform infrared spectroscopy
Gelatin-ADH	Adipic dihydrazide modified gelatin
Gelatin-CDH	Carbodihydrazide modified gelatin
GelMA	Methacrylated gelatin
GG	Gellan gum
GG-CHO	Oxidized gellan gum
GG-MA	Methacrylated gellan gum
GLCM	Gray level co-occurrence matrix
HA	Hyaluronic acid
HCl	Hydrochloric acid
HCM	Hypertrophic cardiomyopathy
hPSC	Human pluripotent stem cell, includes hESC and hiPSC
hESC	Human embryonic stem cell

hiPSC	Human induced pluripotent stem cell
HOBt	*N*-hydroxybentzotriazole
HTS	High-throughput screening
iPSC	Induced pluripotent stem cell
IPN	Interpenetrating network
IUPAC	International Union of Pure and Applied Chemistry
LQTS	Long-QT syndrome
LVER	Linear viscoelastic region
MBF	Methyl benzoylformate
MDA	Multiple discriminant analysis
MMP	Matrix metalloproteinase
MSC	Mesenchymal stromal/stem cell
MWCO	Molecular weight cut-off
MYBPC3	Myosin binding protein C
NaCl	Sodium chloride
NaOH	Sodium hydroxide
$NaIO_4$	Sodium periodate
NGF	Neural growth factor
NMR	Nuclear magnetic resonance
OPT	Optical projection tomography
PAA	Polyacryl amide

PDMS	Polydimethyl siloxane
PEG	Polyethylene glycol
Pen/Strep	Penicillin/Streptomycin
pHEMA	Poly-2-hydroxyethyl methacrylate
PCL	Polycaprolactone
PLA	Polylactic acid
PNS	Peripheral nervous system
PVA	Polyvinyl alcohol
qRT-PCR	Quantitative reverse transcription polymerase chain reaction
RGD	Arginine-glycine-aspartaic acid peptide
RT	Room temperature
SEM	Scanning electron microscopy
SPD	Spermidine
SPM	Spermine
TE	Tissue engineering
TNNT2	Troponin T
UV	Ultraviolet
VEGF	Vascular endothelial growth factor
WI-38	Commercial human lung fibroblast cell line

List of symbols

A	Area
E	Elastic modulus (Compressive modulus or Young's modulus)
E_1	Toe region elastic modulus
E_2	Second linear elastic modulus
F	Force
G'	Storage modulus
G''	Loss modulus
$G*$	Complex modulus
k	Boltzman constant
l	Length
l_0	Original length
M_w	Molecular weight
N_p	Number of polymer chains per volume
T	Temperature
t	Time
γ_0	Sinusoidal oscillatory shear strain
δ	Phase angle
ε	Strain
ε^{eng}	Engineering strain

ε^n	True strain (Hencky strain, logarithmic strain)
η	Viscosity
$\lambda^{emission}$	Emission wavelength
$\lambda^{excitation}$	Excitation wavelength
σ	Stress
σ^{eng}	Engineering stress
σ^c	True stress (Cauchy stress)
τ_o	Sinusoidal oscillatory shear stress

List of original publications

This thesis is based on the following publications that are later referred to in the text as **Publications I-III**. In addition, **Publication IV** has currently been submitted for publication and is listed as **Unpublished Manuscript**. The publications are reprinted here with the kind permission of the publishers.

I.   **Koivisto J.T.***, Joki T.*, Parraga J., Pääkkönen R., Ylä-Outinen L., Salonen L., Jönkkari I., Peltola M., Ihalainen T.O., Narkilahti S.[†], Kellomäki M.[†]: Bioamine-crosslinked gellan gum hydrogel for neural tissue engineering. Biomedical Materials 12 (2017) 2, ID: 025014. [‡]

II. Soto A.M., **Koivisto J.T.**, Parraga J., Silva-Correia J., Oliveira J.M., Reis, R.L., Kellomäki M., Hyttinen J., Figueiras E.: Optical projection tomography technique for image texture and mass transport studies in hydrogels based on gellan gum. Langmuir 32 (2016) 20, pp.5173-5182.

III. **Koivisto J.T.**, Gering C., Karvinen J., Maria Cherian, R., Belay B., Hyttinen J., Aalto-Setälä K., Kellomäki M., Parraga J.: Mechanically Biomimetic Gelatin-Gellan Gum Hydrogels for 3D Culture of Beating Human Cardiomyocytes. ACS Applied Materials & Interfaces 11 (2019) 23, pp.20589-20602.

   [*] These authors contributed equally to this work.
   [†] These authors contributed equally to this work.
   [‡] This publication has been previously included in the doctoral dissertation "Towards Modeling the Human Brain – Human Pluripotent Stem Cell Derived 3D Neural Cultures" by Tiina Joki at the BioMediTech Institute and Faculty of Medicine and Life Sciences, University of Tampere, Finland, 2017.

Unpublished manuscript

This thesis is also based on the following unpublished manuscript, which is later referred to in the text as **Publication IV**.

IV.   Nafar Dastgerdi J.*, **Koivisto J.T.***, Santaoja K., Orell O., Kanerva M., Kellomäki M.: Characterization of compressive behavior of bioamine crosslinked gellan gum hydrogel. *Submitted for publication on 3rd of April 2019*.

   * These authors contributed equally to this work.

During the course of the doctoral thesis approval from the beginning of the pre-examination phase to the dissertation, this submitted manuscript (**IV**) has been in the re-examination at the journal where it was originally submitted. It got rejected in its current form (as attached in this thesis). The criticism received from the journal and reviewers (in submission and re-submission) is directed to the modeling part of the manuscript only and is two-fold:

1. The reviewers question the use of Le Gac and Duval -model, developed for creep experiment, at all for the present stress-relaxation test. Out of the reviewers, the first one suggested that a Stretched Exponential and a Maxwell-solid models display equal quality than the Le Gac and Duval -model and did not find good enough reasoning to use it. The second reviewer suggested to use a Maxwell model (in particular Maxwell-solid). In his opinion, that model could be applicable, and he presented a source where to find a 3D version of the model.

2. Both reviewers stated that it is not clear which values of the stress were used to fit the curve of the Le Gac and Duval -model and requested more information to be added to the manuscript.

Author's contribution

I.   The study was designed together by all the co-authors. J.T. Koivisto was responsible for the hydrogel design and production. Hydrogel characterization and data analysis were done together by the author and by the master's degree student L. Salonen, whose work J.T. Koivisto supervised. The manuscript was co-written together by the shared first authors J.T. Koivisto and T. Joki, who was responsible for all the neuronal cell culture studies.

II.   The study was co-designed together by J.T. Koivisto and the first author A.M. Soto. J.T. Koivisto was responsible for the hydrogel production and assisted in the data analysis, while A.M. Soto was responsible for the imaging and development of data analysis tools. A.M. Soto and J.T. Koivisto co-wrote the manuscript.

III.   The study was designed together by J.T. Koivisto and by J. Parraga. J.T. Koivisto conducted the hydrogel characterization, the cell culture experiments, and a major part of the data analysis, while J. Parraga was mainly responsible for the production of the hydrogel components. J.T. Koivisto wrote the manuscript as the first author.

IV.   The study was designed together by all the co-authors. J.T. Koivisto was responsible for the hydrogel production and the compression measurements. The digital image correlation measurement and analysis were conducted by O. Orell, and the compression data analysis and model development mainly by J. Nafar Dastgerdi. J.T. Koivisto co-wrote the manuscript together with the shared first author J. Nafar Dastgerdi.

1. Introduction

Three-dimensional (3D) cell culturing is required for various applications in biomedical engineering and life sciences. Even though human cells have been cultured for decades on two-dimensional (2D) surfaces, such as a petri dish or a well plate, those conditions are not representative of the real situation inside the human body. To achieve a more representative, biomimicking environment, cell culturing needs to transition from 2D to 3D. Whether the cells are grown for therapeutic clinical tissue engineering, for disease modeling, for studying the basis of developmental biology, or for several other applications, it has been acknowledged that 3D cell culturing will be a necessity in the future. [Gomes et al., 2017, Shah, Singh, 2017, Breslin, O'Driscoll, 2013, Asthana, Kisaalita, 2013]

The basic principle of tissue engineering is to combine living cells with a biomaterial scaffold that provides support and acts as a potential delivery vehicle. The product, an engineered piece of tissue, can then be used in a clinical application to treat an injury or the malfunctioning tissue of a patient or it can be used as a model for the study of normal physiology and the pathogenesis of a disease. [Khademhosseini, Langer, 2016] However, the biomimicking 3D cell culture needs a support structure for the cells, a biomaterial scaffold, where cells can be cultured and monitored, and where they can function as if they were in the human body.

Hydrogels are prime candidates for use as biomaterial scaffolds for tissue engineering. They are crosslinked 3D networks of hydrophilic polymer molecules filled with water [Peppas et al., 2006]. The extracellular matrix of any soft tissue (as opposed to any calcified tissues such as bone and tooth enamel) is essentially a biological hydrogel, while the tissue as a whole can be considered to be a composite material of continuous matrix phase and separate cells [Saldin et al., 2017]. Hydrogels can be produced from various polymers using various crosslinking strategies, from which a few have been chosen for this study.

The success of a hydrogel in the intended application is based on both the physical and biochemical properties of the material. To rationally design novel hydrogels, the most important physical properties include adequate mechanical characteristics for the intended application and a microstructure that allows diffusion and cell migration. From the biochemical viewpoint, the hydrogel must provide enough attachment sites for cells and possibly guide their growth and differentiation. [Brandl et al., 2007, Darnell, Mooney, 2017]

This thesis includes a literature review, an experimental part, a discussion comparing the study results with the previous literature, the conclusions of the studies, and the four original publications. The literature review provides an overview of tissue engineering applicable for various soft tissue types and an overview of the most important material characteristics of hydrogels. In addition, the previous use of selected hydrogel materials is reviewed in more detail. Additionally, existing systems for both clinical applications as well as the disease modeling of neuronal and cardiac tissues are reviewed. In the experimental part, novel hydrogels, based on a polysaccharide called gellan gum, are designed using ionotropic physical crosslinking with endogenous bioamines and hydrazone-based chemical crosslinking together with a gelatin biopolymer. The materials are characterized chemically and physically, with an emphasis on the biomimicking mechanical properties. Physical characterization methods have been developed alongside the hydrogel design, creating novel imaging methods for the structural analysis of hydrogels and applying the new methods for the analysis of the compression behavior of these hydrogels. The biocompatibility of the designed hydrogels has also been studied in cell cultures using cells of human origin. A prospective hydrogel formulation is presented for both human stem cell-derived neuronal and cardiac cells. The designed hydrogels function well in their intended 3D cell culture application.

2. Literature Review

2.1. General principles of tissue engineering

The main goal of the interdisciplinary field of tissue engineering (TE) is to produce new, functional tissues using the principles of engineering and life sciences [Langer, Vacanti, 1993]. In clinical, therapeutic TE, the aim is to repair, regenerate or replace damaged, malfunctioning, or diseased tissue inside a patient's body [Langer, Vacanti, 1993, Khademhosseini, Langer, 2016]. As the population around the world ages, the need for this kind of regenerative therapy will continue to grow [Vats et al., 2005]. Indeed, at present, there are not enough organ donors to fill the current need and most traditional biostable implants do not provide full regeneration of damaged tissue. Instead, they only fix the broken site, but often still leave it in a worse condition than healthy native tissue due to scarring and foreign body reaction and even susceptibility to infection [Langer, Vacanti, 1993, Gomes et al., 2017, Lechler et al., 2005, Place et al., 2009]. The main approaches to tissue regeneration using TE can be divided into four main categories:

1. The implantation of a biomaterial scaffold to fix potential structural damage and to bioactively guide the surrounding healthy tissue to regenerate the site.

2. The implantation of stem cells or other relevant cell types into the treatment site, hoping that they will differentiate into the required cells and tissue.

3. The implantation or controlled release of differentiation-inducing biomolecules, such as carefully selected growth factors, and using them for regeneration.

4. The actual combination of all of the above listed methods into a true TE product built from a bioactive and biodegradable scaffold that encapsulates stem cells and also contains differentiation-guiding growth factors.

Only the fourth approach is real TE as currently understood by the term. The other approaches are closely related methods and are much simpler to perform in an actual clinical setting, but

only when they are combined do they form the three main pillars of TE, as depicted in Figure 1. [Langer, Vacanti, 1993]

Using either acellular biomaterial implants or stem cells alone has been shown to have moderate regenerative capability, depending on the particular tissue, but most of the time, the true regeneration of damaged tissue is not achieved [Khademhosseini, Langer, 2016]. In many clinical applications, such as polymeric stents or nerve guidance conduits, acellular implants are the gold standard, but they often lack the more intricate cell guidance [Kehoe et al., 2012, Khademhosseini, Langer, 2016]. Likewise, implantation of only stem cells or other potentially curative cells, such as insulin producing islet cells, has been a hot topic of discussion, but the poor cell survival without a supporting scaffold is a major obstacle that has still to be overcome. [Vats et al., 2005] Tailoring the combination of a biomaterial scaffold with cells and stimulating biomolecules specifically for the tissue and patient is the true TE approach.
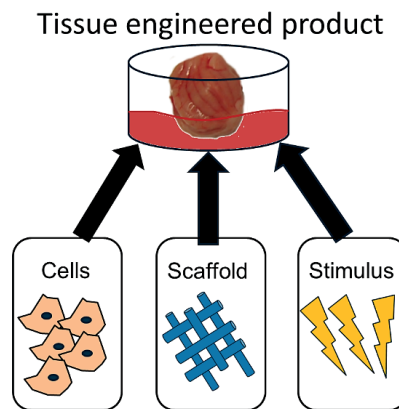
Figure 1. The three equally important aspects of TE to produce a fully functional piece of tissue or organ are living cells, a biomaterial scaffold, and a variety of stimuli.

Another more recent aim for TE is the production of synthetic tissue *in vitro* for use in disease modeling, developmental biology, toxicology, and related biomedical fields with the goal of further studying the produced tissue [Gomes et al., 2017]. Recently, fields even further away from medicine, such as the development of *in vitro* meat or soft biorobotics, have also taken an interest in TE [Khademhosseini, Langer, 2016].

The development of *in vitro* disease modeling is critical in understanding many genetic diseases, such the ones affecting the heart and central nervous system, as these vital tissues function very differently in animals compared with humans [Shah, Singh, 2017, Gomes et al., 2017]. For example, the physiology or even just the size of a rodent heart is magnitudes different than a human heart [Farouz et al., 2014]. Similarly, the intricate network and functioning of a human brain is vastly different from that of a rodent brain, and even measurements with a

monkey brain would need to be extrapolated to humans and are therefore not directly comparable [Hopkins et al., 2015]. A similar observation can be made for any other organ.

In addition to the functioning of organs, another significant field of study is the development of cancer in its multiple forms [Breslin, O'Driscoll, 2013]. All these fascinating issues could be answered by TE in the future. However, because all the underlying problems associated with the complex biomaterial and cell interplay in either *in vitro* or *in vivo* conditions have not yet been solved, more research is needed in this field.

2.1.1. Scaffolds

A biomaterial is any material that can be used in direct contact with a living system, such as the human body or cells *in vitro* [Vert et al., 2012]. Potential biomaterials exist in all the common material groups: metals, ceramics (including glasses), and polymers. Nowadays, the most studied biomaterials are both bioactive and biodegradable. This means that they not only remain passively in the body, but actively transform their surrounding tissue and help the regeneration. Once they have fulfilled their purpose, they degrade away. [D. F. Williams, 2008] In TE, the support structure built from the biomaterial is called a scaffold.

In all tissues of the human body, cells are surrounded by the tissue-specific extracellular matrix (ECM), creating a composite material filled with various biomolecules and water. The main components of this natural scaffold are proteins, glycosaminoglycans, proteoglycans, and matrix metalloproteinases (MMP), all arranged in a unique, tissue-specific 3D microstructure. [Chen, Liu, 2016] A good starting point for producing a TE scaffold is to mimic the ECM as it provides structure, function, and bioactivity for the cells. Decellularized ECM can even be used on its own as a scaffold material, or certain ECM molecules, such as the ubiquitous collagen, can functionalize otherwise bioinert materials. [Geckil et al., 2010, Saldin et al., 2017]

Depending on the specific application, the scaffold can provide structural support to the damaged tissue or have some other functionality, such as the release of drug molecules, or it can just be used to house the cells in a 3D matrix. For TE, the most attractive biomaterials are various bioactive polymers, bioceramics, and bioactive glasses. The biodegradation of these materials can also be utilized in drug delivery systems, where bioactive molecules are released once the encapsulating biomaterial degrades. [Khademhosseini, Langer, 2016, Chen, Liu, 2016] The ability to provide a 3D supporting, tissue mimicking microstructure is the main function of most TE scaffolds. As cells naturally exist in a 3D environment, culturing them on a 2D surface affects both their morphology and their functionality. Some cells may lose their tissue specificity via dedifferentiation, whereas others might gain extra features, for example, they might develop into tumors. In addition, 3D culture conditions are especially important for *in vitro* models because the whole point is to build a model that represents the natural state. [Asthana, Kisaalita, 2013, Breslin, O'Driscoll, 2013, Caliari, Burdick, 2016]

2.1.2. Stem cells

The second main pillar of TE, as stated in the definition above, are cells, the essence of any living tissue [Langer, Vacanti, 1993]. When aiming for the regeneration and production of *in vitro* tissue, the most attractive starting point is stem cells. By definition, a stem cell has two properties: unlimited self-renewal and potency to differentiate. There are several different potencies of stem cells, depending on where the cells originate. Totipotent stem cells can form the entire human body, including extra-embryonal tissues such as the placenta, and they are found only on the very first divisions of fertilized oocyte. Pluripotent stem cells are also able to form all the cells found in the human body, but they lack the ability to form extra-embryonic tissues, and thus cannot form an entire human being on their own. Multipotent stem cells have already started to differentiate in a specific direction and can form multiple cells and tissues specific for that differentiation lineage, such as the adult mesenchymal stem cells (MSC) that form bone, cartilage, and adipose tissue. Oligopotent and unipotent cells are further away on the differentiation track and can only form more restricted cell types that are typically constrained to one organ. Examples of such cells are oligopotent neural progenitor cells that form the neuronal cell types found in the brain and unipotent germ cells that produce oocytes or spermatocytes. [Vats et al., 2005, Horwitz et al., 2006, Avasthi et al., 2008, Robinton, Daley, 2012]

In TE applications, the most commonly used cells are pluripotent stem cells. Human embryonic stem cells (hESC) are pluripotent and found in the developing embryo once it has lost its totipotency. The cells can also be harvested from the inner cell mass of a blastocyst in the early developmental phase and established into a cell line. [Vats et al., 2005] Another, more recent finding are induced pluripotent stem cells (iPSC) [Yamanaka, 2012]. The groundbreaking studies by professor Yamanaka's team first on mouse iPSC [Takahashi, Yamanaka, 2006] and a year later on human iPSC (hiPSC) [Takahashi et al., 2007] created the possibility to use the cells of any adult patient, reprogram them back into a pluripotent state and then use the established hiPSC line for both autologous TE and as a model of the patient. The possibility to differentiate stem cells in a controlled way into target cell- and tissue-types enables access to unreachable parts of human development and to critical cells that cannot be obtained from a living patient [Ojala, Aalto-Setälä, 2016]. The original retrovirus vectors used for the reprogramming of hiPSC have since been changed into safer, non-viral, and non-genome-integrating methods, making the reprogramming process safer, especially if aiming to use the cells for patients [Okita et al., 2011, Robinton, Daley, 2012, Manzini et al., 2015]. When referring to both hESC and hiPSC, the term human pluripotent stem cells (hPSC) is used.

When comparing different hPSCs, the main question is whether the cell types are similar to each other and which should be the gold standard of pluripotency. [Liu, 2008, Robinton, Daley, 2012, Yamanaka, 2012] There are several pluripotency assays that both of the cell types pass, and that are commonly required to prove the newly developed cell line's pluripotency. The

6

example assays include expression of a panel of well-known pluripotency genes and the formation of teratoma tumors containing all germ layers, when implanted in rodents [Robinton, Daley, 2012]. However, iPSCs have also been proven to have some degree of epigenetic memory that likely affects their reprogramming and differentiation efficiency [Robinton, Daley, 2012, Manzini et al., 2015].

The main advantages of hiPSC over hESC include the amount of knowledge about the patient who has donated the cells for the hiPSC reprogramming. Indeed, knowing the medical history of the patient is an advantage when the cells are used for disease modeling. When we use hESC to model a disease, we do not know what kind of individual the cells would have produced, and thus we do not know whether the patient would have symptoms of a specific disease. However, when using hiPSC, the final product of all the genes acting in the stem cells are known, as they are from a living patient. Thus, the invention of iPSC greatly enhanced the possibilities of doing disease modeling. [Robinton, Daley, 2012] Another advantage of hiPSC lines is that they are voluntarily donated by the patients themselves, while hESC lines are produced from surplus embryos from infertility clinics that have been donated by parents. This is sometimes seen as an ethical dilemma because the hESCs could have produced an individual if used successfully in the infertility treatment and, as such, their use in research is seen by some religious groups as being akin to murder [Robinton, Daley, 2012, Murugan, 2009].

2.1.3. Stimulation

The third main pillar of TE is the stimulation of the cell culture and this can mean a large variety of systems. Stimulation activates the differentiation cascade of the stem cells, causing the formation of a wanted cell type or tissue organoid. Without the correct stimulus, the stem cells might just stay in their pluripotent state and proliferate uncontrollably. [Discher et al., 2009] Biochemical stimulation using growth factors and other soluble signaling molecules is the most obvious method of stimulation because they are commonly included in the differentiation protocols of stem cells. Activating the differentiation cascade can also cause the cells themselves to produce more signaling molecules, and thereby enhancing the differentiation process as a whole. [Place et al., 2009, Toivonen et al., 2013]

In addition to biochemical signals, many physical signals can also be used for the stimulation of cell cultures in TE production, as listed in Table 1. Electrically active cells, such as cardiomyocytes and neurons, have been stimulated using electrical fields with the aim of enhancing maturation [Huh et al., 2011, Arslantunali et al., 2014]. In addition to electrical activation, light has also been used for the activation of cells using so-called optogenetics [Pastrana, 2010]. A further active stimulation method, also closely related to the material properties of the growth substrate, is mechanical stimulation that uses the stretching, vibration, or shear stress caused by flow. All these methods aim to mimic the *in vivo* situation, and thus to enhance cell matura-

tion or organoid formation. [Tirkkonen et al., 2011, Chung et al., 2011, Huh et al., 2011] A further aspect of stimulation, providing mechanical cues via mechanotransduction and durotaxis, is discussed in more detail in **Chapter 2.2.4.** [Discher et al., 2009, Walters, Gentleman, 2015].

Table 1. Examples of physical stimuli used for the stimulation of various cell responses.

Stimulus	Cell type	Application	Reference
Electricity	Cardiomyocyte	Maturation	[Kujala et al., 2012]
	Neuron	Neurite outgrowth	[Arslantunali et al., 2014]
Light	Cardiomyocyte	Drug response	[Pastrana, 2010, Björk et al., 2017]
Stretching	Cardiomyocyte	Differentiation	[Kreutzer et al., 2014]
	MSC	Differentiation	[Virjula et al., 2017]
Vibration	MSC	Differentiation	[Tirkkonen et al., 2011]
Flow	Endothelial cell	Vascularization	[Huh et al., 2011]
	Cardiomyocyte	Maturation, Stress induction	[Katipparambil Rajan et al., 2018]
Passive Stiffness	Any	Differentiation & Maturation	[Discher et al., 2009, Walters, Gentleman, 2015]

2.2. Hydrogels

According to the definition given by the International Union of Pure and Applied Chemistry (IUPAC), a gel is a: "*non-fluid colloidal network or polymer network that is expanded throughout its whole volume by a fluid*" [Alemán et al., 2009]. Subsequently, a *hydrogel* is a gel where the expanding fluid or swelling agent is primarily water. Furthermore, in the case of hydrogels, the solid component is usually a polymer network and not a colloid. [Alemán et al., 2009] Another definition by the American Society for Testing and Materials (ASTM) is: "*Hydrogels are water-swollen polymeric networks that retain water within the spaces between the macromolecules; and maintain the structural integrity of a solid due to the presence of crosslinks*" [ASTM F2900, 2011].

As can be seen from both of these definitions, the main components that make up a hydrogel are a crosslinked polymer network and water as a swelling agent. Although there are many other definitions of hydrogels that are formulated in slightly different ways, they are always formed along these lines [Kavanagh, Ross-Murphy, 1998, Hennink, van Nostrum, 2002, Peppas et al., 2006, Buwalda et al., 2014, Chirani et al., 2015] because they are the essential parts required to make a hydrogel. Of particular note for later consideration is the presence of water as a swelling agent. A hydrogel lacking the liquid swelling agent is called either an *aerogel* or a *xerogel*, depending on the drying process [Alemán et al., 2009]. One further case of a dried gel is *cryogel*, where the drying process is done specifically using freezing temperatures [Lozinsky et al., 2003].

The study of hydrogels and the term itself originate from a study by van Bemmelen in 1894 about copper oxides and the colloidal network phase observed in water as $CuO \cdot H_2O$ [van Bemmelen, 1894, Buwalda et al., 2014]. The polymer hydrogels formed from water-swollen crosslinked polymeric networks used nowadays were first reported almost simultaneously by Berkowitch *et al.* and by Danno who both studied the formation of an innadiation crosslinked, water insoluble network of polyvinyl alcohol (PVA) [Berkowitch J. et al., 1957, Danno, 1958, Buwalda et al., 2014]. The first real medical application for hydrogel material was studied by Wichterle & Lím in 1960.They produced a poly-2-hydroxyethyl methacrylate (pHEMA) hydrogel for use as a soft contact lens [Wichterle, Lím, 1960, Buwalda et al., 2014].

There are several key characteristics that are ubiquitous to hydrogels, and thus it is important to quantify their specific properties. The standard IUPAC and ASTM definitions [Alemán et al., 2009, ASTM F2900, 2011] do not specify the amount of water in the network, as this can vary considerably between different hydrogels and depends on the exact physicochemical mechanisms affecting the polymers in question. The water content is often measured as swelling degree, swelling ratio, or water uptake, calculated as a percentage of the weight of the total bound water compared with the dry weight of the polymer. This water content can, however, vary from a few tens of percentage to over 1 000%. Furthermore, the tendency to absorb surrounding water into the hydrophilic network has enabled multiple industrial applications. [Patel, Mequanint, 2011, Chirani et al., 2015] This tendency to absorb water is also directly linked to a hydrogel's crosslinking density, molecular network mesh size, and porosity that are defined further in **Chapter 2.2.5.** A further derivative result related to the properties of the polymer network are the mechanical properties of the hydrogel, usually soft and elastic, as explained in **Chapter 2.2.4.** A third category of important characteristics that is defined further in **Chapter 2.2.6.** is biological response, biocompatibility and cytocompatibility that are especially important in the fields of biomedical engineering and biomaterials science, but often not so critical in the various industrial applications of hydrogels in other fields.

Further simple to understand characteristics include gelation time, optical transparency or turbidity, and degradation [ASTM F2900, 2011]. Sometimes gelation is also called sol-gel transition, by definition a process where a network is formed from a solution by a progressive change from liquid precursor into a sol and then to a gel [Alemán et al., 2009]. However, sol-gel processing is a term more often used in the case of aerogels than hydrogels. The gelation time is simply the time it takes for the crosslinking reaction to finish. After that, the hydrogel behaves like a gel and no longer like a liquid. The simplest method to measure gelation time is perhaps the tube tilt test as defined by Tanodekaew *et al.*, meaning just periodically tilting the vessel where hydrogel components are mixed and, once they stop flowing, the gelation time is recorded. [Tanodekaew et al., 1997, ASTM F2900, 2011] Other methods for measuring gelation time include a falling ball test, optical turbidity, and rheology, all giving roughly the same

amount of information on material behavior, but requiring more sophisticated equipment than the simple tube tilt test [ASTM F2900, 2011].

The importance of the optical properties of the hydrogel depend strongly on the application, but seeing as the first ever biomedical application was a contact lens [Wichterle, Lím, 1960], it can be easily understood that transparency is important. Also, when hydrogels are developed for tissue engineering applications, measuring the transparency and refractive index can provide valuable information. For example, it allows a view of the inside of the hydrogel to study the biological response, even if the actual success of an implantable hydrogel is not dependent on transparency [Vielreicher et al., 2013]. However, the application itself might still require a high degree of transparency, as is the case with ophthalmological applications [Koivusalo et al., 2018]. Another optical property that might be interesting to measure is the autofluorescence of the hydrogel, meaning that the hydrogel emits light on a certain wavelength when illuminated with the appropriate excitation wavelength [Vielreicher et al., 2013].

Measuring the degradation is a more complex task because the variability of hydrogel chemistry results in an equal variability in the degradation behavior. Most hydrogels degrade by hydrolysis and/or by enzymatic biodegradation and both of these can affect the crosslinked sites or the polymer molecules as a whole. This biodegradation is usually beneficial in clinical TE applications as it simply means that the hydrogel disappears when it is not needed anymore at the injury site. Alternatively, it can be used and tailored to produce highly sophisticated controlled drug delivery devices and the so-called spatio-temporal guidance of cells. Overall, the degradation rate in different buffers, temperatures, and pH are often measured and even tuned for specific hydrogel applications. [ASTM F2900, 2011, Chirani et al., 2015, Li, Mooney, 2016, Leijten et al., 2017]

The aforementioned typical characteristics of hydrogels and their general tunability by crosslinking result in their use in a multitude of fields ranging from industrial waste management to diapers and cosmetics, all the way to food and pharmaceutics and into tissue engineering and other biomedical applications [Chirani et al., 2015]. All in all, hydrogels are a highly interesting group of materials that have been under investigation for over fifty years and are still currently taking new and exciting steps forward on a monthly basis.

2.2.1. Classifications and crosslinking methods

Since the 1960s, the number of studies of hydrogels and reports on different materials that can form a gel has been on an exponential rise [Chirani et al., 2015], creating a need for the classification of hydrogels. Figure 2 explores the main classification possibilities for dividing hydrogels into different categories that could be even further divided into subcategories.
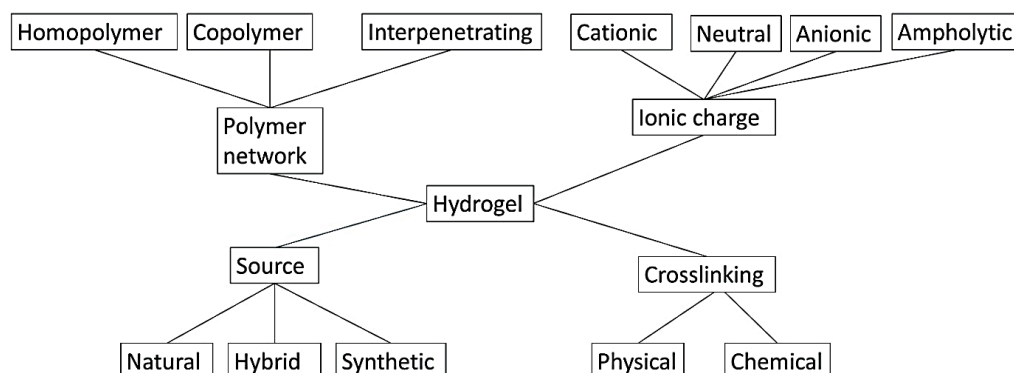
Figure 2. The main classification categories of hydrogels based on polymer source, polymer network type, charge, and crosslinking. Image modified from [Patel, Mequanint, 2011].

The first classification is between natural and synthetic polymers, or hybrids of these. As previously stated, the first hydrogels for biomedical applications were synthetic polymers but currently many natural polymers are also known to form hydrogels. [Malafaya et al., 2007, Hennink, van Nostrum, 2002, Slaughter et al., 2009] Additionally, the water-swollen ECM of any soft tissue can also be considered a natural hydrogel, and is therefore usable either as the full decellularized matrix or as single components, such as collagen and elastin [Saldin et al., 2017].

When designing a hydrogel, the choice of polymer goes hand in and with the choice of crosslinking method. Some crosslinking methods work for many hydrogel-forming polymers while others are more specific, but none works for all. The main categories of crosslinking, as shown in Figure 3, are physical crosslinking, where physical phenomena form the linkage between molecular chains, and chemical crosslinking, where covalent bonds are formed between the functional groups of molecules [Oyen, 2014]. Depending on the exact crosslinking reaction, conditions, such as temperature and pH, might need adjusting for the crosslinking to occur. In general, physical crosslinking is more reversible and chemical crosslinking more permanent and irreversible. However, exceptions exist both ways, such as reversibly light-activated chemical crosslinks and physical irreversibly self-assembled polymethyl methacrylate nanoparticle networks. [Hennink, van Nostrum, 2002, Oyen, 2014]
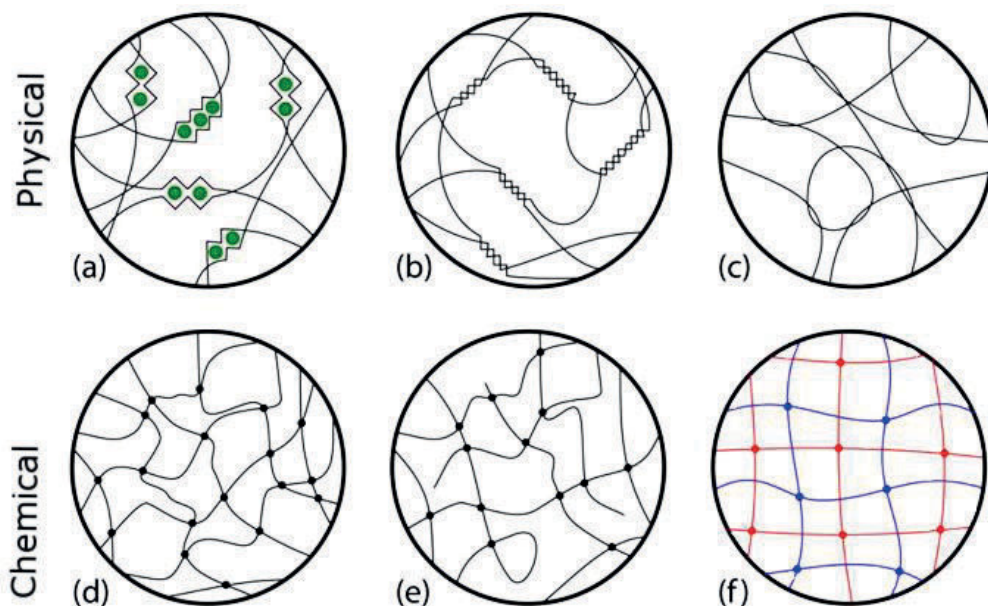
Figure 3. The six main possibilities of hydrogel crosslinking phenomena: a) physical crosslinking with ionotropic or small molecule crosslinker, b) physically crosslinked network with crystallite, stereo complex or helix formation, c) physical entanglement crosslinked network, d) chemical ideal network with tetra-functional crosslinks, e) chemical non-ideal network with tetra-functional crosslinks including ends of polymer chains and loops, f) ideal chemically crosslinked double network or interpenetrating (IPN) network. Image modified from [Oyen, 2014].

One further dividing classification is between a *true gel* and a *weak gel*, terms that describe the physical properties of a hydrogel. Both of these gels pass a gelation test, appearing to have formed a gel. However, only a true gel will retain its shape and appear like a solid if taken out of a mold; whereas a weak gel will collapse without external support and form a puddle, being more of a fluid with an internal structure than a solid gel, hence the term. [Morris et al., 2012, ASTM F2900, 2011] This division between true and weak gels is most often used in the field of rheology, but it is also important for easily distinguishing between different materials when thinking about the suitability for a certain application. From a rheological point of view, gel is a material where elastic behavior dominates over viscous behavior under oscillatory shear stress. Both weak and true gels fulfill this criterion. [Kavanagh, Ross-Murphy, 1998] However, the term weak gel should not be confused with low mechanical characteristics as weak gels can still have a relatively high yield stress and require considerable force to break the network. On the other hand, a true gel can have very low stiffness, even if staying intact without support. [Morris et al., 2012]

2.2.1.1. Physical crosslinking

For physical crosslinking, one of the most used options is ionotropic crosslinking (Figure 3 (a)). This means that positively charged ions or small molecules react with negatively charged polymer chains and form crosslinks. A large subgroup of hydrogels crosslinkable in this way with cations is polysaccharides, including for example alginate, gellan gum, xanthan gum, pectin, pullulan, and carrageenan, all of which are anionic natural polymers. An example of a synthetic anionic polymer that can be ionotropically crosslinked is poly-[di(carboxylatophenoxy)phosphazene]. Different ionotropic crosslinking occurs at the interaction of cationic chitosan with polyanions, also forming a hydrogel. [Hennink, van Nostrum, 2002, Coviello et al., 2007] The downside of ionotropic crosslinking is the ion exchange from higher to lower valence number that is observed to occur in physiological buffers. For example, calcium ions in the polysaccharide crosslinks change to sodium ions, and thus weakens the hydrogel network because the affinity of the polymers towards each other weakens [Coutinho et al., 2010, Lee et al., 2013].

Another physical crosslinking possibility is creating the crosslinks by crystallization of the polymer chains (Figure 3 (b)). Here, the chains physically and reversibly bind together, but can be released by raising the temperature above the melting temperature of the crystallites. A well-known example of this thermal gelation is PVA. Similar systems occur with many different stereo complex formations (Figure 3 (b)), self-assembling systems and variations of hydrophilic and hydrophobic copolymer sequences. For example, block copolymers of polyethylene glycol (PEG) and polylactic acid (PLA) as well as PLA together with pHEMA produce stereo complex hydrogels. Macromolecular proteins or even parts of DNA can form physical crosslinks based on the strong physical affinities they have towards each other or specific antigen-antibody bindings (Figure 3 (a,b,d)). [Hennink, van Nostrum, 2002] The entanglement of chains (Figure 3 (c)) is more common in weak hydrogels and can be triggered by pH or temperature change and strengthened by hydrogen bonds. Examples of hydrogels mainly forming weak gels by this triggered self-assembly and entanglement include the commercially available, natural origin cell culture substrates Puramatrix® [S. Zhang et al., 1995], Matrigel® [Kleinman, Martin, 2005], and Geltrex® [Akopian et al., 2010] as well as other oligopeptide nanofiber systems [Ikonen et al., 2011].

2.2.1.2. Chemical crosslinking

Chemical crosslinking (Figure 3 (d-f)) has wider options than physical crosslinking, dependent on the available functional groups on the polymer chains. Crosslinking by free radical polymerization from the monomers is suitable, for example, for polyacryl amide (PAA), for pHEMA, and for many methacrylate containing polymers [Buwalda et al., 2014]. However, in water solution the degree of substitution and reaction efficiency is low, so the introduction of methacrylate groups has been improved by using methacrylic anhydride and enzymatic catalysts, especially

in the case of polysaccharides. [Hennink, van Nostrum, 2002] The crosslinking of polymers, not monomers, to produce a gel was first done by the irradiation of aqueous PVA solution with ionizing radiation [Berkowitch J. et al., 1957, Danno, 1958]. This crosslinking method has evolved over the years into the currently used ultraviolet (UV) light activated crosslinking, where methacrylate groups polymerize into hydrolysis resistant methacrylate esters [Hennink, van Nostrum, 2002, Buwalda et al., 2014].

Due to several disadvantages, such as heterogenous hydrogel network formation, the possible cytotoxicity of both UV light and the radical polymerization reaction, more attractive options for the production of TE hydrogels include *bio-orthogonal click chemistry reactions* [Ifkovits, Burdick, 2007, Truong et al., 2016]. A *bio-orthogonal* reaction does not interfere with biological processes [Jiang et al., 2014]. A *click chemistry* reaction, as such, means a reaction without any side products, joining polymer units via heteroatom bridge stereospecifically in simple reaction conditions and in a harmless solvent, such as in water [Kolb et al., 2001]. Typical characteristics for this reaction type are high reactivity and selectivity, which enable specific hydrogel design with the required biofunctionalities. Several full- and pseudo-click reactions exist, and all of these can crosslink the hydrogel in aqueous solution in mild reaction conditions and are thus compatible with living cell encapsulation. [Jiang et al., 2014] The first hydrogels formed via click reaction are again based on PVA [Ossipov, Hilborn, 2006]. Examples of the fully click chemistry reaction include norbornene-nitrile oxide in PEG hydrogel production [Truong et al., 2016], Diels-Alder cycloaddition with PEG and hyaluronic acid (HA) [Nimmo et al., 2011], and the tetrazine-norbornene click pair in modified gelatin [Koshy et al., 2016]. The pseudo-click chemistry means not full orthogonality of the crosslinking reaction, having for example water as a side product. Examples of these reactions include thiol–Michael addition reaction [Jiang et al., 2014], Schiff-base amine–aldehyde reaction [M. Khan et al., 2018], and the aldehyde–hydrazide coupling into a hydrazone [Jiang et al., 2014].

As many biopolymers can be easily modified to contain aldehyde and hydrazide functional groups, *hydrazone crosslinking* is an attractive option when designing hydrogels for TE. This reaction is only pseudo-click chemistry, as there is a water molecule by-product. The possibility of free aldehyde groups reacting with unintended targets raises a question of the bio-orthogonality of the reaction. However, in reality, the strongly nucleophilic hydrazide's reaction kinetics will reduce the toxicity to negligible levels in the relevant conditions [Jiang et al., 2014]. For example, the biocompatibility of hydrazone crosslinking HA has been exploited by crosslinking with itself [Koivusalo et al., 2018], with PVA [Karvinen et al., 2018], and with the natural polysaccharides alginate and gellan gum [Karvinen et al., 2017, Karvinen et al., 2019].

2.2.2. Gellan gum

The main polymer studied for hydrogel design and production in this thesis is the bacterial extracellular polysaccharide gellan gum (GG). GG has a linear tetrasaccharide repeating structure of β-D-glucose, β-D-glucuronic acid, β-D-glucose, and α-L-rhamnose (Figure 4). Moreover, GG is produced by the bacterium *Sphingomonas elodea*, formerly known as *Pseudomonas elodea,* and the main producer is the C.P. Kelco company based in the USA and Japan. [Morris et al., 2012] This polysaccharide was originally discovered by Kang *et al*. from Kelco in 1982 [K. S. Kang et al., 1982], and it received approval for use as a food additive in 1992 [FDA, 2018] and the E number E418 refers to GG in the EU [Morris et al., 2012]. GG was first proposed for use as a TE scaffold material by Smith *et al*. [A. M. Smith et al., 2007]. Thereafter, multiple applications have appeared in both hard and soft tissues [Stevens et al., 2016]. The chemical structure, gelation, and material properties of GG hydrogels were thoroughly studied in a special issue of *Carbohydrate Polymers Vol.30, Issue 2/3, 1996* [Nishinari, 1996].
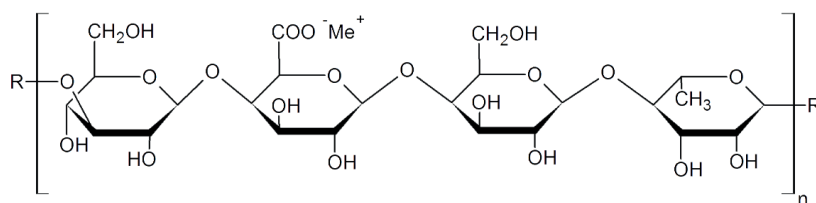
Figure 4. Schematic of the GG tetrasaccharide repeating structure in deacetylated form. The carboxyl group of glucuronic acid is shown in the carboxylate anion form and a generic metallic cation (Me$^+$) is depicted at this typical crosslinking site.

The most commonly used form of GG is the deacetylated version because the bulky acyl and glyceryl groups hinder the compactness of the microstructure. The acyl groups would appear in the left β-D-glucose of the GG molecule (Figure 4). [R. Mao et al., 2000] Like many other linear polysaccharides, GG molecules form stiff double helix coils in water solution, and this helix is tighter for the deacetylated GG [Chandrasekaran, Radha, 1995]. The helix is stabilized by cations and the natural crosslinking process of GG hydrogel then occurs via the ionotropic physical crosslinking resulting from the interaction of the anionic polysaccharide and cationic monovalent or divalent metal ion between the carboxylate groups of several GG molecules (Figure 3 (a)) [Milas, Rinaudo, 1996]. Cooling the water solution of GG from elevated temperatures of over 40 °C increases the helix formation and, even without added crosslinker ions, the gelation will occur due to the residual ions of either sodium or potassium (monovalent cations) present even in purified GG [Milas, Rinaudo, 1996, Morris et al., 2012]. Normally, however, a cationic crosslinker solution is mixed with the GG while cooling down, increasing the crosslink formation and creating a true gel with enough internal structure to be self-standing without support. The most used crosslinker is calcium ion (divalent) [Osmałek et al., 2014], but all the commonly available monovalent and divalent ions alone or as mixtures have been tested

to work for crosslinking. Higher ionic strength increases crosslink strength and there have also been various ions or small molecules used as a crosslinker, such as tetramethylammonium (monovalent) [Morris et al., 2012], aluminium (trivalent) [Maiti et al., 2011], spermidine (SPD, trivalent) [López-Cebral et al., 2013], and spermine (SPM, tetravalent) [Parraga et al., 2014].

The crosslinking process using the SPD and SPM bioamines (Figure 5) is based on the amine groups becoming ammonium groups in water solution, and thus SPD has a trivalent and SPM a tetravalent charge. As a result, they are highly efficient in crosslinking GG, the higher ionic charge of SPM being naturally the most effective. They are also endogenous molecules that are found throughout the body that affect cell survival by reducing oxidative stress and protecting DNA from oxygen radicals. [A. U. Khan et al., 1992] All the biological cascades where these antioxidants are involved are not as yet known. However, it has been suggested that they reduce stress in the endoplasmic reticulum during myocardial infarction, and thus regulate cardiomyocyte apoptosis [Wei et al., 2016], and have a role in the secretion processes of neurons in the brain [Laube et al., 2002]. The use of SPD and SPM bioamines for anionic polysaccharide crosslinking was pioneered by Parraga *et al.* [Parraga et al., 2014] and more specifically for GG by López-Cebral *et al.* [López-Cebral et al., 2013, López-Cebral et al., 2014]. However, these studies concentrated on drug release applications instead of TE and scaffold manufacturing.
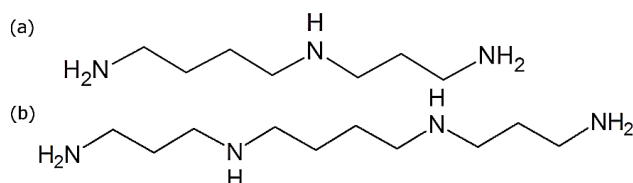
Figure 5. Schematic of the molecular structures of bioamines (a) SPD and (b) SPM. In water solution, each NH or NH$_2$ group gains one H$^+$, thus making the molecules ionically charged, trivalent and tetravalent, respectively.

Another common method for the production of GG-based hydrogels is chemical modification by methacrylation and then crosslinking the methacrylated GG (GG-MA) with UV light. Here, a methacrylic anhydride is reacted with GG in water solution, turning the hydroxymethyl group of glucose into a methacrylate group. UV light can then activate these methacrylate groups to crosslink GG chemically via free radical polymerization. Furthermore, since the carboxylic group is still left free, the crosslinking can be enhanced ionically. [Coutinho et al., 2010, Bacelar et al., 2016] There are two important reasons to use GG-MA instead of normal GG for TE applications. First of all, the stability of ionotropic crosslinking is not as good as that achieved with chemical crosslinking due to possible ion exchange occuring in a physiological solution [Coutinho et al., 2010]. However, the higher ionic charge of bioamines already mitigates this [López-Cebral et al., 2013]. The second reason is to enable advanced manufacturing methods, such as 3D printing for scaffold design in addition to simple casting [H. Shin et al., 2012, M. B.

Oliveira et al., 2016, Mouser et al., 2016]. Here, the only problem is usually the possible cyto-toxicity of the photoinitiator and the UV light [Ifkovits, Burdick, 2007].

The use of GG in different applications has been extensively reviewed elsewhere, so here is only a short compilation listing of the most interesting applications [Fialho et al., 2008, V. D. Prajapati et al., 2013, Osmałek et al., 2014, Bacelar et al., 2016, Stevens et al., 2016]. The initial use of GG was in food applications as a gelling agent, emulsifier, or stabilizer. The material properties that make GG attractive for food application are often also relevant for biomedical applications. GG hydrogel has high thermal and acid stability, high transparency, and good flavor (molecule) release. In tissue, GG goes through enzymatic biodegradation caused by the lysozyme enzyme released by macrophages [Xu et al., 2018]. GG also has easily tunable elasticity and stiffness by changing crosslinker ion concentration. [Fialho et al., 2008] The main food applications include desserts, icings, jams, ice creams, puddings, and vegan candies. Generally, it can be used in many places and one more trendy reason to use GG is as a replacement for animal-origin gelatin [Morris et al., 2012]. The most peculiar GG-containing food product was the short-lived Orbitz™ soft drink with gelated spheres floating in the juice [Skip Rocheford, Hower, 1998].

In addition to food applications, GG is used in various pharmaceutical applications. The first pharmaceutical application being eye droplets that go through weak gelation when in contact with tear fluid, and thus remain on the ocular surface longer than less viscous substances would [Carlfors et al., 1998]. The use of GG in personal care products, such as shampoos and topical creams, is based on the same stabilizing and flavor release properties that are favorable in food applications. As an alternative to gelatin, GG has been used in various drugs as the encapsulating outer layer. [Osmałek et al., 2014, V. D. Prajapati et al., 2013] Combining the food use with more biomedical applications has even produced the suggestion of using GG as an edible electrode [Keller et al., 2016]. To a lesser extent, GG is also used in various other applications, such as the oil and paper making industries [Fialho et al., 2008].

The first intended TE applications were for cartilage in the native form without any additional functionalization [A. M. Smith et al., 2007, J. T. Oliveira et al., 2010]. However, it was soon noted that biological functionalization is needed for most applications because GG on its own is a rather bioinert material, even if it has good biocompatibility [Ferris et al., 2013]. Recently, it has been functionalized in different ways, depending on the application. For example, the addition of bioactive glass, hydroxyapatite or collagen for bone TE [Douglas et al., 2014, M. B. Oliveira et al., 2016, Jamshidi et al., 2016, Bacelar et al., 2016], with ECM-peptides or the electrochemical activity of chitosan for neural TE [Silva et al., 2012, Lozano et al., 2015, Carvalho et al., 2018], as an antibiotic or other drug releasing delivery platform for wound healing [Matricardi et al., 2009, Maiti et al., 2011, López-Cebral et al., 2014, Shukla, Shukla, 2018], or with halloysite nanoclay for soft tissue in general [Bonifacio et al., 2017].

The GG polymer has also been fragmented physically by ultrasonication [Moxon, Smith, 2016] or scissoring chemically by oxidation using sodium periodate (NaIO$_4$) [Gong et al., 2009]. The aim in both cases is to reduce viscosity and enhance 3D printability. The oxidized GG has been further chemically crosslinked into an IPN with chitosan using the Schiff-base reaction, when aiming for cartilage applications [Y. Tang et al., 2012]. For soft tissue applications, functionalizing the oxidized GG with aldehyde modified HA to yield chemical hydrazone crosslinking is a valid option and produces mechanically biomimicking hydrogels similar to brain tissue [Karvinen et al., 2017, Karvinen et al., 2019]. The same components have also been combined by just physical mixing, ionotropic gelation, and freeze-drying to produce cryogels for TE of skin [Cencetti et al., 2011, Cerqueira et al., 2014].

In some cases, not much cell attachment is required. Thus, GG can also work without functionalization as, for example, for adipose TE [Lago et al., 2018] and spinal cord nucleus pulposus TE [Silva-Correia et al., 2012, Tsaryk et al., 2014]. Indeed, GG has even been functionalized specifically to prevent angiogenesis using growth factor blockers [Perugini et al., 2018]. It has even been combined with methylglyoxal-rich Manuka honey to include antimicrobial functionality [Bonifacio et al., 2018]. Furthermore, the original cartilage repair approach with GG-MA has progressed quite far in animal studies [J. T. Oliveira et al., 2010, Vilela et al., 2018].

2.2.3. Gelatin

Collagen is an abundant ECM protein with over 20 different types found in the human body. The different types are present in different tissues, with collagen type I being the most abundant and especially needed in the connective tissues. When a collagen molecule is denatured, it breaks down into smaller linear molecules called gelatin. [Olsen et al., 2003] An understanding of collagen molecular and supramolecular structure is important for also understanding the usability of gelatin as a cell culture substrate. The main difference between different collagen types is the order of amino acids, and thus peptide sequences. However, a defining feature for all collagens is the right-handed triple helix structure formed by three parallel polypeptide chains and stabilized by hydrogen bonds. The total build-up of a collagen fiber starts with protocollagen single strands forming a procollagen triple helix, then a tropocollagen triple helix, which self-assembles into collagen microfibrils that, after enzymatic crosslinking, finally form the collagen fiber. [Shoulders, Raines, 2009] The further crosslinking of these fibers into the actual ECM network makes the understanding of specific cell interactions with these complex molecules more challenging, but the most important aspect is that cells can attach to collagen and collagenous surfaces [Bruckner, 2009].

The gelatin macromolecule is a polyampholyte with hydrophilic groups having both cationic and anionic moieties as well as hydrophobic groups present in the structure in closely 1:1:1 ratio, due to the different constituent peptides. It can form a similar triple helix tertiary structure

as collagen. [Elzoghby, 2013] The basic structure of gelatin is shown in Figure 6. For the pro-
duction of gelatin, the most common sources are bovine or porcine skin, bone, and other left-
over collagenous connective tissues from a slaughterhouse. The collagen is denatured and
broken down by boiling and chemical treatments, yielding a distribution of polypeptide frag-
ments of different sizes and properties, often also causing lot-to-lot variation [Gómez-Guillén
et al., 2011]. Based on the production process, gelatin is divided into acid treated type A and
alkali treated type B, and this also affects the specific polyampholyte nature by controlling
which peptides are present in larger quantities [Elzoghby, 2013]. In addition to this traditional
route which produces gelatin for food and pharmaceutical applications, there have recently
appeared alternative gelatin production routes, such as from fish [Yang et al., 2007], other sea
life [Gómez-Guillén et al., 2011], or recombinantly from bacteria [Olsen et al., 2003, Rutsch-
mann et al., 2014]. Regardless of the production process, the most important parts, i.e., cell
attachment peptides (most importantly the arginine-glycine-aspartaic acid or RGD) and cell
cleavable MMP-sites and some other bioactive sites, retain their functionality. For sensitive
biomedical applications, such as TE, the recombinant gelatins would be the most attractive
option with less lot-to-lot variation and lower risk of contaminating pathogens. [Olsen et al.,
2003, Yue et al., 2015] However, mainly due to high production costs, recombinant versions
are not yet readily available and most of the TE work is done on bovine and porcine gelatin.
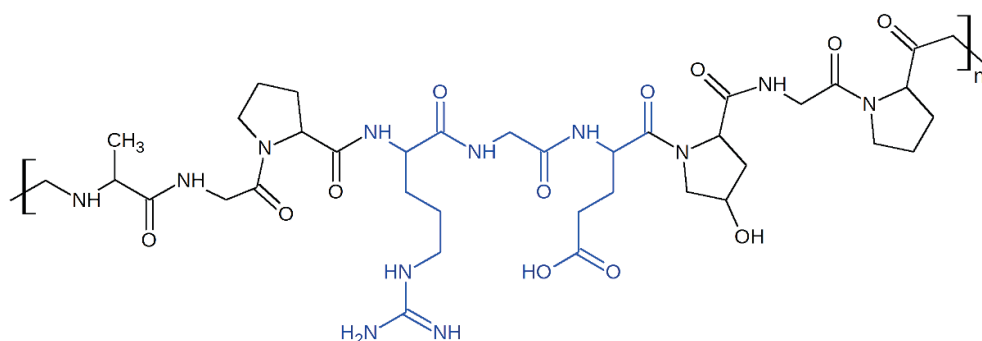
Figure 6. Basic structure of gelatin with the RGD-peptide sequence highlighted in blue.

The use of gelatin in cell culture applications started in the 1970s when it was noted that not
all cells can attach directly to plastic or glass surfaces and needed a coating to enhance at-
tachment [Folkman et al., 1979]. Since then, gelatin coatings have been standard practice in
cell culture studies and stem cell research, providing the RGD and other peptides of connective
tissue for cell attachment. Moreover, when aiming to transfer cell culture from 2D to 3D, gelatin-
based biomaterials are one natural choice as a scaffold material [Yue et al., 2015]. Curiously,
collagen forms a hydrogel when heated above room temperature due to the temperature trig-
gered helical self-assembly stabilized by ions. Then again, gelatin also has coil-to-helix self-
assembly and entanglement in the crosslinking process. However, without further stabilization

it does not reach an equilibrium and gelation occurs when cooling down. Thus, both gelation of collagen and gelatin are thermo-reversible processes, but in opposite directions. [Gómez-Guillén et al., 2011]

As native gelatin does not form a hydrogel at 37 °C, it needs to be chemically modified with stronger crosslinking for cell culture applications [Yue et al., 2015]. Still, it is the main coating material used with many anchorage-dependent cells, such as cardiomyocytes [Folkman et al., 1979, Mummery et al., 2003, Rajala et al., 2010]. The most used hydrogel version is methacrylated gelatin (GelMA), which crosslinks similarly to the GG-MA via UV light activated chemical crosslinking [Van Den Bulcke et al., 2000, Yue et al., 2015]. The UV crosslinking can be combined with many scaffold fabrication methods, and thus GelMA has been used for 3D bioprinting, photopatterning, layer-by-layer assemblies, micromolding, and fiber pulling. The tissue applications vary as well and include, for example, cardiac and skeletal muscle, skin, liver, vascularization, cartilage, bone, and also neural applications [Van Vlierberghe et al., 2011, Yue et al., 2015] However, methacrylation is not the only option. Other chemical modification possibilities include the natural crosslinker genipin as well as the peptide binding transglutaminase. Furthermore, numerous other less studied possibilities for gelatin hydrogel crosslinking strategies also exist [Van Vlierberghe et al., 2011]. After treatment with nordihydroguaiaretic acid, the naturally weak gelatin can be made into hydrogels of remarkably high strength and toughness that reach mechanical properties relevant for bone applications [Koob, Hernandez, 2003].

Gelatin has been combined with various other biomaterials to give the other supporting material gelatin's biofunctionality and increase cell attachment. However, even before TE applications, gelatin has also been combined with GG for food applications, the earliest example being the patent US 4,517,216A [Shim, 1985]. Blending these two biopolymers increases the strength of the hydrogel, regardless of whether the hydrogel was used in food applications or in TE. The combination of hydroxyl apatite particles in a blend of GG and GelMA and the freeze-drying of the system after crosslinking has been used for the production of controlled pore shape scaffolds for cartilage [Canadas et al., 2018]. The production of IPN hydrogels is a more sophisticated process than just blending the polymers together. In the process, gelatin is enzymatically crosslinked via a covalent lysine-amide bond. When gelatin and GG are mixed together with transglutaminase enzyme and an ionotropic crosslinker, an IPN hydrogel is formed. Because the different crosslinking strategies each stabilizes its own network individually, the product is a high strength hydrogel with good cytocompatibility. The major downside of this reported study was the sterilization of the hydrogel via autoclaving, thus preventing any 3D cell encapsulation studies. [Wen et al., 2014] Another IPN strategy for combining gelatin and GG is via photocrosslinking as the methacrylate groups crosslink with each other regardless of the rest of the polymer [H. Shin et al., 2012, Melchels et al., 2014]. The network can be purely chemically crosslinked in a two-step process [H. Shin et al., 2012] or it can be further stabilized by diffusion of cations [Melchels et al., 2014]. Here, GG-MA again increases the

strength of the hydrogel while GelMA increases the cytocompatibility, with the only downside now being the possible phototoxicity of UV light. A further strategy of combination reported is the biofunctionalization of GG microparticles via immersion in $NaIO_4$ to introduce aldehyde groups that can then bind gelatin molecules via 1-ethyl-3-[3-(dimethylamino)-propyl]–carbodiimide (EDC) modification. However, this method was only used for surface modification, and not fully for 3D functionalization. [C. Wang et al., 2008] The favorable attachment to GelMA and lack of attachment in GG has even been utilized in a cell migration study with sandwich hydrogels produced from these two components and cells put in the interface [George et al., 2018].

2.2.4. Biomimicking mechanical properties & mechanical testing

The mechanical properties of tissues are important for the primary biomechanic functioning of the tissue, such as the beating of the heart or the expansion and contraction of the lungs, and additionally they are relevant in the microscopic range for the migration and behavior of cells [Levental et al., 2007]. One logical starting point for the design of a hydrogel biomaterial to be used in a specific tissue is to study the tissue with the aim of producing a hydrogel that is as closely biomimicking to the target tissue as possible [Brandl et al., 2007]. In TE, implants require a certain amount of structural integrity, elasticity, and strength to last in their designated location. However, in most cases, this is not as limiting a factor in soft tissue applications as it can be, for example, in bone applications [Drury, Mooney, 2003].

A major part of TE involves cell culturing and the environment where the cells are grown always affects their behavior, either by stimulating or inhibiting. Traditional cell cultures are grown on 2D surfaces, but three-dimensionality would be needed for the better mimicking of real situations, as the body does not have 2D surfaces for the cells but is a 3D matrix [Murphy et al., 2014, Shah, Singh, 2017]. It has been shown that stem cells respond to mechanical cues from their environment by directing their differentiation towards the tissue that resembles the stiffness of their environment and that this is true for all anchorage-dependent cell types [A. J. Engler et al., 2006, Murphy et al., 2014, Walters, Gentleman, 2015]. The phenomenon of affecting cell behavior via mechanical forces is called mechanotransduction and one of the simplest ways to observe it is to culture MSCs on surfaces of varying stiffness. Due to this effect, they then differentiate into adipocytes on a soft surface and into osteoblasts on a hard surface, even if cultured in the same medium. [Walters, Gentleman, 2015] Another case is the study of the development of cancer in 3D, where the tumorigenic potential of cells is activated by an abnormally stiff microenvironment, and thus improper stiffness can be even harmful [Steimberg et al., 2014]. Between more and less stiff surfaces, most cells change shape drastically. In addition, they change the expression of proteins, which is at least partially the reason for the behavioral change [Murphy et al., 2014, Ihalainen et al., 2015, Walters, Gentleman, 2015].

A kind of subset of mechanotransduction is durotaxis, the phenomenon of controlling cell migration using changes in substrate rigidity [Nemir, West, 2010, Hadden et al., 2017]. The closely related phenomenon of chemotaxis, control of cell migration via chemical gradients, is more well-known and easier to perform than durotaxis experiments. However, during embryonic development, the cells are guided to migrate to their correct positions by both chemotactic and durotactic signals. [Evans, Gentleman, 2014] Translating the durotaxis to the case of 3D hydrogel cell culture requires a careful choice of materials because ideally the mechanical properties should be independent of both the microstructure of the materials and the biochemical composition. The hydrogels that can be manufactured to be closest to this ideal situation are PAA and PEG and in the 2D case membranes made of polydimethyl siloxane (PDMS). [Nemir, West, 2010]

Another valid point is the thickness of the hydrogel substrate. When cells are grown on a very soft gel, the cells can also more easily sense the underlying hard well plate surface, whereas a stiffer gel hides the underlying surface more efficiently [Evans, Gentleman, 2014]. As the cells pull their growth substrate via actin fibers on the attachment sites, they actively deform their surroundings [Evans, Gentleman, 2014, Vogel, 2018]. Indeed, if the growth substrate is stiff enough or thin enough to not deform under the cell's pull, the morphology of the cell will be changed, which in turn affects other functions of the cell, such as differentiation [Trappmann et al., 2012, Evans, Gentleman, 2014, Ihalainen et al., 2015, Walters, Gentleman, 2015].

The most common methods for the mechanical testing of materials are unconfined compression and tensile testing. In the simplest form of both, a force is applied along the sample axis and increased until the sample fractures, either by pressing it or pulling it beyond breaking point. This kind of slow or static testing can be extended into dynamic testing by changing the applied force in a controlled amplitude. Compression testing can be also conducted in a confined fashion, so that the sample is not allowed to expand in the direction perpendicular to the applied force. Other testing methods include shear, bending, torsion, and indentation testing, all of which measure slightly different properties of the material than compression and tensile testing do. [Callister, 2003, ASTM F2150, 2013]

Rheology is a specific field of mechanical testing that combines the material characteristics of solids and fluids and is called "*the science of everything that flows*". In common rheological testing, the sample is situated between two parallel plates, the upper plate rotates controllably and exerts shear force on the sample. The material response to this dynamic shear load is then observed. [Schramm, 1998, Kavanagh, Ross-Murphy, 1998]

Even though there is a scientific consensus on the importance of the mechanical properties of TE scaffolds, there is no such consensus as to which mechanical models best represent the mechanical response of various hydrogel biomaterials or even which represents the actual

tissues [Oyen, 2014]. The oldest, simplest, and generally still widely used is Hooke's law: a linearly proportional rise in the stress when the deformation increases, expressed as: $\sigma = E * \varepsilon$ and shown graphically in Figure 7. Here σ is the stress, ε is the strain, and E is the shape-independent material constant called *elastic modulus* (or Young's modulus) [Callister, 2003, SFS-EN ISO 604, 2004]. Because all the mechanical tests conducted in this thesis are compressive, this modulus is also called *compressive modulus* in the results.
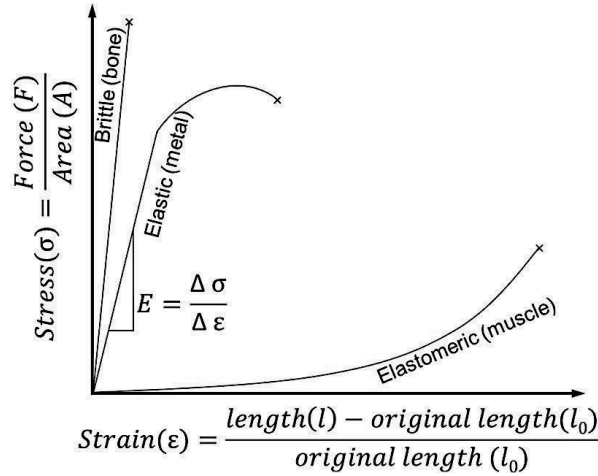
Figure 7. Schematic representation of three typical material classes in mechanical testing and the equations used for calculating elastic modulus (E) based on Hooke's law.

However, this mechanical model was originally postulated in the study of metallic springs and as such does not take into account all the mechanical phenomena occurring in polymeric networks, such as hydrogels, let alone in living tissue [Heidemann, Wirtz, 2004]. The following are background assumptions under which Hooke's law is in effect: continuum, isotropy, small deformation, and linear elasticity [Evans, Gentleman, 2014]. The main concern to raise is with the assumption that energy is stored elastically in the material during deformation, and that deformation recovers instantly after force is released. This is only valid for some materials and even then only in a specific strain range. For example, in metals the 0.2% strain is a commonly used limit, but for polymeric materials such a small strain does not have validity, and for them the realistic elastic ranges are tens of percentage strain [Callister, 2003]. The other assumptions can also be disputed as the isotropy of hydrogels varies and is highly related to the mixing efficiency during gelation [Gering et al., 2018]. Likewise, the recoverable deformations endured by polymers and elastomer-like hydrogels or soft tissues are not small [Y. Mao et al., 2017, Levental et al., 2007].

Over time, more accurate models to study elasticity and specifically the mechanics of polymers, such as Hencky's law of elasticity [Hencky, 1928, Hencky, 1931], Flory's rubber elasticity [Flory,

1985a], non-linear elasticity [Storm et al., 2005], combined Kelvin-Voigt-Maxwell model of viscoelasticity [Schramm, 1998], poroelasticity [Biot, 1941], combinatorial poroviscoelasticity [Caccavo, Lamberti, 2017], and their derivatives [Hong et al., 2010, Chester, 2012, Hu, Suo, 2012, Q. Wang et al., 2014], have been developed. All these models can provide a more accurate understanding of the full mechanical response, but at the same time they are more complicated to use than the simple Hooke's law, and thus Hooke's law is the most widely known and used. The following is a concise review of the most relevant other mechanical models from the view point of hydrogels.

The theory of rubber elasticity as postulated by Flory [Flory, 1985a] is based on studying molecular crosslinked networks and their thermodynamics. The main assumption here is that all the polymers are in contact with each other via the crosslinks and that the network deforms in an affine manner and transforms the macroscopic deformation directly to the microscopic and molecular scales. Rubber elasticity can be most simply expressed as $E = N_p * k * T$, where E is elastic modulus (often depicted as G in the case of rubber elasticity), k is Boltzman constant, T is temperature, and N_p is the number of polymer chains per volume, where polymer chain means part of the polymer between crosslinking points. Even though the basic rubber elasticity has been modified to better take into account the physical interactions of the molecular networks [Flory, 1985b], such as phantom and interpenetrating networks, and the effect of solute [Slaughter et al., 2009], in addition to the effect of just crosslinks, the applicability of the affine deformation has been questioned, for example, in the case of the well-known model hydrogel PAA [Basu et al., 2011, Oyen, 2014]. Another problem is not considering the time dependence of viscoelasticity, and instead assuming purely elastic material response [Oyen, 2014]. However, the applicability of rubber elasticity to studying elastic proteins and muscle was already mentioned in the original studies, so the similarities between soft tissue and rubber are not a new finding [Flory, 1985a].

The non-linear elasticity theory is based largely on rheological observations of ECM protein networks and concentrating on the microscale [Storm et al., 2005, Dobrynin, Carrillo, 2011]. Polymer theory has divided polymer filaments into three categories: flexible, semiflexible, and rigid. Flexible filaments exhibit purely entropic elastic response, rigid filaments exhibit no entropic elasticity, and semiflexible filaments exhibit a response that is much more complex to define. This is where non-linear elasticity theory comes into effect. These semiflexible filaments do not form loops in the network structure like totally randomly crosslinked hydrogels do, but most biological gel networks belong to this category. [Storm et al., 2005] The compression response of cardiac muscle tissue is similarly non-linear, as depicted schematically in Figure 7, and before the formulation of non-linear elasticity theory, cardiac muscle compression was analyzed using tangent modulus, a slope of the stress-strain curve at a single point [Mirsky, Parmley, 1973]. There have also been attempts to put polymers and soft tissue in different categories of mechanical behavior, treating polymers as more freely jointed chains and biological material as a combination of stiff blocks into a worm-like chain. However, hydrogels would

belong in biological material and not in polymers in this division. Currently, the applicability of non-linear elasticity to polymers in addition to soft tissue is a more valid approach than vice versa when the forces used are small enough. [Dobrynin, Carrillo, 2011] The two major short-comings of non-linear elasticity theory are the need for case-specific polymer structure information and the time-dependence of molecules orienting and stiffening due to the applied force, meaning viscoelasticity. The model is currently used mostly in the micromechanic studies of ECM molecules and in rheology, but not in compression. [Storm et al., 2005, H. Kang et al., 2009, Dobrynin, Carrillo, 2011]

Many of the biological materials have a strong strain stiffening effect, easily modeled for polymers with persistent lengths, but more difficult in the case of unfolding protein bundles. Therefore, the unfolding adds an extra microstructural component in the deformation in addition to polymer bending and crosslink breakage, as shown in Figure 8. [H. Kang et al., 2009] This multiphase deformation results in the remarkable ability of protein networks and some hydrogels to deform at relatively low stresses but sustain reversible deformation multiple times their original length [Dobrynin, Carrillo, 2011]. After this low stiffness initial straightening of the more free-moving parts of the molecular network, the load is then taken by the stiff crosslinking points and the now fully extended polymer molecules. The high strength of these structures then causes the pronounced strain hardening effect which can be seen in both soft tissue and hydrogels [H. Kang et al., 2009, Shoulders, Raines, 2009, Furmanski, Chakravartula, 2011, Karvinen et al., 2017].
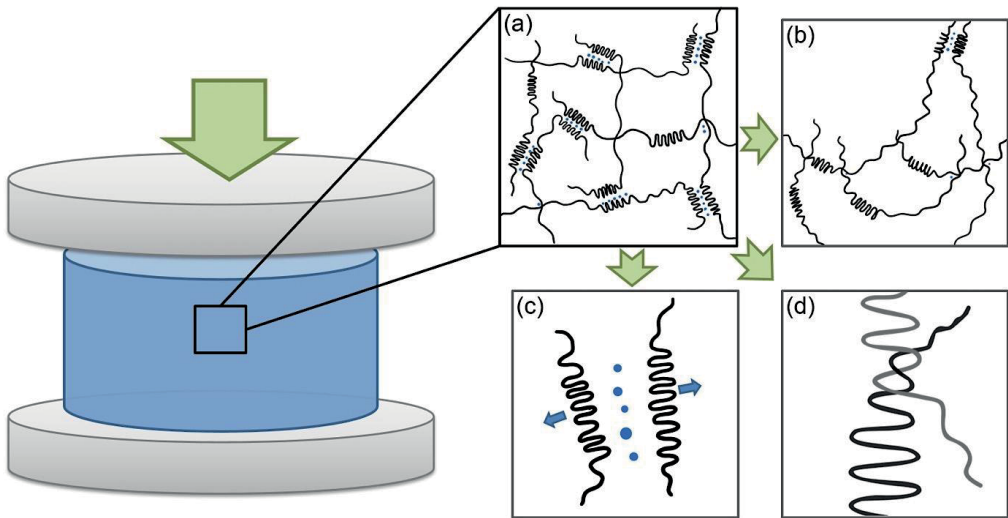
Figure 8. The different molecular level events contributing to the deformation of a crosslinked helical network during compression: (a) the network structure at rest, (b) bending and extension of the free-moving polymer segments, (c) breakage of a crosslink, (d) unfolding of a helix.

Viscoelasticity is the time-dependent deformation of materials under load. It is valid in the study of polymers that tend to have both an immediate elastic response and a delayed viscous response to load. On the molecular scale, viscoelasticity occurs due to long polymer chains adapting to the load in a non-uniform fashion. [Callister, 2003] The first models to understand this mechanical behavior depict the material as being composed of multiple dashpots and springs connected together in series or in parallel (Figure 9). The dashpot depicting viscous liquid is called the Newtonian model and connecting it in series with a Hookean spring creates the Maxwell model. Alternatively, the Kelvin-Voigt model has the dashpot and spring elements connected in parallel. Each dashpot and spring in the system will then have their own material-specific viscosity and elastic modulus, respectively. A multiple element model built from these blocks combining the Maxwell model with the Kelvin-Voigt model is then also called a Burgers model. [Schramm, 1998] This can be even further generalized into an infinite series of parallel dashpots and springs into the Generalized Maxwell model, also called the Wiechert model [Roylance, 2001].
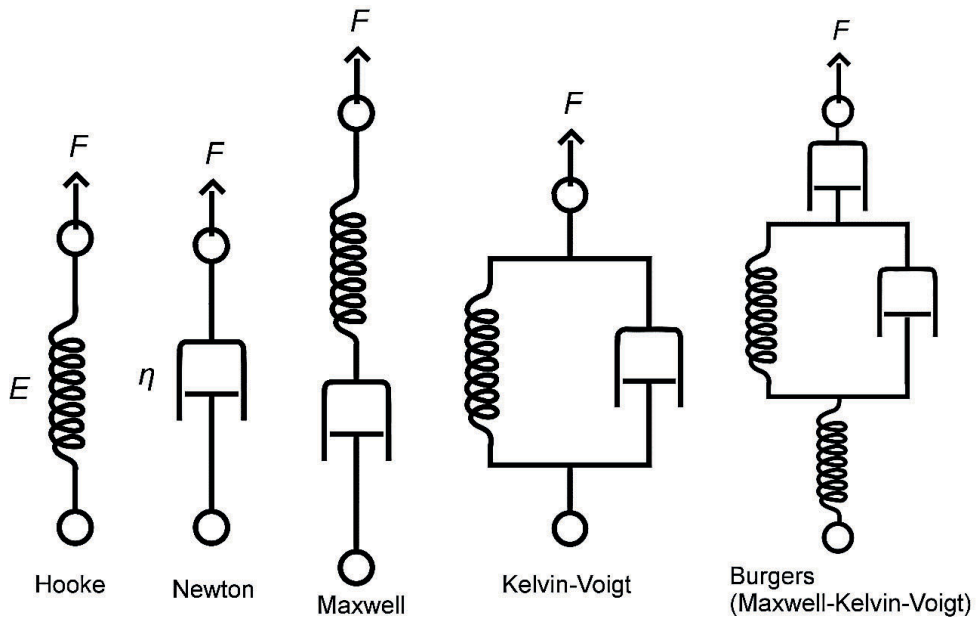
Figure 9. The schematic representation of the components making up the viscoelastic material models with increasing complexity. F depicts the force extending the system and each spring and dashpot has specific elastic modulus E and viscosity η, respectively. Image modified from public domain source [Wikimedia Commons, 2007].

In all the viscoelasticity models, the viscous components make the deformation time-dependent, and thus these properties are mostly studied by creep test, stress relaxation test, dynamic mechanical analysis, or rheology [Roylance, 2001]. However, the viscous component can already have an effect in a compression test, and thus omitting it is not accurate. In a more accurate yet simple analysis of compression, a time-dependent function would replace the elastic constant. [Nakamura et al., 2001, Oyen, 2014] Even though there are theoretical models for the time-dependent function and, for example, for determining the so-called instantaneous and equilibrium modulus, applying it in the analysis is not a simple process. The time-dependent function separates the parts of viscoelasticity, but most of the dynamic mechanical testing studies report only curves of storage and loss of modulus, without further analysis or defining of viscoelastic coefficients [Oyen, 2014].

Yet another phenomenon specific to the hydrogel's mechanical response is the effect of a large amount of incompressible water in the system. The theory of poroelasticity was originally developed for studying the consolidation of soil [Biot, 1941], but it works for other water-containing porous materials and is of especial interest for hydrogels [Cai et al., 2010, Oyen, 2014]. Poroelastic studies have not been widely brought to the 3D case, mostly applying analysis either just uniaxially along the test axis or sometimes also perpendicular to the test axis [Cai et al., 2010, Oyen, 2014, Oyen, 2015]. However, there have recently been several attempts to combine both viscoelasticity and poroelasticity and to update the whole analysis suitability for real 3D case as well. To date, however, these finite element method implementations have been complicated to use [Chester, 2012, X. Wang, Hong, 2012, Q. Wang et al., 2014, Caccavo, Lamberti, 2017]. The use of these methods requires further knowledge of the hydrogel's water content or swelling, the chemical potential of the hydrogel polymer and water, free energy balance equations, and general access to computational modeling for implementation, and thus are not suitable for the simple compression screening of novel hydrogel formulations [Chester, 2012, Caccavo, Lamberti, 2017].

One more special model of viscoelasticity is the Le Gac and Duval model [Le Gac, Duval, 1980, Duval, Le Gac, 1980]. Originally developed for studying the mechanics of ice, more recently the model has also been applied in the case of viscoelastic high-temperature metals [Santaoja, 2014]. The model is used to study the viscoelasticity during creep and stress relaxation and is easily doable using the same measurement setup as conventional compression testing. Moreover, the model is also based on real phenomenological material behavior, and is therefore unrelated to the viscoelasticity models presented in Figure 9 in which the dashpots and springs are a simplification, regardless of how accurate the Generalized Maxwell model is for specific polymers [Le Gac, Duval, 1980, Roylance, 2001, Santaoja, 2014]. The derivation and application of a simplified Le Gac and Duval model is proposed in **Publication IV** for the compression of a hydrogel.

2.2.5. Microstructure and porosity

A scaffold material designed as a support structure for cells with the aim of tissue ingrowth should have a controlled or at least known microstructure that is able to function in the intended application. Additionally, for the TE scaffold to be successful, nutrients, differentiation guiding growth factors, and the waste products of cell metabolism need to diffuse through the hydrogel.

Moreover, as discussed in the previous chapter, the microstructure also holds the key to understanding the mechanical performance of the material. In the case of hydrogels, however, studying microstructure and porosity are not straightforward tasks due to the special nature of these water-filled polymer networks. [Loh, Choong, 2013, Li, Mooney, 2016, ASTM F2900, 2011] An elegant way of defining the terminology related to hydrogel microstructures is by dividing the water-filled voids inside the polymer network into *porosity* and *mesh*, as illustrated in Figure 10 [Li, Mooney, 2016]. A *mesh* is the polymer network itself, consisting of crosslinked polymer molecules and the mesh size is the distance between effective crosslinking points. A *pore* is a larger void inside the material, extending for a much longer distance than the mesh and *porosity* is then the description of this wider property of the microstructure [Li, Mooney, 2016].
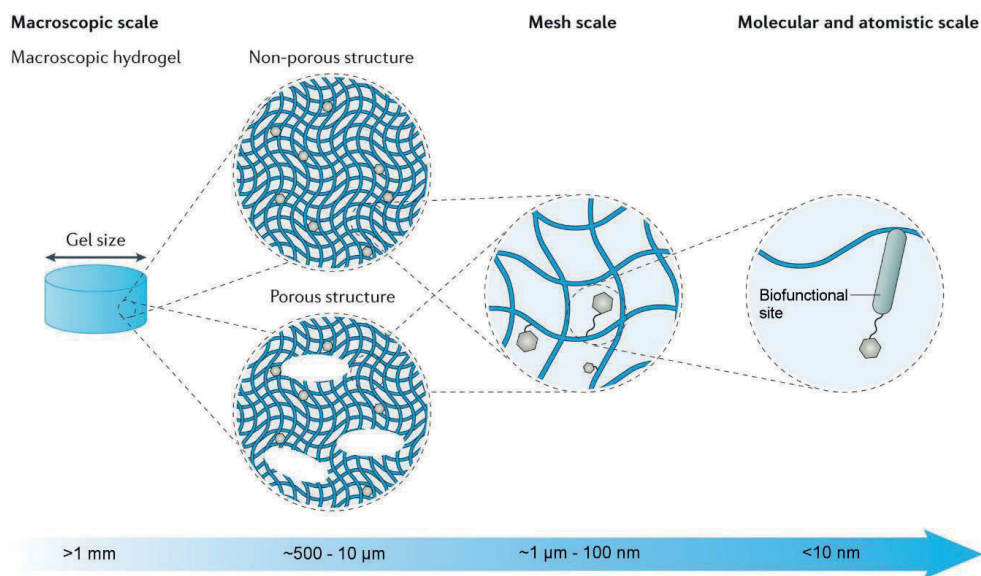
Figure 10. Definition of *porosity* and *mesh* primarily based on their size and in relation to polymer crosslink distances. Image modified from [Li, Mooney, 2016].

Molecular architectures and the crystallization of the polymers can be studied, for example, by x-ray diffraction [Chandrasekaran, Radha, 1995]. In addition, freeze-dried hydrogel scaffolds have been studied a lot with scanning electron microscopy (SEM) [Loh, Choong, 2013] and to

28

some degree with micro-computed tomography (μCT) [Cengiz et al., 2018]. However, the most interesting part is studying the hydrogel microstructure in a wet, water-swollen state. Of course, if the gel is intended to be used as a freeze-dried scaffold and then re-wetted at the application site, then studying the porosity after freeze-drying is relevant. [Lozinsky et al., 2003, García-González et al., 2011, Van Vlierberghe et al., 2011] However, if in the actual application the gel is not freeze-dried after gelation and the gelation is conducted *in situ*, then studying the freeze-dried version of the gel will not give the correct information on the microstructure. Moreover, drying will likely cause the collapse of the polymer network, forming porosity that originally did not exist inside the hydrogel in the swollen state. [Lozinsky et al., 2003, García-González et al., 2011] Thus, the validity of pore size measurements as characterization of hydrogels can be questioned due to the collapse and swelling differences. So studying the gel microstructure via SEM or μCT can give valid information on the pore size of a dry scaffold, which could be *aerogel*, *xerogel,* or *cryogel*, but will not provide exact information on the porosity or mesh size of a water-swollen *hydrogel* [Alemán et al., 2009].

Alternative methods for studying the porosity and mesh size in a swollen state exist, but they have not gained as much popularity as the SEM imaging of dried hydrogels. At the transition between the swollen and dried or frozen state, there are methods based on differential scanning calorimetry (DSC) [Ishikiriyama et al., 1995] and nuclear magnetic resonance (NMR) cryoporometry, also termed thermoporosimetry [Nedelec et al., 2006], both usually combined with gas adsorption-desorption cycle measurements. However, neither of these methods give information at exactly the swollen state, and thus they should be considered more as auxiliary tools in the study of porosity that are more useful in the case of membranes or hybrid materials than scaffolds in a purely hydrogel form [Ishikiriyama et al., 1995, Nedelec et al., 2006].

Studying the mesh size based on knowledge about the crosslinkage is possible mathematically based on the rubber elasticity theory mentioned in **Chapter 2.2.4**, especially in the case of stoichiometric chemical crosslinking [Flory, 1985b]. The requirement is to know the average molecular weight between the crosslinks and the polymer volume fraction in the swollen state, which could be further determined using applied mechanical testing [Slaughter et al., 2009]. Mechanical testing data can also be used to measure the transport of water or other solute through the hydrogel, if applying the poroelasticity theory. The problems with this approach include the difficulty in solving coupled poroelasticity equations and an unknown water chemical potential in each hydrogel case. However, once these problems are overcome, the theory could be used to determine mesh size [Cai et al., 2010, Oyen, 2014, Caccavo, Lamberti, 2017]. Another option for mesh and crosslink analysis is the use of rheology, where measuring the storage modulus *G'* can yield both average mesh size and average crosslink density in the swollen state [Karvinen et al., 2019]. However, because a GG network contains the double helix structures and can have coil-helix transitions independent of crosslinking as well, the

interpretation of crosslink density is more complicated than with more linear or single coil polymer networks. [Morris et al., 2012]

Various diffusion-based or forced mass transport methods have also been used for the characterization of hydrogel microstructure. Mercury intrusion porosimetry is usually more suitable for more rigid structures than hydrogel-type polymer networks because the pressures required to push mercury through the porous material are quite high, but it has also been used in the characterization of hydrogels [Gemeinhart et al., 2000]. More suitable methods for hydrogels include the confocal microscopy technique fluorescence recovery after photobleaching (FRAP) [J. White, Stelzer, 1999]. This method was originally developed to study the lateral transport of proteins and lipids in the cell membrane [Axelrod et al., 1976]. The main principle is embedding fluorescent molecules inside the studied volume, and then bleaching the fluorescence from a small spot and recording time lapse fluorescence images to study how the fluorescence recovers in the bleached area [J. White, Stelzer, 1999]. The recording can be combined with computational diffusion simulation to yield the diffusion coefficients of a specific molecule in a specific medium, even inside a hydrogel [Karvinen et al., 2019].

When the diffusing agent is a well-known molecule with a controlled size, the diffusion data can be used to calculate pore or mesh size. The main parameter needed for this is the Stokes radius, defined as the radius of a smooth sphere with the molecular weight and frictional coefficient of the diffusing agent molecule [Erickson, 2009]. The hydrodynamic radius is a similar parameter that better takes into account the shape of the molecule, thus no longer expecting a spherical shape, even though in certain applications, such as size exclusion chromatography, these can be interchangeable. Knowing the size of a molecule that can go through the hydrogel essentially tells the pore or mesh size of the hydrogel. However, this indirect method of measuring the microstructure only works if there are no additional relevant interactions between the hydrogel polymer and the diffusing agent, such as binding to the network. [Frigon et al., 1983, Venturoli, Rippe, 2005, Erickson, 2009]

A method combining rheology with the imaging of movement inside the hydrogel is called multiple particle tracking microrheology, where the Brownian motion of fluorescent particles enables the imaging of porosity with a laser scanning confocal microscope. This method has even been used to correlate microstructure with mechanical properties from compressive and conventional rheology measurements. However, it has so far only been used with freeze-dried scaffolds. [Oelschlaeger et al., 2016] Recording the movements of fluorescent molecules is also the main point in fluorescence correlation spectroscopy (FCS), another confocal microscopy method already used in hydrogel characterization as well [Kisley et al., 2015]. Other diffusion methods include recording the movement of fluorescent molecules out of the hydrogel with a simple diffusion chamber and measuring the output either microscopically or spectroscopically [ASTM F2900, 2011]. Even studying the diffusion of pure water using NMR and spectroscopic methods has been tried with GG hydrogels. The hydrogel network has been

proven to not interfere with water diffusion, thus the diffusion coefficient of a water molecule inside ionotropically crosslinked GG is very close to diffusion coefficient purely in water. [Ohtsuka, Watanabe, 1996]

One aspect related to both the microstructure and transparency of a hydrogel is the optical density, or turbidity, of the material [ASTM F2900, 2011]. This can be measured with a spectrophoto-meter as a bulk property [Lau et al., 2000]. Alternatively, a novel method for studying the variations in optical density of a hydrogel is to use optical projection tomography (OPT), a microscopy method originally developed for the study of embryonal development in the mesoscopic scale [Sharpe et al., 2002, Figueiras et al., 2014]. OPT is based on the sample rotation and reconstruction of individual 2D projections into a full 3D view of the sample. It is a good method for hydrogel studies because the samples can be in the swollen-state throughout the imaging. While OPT is a 3D imaging method, spectrophotometry just measures the amount of light passing through the sample, essentially being a one dimensional measurement which does not take into account the 3D volume aspect [Lau et al., 2000, Figueiras et al., 2014]. Additionally, OPT can fit a significantly larger volume in the field-of-view than the more conventional 3D imaging method confocal microscopy. In OPT, the image size can cover several millimeters, while confocal microscopy can cover a maximum depth of a few hundred micrometers. [L. E. Smith et al., 2010, Figueiras et al., 2014]

When imaging pure hydrogel samples in bright field OPT without any added dye or contrast agents, it was noted that hydrogels of different concentrations show variations in optical density. Furthermore, these variations can be studied in the reconstructed 3D images. [Figueiras et al., 2014] This variation is not directly the microstructure of the hydrogel but characterizes the differences as image texture [Haralick et al., 1973], which can also yield insight into the microstructure of hydrogels. In short, all digital images have the properties of tone and texture and image texture contains information on the spatial distribution of tonal variations [Haralick et al., 1973]. The image texture analysis should not, however, be confused with the mechanical texture analysis performed in materials science and the food industry. Mechanical texture is a widely used characteristic of a human sensory property that describes how food feels in the mouth [Szczesniak, 2002]. When studying hydrogels, it is of primary importance to distinguish which texture is studied because the mechanical texture of gels, such as GG and gelatin used in food applications, has been generally more studied than their image texture [R. Mao et al., 2000, Lau et al., 2000]. Thus, variations in the optical density of a hydrogel, even for gels transparent to the naked eye, can be used to gain information on the 3D microstructure in the swollen-state.

2.2.6. Biocompatibility and cytocompatibility

To be able to call something a *biomaterial*, the biological response, so-called biocompatibility, is key. The general term biocompatibility has several widely accepted definitions in the literature. For example, the IUPAC gives the following definition: "*Ability to be in contact with a living system without producing an adverse effect*" [Vert et al., 2012]. Another way to express this is the famous *Williams definition*: "*The ability of a material to perform with an appropriate host response in a specific application*", defined by Professor Williams the researcher who originally defined biocompatibility in 1987 [D. F. Williams, 2008]. One more definition, modified from the Williams definition, is "*An expression of the benignity of the relation between a material and its biological environment*" [Kohane, Langer, 2010]. All in all, there is a consensus that biocompatibility is of great importance for any biomaterial application, but then opinions vary on how to exactly measure biocompatibility. Methods of measuring biocompatibility can be divided into multiple subcategories that include, for example, cytotoxicity, systemic toxicity, hypersensitivity, genotoxicity, chronic toxicity, haemocompatibility, and carcinogenicity. All these require their own specific tests for a material to be called fully biocompatible and to be accepted for clinical therapeutic use by the regulatory authorities. [SFS-EN ISO 10993-1, 2009, ASTM F748, 2010, ASTM F2900, 2011]

However, in most cases when developing novel biomaterials, not all of these aspects are addressed at once. When novel hydrogels are designed for TE, the main property for initial study is cytotoxicity and its reverse side cytocompatibility [Caliari, Burdick, 2016]. When developing bioinert implant materials, it is enough during the intial phase to prove that the material is not cytotoxic. However, for TE and regeneration, the material should be bioactive and allow attachment and interaction. [Kohane, Langer, 2010, Khademhosseini, Langer, 2016] Thus, when studying cytocompatibility *in vitro*, cells are cultured in direct contact with the material, for example, on top of it or encapsulated inside of it, and the focus is on the cell response. This can be done with a more general multipurpose cell line at first and then later with the specific cells of the intended application. In addition, it can be done directly using the application-specific cells if they are not too expensive or too hard to get, or no suitable preliminary model cell line is available. [SFS-EN ISO 10993-5, 2009]

There are several aspects of cytocompatibility to be tested. Culturing cells on top of the studied material gives information on how they react when in direct contact with the material. For example, do the cells attach, spread, migrate, and proliferate on the material [Naahidi et al., 2017]. Moreover, when encapsulating the cells inside a hydrogel, further information is also gained on the crosslinking process and its cytocompatibility [Caliari, Burdick, 2016]. Detached cells are in a more vulnerable state and harsh chemical reactions, high ion concentrations, or UV irradiation are often cytotoxic [C. G. Williams et al., 2005, Truong et al., 2016, Shukla, Shukla, 2018]. This should to be kept in mind when designing crosslinking strategies and, as already stated in **Chapter 2.2.1.2.**, when the bio-orthogonality of chemical crosslinking is desired

[Jiang et al., 2014]. Thus, initial cell survival can be studied within a few days of cell plating, while longer time effects, such as proliferation and migration, can take at least a week to be distinguishable [SFS-EN ISO 10993-5, 2009, Nam et al., 2015]. Furthermore, the effect on cell attachment and the long-time response can also be seen in encapsulation studies. However, if there is a problem with the crosslinking and encapsulation process itself, this can cause a false negative result on the cell attachment. Moreover, if the hydrogel microstructure restricts nutrient transport or cell movement too much, this problem can also be traced by culturing cells both on top of and encapsulated inside the hydrogel. [ASTM F2900, 2011]

The most common method to study cytocompatibility is microscopy of the cells living in contact with the material, which can be either a qualitative or quantitative assay. In general, a reduction of quantitative cell viability by more than 30% is considered a cytotoxic effect. [SFS-EN ISO 10993-5, 2009] A common method of distinction between live and dead cells with fluorescent microscopy is the Live/Dead® assay. The method is based on calcein acetoxymethyl ester (Calcein-AM or Ca-AM) and ethidium homodimer-1 (EtHD-1) fluorescent probes. Most viable mammalian cells have a ubiquitous presence of esterase enzyme capable of cleaving the acetoxymethyl ester off Ca-AM and enabling calcein to be excited by 488 nm wavelength fluorescent light, subsequently emitting green fluorescence and labeling the cell alive. Then, only in dead cells can the EtHD-1 penetrate the compromised cell wall, bind to the nucleus, and emit red fluorescence and labeling the cell dead. [Poole et al., 1993] Other cell viability assays include the 3-(4,5-dimethylthiazol-2-yl)-2,5-diphenyltetrazoliumbromid (MTT) assay that detects metabolic activity or the 2,3-bis(2-methoxy-4-nitro-5-sulfophenyl)-5-[(phenylamino)carbonyl]-2H-tetrazolium-hydroxide (XTT) assay that detects the mitochondrial dehydrogenase activity of live cells. Both MTT and XTT assays are used on a whole culture well at once and the result is read with a colorimetric or fluorimetric microplate reader as color change in the wells with cytotoxic compounds. [SFS-EN ISO 10993-5, 2009]

For 3D hydrogel cell cultures, the microscopy-based Live/Dead® assay is the most commonly used option, mainly because it can detect more than just the viability status. As the Ca-AM stains the whole cell, estimations on cell morphology can be done in addition to the live/dead-status [Poole et al., 1993]. The morphological changes lead to studying cell attachment and spreading or elongation, which are important indicators of cytocompatibility in addition to the cells just being alive in contact with the material. Any bioactive function of a material requires cell attachment as the first step. [Cukierman et al., 2001, SFS-EN ISO 10993-5, 2009, Naahidi et al., 2017] However, most viability assays as well as microscopy methods are designed primarily for 2D cell cultures and to be compatible with standard well plate formats. However, because hydrogel samples have a significantly higher thickness and the cells are encapsulated randomly throughout the volume in 3D, they often create imaging problems [Appel et al., 2013]. For example, the imaging depth reachable by the objective might not be enough, out-of-focus fluorescence from the cells above or below the studied spot can interfere, or the hydrogel itself may not be fully transparent [L. E. Smith et al., 2010, Appel et al., 2013]. An attractive option

33

that has not been used much for hydrogel imaging is OPT [Sharpe et al., 2002, Figueiras et al., 2014]. As mentioned previously in **Chapter 2.2.5.**, OPT is a mesoscale imaging method that has larger sample volumes and imaging depths than traditional confocal microscopy. OPT is a highly attractive method for studying larger hydrogel volumes in a single imaging step, either in transmission or fluorescent imaging mode. Imaging a larger volume reduces the ambiguity of what is a representative image of the cells and, as the whole 3D volume is reconstructed, it opens new possibilities to analyze the details of 3D cell cultures. [Belay et al., 2018]

2.3. Tissue engineering applications for soft tissue

As stated in **Chapter 2.1**, current trends in TE can be divided into therapeutic clinical TE and research focused *in vitro* TE. In this work, the number of TE applications were narrowed down to soft tissue applications for two main reasons. First of all, hydrogels designed to be mechanically biomimicking and suit the needs of one type of soft tissue are likely to suit other soft tissues as well, at least more so than bone and other hard tissues. Even though the elastic modulus varies between muscle, internal organs, and brain, it is still closer than that of bone and cartilage. [Levental et al., 2007, Brandl et al., 2007] The second reason stems from the World Health Organization Global Disease Burden studies that show that cardiovascular diseases are one of the leading causes of death globally [Naghavi et al., 2017, Vos et al., 2017]. Furthermore, although not reaching the top five causes of death, neurological disorders are also a major cause of death and disability. The importance of cardiac and neural treatments further increases when the number of injuries and years lived with non-fatal disease or injury are taken into account [Vos et al., 2017].

In addition to clinical treatments, iPSC technology has opened up new and exciting ways for disease modeling, which would have been impossible if only animal models or even hESC-derived cell types were used [Robinton, Daley, 2012]. The problems of animal models and primary cell line studies include differences between animal and human cell responses, missing the systemic and metabolic effects, and differences based on age, sex, and ethnicity [Ribas et al., 2016]. When using hiPSC, it is possible to know the full medical record of the cell donor patient and to study the phenotype of a genetic disease specifically occurring in that patient via *in vitro* disease modeling. This can lead to both a more thorough understanding of the disease pathogenesis and the personalized medicine and drug discovery suitable for the specific patient [Gomes et al., 2017, Monteiro et al., 2016]. The human-based experimental setups aim for more precise drug development based on the disease pathway analysis and, while aiming to produce more efficient drugs, simultaneously reduce the amount of pre-clinical animal testing [Langley et al., 2016].

2.3.1. Neural tissue engineering

The nervous system of the human body is divided into the central nervous system (CNS) and the peripheral nervous system (PNS). The CNS consists of the brain and spinal cord and the PNS consists of the neuronal innervation of all the tissues, transmitting sensory and excitatory input between the CNS and other tissues [Schmidt, Leach, 2003]. There are multiple cell types present in the nervous system. The most important of these, *neuronal cells,* being a top category term which can be divided into neurons that actually transmit the electrophysiological signals, astrocytes, that function as supporting cells, and oligodendrocytes and Schwann cells in CNS and PNS, respectively. The last ones produce the insulating myelin sheath that increases neural signal transmission speed [Schmidt, Leach, 2003, Merryweather, Roach, 2017]. Typical neural cell architecture is presented in Figure 11.
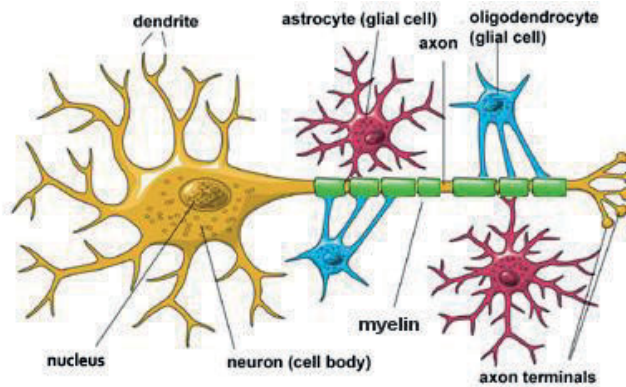
Figure 11. Schematic presentation of the most relevant neuronal cell types and their interactions. Image modified from public domain source. [National Institutes of Health, 2018]

The strategies for clinical neural TE mainly comprise guidance systems to allow broken neural axons and dendrites to regenerate lost nerve contacts caused by injury or pharmacological prevention of neurodegenerative disease progression in the brain [Schmidt, Leach, 2003, Aurand et al., 2012, Kornev et al., 2018]. Both physical and biochemical cues have been used as conduits to guide a neuronal axon to regrow in the correct direction, for example, in the case of spinal cord injury [Schmidt, Leach, 2003]. One further important aspect related to axonal regeneration is the repairing of the myelin sheath that covers the axons that is specifically required in the treatment of diseases, such as multiple sclerosis [Narkilahti et al., 2009]. Requirements for the scaffolds, cells, and bioactive molecules vary depending on the specific clinical application. Very few neural TE approaches have yet advanced to clinical trials, so most are just suggested strategies [Kornev et al., 2018]. The ones that have been tested clinically are mainly just cell injection treatments, both for neurodegenerative diseases and for injury treatments and axonal regeneration, but not for full TE with cells and scaffold combined

[Lindvall, Kokaia, 2010, Feldman et al., 2014, Trounson, McDonald, 2015]. However, several commercial products, composed of scaffolds without added cells acting as a guidance conduit, have gained approval for clinical testing and have been reviewed thoroughly elsewhere [Kehoe et al., 2012, Arslantunali et al., 2014]. To date, the most promising guidance conduit scaffolds have been based on collagen type I [Means Jr et al., 2016].

The scaffold material choice for neural TE is often a soft hydrogel that mimics brain tissue or a composite scaffold with a porous soft matrix and long fibrous phase for axonal guidance. In the case of spinal cord injury, adding a stronger scaffold to account for the nucleus pulposus tissue surrounding the gentle axons is a valid option. [Pereira et al., 2011, van Uden et al., 2017, Kornev et al., 2018] For the rational scaffold design, it is good to note that the main components of neural ECM are proteins, such as laminin and collagen type IV, together with the glycosaminoglycan HA and chondroitin sulfate proteoglycan complexes [Merryweather, Roach, 2017]. The low elastic modulus of brain tissue has been attributed to a low amount of collagen type I [Shoulders, Raines, 2009, Hopkins et al., 2015]. Even though endogenously collagen type I is not a major component in neuronal ECM, it is still the most used in commercial treatment applications so far, but not often in the hydrogel state [Kehoe et al., 2012, Arslantunali et al., 2014, Means Jr et al., 2016, Sensharma et al., 2017].

All the common neural ECM molecules have been previously used in research for nerve guidance scaffold production [Kornev et al., 2018]. These include axon guiding PLA fibers functionalized with laminin [Ylä-Outinen et al., 2010] and polycaprolactone (PCL) fibers functionalized with laminin molecule fragments [Hyysalo et al., 2017]. From synthetic polymer hydrogels, there exists a freeze-dried gel product made out of PVA [Ku et al., 1997, Kehoe et al., 2012]. Decellularized ECM is another basis for neural TE scaffolds, both as the commercial Matrigel® [Kleinman, Martin, 2005] as well as in many in-house built systems [Saldin et al., 2017]. The advantage of these is the inherent functionality when retaining the cell attachment sites during processing. However, a major disadvantage is the varying product quality between batches and possible pathogen transmission, both of which hinder their advancement to clinical treatments [Huebsch et al., 2005, Saldin et al., 2017, Kornev et al., 2018].

When considering other hydrogel systems instead of the full ECM products, the HA is one valid option for use as a base for a neural hydrogel scaffold, if, for example, hydrazone is crosslinked together with alginate or PVA for increased stability. HA promotes neuronal cell attachment and neurite spreading, and the cells survive the bio-orthogonal crosslinking reaction. [Karvinen et al., 2018] Further enhancement could be achieved with functionalization using ECM molecules, for example, GelMA photocrosslinked with tropoelastin [Soucy et al., 2018]. Another hydrogel already tested for neural applications is GG. For example, GG-MA together with chitosan has been used as a freeze-dried and re-hydrated nerve guidance scaffold in rats with positive results [Carvalho et al., 2018]. Without the freeze-drying step, RGD-functionalized GG has at least been shown to have good cytocompatibility with glial cells and neural precursors

[Silva et al., 2012]. A similar composition also proved to be a suitable growth substrate for primary rat cortical neurons [Lozano et al., 2015].

From the biochemical stimulation point-of-view, the small polyamines suggested for GG iono-tropic crosslinking in **Chapter 2.2.2.**, have been shown to be secreted in both the CNS and the PNS [Fujiwara et al., 1997]. Certain neuron subtypes, mainly motor neurons and somatosensory neurons, have specific receptors for both of the bioamines SPM and SPD, and thus it is speculated to have a more special function in the synaptogenesis than just common DNA protection as oxygen radical scavengers [Laube et al., 2002]. Furthermore, SPD has been shown to even promote axonal regeneration *in vivo* in a rat wound healing model for both the spinal cord and the optic nerve [Deng et al., 2009]. Another, obvious biochemical stimulation possibility is drug release systems that deliver, for example, neural growth factor (NGF) or brain-derived neurotrophic factor (BDNF) to the injury site. [Aurand et al., 2012, Arslantunali et al., 2014, Sensharma et al., 2017]

2.3.2. Neural disease modeling

In addition to clinical TE treatments, there are two main aspects for *in vitro* neuronal cell culture systems: disease models for drug development and tissue models for modeling injuries. When successful, both of these reduce the need for animal testing and can provide valuable data on the cellular and organoid level functions and eventually lead to improved medical treatments. [Mobini et al., 2017] Multiple neurological disorders and neurodegenerative diseases, such as Parkinson's, Alzheimer's, Huntington's disease, multiple sclerosis, and epilepsy, are still poorly understood and would benefit from more accurate, human cell–based *in vitro* models [Lindvall, Kokaia, 2006]. The main reason for the need for *in vitro* models is the vast differences in size, shape, and physiology of human neurons compared to neurons from any other animal source [Hopkins et al., 2015, Mertens et al., 2016]. Furthermore, human primary neuronal cells are not readily available, so they need to be first differentiated from stem cells to be used in the models. What is more, the neuronal cells, organoids, or tissues produced by TE from hiPSC, with a known genetic background, can be used for the disease modeling of the specific genetic neural disease that the donating patient has. This can yield information on disease progression, morphological changes in the diseased cells and their function as well as help in finding drugs to prevent or treat the diseased phenotype.

The hPSC-derived neuronal cells can also be used for studying developmental biology, be it with developmental diseases or just for better understanding the embryological development of the CNS and PNS in healthy cases. [Mertens et al., 2016] Other specific parts of neuronal tissue that need the attention of *in vitro* modeling are the myelination of axons [Narkilahti et al., 2009, Narkilahti et al., 2016], the modeling of spinal cord injury [Führmann et al., 2016], traumatic brain injury [Tang-Schomer et al., 2014], the modeling and treatment of stroke [Lindvall, Kokaia, 2010], and the pain sensing ability of sensory neurons [Woolf, Ma, 2007].

Multiple specific parts of neuronal tissue, such as organoids of cerebellum and hippocampal origin for developmental studies or blood-brain-barrier for studying drug transport into the brain, have already been modeled *in vitro* [Hopkins et al., 2015]. The stem cell differentiation into organoids is often conducted purely in cell aggregates in suspension culture or with the hanging drop method. However, the organoid cultures have notable heterogeneity and lack support structures, but better structural control can be provided by a TE scaffold. [Mertens et al., 2016] Many of the materials deemed suitable for clinical neural TE are used in disease modeling as well, such as Matrigel®, collagen type I, and various polysaccharides. [Kornev et al., 2018]

The differentiation methods used to produce the various different neuronal cell subtypes are already well characterized and reproducible, as is required for the high-throughput screening (HTS) needed by the pharmaceutical industry for drug discovery applications [Lappalainen et al., 2010, Reinhardt et al., 2013, Mertens et al., 2016, Langley et al., 2016]. Thus, the next step is to produce the cells into the relevant model systems and platforms. For example, limiting and guiding the spreading of neuronal processes with PDMS structures on top of microelectrode arrays allows both the measuring of the propagation of the neural signals along the axons and dendrites as well as studying the myelination of axons with separated neuron and oligodendrocyte chambers [Narkilahti et al., 2016, Toivanen et al., 2017]. Examples of hydrogel nerve-on-a-chip systems include bulk PEG with poor cell attachment and tunnels made out of Puramatrix® with good attachment, allow 3D growth guidance *in vitro* [Mobini et al., 2017]. As yet, these systems have not been combined with hiPSC-derived cells and PDMS-microelectrode arrays, but they do seem compatible. In both drug testing and neurotoxicology, the culture system needs a suitable exposure method for the studied molecules and a distinction between acute and chronic toxicity, most often applied together with the culture medium or via microfluidistic channels in the on-chip systems [Kumar et al., 2012].

2.3.3. Cardiac tissue engineering

Cardiovascular diseases are currently the most common cause of death in Western countries and a major cause of disabilities and reduction in the quality of life globally [Naghavi et al., 2017, Vos et al., 2017]. The shortage of donor organs grows as the general patient life-span increases and medical treatments that can prolong the life of even poorer condition patients needing transplants are developed [Lechler et al., 2005]. Multiple treatment and prevention methods are constantly being studied to alleviate the effects of cardiovascular disease, and clinical cardiac TE is one of the methods [Simon-Yarza et al., 2017, Duan, 2017]. The main application of clinical cardiac TE is the treatment of myocardial damage caused by ischemia or heart failure due to some other causes [Madonna et al., 2016]. Another important application relevant to all the organs is the regeneration of vasculature, whether it is for the treatment of ischemia due to atherosclerosis or the neovascularization of *in vitro* produced TE organoids. More examples include the treatment of major arteries, such as the aorta, that are critical for patient survival. Likewise, vascular grafts are in demand for various surgeries, regardless of

the target site. [Gomes et al., 2017, Di Franco et al., 2018] Yet another, functionally different parts of the heart that are being studied in cardiac TE are the heart valves. They require more stiffness but an equal amount of creep resistance and dynamic stability compared to vasculature [Sanz-Garcia et al., 2015, Duan, 2017]. The heart and the main treatment areas are shown in Figure 12.
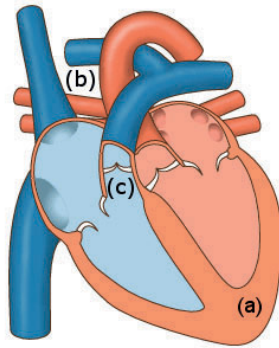
Figure 12. Schematic presentation of the structure of the human heart. (a) The cardiomyocyte-rich muscle tissue, a typical spot for ischemia. (b) Essential vasculature, snculind aorta. In the case of coronary artery disease, the treated blood vessels are actually all over the surface of the heart, not depicted in this figure. (c) The heart valves separating heart compartments. Image modified from public domain source [Wikimedia Commons, 2010].

The three cardiac TE application areas are very different and require different properties from the TE products. The cells used in each of these applications are different. For example, treatments to repair damaged heart muscle due to ischemia require actual cardiac muscle cells, or cardiomyocytes, [Madonna et al., 2016] while vasculature mainly requires endothelial cells, pericytes, and smooth muscle cells [Potjewyd et al., 2018]. In addition, heart valves are compose of specialized valvular interstitial and endothelial cells [Sanz-Garcia et al., 2015]. The TE of heart muscle tissue (Figure 12 (a)) is the focus here. Because cardiac cells cannot be easily transplanted from one patient to another, the best option to access them for use is via stem cell differentiation. Several methods exist for the differentiation of hPSCs into cardiomyocytes. Currently, the most used systems are either co-culture together with mouse endothelial cells on top of a gelatin coating [Mummery et al., 2003] or in defined conditions on top of a thin Matrigel® or Geltrex® gel by modifying the differentiation pathways using small molecules [Lian et al., 2012]. Both methods produce spontaneously beating cardiomyocytes which can be easily processed further in the final application, be it for clinical TE or disease modeling [Mummery et al., 2003, Lian et al., 2012]. The main challenges in hPSC-derived cardiomyocyte generation are the maturity of the differentiated cells and the purification and scalability of the culture systems to a clinically relevant scale [Talkhabi et al., 2016].

In clinical trials to treat ischemic heart tissue, MSCs have been used more than hPSCs, mainly because MSCs are more readily available in large numbers, even autologously. Still, their differentiation to actual cardiomyocytes is questionable, and therefore hPSCs provide a more promising cell source for the future. The hPSCs could be transplanted as cardiac progenitor cells while MSCs are also being tested at the multipotent state. [Madonna et al., 2016] The cardiac progenitors are oligopotent cells that have been committed to the cardiac lineage but are more potent than just cardiomyocytes. In either case, the regenerative effect of these cell transplantations has thus far been largely attributed to the paracrine effect of the cells' secreted biomolecules and not on actual regeneration. [Farouz et al., 2014, Madonna et al., 2016, Duan, 2017, Menasché et al., 2018]

Similar to neural TE, the injection of regeneration stimulating growth factors alone, such as vascular endothelial growth factor (VEGF) and basic fibroblast growth factor (bFGF), has been studied [Simon-Yarza et al., 2017]. And other molecules, even the oxygen radical scavenging-bioamines mentioned in **Chapter 2.2.2.** have been tested as injectable drugs to the infarcted site [Han et al., 2007, Wei et al., 2016]. Based on these, the actual regeneration of ischemic cardiac tissue still seems to require a full TE product with cell-supporting scaffold and stem cells combined, possibly with added growth factor release. [Madonna et al., 2016, Simon-Yarza et al., 2017]

Even though the mechanical properties of CNS and heart are very different, there is high similarity within the biomaterial choices for both of these tissues. In fact, one of the earliest studies on the effect of substrate stiffness on cell response was done with muscle cells on top of collagen coated PAA hydrogels [A. J. Engler et al., 2004]. Due to the non-linear elasticity and highly varied testing and data analysis methods, as discussed in **Chapter 2.2.4.**, the elastic or compressive modulus of cardiac muscle tissue has been reported to be between 10-150 kPa [Levental et al., 2007], with the most agreement in the lower end of this scale at 10-25 kPa [Mirsky, Parmley, 1973, Karvinen et al., 2017]. This result is further diversified by the number of different animals used, as human cardiac muscle is not readily available for mechanical testing [Mirsky, Parmley, 1973]. However, cardiac muscle stiffness seems to be well preserved across the mammals. For example, rat and human stem cells give similar results with a reported sweet-spot for muscle cell differentiation and functionality in the aforementioned ~10 kPa range [A. J. Engler et al., 2006, Xi et al., 2010, Young, Engler, 2011, Murphy et al., 2014, Scuderi, Butcher, 2017].

Further structural properties of materials to consider are fibers and topographies which induce cell orientation. The mature cardiomyocytes are highly oriented and elongated, and this structural maturation is sought after using topographies as stimulator cues [M. Zhang et al., 2015, Scuderi, Butcher, 2017]. An intertwined polymer fiber network, such as a textile structure or electrospun mat, is one possible scaffold type and the material options include PLA, PCL, or a copolymer consisting of these and other biodegradable polymers [Kitsara et al., 2017]. Another

approach is to use a hydrogel with a distinct nanofibrillar microstructure [Ikonen et al., 2011, Ikonen et al., 2013, Farouz et al., 2014, Y. S. Zhang et al., 2016] The elastic hydrogel environment can fulfill the cardiac requirements as heart ECM contains mainly different types of collagen, a protein with a fibrillary microstructure [Shoulders, Raines, 2009]. Decellularized rodent and porcine heart ECM have been tested pre-clinically with positive results [Saldin et al., 2017]. Other hydrogel system examples for cardiac TE include photocrosslinked complex containing GG-MA, PEG and chitosan [Coutinho et al., 2012], alginate and gelatin reinforced Matrigel® with the possibility to release VEGF [Duan, 2017], hydrazone crosslinked alginate HA [Dahlmann et al., 2013], thiol-based pseudo-click reaction hydrogels combining PEG and HA [Jiang et al., 2014], and mechanically tunable gelatin-PEG hydrogel [Choi et al., 2017] to name just a few in addition to the gel systems already mentioned in **Chapters 2.2.1.1.** and **2.2.3.** The cardiac biomaterials have been more conclusively reviewed elsewhere [Di Franco et al., 2018].

An advanced TE product for the treatment of ischemic heart tissue is the so-called cardiac patch or engineered heart tissue (EHT), originally designed by Eschenhagen and Zimmermann *et al.* [Eschenhagen et al., 1997]. In EHT, the cells are densely cultured inside collagen type I or fibrin hydrogel in a silicone mold and stimulated with a pacing electrode, and the dynamic mechanical contraction is recorded via a force transducer [Eschenhagen et al., 1997, Eder et al., 2016, Mannhardt et al., 2016]. Recently, the size of EHT patches has been scaled up and hiPSC can be differentiated into cardiomyocytes in robust ways. Moreover, after successful preclinical studies in a macaque ischemia model, they are actually advancing to clinical trials [Zimmermann, 2018]. The shapes of the patches can be controlled based on the mold used and building the patch has even been automatized to a certain degree [Ong et al., 2017]. However, the main disadvantage of the EHT cardiac patch is the requirement for open heart surgery during implantation, in contrast to the injectable and *in situ* crosslinkable hydrogel systems [Reis et al., 2015, Roshanbinfar et al., 2017, Simon-Yarza et al., 2017]. A minimally invasive surgical procedure that reduces the need for an injection into cardiac muscle has been presented based on photocrosslinked hyaluronic acid and cathecol hydrogel with glue-like adhesivity to tissue that can encapsulate cells and be applied directly on top of injured organ [J. Shin et al., 2015].

Other advanced TE constructs in the cardiac field include the so-called Biowire®, a platform for cardiomyocyte maturation built out of collagen type I, a rigid polymer surgical suture wire, and hESCs in a PDMS mold. The whole platform can be used for either the production of transplantable cardiac TE products or for studying the maturity of the cells in disease modeling as the cells can be studied both electrophysiologically and for gene and protein expression. [Nunes et al., 2013] Another advanced system is based on the GelMA hydrogel, either where the carbon nanotubes increase the conductivity of the material, representing the conductive Purkinje fibers of a heart conduction track [S. R. Shin et al., 2013] or by producing structures via 3D bioprinting [Y. S. Zhang et al., 2016]. Further strategies include combining endothelial cells with cardiomyocytes in a co-culture [Vuorenpää et al., 2017].

2.3.4. Cardiac disease modeling

Cardiovascular diseases cover a wide range of diseases from coronary artery disease and heart failure to genetic arrhythmias and cardiomyopathies and not all of these can be treated with a TE implant [Vos et al., 2017]. Thus, learning the disease mechanisms on a cellular level using *in vitro* disease modeling is important for drug discovery. Furthermore, in the development of any novel drugs, cardiotoxicity is a major cause of failure of a potential drug molecule in clinical trials or even cause withdrawal of a drug from the market, and thus increasing drug development costs significantly [Tzatzalos et al., 2016]. The most common cardiotoxic effect is drug-induced long-QT syndrome (LQTS). LQTS can be genetic or a patient can just have a higher genetic susceptibility to acquire it from a drug. The syndrome appears as prolonged repolarization, meaning the interval in the recovery phase of a heartbeat, which can lead to multiple problems when combined with increased heart rate or ectopic beats and results in severe ventricular tachycardia and even sudden cardiac death. [Roden, 2004] The current approved methods for cardiotoxicity drug testing with various animal cells are not precise enough to reveal all the possible risks, so human cells are needed. [Tzatzalos et al., 2016, Eder et al., 2016] To solve the problem of cardiotoxicity during drug discovery, there is even a global initiative to create a Comprehensive in Vitro Proarrythmia Assay (CiPA), put together by the regulatory agencies, the pharmaceutical industry, and academia [Colatsky et al., 2016, Wallis et al., 2018]. A result of this initiative is the recently published calcium imaging scoring protocol for screening early drug safety [Kopljar et al., 2018].

In addition to cardiotoxicity, an encouraging reason to specifically do disease modeling with patients from Finland is the historical isolation of this country. The genetic background of people living in Finland is highly separated from the gene pool of people from elsewhere in Europe. [Lao et al., 2008] The isolated gene pool has caused certain genetic mutations, such as the prevalence of LQTS, hypertrophic cardiomyopathy (HCM), and catecholaminergic polymorphic ventricular tachycardia (CPVT), to enrich in the Finnish population. The LQTS has four founder mutations found in the Finnish population with disease prevalence as high as 0.4% in the whole population [Marjamaa et al., 2009, Kuusela et al., 2016]. Similarly, 20% of HCM cases in Finland can be covered by studying just two different genetic mutations, even though the disease as a whole has over 1400 identified mutations causing it. The HCM causes the ventricular wall of the heart to become enlarged, thus limiting the volume pumped per beat. [Jääskeläinen et al., 2013, Ojala, Aalto-Setälä, 2016]. The genetic cause for the third genetic cardiac disease, CPVT, was originally identified in Finland [Swan et al., 1999]. The disease mechanism of CPVT is malfunction in the calcium handling vital for cardiomyocyte beating and is caused by mutation in gene encoding of cardiac ryanodine receptor protein [Swan et al., 1999, L. Antoine et al., 2012].

Since the first established differentiation protocols to produce cardiomyocytes *in vitro* [Mummery et al., 2003], several differentiation methods to produce hPSC-derived cardiomyocytes

have been published and recently reviewed by Talkhabi *et al*. [Talkhabi et al., 2016]. Disease modeling has been an important application for the cardiomyocytes since the invention of cardiac differentiation [Mummery, 2018]. Even before the availability of human cells, disease modeling was conducted as part of cardiac TE with rat cells [Carrier et al., 1999]. The aforementioned cardiac diseases have all been well established in human cell-based 2D *in vitro* disease models: LQTS [Kiviaho et al., 2015], HCM [Ojala, Aalto-Setälä, 2016], and CPVT [Penttinen et al., 2015]. They have even been used already to find drugs leading to clinical trials [Penttinen et al., 2015].

The human body is not, however, composed of 2D surfaces; the body is a 3D structure. Thus, hydrogel scaffolds are needed as an option to produce more biomimicking model tissues that can later advance into disease models [Fang, Eglen, 2017]. It has already been proven that when comparing cardiomyocytes in 2D and 3D cultures, both their gene expression and their electrophysiological properties change towards a more mature phenotype, even in just a spheroid suspension 3D culture without a hydrogel support scaffold [M. Zhang et al., 2015]. Adding a scaffold as a fibrillary orienting structure or an encapsulated 3D hydrogel culture also increases the maturity of the cells [Scuderi, Butcher, 2017]. The stiffness of the growth substrate is well known to affect cardiomyocyte functions due to mechanotransduction, another reason to transition the disease models in 3D [A. J. Engler et al., 2008, Young, Engler, 2011]

The EHTs introduced in the previous chapter are an attractive TE product for disease modeling, as they biomimic muscle tissue. They can be used in all the modeling aspects, be it cardiotoxicity, genetic cardiac diseases [Eder et al., 2016], or even an *in vitro* heart failure model [Malte et al., 2017]. The cells can be stimulated as well as measured electrically or mechanically in the EHT, thus allowing the study of the effects on cellular electrophysiology. Examples of published EHT disease models include the electrophysiological defect diseases LQTS and CPVT. [Eder et al., 2016] In the case of HCM, the EHT or any other 3D culture system is even more attractive since the ECM and cell-to-cell interactions play a bigger role in abnormal muscle formation than they do in purely electrophysiological diseases. For example, in addition to the cardiomyocytes themselves, cardiac fibroblasts can also play a significant role in HCM. So far, the main use of EHTs in disease modeling has been in the electrophysiological and mechanical effects of tested drugs. [Eschenhagen et al., 2015]

In addition to the EHT, examples of systems designed more specifically for cardiac disease modeling and drug discovery include various heart-on-a-chip constructs, where microfluidistic flow delivers nutrients and drug molecules to the cells and the functionality can be monitored. There are again many similarities between neuronal and cardiovascular organ-on-a-chip systems with requirements for electrophysiological measurements, orientation, and interest in barrier properties. [Ribas et al., 2016, B. Zhang et al., 2018] Currently, the most advanced heart-on-a-chip constructs have mostly featured rat cardiomyocytes, when concentrating on the proof-of-concept studies related to fluid flow and topography [Y. S. Zhang et al., 2016, Sheehy

et al., 2017]. Even if using hiPSC-derived cardiomyocytes, the heart-on-a-chip systems are lacking an ECM mimicking hydrogel support because these components have not been combined together thus far [Mathur et al., 2015].

One of the main disadvantages of 3D disease models from the pharmaceutical drug development point-of-view is the difficulty to apply the same HTS methods that are used in the 2D cultures [Eglen, Randle, 2015]. Indeed, at the starting point of drug discovery, there can be over 1,000,000 molecules to start the screening with. Such amounts require automation and HTS to be feasible and, in the 2D cell culture case, the methods for this already exist. [Molokanova et al., 2017] However, regardless of the higher degree of biomimicry, 3D hydrogel cell cultures are more difficult to study and it is more difficult to get accurate signals from the cells, especially in an HTS manner. Currently, various methods based on imaging and electrical measurements are being developed that will allow the full transition from 2D to 3D in HTS drug development [Edmondson et al., 2014, Eglen, Randle, 2015, Nam et al., 2015, Hoffman et al., 2017].

2.3.5. Other soft tissue applications

Various soft tissues have similar requirements for their TE scaffold as neuronal and cardiac tissues, mainly a controlled structure with adequate strength and elasticity and enough sites for cell attachment [Place et al., 2009]. As collagen isoforms are a major component in all soft tissues, adding collagen or its derivative gelatin to enhance cell attachment is a valid functionalization strategy, regardless of the exact target tissue [Shoulders, Raines, 2009, Yue et al., 2015]. Similarly, the mechanical properties of soft tissues generally fall in between the values measured for cardiac muscle and for brain [Levental et al., 2007]. Thus, once a suitable hydrogel candidate has been found for these two tissue types, it can easily be fine-tuned by adjusting crosslinker concentrations, the number of crosslinking sites, or exact collagen or gelatin types to suit other applications [Shoulders, Raines, 2009, Place et al., 2009].

The first clinical TE products to enter the market included Dermagraft®, a skin substitute scaffold with allograft skin cells in a polymer mesh. The treatment of skin and wounds remains one of the most used clinical soft TE products, with various applications using hydrogels in filling deep scars and treating burn wounds [Place et al., 2009]. In addition, filling wrinkles with hydrogels in plastic surgery has become a popular option due to the biocompatibility and injectability. [Geckil et al., 2010, Cerqueira et al., 2014] However, the use of hydrogels in plastic surgery is not always without complications. For example, the inflammation and instability of PAA hydrogel injections has been reported to cause severe problems in roughly 1% of patients [Manafi et al., 2010].

Another, seemingly simple clinical TE application is the regeneration of adipose tissue needed, for example, in breast reconstructive surgery after breast cancer tumor removal, or for various

trauma patients, and also in aesthetic plastic surgery. Hydrogels are an attractive material choice for these applications because they can be used in minimally invasive surgery and even injected in patients without anesthesia. Additionally, the human adipose MSCs are an easily available autologous cell source for adipose TE [Nam et al., 2015, Lago et al., 2018] This has been done for example with human MSCs in GG microgels, where the cells seem to go through adipogenesis even without the biofunctionalization of GG, if cultured in adipogenic medium [Lago et al., 2018].

Tissue models for specific internal organs have been aimed for and developed for as long as TE has existed as a methodology. Production of hepatocyte-based TE of the liver was already in focus in early TE studies because liver cirrhosis, cancer, and other liver diseases are significant disease burdens [Langer, Vacanti, 1993, Vos et al., 2017]. As liver is the main metabolic site for most drug molecules, the use of hepatocytes in drug discovery is also a major point for pharmaceutical companies [Langley et al., 2016, Kiamehr et al., 2017]. Even though liver cancer cell lines have already been cultured in 3D nanocellulose hydrogels [Bhattacharya et al., 2012], due to the recent development of hiPSC-derived hepatocytes [Kiamehr et al., 2017], 3D culture in mechanically more biomimicking hydrogel than nanocellulose is interesting for future investigations [Langley et al., 2016]. Another organ of longstanding interest for TE is the pancreas and the implantation of insulin-producing islet cells, since diabetes is one of the major diseases in the Western countries associated with increased morbidity and mortality [Langer, Vacanti, 1993, Place et al., 2009, Langer, 2017, Vos et al., 2017].

The production of whole organs to supply the demand of organ transplantations was one of the first named goals of TE. However, in reality, the production of fully functioning macroscale internal organs has proven more difficult than anticipated [Langer, Vacanti, 1993, Langer, 2017]. The first fully functioning TE organ was a urinary bladder, produced and implanted in patients by Atala *et al*. [Atala et al., 2006, Place et al., 2009]. The used scaffold was a composite of collagen and polyglycolic acid and the cells were autologous urothelial and smooth muscle cells. In the end, all seven patients benefitted from the TE bladder transplantation based on a follow-up after several years [Atala et al., 2006]. Still, for most organs the only successful TE strategy so far has been the decellularization of donated organs and the repopulation of them with autologous hiPSC, and not production of the complex macroscale structures from scratch [Khademhosseini, Langer, 2016].

On the side of disease modeling, the 3D models of cancer are yet another important aspect of hydrogel applications. Comparable to the cardiotoxicity issues, cancer drugs sometimes have difficulties to advance from preclinical trials to clinical trials, and this can at least partially be attributed to non-representative *in vitro* models [Rijal, Li, 2017]. Various cancer studies are conducted on Matrigel®, but the suitability of this very soft and weak hydrogel can be questioned because it mostly functions as a thick coating and does not necessarily provide a true

3D environment [Kleinman, Martin, 2005, Steimberg et al., 2014, Rijal, Li, 2017]. Other alternative hydrogel materials currently in use include decellularized ECM, alginate, and HA [Rijal, Li, 2017, Gomes et al., 2017]. Other, more novel ways of disease modeling *in vitro,* where 3D structures are important, include inflammatory disorders of the lungs. In addition to cancer and drug molecule penetration through lung tissue, models can be used to study infection of tuberculosis into human lung tissue. [Huh et al., 2011, Nam et al., 2015, Tezera et al., 2017, Gomes et al., 2017]

3. Aims of the Study

The overall aim of this thesis is to find hydrogel biomaterials suitable for 3D cell culturing and to develop methods to characterize the most relevant properties of these hydrogels in TE applications. The hypothesis was that gellan gum or its derivatives would provide a simple to use and functioning hydrogel for TE and additionally provide a usable model hydrogel for the development of hydrogel material characterization methods. As the focus is on pluripotent stem cell-derived neuronal and cardiac cells, the development concentrated on hydrogels and characterization methods relevant for soft tissue applications, with potential for wider use within soft tissue than the two main focus areas. Similarly, the material characterization methods developed here are widely usable for studying hydrogels, even beyond the biomedical field.

More specific aims for each **Publication**, denoted by their Roman numerals, are defined as follows:

I. To produce a hydrogel suitable for 3D culturing of human induced pluripotent stem cell-derived neuronal cells and to characterize the relevant properties of this hydrogel.

II. To develop an optical, non-destructive method to gain insight of the bioamine cross-linked gellan gum hydrogel microstructure in the water-swollen state.

III. To produce a hydrogel suitable for 3D culturing of human induced pluripotent stem cell-derived cardiomyocytes and to characterize this hydrogel for the relevant properties. Additionally, to develop cytocompatibility testing methods for hydrogel screening.

IV. To develop more representative mechanical testing methods for the compressive response of hydrogels and to develop more reliable analysis methods to measure elastic modulus.

4. Materials & Methods

4.1. Hydrogel design

4.1.1. Materials (I-IV)

The reagents needed to prepare the hydrogels: gellan gum (GG, Gelzan™, low acyl, M_w 1 000 g/mol), spermidine trihydrochloride (SPD), spermine tetrahydrochloride (SPM), sucrose, gelatin A from porcine skin, adipic dihydrazide (ADH), carbodihydrazide (CDH), dimethyl sulfoxide (DMSO), ethylene glycol, 1-ethyl-3-[3-(dimethylamino)-propyl]–carbodiimide (EDC), hydroxylamine hydrochloride, *N*-hydroxybentzotriazole (HOBt), 4-hydroxybenzaldehyde, deuterium oxide (99.9 atom % D, containing 0.05 wt. % 3-(trimethylsilyl)-propionic-2,2,3,3-d4 acid, sodium salt), hydrochloric acid (HCl), sodium hydroxide (NaOH), sodium chloride (NaCl), and sodium periodate ($NaIO_4$) were obtained from Sigma-Aldrich (St. Louis, MO, USA and Sigma-Aldrich Finland). GG, SPD, SPM and sucrose were acquired at the highest level of purity available. Methacrylated gellan gum (GG-MA) and the photo-initiator methyl benzoylformate (MBF, 98%) were a kind gift from the collaborators in the 3B's research group at the University of Minho, Portugal. Calcium chloride ($CaCl_2$) was obtained from Honeywell Riedel-de Haën (Germany). Phosphate buffered saline solution (PBS) was obtained from Lonza (Basel, Switzerland). Laminin (laminin-111, Engelbreth-Holm-Swarm mouse origin) was obtained from Thermo Fisher Scientific (Waltham, MA, USA).

Auxiliary materials for hydrogel sample preparation were obtained as follows: dialysis membrane (Spectra/Por® 12-14 kDa molecular weight cut-off (MWCO)) from Spectrum Laboratories (Rancho Dominguez, CA, USA). Syringe sterile filters Whatman FP 30/0.2 CA-S filter from Thermo Fisher Scientific (Waltham, MA, USA) and Whatman Plc, (Little Chalfont, UK), Sterivex-GP 0.22 μm Millipore Express (PES) filter from Merck Millipore (MA, USA), and Acrodisc® 0.8/0.2 μm filter from PALL Corporation (Port Washington, NY, USA). Compression and rheological testing sample molds, for non-sticky gels, were prepared from cut BD Discardit II™

syringes at sizes 5mL, 10mL, and 20 mL (Mediq, Espoo, Finland). Polydimethyl siloxane (PDMS) was fabricated from Sylgard 184 base polymer and curing agent (10:1, w/w, Sylgard 184, Dow Corning, USA) and acquired from Ellsworth Adhesives AB (Sweden). PDMS was used to manufacture custom-made platforms for OPT sample support with fluorinated ethylene propylene (FEP) tubes from Adtech (Lochgelly, UK) and for single-use compression sample molds for sticky gels.

For the OPT mass transport study, FITC-Dextran ($\lambda^{excitation}$ 493 nm, $\lambda^{emission}$ 520 nm) with defined molecular weights of 20 kDa, 150 kDa, and 2000 kDa were obtained from TdB Consultancy AB (Uppsala, Sweden). Each FITC-Dextran solution was prepared by dissolving the powder in distilled water at a concentration of 10 mg/ml. For the *in vitro* degradation study, collagenase II and fluorescamine were obtained from Sigma-Aldrich (St. Louis, MO, USA).

4.1.2. Chemical modification (III)

4.1.2.1. Preparation of adipic dihydrazide modified gelatin (gelatin-ADH)

First, 300 mg of gelatin was dissolved in 100 mL water, and 3.92 g of ADH was added to this solution. Excess of hydrazide is used to avoid concurrent crosslinking during functionalization [Ossipov et al., 2010]. The pH of the reaction mixture was adjusted to 6.8. Then, 576 mg of EDC and 405 mg of HOBt were dissolved in 3 mL DMSO/water (1.5:1 v/v) and added dropwise to reaction mixture, while keeping the pH at 6.8 with 0.1 M NaOH and 0.1 M HCl during the addition of the mixture and for a further 4 hours. Then, the reaction was continued for a further 20 hours. The pH was adjusted to 7 and gelatin-ADH was exhaustively dialyzed against water for 2 days. Then, NaCl was added to produce a 7% (w/v) solution, and the product was precipitated in cold ethanol (4 vol eq.). Then, the product was dissolved in water and dialyzed in RT against water for 2 days through a MWCO 12-14 kDa membrane followed by freeze-drying.

4.1.2.2. Preparation of carbodihydrazide modified gelatin (gelatin-CDH)

Similar to the above, 300 mg of gelatin was dissolved in 100 mL water, and 3.6 g of CDH was added to this solution. The pH of the reaction mixture was adjusted to 4.7 with 0.5 M HCl. Then, 575 mg of EDC and 405 mg of HOBt were dissolved in 3 mL DMSO/water (1.5:1 v/v) and added dropwise to the reaction mixture, while keeping the pH at 6.8 with 0.1 M NaOH and 0.1 M HCl during the addition of the mixture and for a further 4 hours. Then, the reaction was kept for 20 hours more. Gelatin-CDH was exhaustively dialyzed in RT against water for 2 days. Additional purification was carried out, as described above, followed by freeze-drying.

4.1.2.3. Preparation of oxidized gellan gum (GG-CHO)

GG was modified by periodate oxidation according to the method previously reported by our group to produce GG-CHO at the modification degree of 25% [Karvinen et al., 2017]. Briefly,

500 mg GG was dissolved in 50 mL deionized water at 60 °C for a few hours. NaIO$_4$ (0.05 M; 48 mg) was added dropwise and stirred for 4 hours at room temperature (RT) under nitrogen. Ethylene glycol (4 equivalents) was added to inactivate any unreacted NaIO$_4$ and the reaction was stirred for 1 hour. The produced GG-CHO was dialyzed with MWCO 1000 dialysis membrane against deionized water for 4 days followed by freeze-drying. [Karvinen et al., 2017]

4.1.3. Chemical analysis (III)

To confirm the presence of hydrazide functionality, 20 mg of gelatin-ADH or gelatin-CDH were treated with 10 mL of 4-hydroxybenzaldehyde (20 mg/mL) in distilled water for 24 hours at RT. The product was dialyzed and lyophilized, as described in **Chapter 4.1.2.1.** and analyzed by NMR spectroscopy. All the experiments were measured with a Jeol JNM-ECZR 500 MHz NMR spectrometer (Tokyo, Japan). Samples (5 mg) were dissolved in deuterium oxide (600 µL) containing an internal standard (0.05 wt-% 3-(trimethylsilyl)-propionic-2,2,3,3-d4 acid, sodium salt). The samples were measured at 40 °C. The relative substitution was calculated by comparing the integral of the lysine amino acid peak at δ 3.0 ppm to the aromatic proton peak of 4-hydroxybenzaldehyde at δ 7.6 ppm. The presence of aldehyde groups in GG-CHO polymer was qualitatively evaluated using FTIR, measured on a Perkin Elmer Spectrum One ATR-FTIR Spectrometer (Waltham, MA, USA) in a spectral range of 400 to 4000 cm^{-1}.

4.1.4. Hydrogel formulation (I, III)

In **Publication I,** the formulation of ionotropic crosslinking of GG using bioamines SPD and SPM was based on the findings of López-Cebral *et al*. and Parraga *et al*. [López-Cebral et al., 2013, Parraga et al., 2014]. During formulation, the highest crosslinker concentration that produces hydrogel without apparent turbidity and transparent to the naked eye was first screened. After finding the highest usable concentration, we halved the concentration and used that as one composition and then screened for the lowest concentration that still produced a self-standing, true hydrogel. The same procedure was used for both SPD and SPM and the names of the formulated hydrogel compositions along with concentrations are found in Table 2. To enhance neuronal cell attachment, laminin was added as a physical mixture into the hydrogel components at 1, 5, and 10% (v/v) of the final hydrogel volume.

In **Publication III**, the formulation of chemical hydrazone crosslinking of gelatin and GG was based on the results of Karvinen *et al*. [Karvinen et al., 2017]. The formulation was started by screening for the highest solubility of the polymers while still being able to sterile filter the solutions. The breakage of polymer chains and carbohydrate rings makes the polymers more flexible during the chemical modification, and thus allows for higher soluble concentrations than with unmodified polymers. The starting point for the combination of both gelatin-ADH and GG-CHO was 40 mg/mL, and for both gelatin-CDH and GG-CHO it was 60 mg/mL. After finding the highest concentration and verifying gelation, the concentration was reduced for further

formulations. For gelatin-ADH, the concentration of GG-CHO was reduced in 10 mg/mL steps, yielding three usable compositions of true hydrogels. For gelatin-CDH, the concentration of GG-CHO was first reduced to 40 mg/mL, still yielding a true hydrogel. Then, the gelatin-CDH concentration was also reduced to 40 mg/mL, again yielding a true hydrogel. In this study, we did not screen any further to find the lowest possible concentrations. The names of the formulated hydrogels along with their concentrations are presented in Table 2. All the gelatin-GG hydrogels had good transparency.

4.1.5. Hydrogel production (I-IV)

All the hydrogel components were dissolved in 10% w/w sucrose to adjust osmolarity on the same level as tissues, with the exception of the components of gels containing gelatin-CDH that were dissolved in DMEM/F-12. The solutions used in **Publications I, II,** and **IV** were sterile filtered using an Acrodisc® 0.8/0.2 µm sterile filter at 60 °C. In **Publication III,** due to higher viscosity and reactivity that caused more difficult filtration, the GG-CHO solutions were filtered using a Sterivex-GP 0.22 µm Millipore Express filter at 60 °C. Furthermore, gelatin-ADH and gelatin-CDH were filtered using a Whatman FP 30/0.2 CA-S filter at 37 °C. Using the wrong filter membrane material or wrong temperature causes clogging of the filter and the loss of polymer material. After filtration, solutions can be stored for 1 month at 4 °C.

To produce the bioamine-GG of **Publication I, II,** and **IV**, SPD or SPM crosslinker was mixed together with unmodified GG (5 mg/mL) at a volume ratio of 4:25 and heated to 37 °C, cast into a mold, and stored overnight at RT for material characterization. In **Publication IV**, the mixing of gel components was done using the magnetic stirrer method as described by Gering *et al.* [Gering et al., 2018].

The iGG-Ca in **Publication II** was prepared in a similar way as the bioamine GG gels, except the volume ratio was 1:3 $CaCl_2$ to GG (5 mg/mL). In the same publication, iGG, iGG-MA, and photoGG-MA with UV photo-cross-linker were prepared, as described by Silva-Correia *et al.* [Silva-Correia et al., 2011]. To produce the iGG and iGG-MA hydrogels, the solutions were heated progressively to 90 °C, and this temperature was maintained for 30 min. Then, the temperature was gradually decreased to between 60 and 65 °C and PBS (pH 7.4) was added to a final concentration of 10% v/v in the GG solution. The temperature was continuously decreased to 50 °C and the hydrogel was poured in a mold. Then, the hydrogels were allowed to crosslink and stabilized by immersion in PBS. To produce photoGG-MA, the photoinitiator MBF was mixed to the GG-MA and the solution was then cast in a mold and exposed to UV light (366 nm; UV lamp Triwood 6/36, Italy) for either 10 min in FEP tube or 40 min in cuvette, 10 min for each face of the cuvette.

In **Publication III**, the GG-CHO and either gelatin-ADH or gelatin-CDH were heated to 37 °C, mixed together by pipetting at 1:1 volume ratio and cast into a mold.

Table 2. Abbreviations for the different hydrogel compositions used in **Publications I-IV**.

Abbreviation	Polymer	Cross-linking	Crosslinker concentration	Solvent	Publica-tion
GG 1.10%SPM*	GG (0.5% w/v)	Ionic (SPM)	0.350 mg/mL	10% sucrose	**I, IV**
GG 0.60%SPM**	GG (0.5% w/v)	Ionic (SPM)	0.175 mg/mL	10% sucrose	**I, IV**
GG 0.40%SPM	GG (0.5% w/v)	Ionic (SPM)	0.125 mg/mL	10% sucrose	**I**
GG 3.00%SPD	GG (0.5% w/v)	Ionic (SPD)	1.00 mg/mL	10% sucrose	**I**
GG 1.50%SPD***	GG (0.5% w/v)	Ionic (SPD)	0.50 mg/mL	10% sucrose	**I**
GG 1.25%SPD	GG (0.5% w/v)	Ionic (SPD)	0.40 mg/mL	10% sucrose	**I**
iGG	GG (2% w/v)	Ionic (PBS)	10% (v/v)	10% sucrose	**II**
iGG-MA	GG-MA (2% w/v)	Ionic (PBS)	10% (v/v)	10% sucrose	**II**
photoGG-MA	GG-MA (2% w/v)	Chemical (UV light; MBF & PBS)	MBF 0.1% (w/v) + PBS 10% (v/v)	10% sucrose	**II**
iGG-SPM-H*	GG (0.5% w/v)	Ionic (SPM)	0.350 mg/mL	10% sucrose	**II**
iGG-SPM-L**	GG (0.5% w/v)	Ionic (SPM)	0.175 mg/mL	10% sucrose	**II**
iGG-Ca	GG (0.5% w/v)	Ionic (Ca^{2+})	1.110 mg/mL	10% sucrose	**II**
F1-ADH	GG-CHO (40 mg/mL) & gelatin-ADH (40 mg/mL)	Chemical (hydrazone)	-	10% sucrose	**III**
F2-ADH	GG-CHO (30 mg/mL) & gelatin-ADH (40 mg/mL)	Chemical (hydrazone)	-	10% sucrose	**III**
F3-ADH	GG-CHO (20 mg/mL) & gelatin-ADH (40 mg/mL)	Chemical (hydrazone)	-	10% sucrose	**III**
F4-CDH	GG-CHO (60 mg/mL) & gelatin-CDH (60 mg/mL)	Chemical (hydrazone)	-	DMEM/F-12	**III**
F5-CDH	GG-CHO (40 mg/mL) & gelatin-CDH (60 mg/mL)	Chemical (hydrazone)	-	DMEM/F-12	**III**
F6-CDH	GG-CHO (40 mg/mL) & gelatin-CDH (40 mg/mL)	Chemical (hydrazone)	-	DMEM/F-12	**III**
F7-SPD***	GG (0.5% w/v)	Ionic (SPD)		10% sucrose	**III**

*, **, *** marked compositions are exactly the same, respectively based on the marks, but with different naming convention used in the original publications.

4.2. Hydrogel characterization

4.2.1. Gelation time (I, III)

Gelation time was estimated with the tube tilt test, as described by Tanodekaew *et al.*1997 [Tanodekaew et al., 1997, ASTM F2900, 2011]. The reagents were mixed in a small glass vial. After mixing, the vial was slowly turned upside down at 30 s time intervals, and the flow of gel was observed. If the solution started to move even slightly once tilting started, it was not tilted further to let the gelation continue. Once the solution did not flow, the gelation was considered complete, and the time was recorded.

4.2.2. Hydrogel degradation *in vitro* (III)

For the *in vitro* degradation tests, 500 μL hydrogels were cast in Eppendorf® tubes. A solution of 10 U/mL of collagenase II was then added to the tubes. After that, they were incubated, and aliquots were collected at 1, 3, 5, 7, 24, 30, 48, and 56 hours and refreshed with fresh enzyme solution. The fluorescamine ($\lambda^{excitation}$ 390 nm, $\lambda^{emission}$ 465 nm) test was used to determine the presence of gelatin in the collected samples using a QuantaMaster PTI spectrofluorometer (Photon Technology International, Inc., Lawrenceville, NJ, USA).

4.2.3. Rheology (I)

Rheological experiments were carried out with a rotational rheometer (Haake RheoStress RS150) equipped with Rheowizard 4.3 software (ThermoHaake, Germany). Parallel plate geometry with 20 mm diameter metal plates was used. All the experiments were conducted at room temperature (~25 °C) in the oscillatory mode. In the oscillatory mode, the sample is subjected to sinusoidal oscillatory shear strain with amplitude γ_0. In the linear viscoelastic region (LVER) with sufficiently small strain amplitudes, the resulting stress amplitude τ_0 will also be sinusoidal of the same frequency and corresponding to phase angle δ. The complex moduli (G^*) represents the rigidity of the sample and in the LVER the following relationship applies:

$$G^* = \frac{\tau_0}{\gamma_0} = \sqrt{(G'^2 + G''^2)} \qquad (1)$$

The storage modulus (G') is the in-phase and the loss modulus (G'') the out-of-phase components of the response:

$$G' = \frac{\tau_0}{\gamma_0} cos\delta \qquad (2)$$

$$G'' = \frac{\tau_0}{\gamma_0} sin\delta \qquad (3)$$

The G' represents the elastic and G'' the viscous behavior of the sample. The loss factor tanδ is the ratio of the viscous to the elastic portion. [Schramm, 1998]

The samples for rheological testing were cast in cut syringe molds with a maximum height of 1 mm and a cross-section diameter of 20 mm. Prior to each measurement, the hydrogels were stored overnight at RT to ensure complete gelation. During the measurements, the gap between plates was set to 0.8 mm. All measurements were done in oscillatory shear deformation mode and both amplitude and frequency sweeps were used for all samples. The strain amplitude range for the amplitude sweeps was from 0.01 to 5.00 rad (0.1 rad = 1.6% displacement) with 1 Hz frequency. Six parallel samples were tested with amplitude sweeps and two parallel samples with frequency sweeps, both in ambient conditions. The frequency sweep was done in the range of 0.1 to 3.0 Hz, with constant 0.1 rad strain amplitude, which is in the LVER for all samples.

4.2.4. Compression testing (I, III, IV)

Mechanical testing was performed with a Bose Electroforce BioDynamic 5100 machine using WintTest 4.1 software and 225 N load cell (TA Instruments, Eden Prairie, MN, USA). The common method in **Publications I, III,** and **IV** was unconfined compression in ambient air at 10 mm/min displacement rate until 65% displacement for bioamine-GG and until 75% displacement for gelatin-GG. Additionally, 22 N load cell and 1 Hz digital filtration was used in **Publication IV** for the softer GG 0.6%SPM due to an otherwise poor signal-to-noise ratio in the load data. The displacement rate was originally decided based on the Nakamura *et al.* study, determined to be in the viscoelasticity dominated and not in poroelasticity dominated range [Nakamura et al., 2001]. In **Publications I** and **IV**, cut syringe molds with an approximate height of 6.5 mm and a cross-section diameter of 12.2 mm were used. Due to the very sticky surface property of gelatin-GG hydrogels, custom-made PDMS molds, with similar dimensions to those stated above, were used in **Publication III** and the samples were cut from the mold with a scalpel.

Each composition was tested in five parallel samples. The exact dimensions of each sample were measured with calipers before testing. To avoid slippage of the samples, the compression plates were covered with a piece of wet lint-free cellulose wadding paper to increase friction between the hydrogel and the metal plate. The sample was set in between the compression plates so that the upper plate touched the sample, but no pre-load was used.

To obtain a good reference in terms of the biomimicking of mechanical properties in the design of hydrogels for soft tissue TE, compression testing was also performed with brain and heart muscle tissue samples. New Zealand white rabbits (age 10 weeks, male) were sacrificed with deep anesthesia, after which the heads and hearts were removed and stored in ice for a max-

imum of 8 h. The brains were removed from the skulls, and samples containing midbrain, cerebellum, or cortex were prepared. For heart tissue, both the left and right ventricle were used, and the data were pooled together. The samples were then cut with a biopsy punch to the same size and shape as the hydrogel compression samples and stored on ice until compression testing. The test parameters used were the same as those described above. The rabbit tissues were obtained from animal experiments conducted at the Medical School of University of Tampere.

In **Publications I** and **III**, the compression data were analyzed with MS Excel (Microsoft, Redmond, WA, USA). According to Hooke's law, $\sigma = E * \varepsilon$, the compressive modulus was calculated from the stress–strain curve as the slope of the perceived elastic region [Callister, 2003]. In addition, the fracture strength and fracture strain were recorded as a sudden drop in the stress–strain curve.

In **Publication I**, the statistical analysis was conducted using SPSS Version 25.0 (IBM SPSS Statistics for Windows, NY, USA). The nonparametric Kruskal Wallis test and Mann–Whitney U-test were used due to non-Gaussian distribution of the data. A p value of less than 0.05 was considered statistically significant. If more than two groups were compared, the resulting p values were multiplied by the number of comparisons (Bonferroni correction).

In **Publication III**, the statistical analysis was conducted using SPSS Version 25.0. The data were presented as mean +/- standard deviation. One–way analysis of variance (ANOVA) was performed with confidence level of 95%. A p value less than 0.05 was considered as statistically significant. Pair comparisons of data were done with Tukey post-hoc test to identify significant differences between the hydrogels.

In **Publication IV**, compression parameters were varied from the common method for GG 1.1%SPM hydrogel to gain further insight on the viscoelasticity of the bioamine-GG hydrogel. A lower 1 mm/min displacement rate was used to observe the rate dependency of the compression behavior. Then, the repeatability of the measurements was studied by varying the starting point of the measurements and the friction between the compression plates and the sample. To distinguish any possible machine artifact in the early phase of compression, measurements were started both clearly ~1 mm above the sample surface and with a machine-indicated pre-load value of 0.06 N as well as at the standard position of compression plate touching the sample from both sides. The friction was varied by either removing the wet piece of paper from the compression plate or by varying how often it was changed. Without the paper, the compression was only possible until ~30% displacement, after which the sample tended to slip off. Changing the paper between each and every sample helped to keep the contact friction constant between tests because the pores of the paper were not filled with hydrogel residue from previous tests. This step is recommended for further compression tests.

A stress-relaxation test was conducted in **Publication IV** on the GG 1.1%SPM and GG 0.6%SPM hydrogels. In the first step of the relaxation test, the specimen is compressed with a 10 mm/min compression velocity to 50% of the fracture load value obtained in the measurements of parallel samples. Then, in the second step (relaxation step) the specimen is held in this condition under constant strain for 60 seconds to observe the viscous flow.

4.2.5. True stress and true strain in hydrogel compression (IV)

The engineering stress and engineering strain used in other publications were converted to true stress σ^c (or Cauchy stress) and true strain ε^n (or logarithmic strain or Hencky strain) in **Publication IV**. In the uniaxial case, the Cauchy stress takes the following form:

$$\sigma^c = \frac{F}{A},$$ (4)

where F is the applied force and A is the true, current cross-sectional area.

The true strain is defined as follows:

$$\varepsilon^n := \int_{l_0}^{l} \frac{dl}{l} = ln\frac{l}{l_0},$$ (5)

where l_0 and l are the initial and current gauge length of the sample, respectively. Here, the positive directions are defined so that the strain for tensile deformation is positive and, likewise, the stress for tensile loading is positive. After mathematical manipulations, the logarithmic strain and the Cauchy stress are obtained in terms of engineering strain and stress as follows:

$$\varepsilon^n = \ln(1 + \varepsilon^{eng})$$ (6)

and

$$\sigma^c = \sigma^{eng}(1 + \varepsilon^{eng}).$$ (7)

The applicability of these conversion equations was verified with the digital image correlation technique (**Chapter 4.2.6.**). To precisely analyze the material response, this elastic deformation was divided into bilinear or piecewise linear elastic deformation phases. The first phase describes the toe region and the second phase the linear elastic region. Then, the elastic modulus of each region is calculated using Hooke's law [Callister, 2003, Gentleman et al., 2006]. This piecewise analysis solves the issue of the ambiguity of the linear elastic region and is supported by the macromolecular structures of these studied hydrogels.

4.2.6. Digital image correlation (IV)

The three-dimensional digital image correlation (3D-DIC) technique using lenses with a focal length of 100 mm was used to study the surface deformations during the compression tests of the hydrogel samples (Figure 13) [Schreier et al., 2009, Palanca et al., 2016]. By using this technique, the sample surface having unique features is recorded simultaneously with two cameras (5 Mpix Imager E-Lite, LaVision, Germany). From the recorded images, a full-field surface deformation map was obtained by tracking the movement of the surface divided into small subsets. The surface pattern required for carrying out the experiments was made by blowing fine carbon black powder (Corax® N550, Evonik, Germany) on the naturally transparent, moist sample.
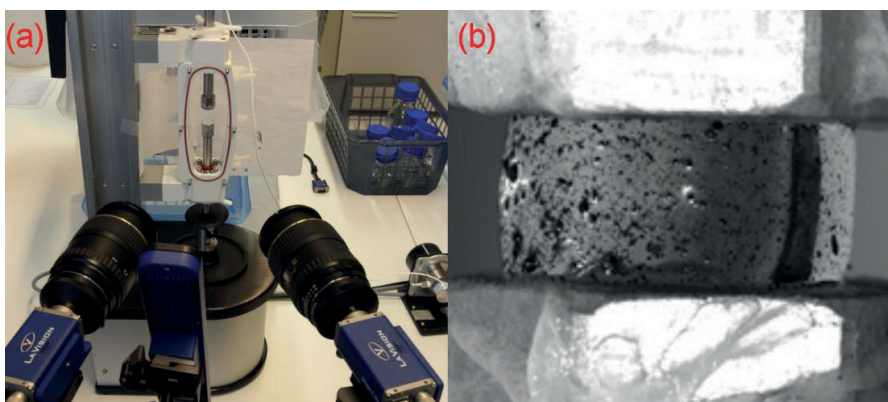
Figure 13. (a) The 3D-DIC test setup, (b) an image taken of a sample with carbon black speckle pattern. Image modified from **Publication IV**.

The lighting of the sample was performed using two synchronized pulsed led lights operated directly via DIC software (Davis 8.4, LaVision). To achieve constant and flat light throughout the sample, the reflections caused by the curved, wet, and transparent sample had to be optimized and balanced. The recording rate of the 3D-DIC measurements ranged from between 1 Hz (stress-relaxation test) and 8 Hz (standard compression method), depending on the total time for each compression test. The scale factor of the images was 8 μm / pixel and the root mean square (RMS) fit of the calibration was 0.4 pixels.

The deformation analysis was performed using Davis 8.4 software. The used subset and step sizes were 55 × 55 pixels and 15 pixels, respectively. In order to ease the tracking process and to minimize the effects by artificially changing pattern (for example due to water seeping on the surface), the applied correlation mode in the analysis was the sum of differential images instead of the more conventionally used mode (i.e., relative to the first image) [Schreier et al., 2009]. From the correlation results, axial surface strains and radial surface displacements were calculated in addition to the qualitative examinations of the sample deformations.

4.2.7. Optical projection tomography (II, III)

An in-house built optical projection tomography (OPT) system with transmission and emission modes was used for materials characterization in **Publication II**. The OPT system used for materials characterization, as explained in the following **Chapters 4.2.7.1. – 4.2.7.4.** and initially described by Figueiras *et al.*, is shown in Figure 14 [Figueiras et al., 2014]. For 3D cell culture visualization imaging, the OPT setup was updated, as shown in **Publication III** and explained in **Chapter 4.4.5.**
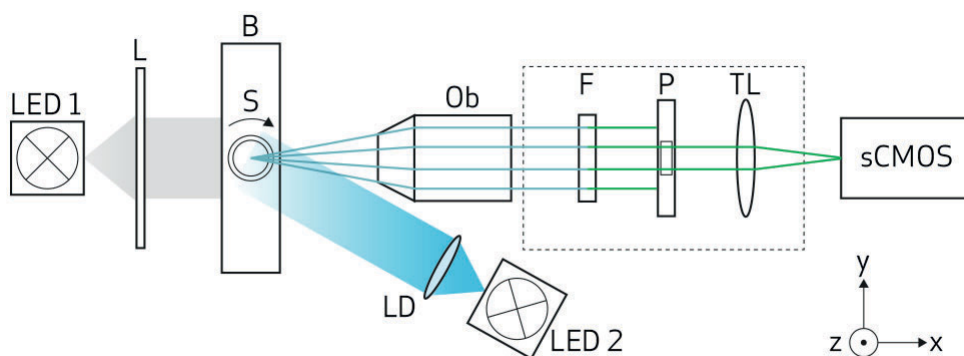
Figure 14. Schematic diagram of the OPT setup (from **Publication II**): the hydrogel samples inserted in FEP tubes are rotated in the rotation stage (S) inside a water bath (B). For brigth field illumination, a white light (LED 1) and a telecentric lens (L) are used. For fluorescence illumination, 470 nm wavelength (LED2) collimated with a lens with difuser (LD) are used. The detection system consists of an objective lens (Ob), a band pass filter (F) used only for fluorescence imaging, a pinhole (P), a tube lens (TL), and a sCMOS camera.

Image processing and the analysis of all the OPT materials characterization experiments were performed using MATLAB®. The data normality and homoscedasticity were verified using Shapiro–Wilk and Levene statistics, respectively. Due to the non-Gaussian distribution of the data, the non-parametric Mann–Whitney U test was used to compare the differences between groups. Analysis was performed with SPSS v13.0 for Windows (SPSS Inc, Chicago, IL, USA).

4.2.7.1. Bright field OPT imaging

Five samples of each hydrogel composition iGG, iGG-MA, photoGG-MA, iGG-SPM-H, iGG-SPM-L, and iGG-Ca, as described in Table 2, were imaged using transmission mode OPT. The hydrogels were prepared into FEP tubes with water matching refractive index and submerged inside a large cuvette filled with water for imaging. Projection images were taken around an entire 360° rotation at steps of 0.9°, resulting in 400 images. The transmitted light

was detected by a 5x infinity-corrected objective with a numerical aperture of 0.14 and imaged with a sCMOS camera (ORCA-Flash 4.0, Hamamatsu, Japan). The used 5x objective provided a resolution of ~3 μm. The 3D images of the samples visualizing the 3D internal structures were reconstructed from the projection images using a filtered back projection (FBP) algorithm [Jochen Birk et al., 2011, Figueiras et al., 2014].

4.2.7.2. Image texture analysis

Image texture analysis was carried out using multiple discriminant analysis (MDA) [Duda et al., 2001]. The analysis was performed to assess and compare the microscopic structures of the hydrogels in the projection images and in their 3D reconstructions using Haralick's textural features in the five samples of each hydrogel type [Haralick et al., 1973]. Pre-processing of the projection images included flat field correction of the illumination non-uniformity created by the white LED (LED1 in Figure 14) using 2D polynomial fitting, and the removal of the tube from the images by manual segmentation. Histogram equalization was applied to the projections and sliced images before performing the textural analysis. The gray-level co-occurrence matrix (GLCM) was computed for each image using 1 and 3 pixel lengths in different directions, i.e., 0°, 45°, 90°, and 135° respectively. From the calculated GLCM of each image, 13 textural features were computed using the toolbox originally developed by Gupta *et al*. [Gupta, Markey, 2005]. Due to the high dimensionality of Haralick's features, MDA was used as a method to reduce dimensionality and to find differences between the textural features of the hydrogels. MDA projects the feature space onto a lower dimension space in such a way that maximizes the inter-class scatter and minimizes the intra-class scatter. [Duda et al., 2001]

4.2.7.3. Fluorescent OPT imaging

For imaging the mass transport, OPT fluorescent projections were always taken in the same angular position of the sample using the OPT in emission mode as represented in Figure 14. For the fluorescence mode, a collimated LED of 470 nm (LED 2 in Figure 14, M470L3; Thorlabs, Newton, NJ, USA) was used to excite the samples and a band pass filter with a center wave-length of 520 nm (EO 67-030; Edmund Optics, Barrington, NJ, USA) was added to the detection system (F in Figure 14).

4.2.7.4. Mass transport assay of fluorescent molecules and index of homogeneity

The hydrogel samples (~1 mL) for mass transport studies were prepared in 5 mL polystyrene cuvettes. Fluorescent FITC-labeled dextran with defined molecular weights of 20 kDa, 150 kDa, and 2000 kDa were used to characterize the transport of molecules. Each type of dextran molecule experiment was replicated five times.

The experiments were performed as follows: (a) the focal plane of the imaging system was placed approximately in the middle plane of the cuvette at the upper part of the hydrogel; (b)

100 μL of solution of one type of molecular weight dextran was pipetted to the surface of the sample; and (c) projections were acquired each minute for 4 hours with an exposure time of 0.04 seconds. The first image was taken before pipetting the dextran on the top of the samples. The imaged area consisted of a square 3 mm in length.The data were pre-processed by subtracting the background to remove common elements, such as non-uniformity produced by the LED, in all images. This was performed by subtracting the first image acquired before the addition of the dextran molecules.

We devised a new method to assess the homogeneity of the hydrogel microstructure by defining an index of homogeneity. The acquired images were first binarized by Otsu´s method [Gonzalez, Woods, 2008], a heuristic method which iteratively calculates the optimum threshold automatically based on the histogram of the image. This threshold value was calculated for each sample. Thus, when the gray level intensity of the pixel is higher than the calculated threshold, the value of the pixel is converted to 1 (white). In turn, if the value of the pixel is inferior to that for the calculated threshold, the pixel value is converted to 0 (black). This produces a wavefront descending through the image. We assume that when the binarized signal from dextran does not travel uniformly, the hydrogel is less homogenous than when traveling uniformly. The index of homogeneity was defined as a measure of the smoothness of the wavefront descending through the hydrogel. To calculate the index of homogeneity, the gradient in the black and white interface was calculated. The gradient points towards the direction of greatest change in every pixel, and thus it is possible to determine the flatness of the said interface by analyzing the gradient interface. In this manner, when the interface between black and white pixels is flat, the angle of the gradient vector is 90° (pointing downwards in the image). If the interface is not flat, i.e., irregular, however, its gradient will also be irregular, and the angles will be different than 90° (they will point in random directions other than downwards). Motivated by this behavior, the index of homogeneity is calculated as the ratio between the total number of 90° angles and the total number of angles. When the value of the index is closer to 1, a greater number of 90° angles is present, and thus indicates a flat interface. The binary images were also used to analyze the position of the wavefront at different times giving us the velocity of the mass transport. We calculated the velocities of the wavefront at time ranges of 50 minutes by polynomial fitting of first degree.

4.3. Cell culture

4.3.1. Ethical considerations

BioMediTech Institute of Tampere University has approval from the Ethics Commitee of Pirkanmaa Hospital District to derivate, culture, and differentiate hESCs (Skottman R05116) and hiPSCs (Aalto-Setälä R08070) and permission from the National Authority for Medicolegal Affairs (FIMEA 1426/32/300/05) to conduct human stem cell research. Patients donating cells for research have provided written, informed consent.

4.3.2. Cell culture reagents (I, III)

The following reagents were used for cell cultures and fluorescent staining of cells: Dulbecco's Modified Eagle Medium/Ham's Nutrient Mixture F-12 1:1 (DMEM/F-12), Penicillin/Streptomycin (Pen/Strep), Neurobasal medium, N2 supplement, Geltrex®, Roswell Park Memorial Institute 1640 Medium (RPMI), B27(-insulin), B27(+insulin), KnockOut-Dulbecco's Modified Eagle Medium (KO-DMEM), GlutaMAX™, TrypLE Select, poly-L-lysine (M_w 70,000-150,000) Alexa Fluor 488 conjugated to donkey anti-rabbit (A21206) and anti-mouse antibody (A21202), Alexa Fluor 568 conjugated to donkey anti-goat antibody (A11057), Calcein-AM (Ca-AM, $\lambda^{excitation}$ = 568 nm) and Ethidium Homodimer-1 (EtHD-1, $\lambda^{excitation}$= 568 nm) acquired from Thermo Fisher Scientific (Waltham, MA, USA). Paraformaldehyde (PFA), pronase, bovine serum albumin (BSA), normal donkey serum (NDS), Triton X-100, phosphate buffer (PB), alpha-actinin (ACNT2, mouse IgG, A7811), 4',6-diamidino-2-phenylindole (DAPI) and tetramethyl-rhodamine isothiocyanate conjugated to phalloidin (TRITC-phalloidin, P1951) acquired from Sigma-Aldrich (St. Louis, MO, USA and Espoo, Finland). Basic fibroblast growth factor (bFGF) acquired from R&D Systems (Minneapolis, MN, USA). Brain-derived neurotrophic factor (BDNF) acquired from Prospec Bio (Germany). Fetal bovine serum (FBS; South American origin) acquired from Biosera/Bionordika (Helsinki, Finland). mTeSR1™ medium acquired from STEMCELL Technologies (Vancouver, Canada). CHIR99021 acquired from REPROCELL (Glasgow, UK). IWP-4 acquired from R&D Bio-Techne (Minneapolis, MN, USA). Non-essential amino acids (NEAA) acquired from Cambrex (East Rutherford, NJ, USA). Phosphate buffered saline (PBS) and trypsin acquired from Lonza (Basel, Switzerland). Rabbit anti-microtubule associated protein 2 (MAP-2, AB5622) acquired from Merck (Kenilworth, NJ, USA). Rabbit anti-β-tubulin isotype III (β-tub, IgG, A01627) acquired from GenScript (Piscataway, NJ, USA). Goat anti-troponin T (TNNT2, IgG, ab64623) acquired from Abcam (Cambridge, UK). Mounting medium VECTASHIELD containing DAPI acquired from Vector Laboratories (UK). Qiagen RNeasy® kit acquired from Qiagen (Hilden, Germany). cDNA Reverse Transcription kit and TaqMan Universal Master Mix acquired from Applied Biosystems Foster City, CA, USA). The

compositions and producers of enzymatic dissociation buffers used in cardiomyocyte cell culture and TaqMan assays used in Quantitative reverse transcription polymerase chain reaction (qRT-PCR) are listed in **Appendix I**.

Cell cultures were conducted on T75 and T175 culture flasks and Nunc 12- and 24-well plates acquired from Thermo Fisher Scientific (Waltham, MA, USA), 48-well plate from Greiner Bio-one (Kremsmünster, Austria), and glass bottom well plates from MatTek Corporation (Ashland, MA, USA). All cell cultures were maintained at 37 °C in 5% CO_2 atmosphere and 95% humidity.

4.3.3. Commercial fibroblast cell line WI-38 (III)

The commercial human lung fibroblast cell line WI-38 was obtained from European Culture Collections (Public Health England, United Kingdom) [Hayflick, Moorhead, 1961]. The fibroblasts were cultured and expanded in T175 or T75 culture flask with DMEM/F-12 supplemented with 10% FBS and 50 U/mL Pen/Strep. For cytocompatibility tests, the fibroblasts were detached with trypsin treatment, counted and plated with 30,000 cells/cm^2 in 2D conditions and 300,000 cells/mL hydrogel in 3D conditions. To test the cytocompatibility of the modified gelatins, separate cell culture wells were dip coated with gelatin-ADH or gelatin-CDH (40 mg/mL) with 1 hour incubation at 37 °C. Dip coating with unmodified gelatin (1 mg/mL) was used as 2D control for all the cell experiments in **Publication III**. This is a well-known method for cardiomyocyte culture and gelatin molecules adsorb to the surface strongly enough to facilitate the cell attachment [Mummery et al., 2003, Ikonen et al., 2013, Kiviaho et al., 2015].

Cytocompatibility testing of hydrogels were conducted both on top of the gel (2D) and encapsulated inside the gel (3D) using the compositions F1-ADH, F2-ADH, F3-ADH, F4-CDH, F5-CDH, F6-CDH, and control unmodified bioamine-GG composition F7-SPD. In the 2D experiment, the hydrogel was cast in the well plate 20 minutes before the cells were plated on top. In the 3D experiment, 30 µL cell suspension was mixed with the gelatin-ADH or gelatin-CDH and GG-CHO simultaneously during gelation to form a total of 330 µL of hydrogel. Cell culture medium was applied on top of the samples after ~20 minutes gelation time. Cell were cultured for 1 week and used for Live/Dead® viability assay on day 3 and day 7.

4.3.4. Human pluripotent stem cells (I, III)

Both hESC- and hiPSC-origin cells were used and the derivation and pluripotency of all the used lines has been studied and published before. In **Publication I**, the used hESC-lines were Regea 08/023 [Skottman, 2010] and Regea 11/013 [Sorkio et al., 2015] and the used hiPSC-lines were UTA.04511.WT [Ojala et al., 2016], Hel24.3, and A116 [Toivonen et al., 2013] (the latter two being kind gifts from the University of Helsinki). In **Publication III**, only one hiPSC line, UTA.04602.WT [Kiviaho et al., 2015], was used. All the hPSCs were cultured in the stem cell state as previously described [Rajala et al., 2010, Kiviaho et al., 2015].

4.3.4.1. Neuronal-hydrogel cell culture (I)

The neuronal differentiation of hPSCs were performed as described previously by Lappalainen *et al*. [Lappalainen et al., 2010]. Briefly, undifferentiated stem cell colonies were mechanically cut into small aggregates and placed in a suspension culture on neural differentiation medium (NDM) containing 1:1 DMEM/F12 and Neurobasal medium, 2 mM GlutaMax™, 1 × B27, 1 × N2, 20 ng/mL bFGF, and 25 U/mL Pen/Strep. During suspension culture, the cell aggregates formed round, floating neurospheres. The neurospheres were kept small via mechanical cutting once per week and 1/3 of the medium was changed three times per week. Cells were kept for 8 to 17 weeks in the differentiation phase prior to use in the hydrogel experiments. The cells were constantly monitored for the quality of differentiation. Only experiments in which cells formed good neuronal cultures in 2D control were included to the analysis (representative images of good quality 2D cultures are presented in **Appendix II**).

To evaluate the suitability of the hydrogels for neural TE, three approaches were taken to study the cell/biomaterial interactions, as shown in Figure 15. In each case, the control cells were plated on laminin-coated cell culture wells (positive control) and on non-coated cell culture wells (negative control). Cell behavior on the studied materials was always compared to that of the controls. Depending on the well type used, either plastic Nunc or glass bottom MatTek wells, the wells were coated with either 10 μg/mL laminin or 10 μg/mL poly-L-lysine followed by 10 μg/mL laminin, respectively.

Gelation was performed as described in **Chapter 4.1.5.** and in Figure 15. A drop of crosslinking agent was added on top of the cell culture, followed by the gentle addition of GG solution in cases of cultures beneath the gel. To avoid disturbing the cells, no additional mixing was performed. For cell encapsulation, the cells were suspended in GG solution with a minimal amount of medium prior to crosslinking. After complete gelation, medium was gently added on top of the gel. In 3D cell encapsulation studies for gels with slow gelation (all except GG 3.00%SPD), a thin bottom layer of gel was cast beforehand to prevent cell aggregates from sedimenting to the well bottom during gelation.

Cells were plated either as mechanically cut small cell aggregates or as enzymatically dissociated single cell suspensions prepared using 1 × TrypLE Select. For the 2D experiments (controls, cells embedded or on top), the plating density was 60,000 cells/cm^2 or 7 to 20 small aggregates/cm^2 (3000-7000 cells/aggregate). The cell density for the 3D experiments (cells encapsulated) was ~3.5 × 10^6 cells/mL of gel, or a corresponding number of small mechanically cut cell aggregates.
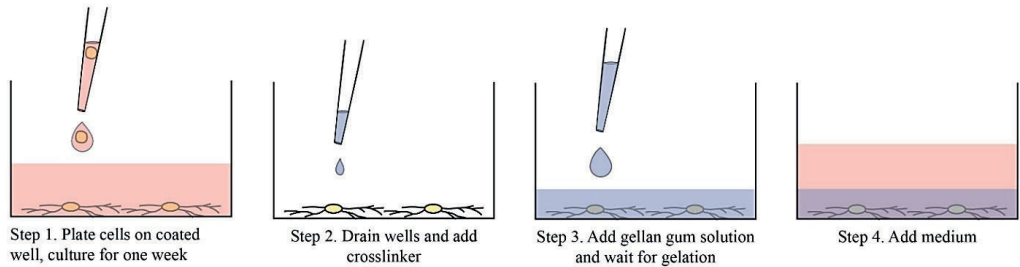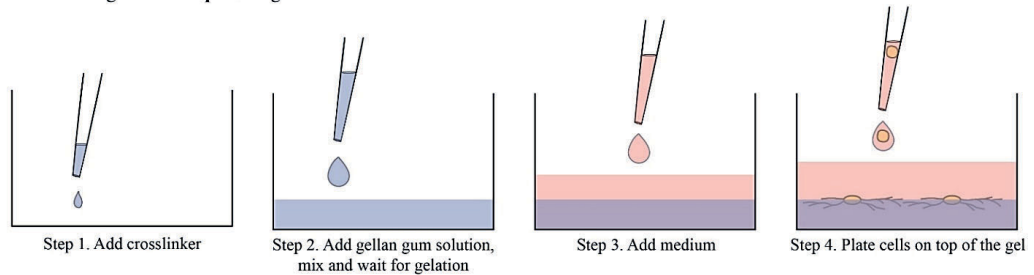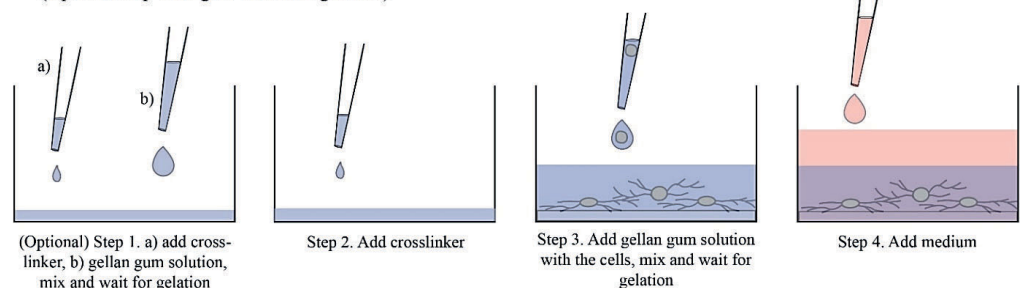
Figure 15. Schematic presentation of plating cells with the hydrogels (from **Publication I**). All components were kept at 37 °C to ensure homogeneous and complete gelation.

The cells were cultured with the gel for 2 weeks. NDM without bFGF was used during the first week of the experiments. After one week of culture, NDM containing 5 ng/mL bFGF and 4 ng/mL BDNF was used. Half of the medium was changed three times per week and the cells were monitored periodically throughout the experiments. Phase contrast images of neuronal-GG cultures were taken using a Zeiss AxioVert.A1 microscope and an AxioCam ERc 5s camera system (Carl Zeiss, Germany) or with a Nikon Eclipse TE 2000-S and a Nikon Digital Sight DS-Fi1 camera system (Nikon, Japan).

4.3.4.2. Cardiomyocyte-hydrogel cell culture (III)

The cardiomyocyte differentiation was done by modulating Wnt signaling, according to the protocol published by Lian *et al.* [Lian et al., 2012]. In short, differentiation was initiated by plating 700,000 hiPSCs/well in a Nunc 12-multiwell plate in feeder-free condition on Geltrex®-coating and cultured with mTeSR1 medium supplemented with 50 U/mL Pen/Strep for four days. For 10 days after initiation, the medium was changed to RPMI supplemented with B27(-insulin) and 50 U/mL Pen/Strep. During this period, 8 μM CHIR99021 was applied to the cells at day 1. After 24 hours, the CHIR99021 was removed. At day 3, 5 μM IWP-4 was added for 48 hours. From day 10 onwards, the B27(-insulin) was changed to B27(+insulin) and the cells were cultured in this medium until they were used for the hydrogel experiments.

After differentiation, beating cardiomyocyte areas were cut with a scalpel under a microscope and collected. Then, the aggregates were partially dissociated to loosen the cell-to-cell bonds inside the aggregate and to better allow the attachment on the hydrogel. The dissociation protocol of Ahola *et al.* was modified as follows: the enzymatic dissociation buffers were applied to the cells incubated at 37 °C: 1st buffer for 45 minutes, 2nd buffer for 15 minutes, and 3rd buffer for 10 minutes, but no mechanical dissociation was done [Ahola et al., 2014]. This gentle dissociation treatment loosens the cardiomyocyte aggregate and makes it more susceptible to attach to the hydrogel. Four aggregates were plated per well with all coating and hydrogel preparations (2D & 3D) in a similar way to that described above for fibroblasts. Cells were cultured with KO-DMEM supplemented with 20% FBS, 1% NEAA, 2 mM GlutaMAX™, and 50 U/mL Pen/Strep. The medium was changed every 3 days, always 1 day before analysis, and cells were cultured for 7 days maximum, monitoring their beating throughout the culture time.

4.4. Cell culture analysis

4.4.1. Live/Dead® staining (I, III)

The Live/Dead® cell viability kit was applied to fibroblast samples after 3 and 7 days of culturing (**Publication III**) and to neuronal samples after 2 weeks of culturing (**Publication I**). Dye concentrations were diluted in PBS and optimized further between the publications. The fluorescent Ca-AM (at 0.1 μM in **Publication I** and 0.2 μM in **Publication III**) stains intact cells green, and Et-HD-1 (at 0.4 μM in **Publication I** and 1.0 μM in **Publication III**) stains dead cell nuclei red. After 1 h of incubation at RT with a rocker plate the samples were imaged.

4.4.2. Immunocytochemical staining (I, III)

We optimized the protocol for immunostaining cells within macroscopic (up 300 μL) hydrogel blocks. In brief, cultures were fixed with 4% PFA pre-heated to 37 °C for 30 min. After a brief

wash in PBS, non-specific staining was blocked with 10% NDS, 0.1% Triton X-100, and 1% BSA in PBS for 1 h at RT, followed by another wash in 1% NDS, 0.1% Triton X-100, and 1% BSA in PBS. Then, the cells were incubated with a combination of primary antibodies at 4 °C for at least 2 days. These antibodies included MAP-2 (1:400) and β-tub (1:1000) (**Publication I**) or troponin T (1:1750) and α-actinin (1:1250) (**Publication III**) in 1% NDS, 0.1% Triton X-100, and 1% BSA in PBS. The samples were washed three times with 1% BSA in PBS (first briefly, followed by 2 × 1 h washes) and then incubated overnight at 4 °C with Alexa Fluor 488 conjugated to donkey anti-rabbit antibody (1:400) and TRITC-phalloidin (0.625 μg/mL) (**Publication I**) or Alexa Fluor 488 conjugated to donkey anti-mouse (1:800) and Alexa Fluor 568 conjugated to donkey anti-goat (1:800) (**Publication III**) in 1% BSA in PBS. The samples were washed three times (first briefly, followed by 2 × 1 h washes) in PBS and then mounted with VECTASHIELD containing DAPI (**Publication I**) or stained with DAPI (1:2000) in PBS (**Publication III**).

4.4.3. Wide field fluorescence microscopy and image analysis (I, III)

The samples stained either using Live/Dead® viability assay or immunocytochemical staining were imaged with an Olympus IX51 inverted microscope and an Olympus DP30BW digital camera. Gray scale images were post-processed (merging and pseudo-coloring) using Adobe Photoshop CS4 (version 11.0, Adobe Systems Inc., CA, USA) and Adobe InDesign CS4 (version 6.0, Adobe Systems Inc.) in **Publication I** and ImageJ (Version 1.39, US National Institutes of Health, Bethesda, MD, USA) in **Publication III** [Schneider et al., 2012].

In **Publication I**, the neurite migration was measured with the ImageJ measurement tool: drawing a straight line from the cell aggregate surface to the visible end of a neuronal process and recording the length. For each cell aggregate analyzed, the four longest separately distinguishable neurites were measured. Values of less than 10 μm were considered as representing no migration. The analysis was conducted with at least two individual experiments with at least two replicative wells. For each studied group, 7 to 16 images were analyzed. The same statistical analysis as described in **Chapter 4.2.4.** was applied in neurite migration analysis.

In **Publication III**, the cell number quantification was done using the ImageJ particle counting algorithm based on at least 3 parallel Live/Dead® stained images taken with 4x magnification from all the studied conditions. Fibroblast viability percentage was calculated from the detected live and dead cell area according to the following equation:

$$\text{Viability\%} = \frac{area\ of\ live\ cells}{area\ of\ live\ cells\ +\ area\ of\ dead\ cells} = \frac{\sum_{i=1}^{n} L_i}{\sum_{i=1}^{n} (D_i + L_i)} \tag{17}$$

4.4.4. Confocal microscopy (I)

Confocal scanning of the samples was performed with a Zeiss LSM 780 mounted into an inverted Cell Observer microscope (Carl Zeiss, Jena, Germany) using 10x (NA 0.45) or 20x (NA 0.80) air objectives. The samples were scanned through MatTek #1.5 glass bottom well plates or through high performance #1.5 coverslips. The confocal data were visualized with ZEN Black 2012 software (Carl Zeiss) and ImageJ [Schneider et al., 2012].

4.4.5. Optical projection tomography for 3D cell imaging (III)

An updated version of the in-house built OPT system presented in Figure 14 (**Chapter 4.2.7.**) was used to visualize the 3D morphology of fibroblasts in selected hydrogel conditions [Figueiras et al., 2014, Belay et al., 2018]. Cell samples were transferred into FEP tubes by puncturing the 3D hydrogel cultures. A white LED source was used to illuminate the sample in transmission mode and imaging was conducted in a similar way to that stated for texture analysis (**Chapter 4.2.7.1**). 3D reconstruction was computed in MATLAB® from projection images using the standard FBP algorithm [Figueiras et al., 2014]. Visualization in 3D was done with Avizo software (Thermo Fisher Scientific, Waltham, MA, USA).

4.4.6. Video recording and beat analysis (III)

The cardiomyocyte cultures were primarily analyzed by phase contrast microscopy using a Nikon Eclipse TS100 (Nikon Corporation, Japan) microscope, and monochrome 8-bit videos were acquired with an Optika DIGI-12 (Optika Microscopes, Italy). The video recording of beating cardiomyocytes was done with the same setup using 60 frames per second recording for 30 seconds. The videos were analyzed based on particle image velocimetry with BeatView® software, i.e., creating and comparing velocity vector fields based on pixels in two consecutive video frames [Ahola et al., 2014]. Figure 16 shows a representative beating pattern of a cardiomyocyte aggregate. It should be noted that this analyzed beating is a record of purely mechanical movement, so no further information is known about the electrophysiology and electrical phenotype of the cardiomyocytes.
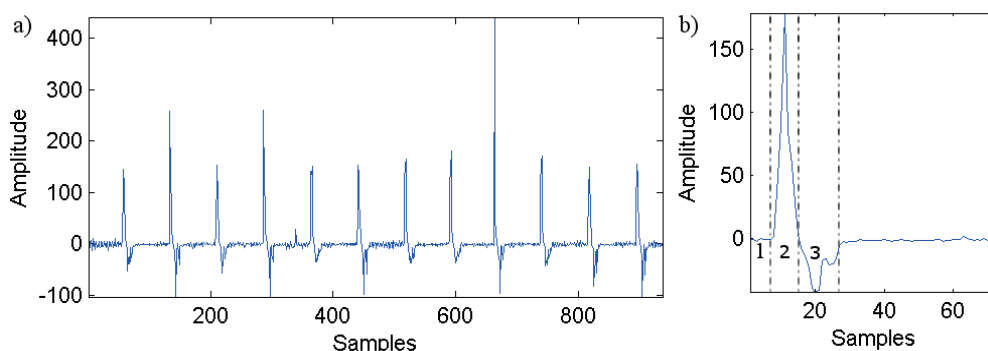
Figure 16. Beating pattern of cardiomyocyte aggregate in F4-CDH hydrogel as an example of the BeatView® analysis (from **Publication III**). Graph a) shows regular beating rhythm for 30 s, b) shows the breakdown of a single beat into (1) relaxed state, (2) contracting movement, and (3) relaxing movement. Each of the x-axis samples consists of two consecutive video frames.

4.4.7. Gene expression (III)

The expression of three main cardiac marker genes was studied to further verify the cardiac nature of the hiPSC-derived cells using qRT-PCR. The total RNA was isolated from 3D hydrogel culture using the Qiagen RNeasy® kit after two weeks of culture. The culture medium was removed, and the hydrogel was briefly washed with PBS. The cardiomyocyte aggregates in the hydrogel were cut and extracted under microscope with a scalpel and transferred to a microcentrifuge tube. The excess hydrogel in the sample tube was digested by the addition of 100 µL pronase solution (stock 10 mg/mL in water) incubated at 37 °C for 5 minutes. This digested cell-hydrogel solution was added directly to the RNeasy® lysis buffer, homogenized, and RNA extracted according to the manufacturer's instructions. DNase I treated total RNA was reverse-transcribed using the high capacity cDNA Reverse Transcription kit. The cDNA was amplified with TaqMan Universal Master Mix using the BioRad CFX384 Real-Time PCR Detection System (Hercules, CA, USA) Samples were analyzed in triplicates and GAPDH was used for normalization of expression levels of individual genes, which was calculated by the $\Delta\Delta$CT method [Livak, Schmittgen, 2001]. The studied marker genes were troponin T (TNNT2), α-actinin (ACNT2), and myosin binding protein C (MYBPC3), as listed in **Appendix I**.

5. Results

Hydrogels based on GG (**Publications I, II & IV**) and gelatin with GG (**Publication III**) were successfully designed and produced. The material characterization methods for hydrogels in the wet state were developed and used for studying relevant parameters for TE and 3D cell culture applications. All studied hydrogels satisfy the true gel definition and are transparent. The names of the studied hydrogel compositions are presented in Table 2 in **Chapter 4.1.4.** The cytocompatibility of the developed hydrogels is generally good; however, bioamine crosslinked GG without ECM protein functionalization does not provide enough attachment sites to enable cell spreading. Functionalization with laminin for neuronal cells and with gelatin for cardiomyocytes greatly enhances the cell attachment, spreading, and also viability.

5.1. Polymer modification for hydrazone crosslinking

Hydrogel producing polymers were chemically modified to enable chemical crosslinking of gelatin-GG in **Publication III**. Successful crosslinking requires introducing the hydrazide groups in gelatin, as using only the native amine groups available can form imine crosslinks, but those are not as stable as the hydrazone crosslinks [Kalia, Raines, 2008]. In other publications, the polymers were used as-received for production of physically crosslinked hydrogels (and chemically crosslinked photoGG-MA in **Publication II**). Figure 17 shows the chemical reaction schemes for modification of gelatin and GG yielding the hydrazone crosslinked hydrogels, and the NMR spectra comparing ADH and CDH modified gelatin to the unmodified gelatin. During the modification reaction 0.24 millimoles of free carboxylic groups of gelatin react with 3 millimoles EDC and either 22.5 millimoles of ADH or 20 millimoles of CDH. The Figure 17 also shows higher modification degree of gelatin-CDH compared to gelatin-ADH. As the CDH is a smaller molecule, the higher mobility can affect the modification degree, which then affects the required concentrations. Additionally, the success of the oxidation of GG-CHO is shown by FTIR in Figure 18 as a change in the bend of the curve at wavenumber 1500 cm^{-1}. The degree of substitution of GG-CHO has been previously reported [Karvinen et al., 2017].
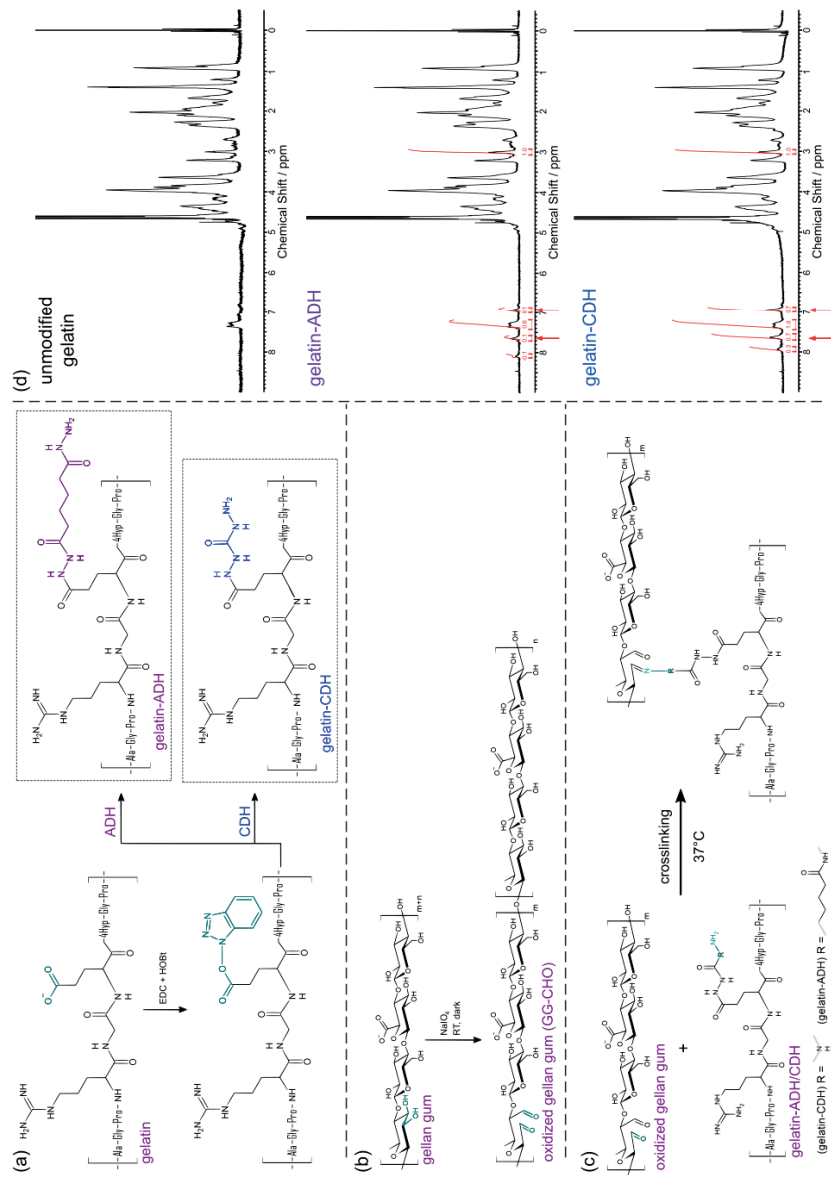
Figure 17. (a)-(c) Chemical modification of gelatin and GG to produce hydrazone crosslinked hydrogel. (d) Comparison of NMR spectra of unmodified and modified gelatin molecules. (from **Publication III**)

70
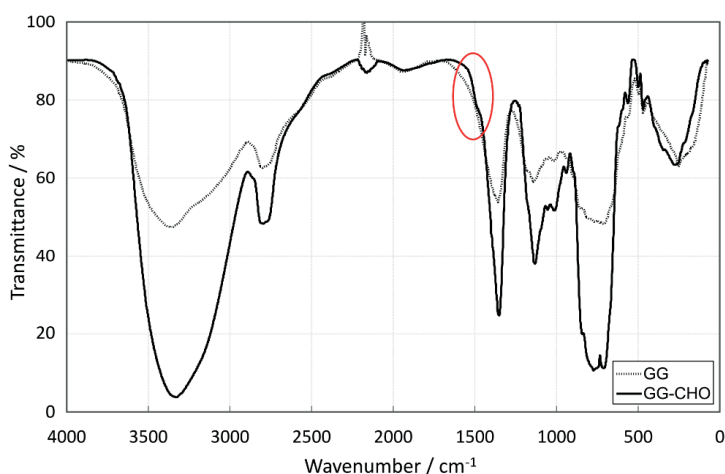
Figure 18. Comparison of the FTIR spectra of unmodified and modified GG with the main change highlighted with a red circle (from **Publication III**).

5.2. Gelation & biodegradation

During the formulation of new hydrogels, the components were mixed in a syringe mold and a tube tilt test was performed. Once the composition in question did not flow anymore, it was examined further. Only hydrogels which were fully transparent and self-standing when taken out of the mold were considered to be proper, true gels and used in the publications. Omitting weak gels was a decision done with clinical TE applications in mind. Weak gels might still be suitable growth substrates for disease modeling. All the used hydrogels were also structurally stable enough to be handled with tweezers, as can be seen in Figure 19.

Figure 19. Photograph of a GG 3.00%SPD hydrogel sample lifted with tweezers after overnight incubation in cell culture medium.

Ionotropic, physical crosslinking of native GG using the bioamines SPM and SPD was studied in **Publication I**. The maximum and minimum crosslinker concentrations still producing transparent, true gels were from 1.1% to 0.4% (w/v) in SPM and from 3.0% to 1.25% (w/v) in SPD. The recorded gelation times are presented in Table 3. The crosslinker:GG ratio was a constant 4:25. Higher concentrations than these caused the gelation process to be too fast for uniform mixing, causing a white turbidity to form inside the gel. Lower concentrations formed weak gels that could not keep their shape unsupported. The bioamine-GG hydrogels functioned as 3D cell culture platform in **Publication I** and as model hydrogels for the methods development done in **Publication II** and **IV**.

Table 3. Gelation times of bioamine crosslinked GG estimated by tube tilt test.

Composition	1.10%SPM	0.60%SPM	0.40%SPM	3.00%SPD	1.50%SPD	1.25%SPD
Gelation time	1 min	5 min	10 min	5 sec	5 min	10 min

The chemical hydrazone crosslinking of gelatin-ADH/CDH and GG-CHO was studied in **Publication III**. Again, the maximum and minimum polymer concentrations used still produced transparent, true gels. Weak gels were noted at gelatin-ADH concentrations below 2% (w/v) and gelatin-CDH concentrations below 3% (w/v). Forming the gels at a 1:1 volume ratio yielded the best gelation. Due to higher modification degree, the highest total gelatin content was achieved with gelatin-CDH, reaching 60% w/w. The gelation time of gelatin-ADH gels was approximately 5 minutes and gelatin-CDH gels approximately 10 minutes. The hydrogels produced with either of the modified gelatins were definitely stickier and more difficult to handle than the gels produced by bioamine crosslinking, which actually had a rather low surface friction and slid easily on surfaces.

The biodegradation of gelatin-GG was studied in **Publication III** using collagenase enzyme, and the presence of gelatin was evaluated using fluorescence spectrophotometry. Figure 20 shows the degradation profiles. The degradation of gelatin-CDH gels is faster initially but slows down around the 24 h time point, after which the gelatin-ADH gels degrade faster. The CDH-hydrazone bond is known to be more resistant to hydrolysis than the ADH-bond because of electron resonance stabilization effect provided by nitrogen heteroatom neighbouring the CDH-bond [Kalia, Raines, 2008, Oommen et al., 2013, Koivusalo et al., 2018]. Thus, it is assumed that the initial part of degradation observed is caused by the collagenase affecting gelatin, while after 24 h the degradation effect is more related to hydrolytic vulnerability of the ADH-bond. The polymer concentrations in either gel type did not have a significant effect on the degradation rate.
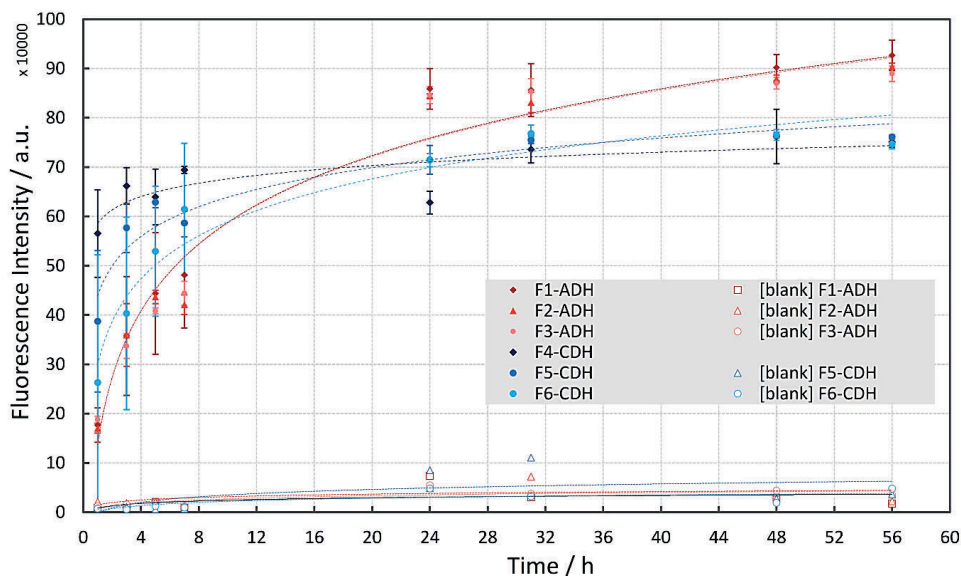
Figure 20. Enzymatic degradation of hydrazone crosslinked gelatin-GG hydrogels incubated in col-
lagenase at 37 °C, over 56 h (from **Publication III**). The release of gelatin was studied
by staining with fluorescamine and recording fluorescence intensity. The blank control
is a sample without collagenase.

5.3. Mechanical properties

Compression testing is one of the cornerstones of this research aiming to design and produce
mechanically biomimetic hydrogels. The compression testing of both hydrogel samples and
reference tissue samples was conducted in the exact same conditions to ensure the compa-
rability of the data in **Publications I, III, IV**, unless otherwise specified. In general, the compa-
rability of the mechanical testing data between hydrogel studies is problematic, mainly due to
viscoelasticity, poroelasticity, definitions of linear elasticity, and differences in applying forces
on anisotropic samples in various test setups. Thus, the results presented here are comparable
with each other, but care needs to be taken when comparing them with other test setups. In
Publications I, the compression data were analyzed using Hooke's law and engineering
stress and strain [Callister, 2003]. In **Publication III**, only the stress-strain curves and fracture
parameters were analyzed. In **Publication IV**, the standard compression data were analyzed
using true stress (Cauchy stress) and true strain (Hencky strain) instead of the engineering
stress and strain [Hencky, 1928, Hencky, 1931, Xiao et al., 2004]. This analysis was supple-
mented with 3D-DIC compression analysis [Palanca et al., 2016].

The compression testing of bioamine crosslinked GG in **Publication I** shows biomimicking material response compared to rabbit brain tissues until ~30% strain, after which point the hydrogel fractures, while the more elastic brain tissue only strain hardens. The representative stress-strain curves, and compressive moduli calculated from 10-35% strain, are shown in Figure 21. Different sections of rabbit brain: midbrain, cerebellum, and cortex, all have a very similar response to compression without significant differences in stress-strain curve or compressive moduli. It was also noted that both SPM and SPD crosslinked GG have linear dependence between crosslinker concentration and compressive modulus, and thus enable the easy tuning of the mechanical characteristics by changing concentration. Fracture strength and fracture strain were also measured, and the fracture strength had a similar linear dependency on crosslinker concentration as the compressive modulus (Figure 21). Fracture strain only changed slightly over the studied crosslinker range, staying around 30 to 40%, which is rather brittle for a hydrogel. The addition of laminin as a physical mixture did not affect the mechanical properties (data not shown).

The hydrazone crosslinked gelatin-GG in **Publication III** had a much stickier surface characteristic than the bioamine-GG and made handling more difficult. Thus, the compression samples had to be prepared in single-use PDMS molds, from which the samples were cut. The difficult handling likely decreased the reproducibility between parallel samples and increased error in the results. However, at least five parallel samples were still tested per composition. Figure 22 shows the comparison of gelatin-GG compositions between each other and with rabbit heart tissue. The most noteworthy result is the highly biomimetic stress-strain curve of F5-CDH that closely follows the shape of the heart muscle curve. The brain and heart tissue have a similar elastic shape of the curve, but the heart muscle is much stronger. When increasing concentrations, the trends were not as clear as those seen in **Publication I**. The compressive moduli were analyzed according to Hooke's law. An interesting result with the same F5-CDH gel was a significantly higher modulus and fracture strength compared with all other studied hydrogels. This gel had disproportioned amounts of gelatin (more) and GG (less), potentially finding a sweet spot of crosslinking efficiency.
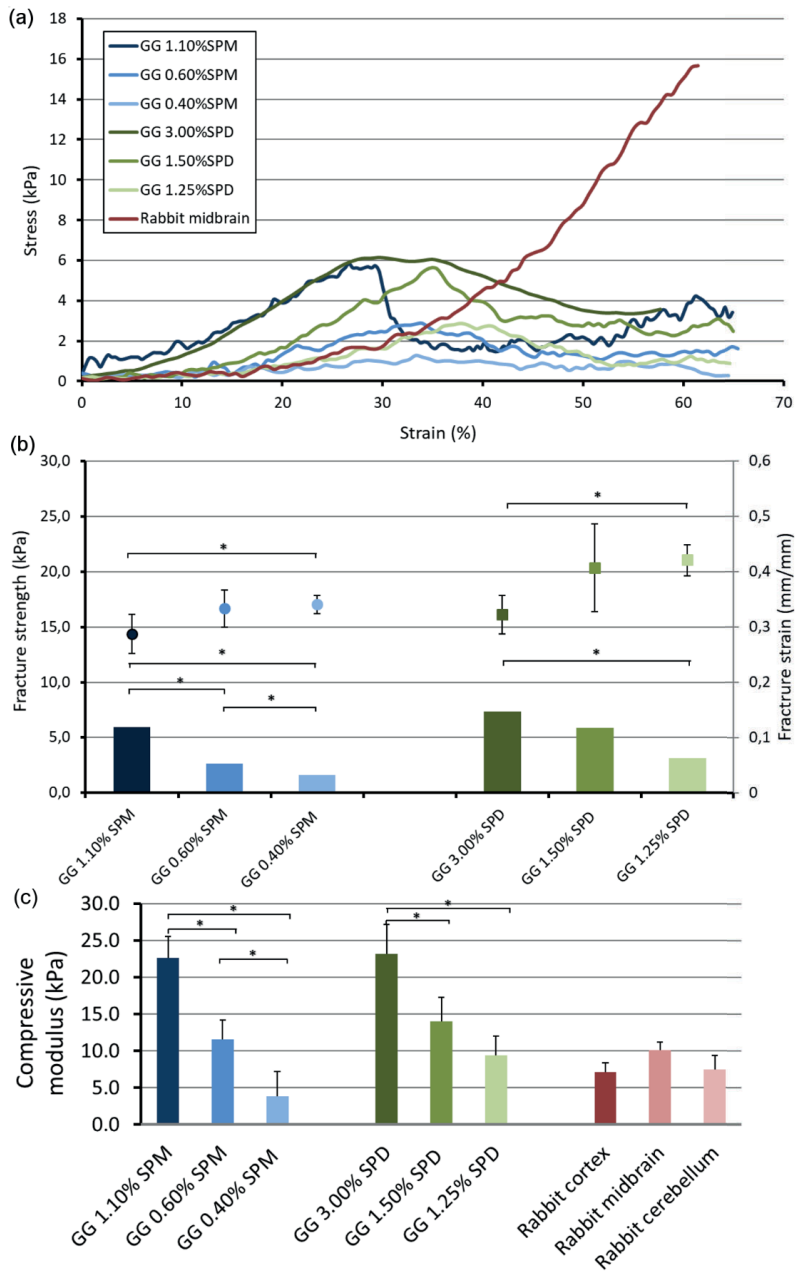
Figure 21. (a) Representative stress-strain curves of the six tested bioamine GG hydrogels com-
pared with rabbit midbrain. (b) Average compressive moduli of the bioamine cross-
linked GG hydrogels with error bars showing the standard deviation. (c) Fracture
strengths and fracture strains of the studied hydrogels, strength on primary y-axis,
strain on secondary y-axis. In (b) and (c) n=5, *=significant difference at $p \leq 0.05$. Image
modified from **Publication I**.
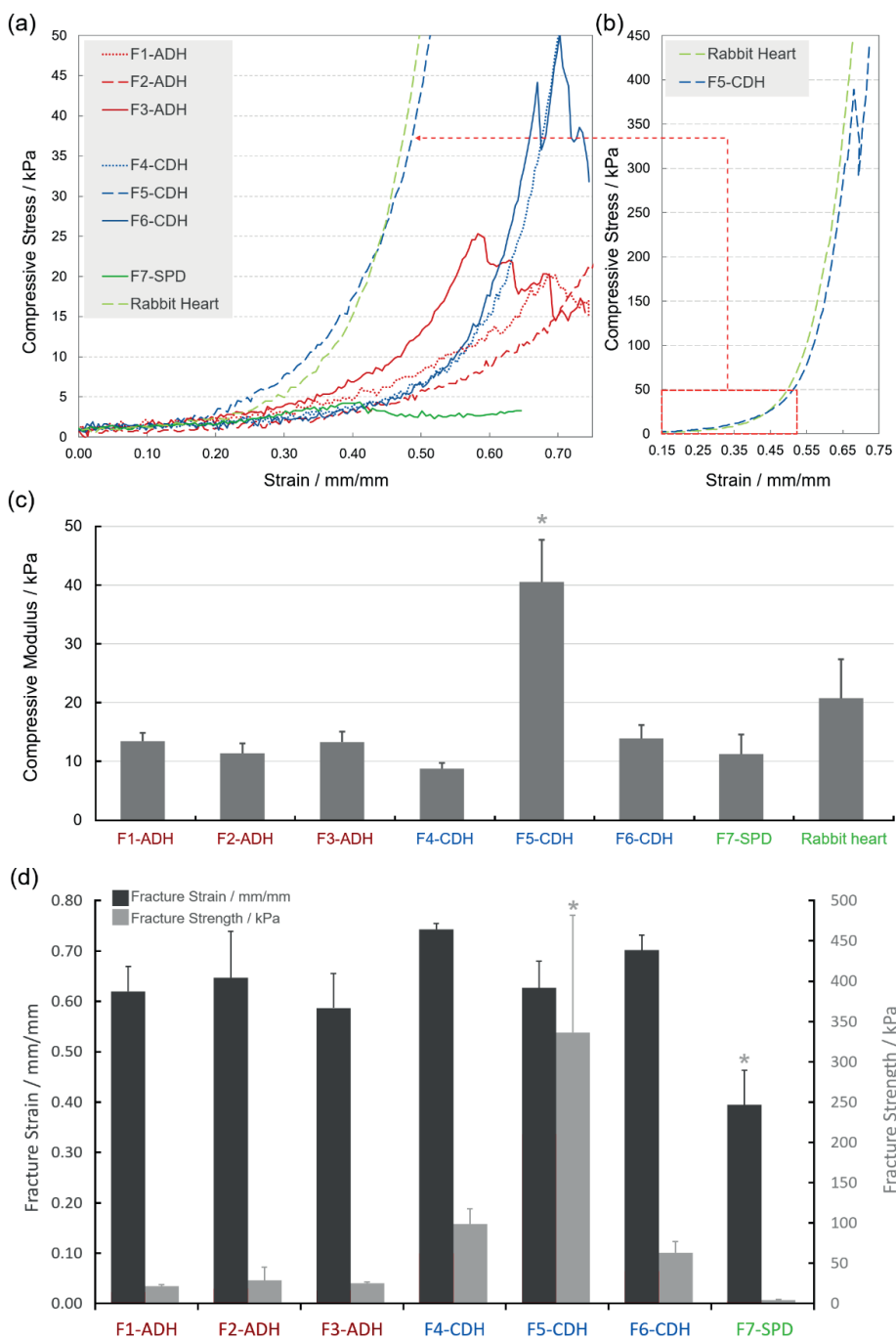
Figure 22. (a) Representative stress-strain curves of F1-F7 hydrogels compared with rabbit heart tissue. (b) Zoomed-out view of the comparison between F5-CDH composition and rab-

76

bit heart, showing very close mechanical biomimicking. (c) Compressive moduli measured case-by-case at the perceived LVER. (d) Fracture strains (primary y-axis) and fracture strengths (secondary y-axis). n=5, *=significant difference at p ≤ 0.05 (from **Publication III**).

Only SPM crosslinked GG hydrogels were successfully tested rheologically in amplitude sweep, SPD crosslinked GG did not have a discernible LVER, which was likely due to the too high anisotropy of the microstructure and the polymer mesh. All the SPM gels had LVER in a similar range and both storage and loss moduli of between 1 and 10 kPa (data not shown). The calculated complex moduli again showed comparable dependency on crosslinker concentration to the compressive modulus (Figure 23). The frequency sweep showed a linear line with storage modulus higher than loss modulus, proving a typical gel-like material response (data not shown). Overall, the rheological studies did not yield significantly different information on the mechanical response than compression testing.
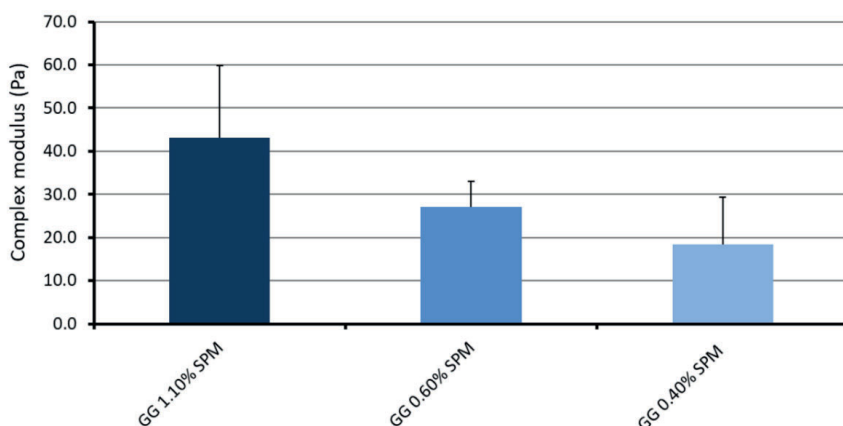
Figure 23. The rheologically measured complex moduli of SPM crosslinked GG hydrogels. Image modified from **Publication I**.

The hydrogel composition GG 1.10%SPM was selected for more careful study in **Publication IV** to gain a deeper understanding on the compression response of this rather brittle, physically crosslinked hydrogel type. First, the effect of measurement parameters was studied further by changing the starting point of measurement with and without pre-load, by increasing and decreasing friction between the sample and the measurement plate, and by varying the displacement rate. The resulting suggested protocol for hydrogel compression testing based on these experiments is presented in **Appendix III**. Then, the compression analysis was conducted using true stress (Cauchy stress) and true strain (Hencky strain) and supplemented with 3D-DIC measurement conducted simultaneously with the compression testing. Figure 24 shows example stress-strain curves with both engineering and true parameters and the validation of the suitability of the true parameters and the deviation of the engineering parameters based on 3D-DIC.
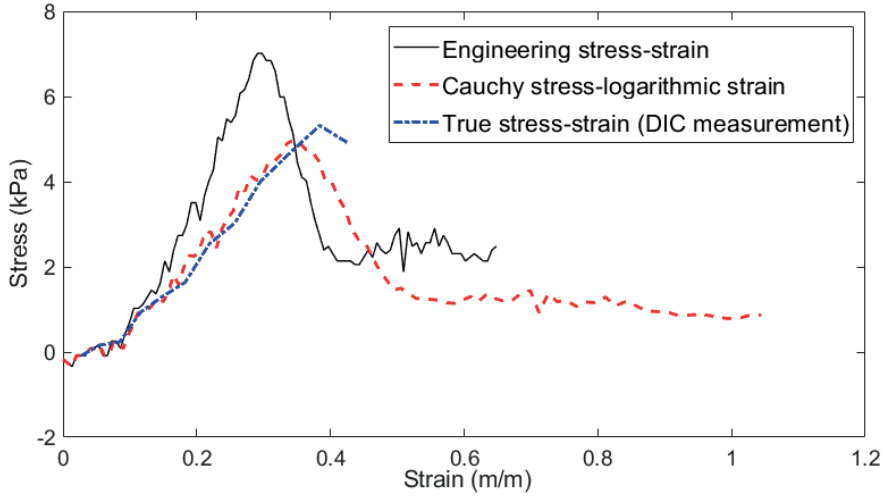
Figure 24. Comparison of a GG 1.10%SPM engineering stress-strain curve with the true stress-strain curve based on 3D-DIC measurement and the calculated Cauchy stress–Hencky strain curve, with a displacement rate of 10 mm/min. Image modified from **Publication IV**.

The 3D-DIC measurement gave additional insight on both the strain distribution in the sample during compression as well as on the deformation of the sample. This was used here as validation of the change of cross-sectional area and for determining true strain. The Poisson ratio of the hydrogel could be measured with a further development of 3D-DIC, but currently the literature value of 0.5 for GG [J. Tang et al., 1996], indicating incompressible hydrogel with constant volume, was used in the analysis. The full-field axial strain map from 3D-DIC is shown in Figure 25 (a). Based on this, it can be concluded that the calculated true strain reliably represents the strain in the middle of the sample, as presented in Figure 24. Figure 25 (b) shows the verification of engineering strain between machine recorded and DIC measured values as well as the fracture of the sample. Even though the DIC correlation fails due to a too rapidly changing sample surface after fracture, 3D-DIC or just the magnified video could also be a valuable tool for studying hydrogel fracture mechanics and crack initiation. A clear, procedural change in the sample cross-sectional area is seen in Figure 25 (c) and (d), illustrating why simply defined engineering stress and strain values are not accurate in demonstrating the compression response of a hydrogel. Figure 25 (c) and (d) also depict the radial surface deformation with varied friction between sample and compression plate and a clear barreling effect is observed. The barreling is approximately symmetrical when the friction is higher, and the sample deformation is even. The combinatorial effect of uneven deformation and anisotropic sample microstructure are likely causing high standard deviation between parallel hydrogel samples.
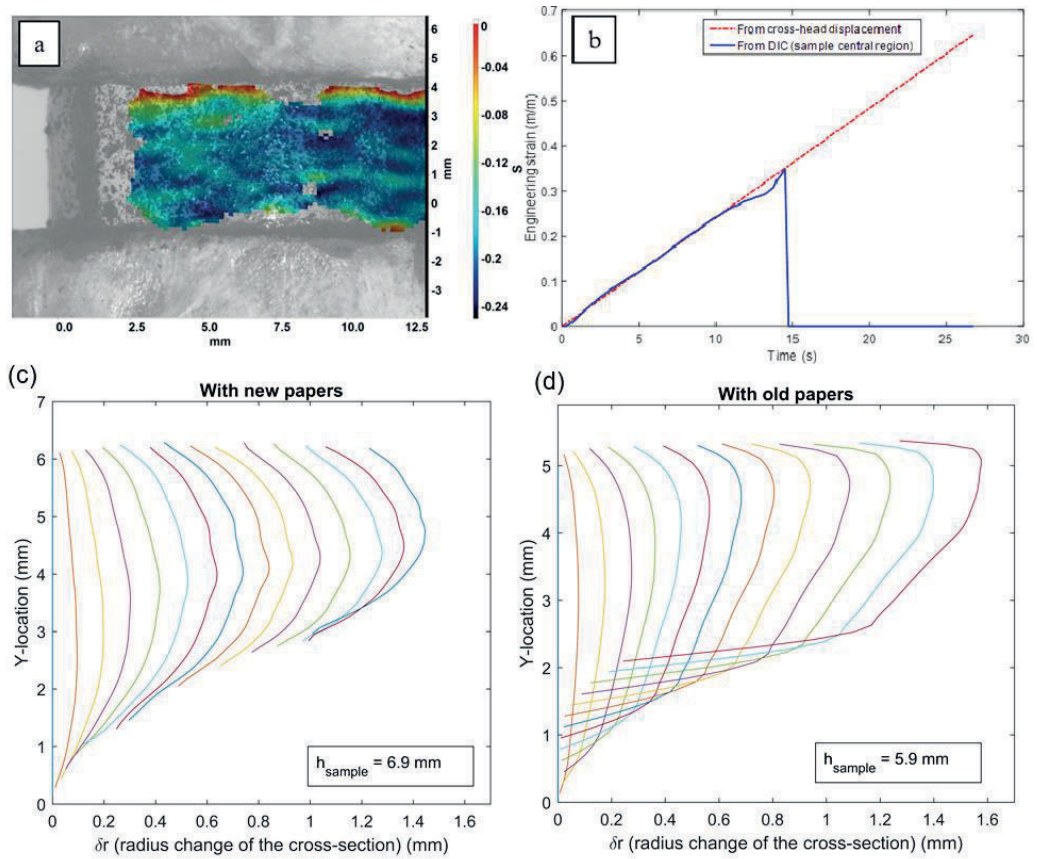
Figure 25. (a) Representative image of 3D-DIC measured strain field in the loading direction at GG 1.10%SPM sample surface 8 seconds after start of compression with displacement rate of 10 mm/min. (b) Verification of engineering strain measurement based on DIC. Fracture of the sample at 14.5 second time point. (c) and (d) the radial surface deformation for hydrogel samples during compression, time interval between each curve is 1 second. (c) Fresh paper between sample and compression plate to increase friction. (d) Reused paper with pores filled with hydrogel residue and reduced friction. Image modified from **Publication IV**.

The experiments with varied pre-loading conditions proved the existence of a so-called toe region as part of the material response. This type of increase in strain with very small stress before a more pronounced linear stress-strain response is typical for biological materials and tissue, but unseen, for example, with metallic materials. In most soft tissues, there are two different molecular parts of the ECM that take the load and are responsible for the material response. First, very elastic elastin fibers elongate and, after they have reached their limits, collagen fibers take over the load, resisting deformation more and in a more linear fashion. Purely nonlinear elasticity is possible on the microscopic scale. As GG has a double helix molecular structure and collagen is a triple helix, when GG hydrogels are deformed, their initial

response is highly biomimicking, with helix unfolding occurring in both cases. Based on this finding, the stress-strain curves were interpreted and analyzed as piecewise linear elastic region, determining two elastic moduli: E_1 for toe region elastic modulus and E_2 for second linear elastic modulus, as shown in Figure 26 for GG 1.1%SPM and GG 0.6%SPM hydrogels.
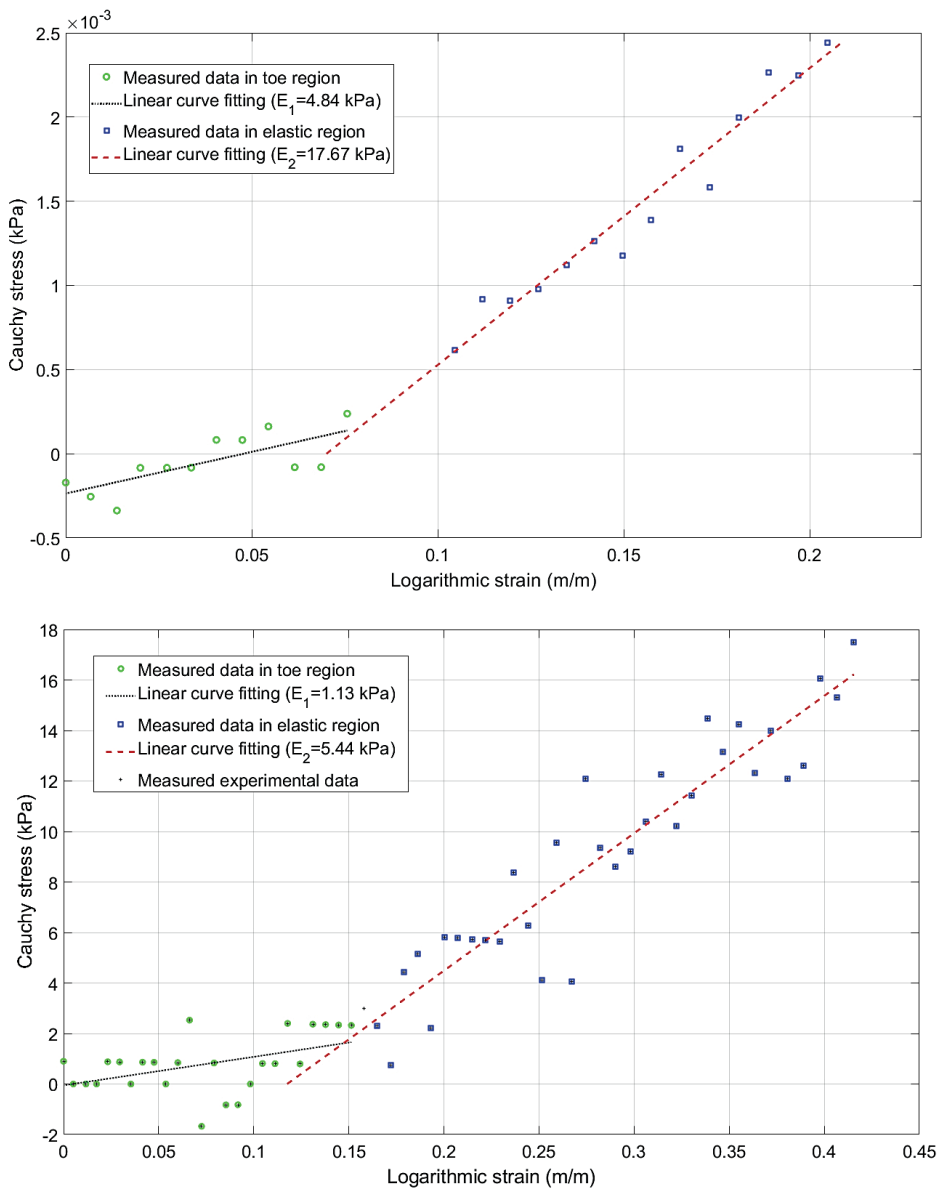
Figure 26. Determination of bilinear elastic moduli with linear fitting using true stress and true strain, graph above for GG 1.1%SPM and below for GG 0.6%SPM. Image modified from **Publication IV**.

5.4. Microstructure

The microstructure of six different hydrogel compositions were analyzed in **Publication II** using OPT via Haralick's textural features and MDA [Haralick et al., 1973, Duda et al., 2001, Gupta, Markey, 2005]. For image processing, the texture is just the spatial arrangement of pixel intensities. As it was noted that pixel intensity histograms do not reveal all the information ingrained in the texture, the GLCM method was used to extract the spatial dependence of gray level values and to characterize the texture. As GLCM does not describe shape properties, it should only be used for microstructure analysis and not on large scale structures. The texture was analyzed from both projection images and from the reconstructed images of OPT to verify if one produces easier to interpret data. It was, however, noted that either image type could be used for texture analysis alone. The only benefit of using a reconstructed image is getting the full 3D image analyzed. Different textural features are highlighted between image types, as can be seen in Figure 27, but the information gained is essentially the same.

Because the total of 13 Haralick's features are too many to present in comparison, MDA was used to reduce the dimensionality of the data to three dimensions with three discriminant functions, implementing a previously published toolbox [Gupta, Markey, 2005]. These show the combination of features that contribute most to the separation of different hydrogel formulations. The exact names of the features are irrelevant on this level of analysis, the major result is how they contribute to distinguishing between the different hydrogel formulations. As shown in Figure 27, both GG-MA gels differ from all the GG gels without the methacrylate modification more than any unmodified GG formulations differ between each other. This is logical because the photoGG-MA is also more densely crosslinked and has both chemical and ionic crosslinking, while the others are only ionically crosslinked. It was additionally noted that GG-MA gels also have poorer transparency than SPM crosslinked gels, which can affect the monitoring of cell cultures and especially disease modeling. This indicates that even though the resolution of OPT is not enough to visualize the actual polymer network and its crosslinks, the variations in crosslinking density carry over to be contrast enhancing variations in optical density as well.

When concentrating on the ionically crosslinked GG, it is clear that the SPM crosslinked gels have the most similar texture, but even they are distinguishable from each other. The separation between iGG-Ca and iGG-SPM-H or iGG-SPM-L is more distinctive, clearly presented in Figure 27(c). This can be directly traced to the different charge of Ca^{2+} and SPM molecules, affecting both the structure of the hydrogel network and the texture. The high separation of iGG and iGG-Ca can be easily explained by the different polymer concentration, as iGG was used as a reference to photoGG-MA and iGG-MA, while iGG-Ca was primarily a reference to iGG-SPM-H and iGG-SPM-L. It was later attempted to correlate the high amount of numerical data provided by Haralick's textural feature analysis with other properties of hydrogels, but an

insufficient amount of data prevented further correlation between image texture and mechanical properties or neurite length [Koivisto et al., 2018].
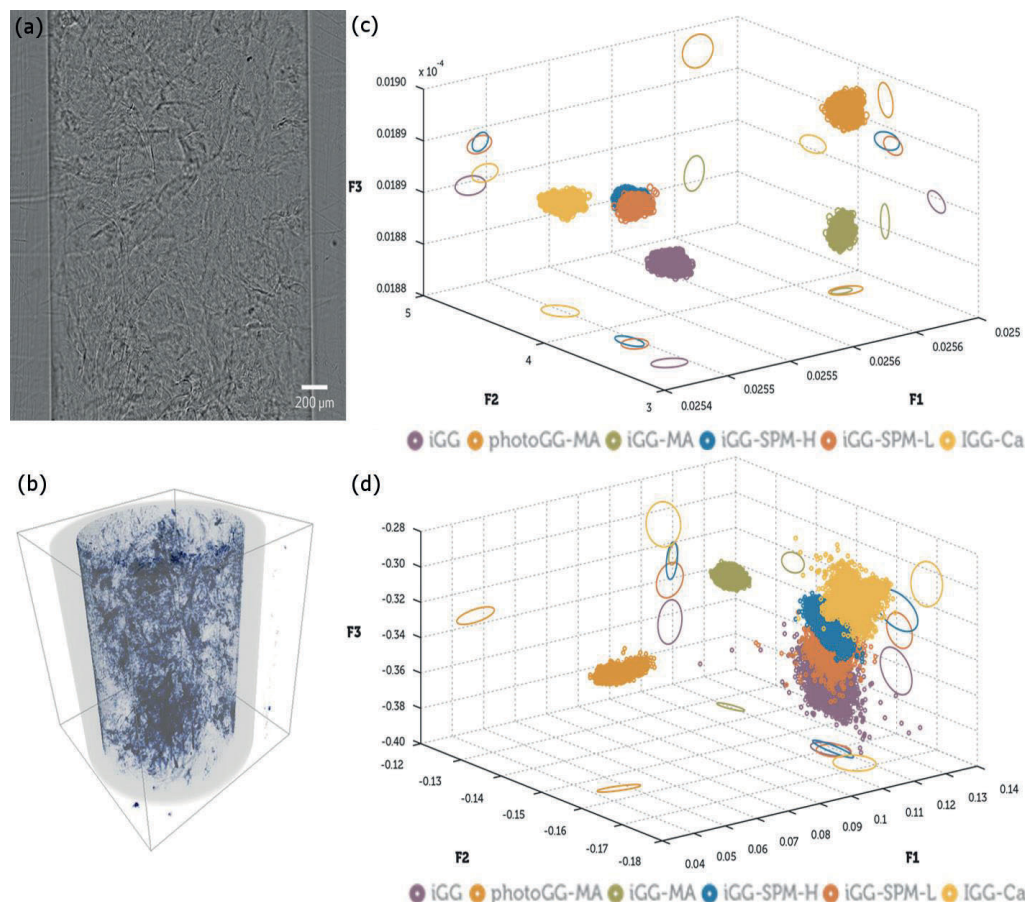
Figure 27. Image texture analysis workflow and results. (a) Example single projection image of iGG-Ca hydrogel with visible texture. (b) Reconstructed 3D image of the same hydrogel highlighting the texture. Haralick's textural features of all the studied hydrogels projected onto 2D subspace after MDA, (c) projection images, (d) reconstruction images. Image modified from **Publication II**.

In addition to texture analysis, the OPT setup was used for studying mass transport of known-sized (20 kDa, 15k Da, 2000 kDa) fluorescent dextran molecules through the six hydrogel compositions of **Publication II**. Dextran sizes were chosen to represent different types of molecules in the cell culture: 20 kDa or smaller is relevant for nutrients and growth factors, 150 kDa for smaller ECM proteins, and 2000 kDa covers all ECM molecules except for the largest proteoglycans [Leddy, Guilak, 2003]. The mass transport was recorded as the progression of the fluorescent wavefront through the hydrogel, downwards from the top. The imaging was done

in purely 2D without rotating the sample, just taking advantage of the large field-of-view of the OPT setup. As expected, it was noted that 20 kDa dextran travels much faster through the gel than the 150 and 2000 kDa dextran. These other two have a more similar velocity together and they do not reach as far inside the gel during the measurement. This indicates a threshold pore size somewhere between 20 kDa and 150 kDa molecules, the smaller ones passing through smaller microstructures than the larger ones. Then, there was another threshold between the middle and the largest dextran, but even the largest of these molecules will pass through the hydrogel eventually.

The penetration depth for the studied dextran-hydrogel conditions over time are shown in Figure 28. In all the tested conditions, 20 kDa dextran had a statistically significant difference in transport velocity compared with the other dextrans in the same hydrogel. Furthermore, when comparing the transport of same dextran size in different compositions, no statistical difference was found in comparison between iGG-SPM-L, iGG-SPM-H, and photoGG-MA, and indicates similar pore sizes in all these compositions. The observed penetration velocity is not linear due to dilution of the diffusing agent and photobleaching of the fluorophore, thus causing a loss of fluorescence signal over time during the test.

Due to the observation of the wavy mass transport wavefront, we defined an index of homogeneity to quantify the effect of different crosslinking methods on the isotropy of hydrogel's microstructure, indicated already in the texture reconstruction and analysis. This index states the uniformity of parallel samples within a single composition as well as the differences between compositions related to single dextran size. As Figure 28 shows, the SPM crosslinked gels were the most homogenous, while iGG-MA and iGG-Ca gels had the greatest variability both within their groups as well as the lowest homogeneity overall compared with other gels. Even though this mass transport study does not directly give a value for the pore size, the knowledge of how fast certain molecules travel through the hydrogel can be actually more valuable, as the effects of molecular charge and shape are already summed in the transport behavior.
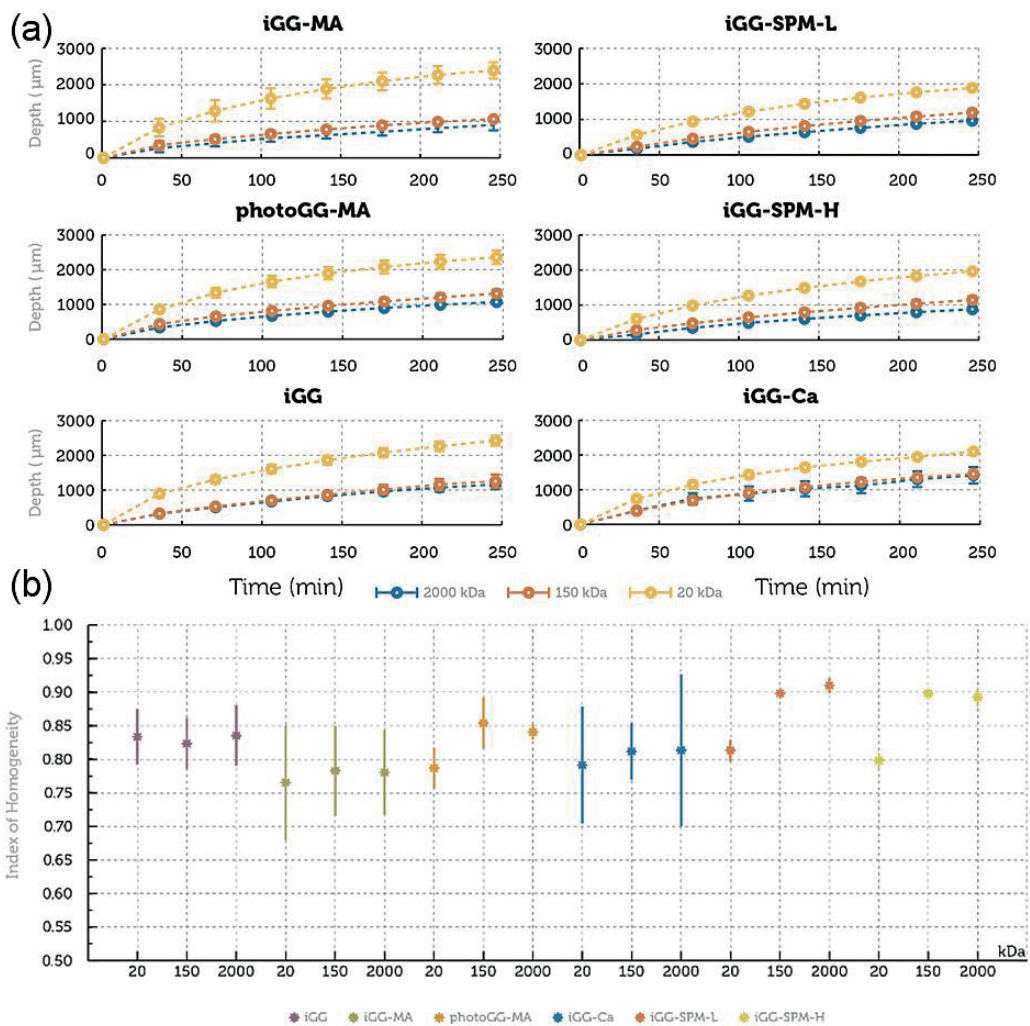
Figure 28. Mass transport of three differently sized dextran molecules in GG hydrogels. (a) Penetration depths over 250 min imaging time. (b) Defined indices of homogeneity based on the uniformity of diffusion wavefront progression. Image modified from **Publication II**.

5.5. Cell response

The designed hydrogel compositions were tested for cytocompatibility in both 2D and 3D conditions using various human cell lines relevant for soft tissue engineering. As explained in Figure 15 in **Chapter 4.3.4.1**, the 2D culture on top of a hydrogel gives information on cell attachment, while 3D culture is the actual application sought, where the diffusion of nutrients and the microstructure of the hydrogel also play a major role in cell response. In both conditions, the hydrogel will also provide mechanical cues for the cell's mechanotransduction provided the gel is thick enough. Neuronal cell cultures were conducted in **Publication I** and fibroblast and cardiomyocyte cultures in **Publication III**.

5.5.1. hPSC-derived neuronal cells

Neuronal cells of both hESC and hiPSC origin were used when characterizing the cell response. However, no significant differences were observed in any of these experiments and the results were reproducible with all the cell lines used. The cytocompatibility of the gelation process was studied by casting different bioamine crosslinked GG hydrogels on top of a week-old, attached neural culture. The gelation process or exposure to pure bioamine prior to gelation did not cause any acute cytotoxicity and the neuronal maturation continued similarly as in the positive 2D control cultures without hydrogel. Good viability was shown by Live/Dead® staining (Figure 29). Immunocytochemical staining shows expected neuronal protein expression and also proves the adequate diffusion of both nutrients and staining antibodies through the hydrogel to the cells underneath (Figure 29).

On top of the bioamine crosslinked GG, the neuronal cells remained viable during a prolonged culture period of 2 weeks. Cell-type specific behavior, i.e., neurite migration, was observed in approximately 50% of cases. When the gel was functionalized with the addition of laminin as a physical mixture, the neurite migration increased the most dramatically in the GG 3.00%SPD gel. Figure 29(d) shows a representative neurite migration on top of the GG 3.00%SPD gel functionalized with 1% laminin compared with non-functionalized gel. When increasing the amount of laminin up to 10%, a significant increase was found in the neurite length, the more laminin the better the cell response. A similar result was found in encapsulated 3D condition, where neurite migration, density, and length all increased in 3D culture when the amount of laminin was increased. A full 3D neuronal network expressing typical neuronal markers is shown in Figure 30. However, the best composition, 10% laminin per hydrogel, is not a sustainable composition for further use simply due to the high cost of laminin reagent, and we did not even use the more expensive recombinant laminin here. Thus, alternative functionalization methods, such as the laminin fragment E8, peptides, or fibronectin protein, are required for the actual routine use of GG-based hydrogels in neural disease modeling or clinical tissue engineering applications.
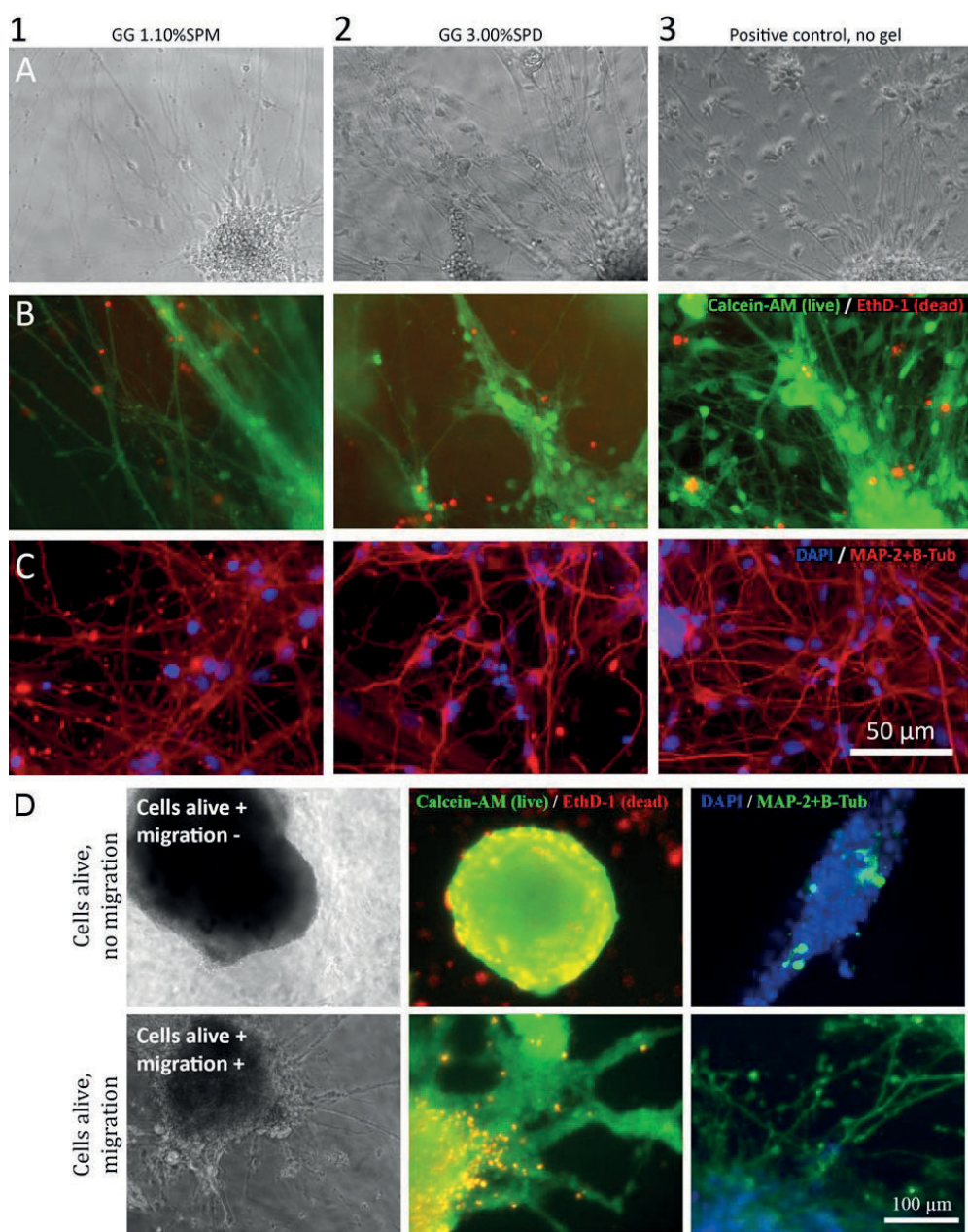
Figure 29. Representative micrographs of neuronal cell cultures under and on top of the bioamine crosslinked GG hydrogel. Row (a) phase contrast images, row (b) Live/Dead® viability analysis, row (c) immunocytochemical staining against MAP-2 and β-tub (red) and DAPI (blue). Scale bar 50 μm for rows (a-c). (d) Neurite migration from neurospheres on top of the GG 3.00%SPD hydrogel with (above) and without (below) 1% laminin functionalization. Scale bar 100 μm for panel (d). Image modified from **Publication I**.
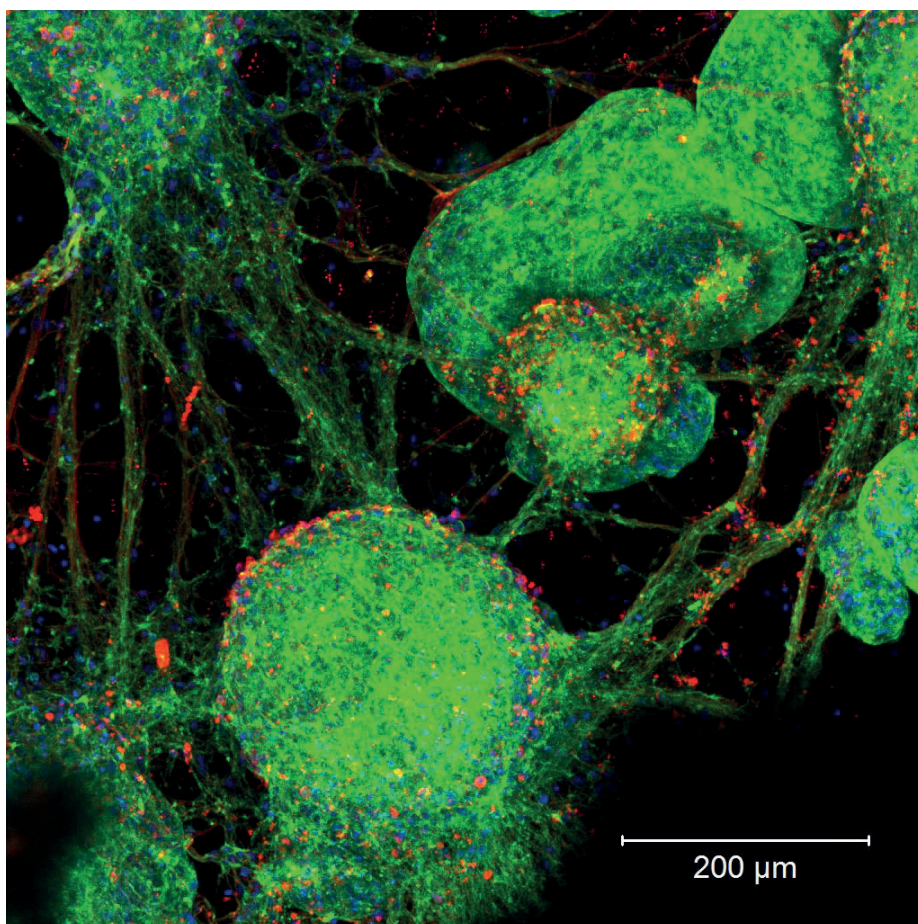
Figure 30. Confocal microscope maximum intensity projection of the neuronal cell network growing encapsulated in 3D in the GG 3.00%SPD hydrogel functionalized with 10% laminin. Immunocytychemical staining against MAP-2+β-tub (green), labeled with phalloidin (red) and DAPI (blue). Image modified from **Publication I**.

5.5.2. Human fibroblasts

The cytocompatibility of hydrazide modified gelatin (gelatin-ADH & gelatin-CDH) was first tested as a coating material with human WI-38 fibroblasts plated on top of the coating. Even though the hydrazone crosslinking occurs in mild conditions, it is important to check the compatibility of the reactive groups, as that will greatly affect cell encapsulation later. The fibroblasts attached, elongated, and proliferated on the modified gelatin coatings as well as on the control native gelatin coating.

The actual hydrazone crosslinked gelatin-GG hydrogels were tested by culturing fibroblasts on top of the gels in 2D and encapsulated inside the gel in 3D. The gelatin coating test essentially

replaced the underneath gel culture condition, which was used with neurons, as explained in Figure 15 in **Chapter 4.3.4.1**. Cells were studied at day 3 and day 7 with Live/Dead® staining to examine both the initial and prolonged effect of the hydrogel conditions. The cells tolerate the aldehyde groups of GG-CHO, so cytotoxic effect is observed. The length of the polymer chain attached to the aldehyde is speculated to have importance on cytotoxicity, smaller molecules penetrating the cell more easily. The calculated cell viability percentage is shown Figure 31 and a clear improvement in the viability is seen in all 3D gelatin-GG conditions compared with unmodified GG. The majority of the cells were alive and showed elongation already at day 3 and more so on day 7, as can be seen in Figure 32. On top of the gelatin-ADH gels, the fibroblasts seemed to randomly form either loose cell aggregates or a continuous cell mat, likely due to active proliferation and confluence. On top of the gelatin-CDH gels, the cells did not form as many clusters, but instead preferred to stay individual and even more elongated.
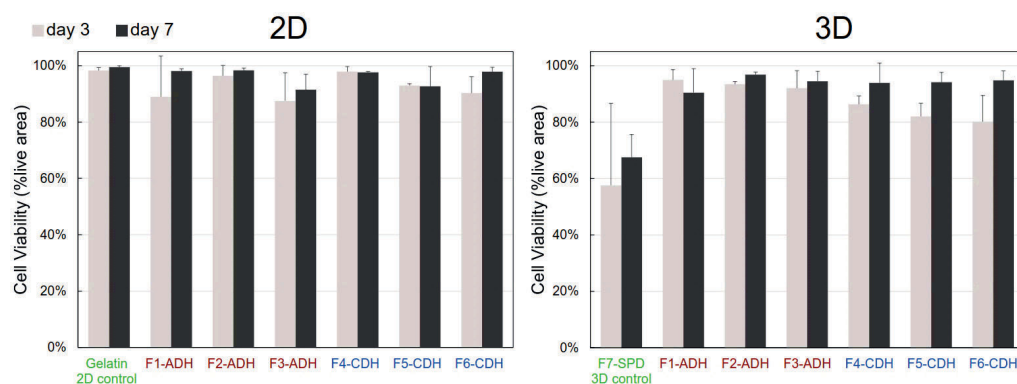
Figure 31. Measured fibroblast viability percentage based on the number of live cells compared with all cells in the image, 4x magnification images (from **Publication III**). Error bars represent mean values ± standard deviation, $n \geq 3$, $p^* < 0.05$.

A remarkable amount of fibroblast elongation was seen in the 3D cultures in all hydrazone crosslinked gels. The cells were very long and elongated in all directions, as seen in Figure 32. The open aldehyde groups in modified GG did not have a cytotoxic effect on the cells, and neither did the gelation process. As wide field fluorescence microscope was not enough to fully deliver the 3D information, OPT in bright field mode was used to better visualize the cell response in 3D. Figure 33 shows representative results from OPT imaging in control F7-SPD gel compared with gelatin containing F3-ADH. Especially the reconstruction video was deemed a great tool for the assessment of large cell populations in 3D culture conditions at mesoscopic scale. In addition to qualitative analysis, the cell numbers and morphology can be also further analyzed from the OPT reconstruction images [Belay et al., 2018]. This makes OPT a highly desirable imaging method for any hydrogel 3D cell culture application, whether it is for studying the development and myelination of neural networks, the maturation of cardiomyocytes, or tissue formation in a TE scaffold.
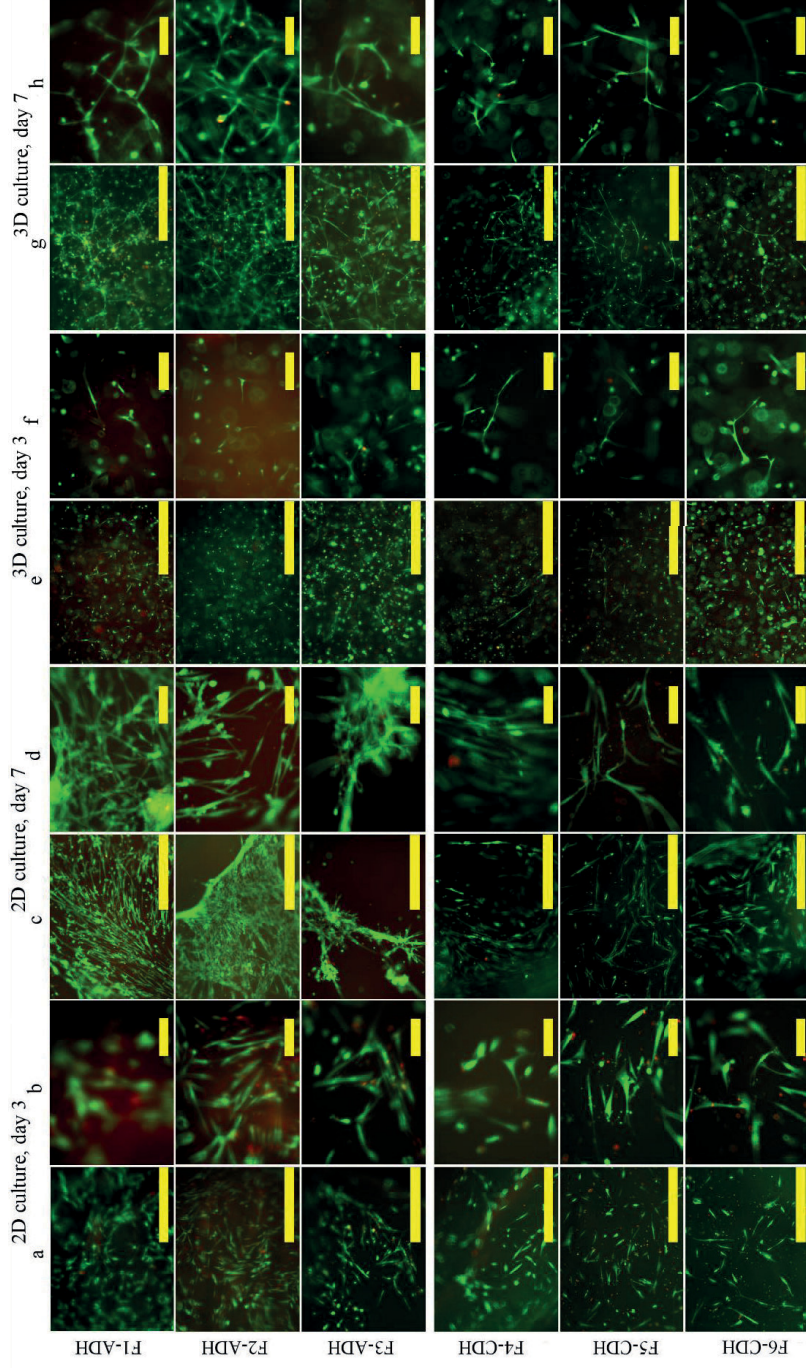
Figure 32. Live/Dead® stained fibroblast cell cultures in all the tested hydrogel formulations and in both 2D and 3D culture conditions (from **Publication III**). Green indicates live cells and red indicates dead cells. Rows a), c), e), and g) are with lower magnification and scale bar length is 1000 μm and rows b), d), f), and h) are with higher magnification with scale bar length of 200 μm.
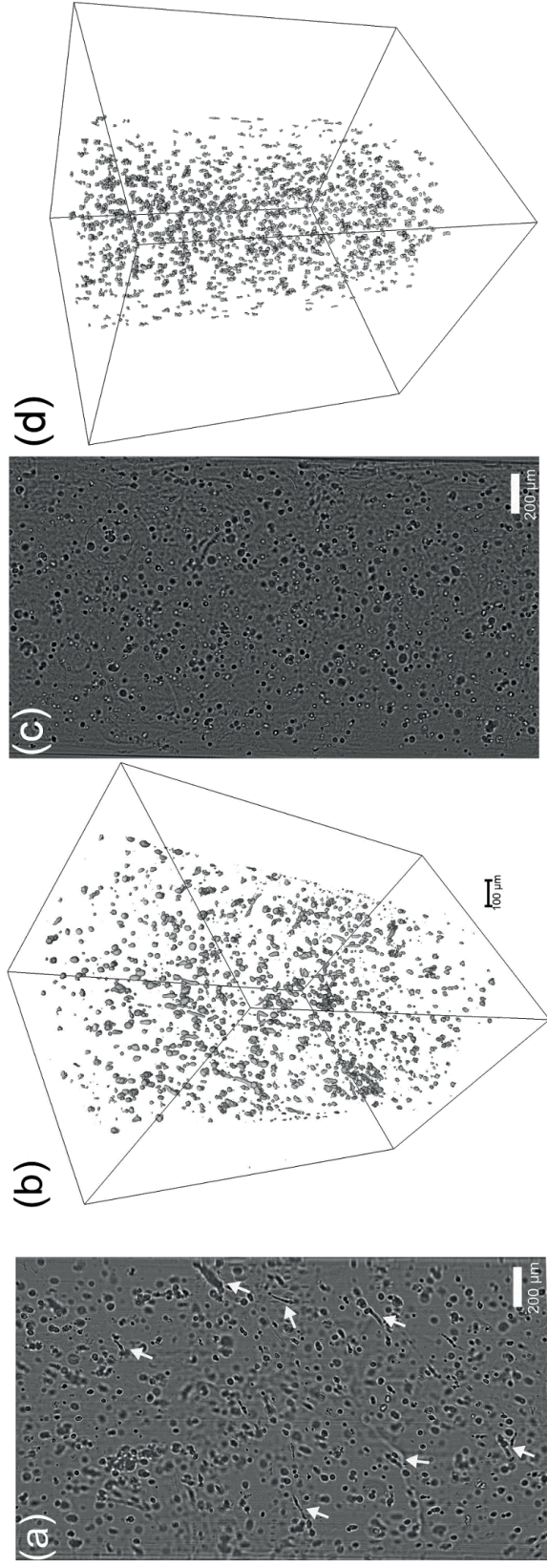
Figure 33. Visualization of 3D encapsulated fibroblast cultures imaged with OPT (from **Publication III**). (a) & (b) F3-ADH, (c) & (d) F7-SPD. In (a) & (c) are shown single projection images with arrows in (a) highlighting elongated cells and in (b) & (d) are shown the respective 3D reconstructions. Cell size is larger and shape more elongated in F3-ADH culture.

5.5.3. hiPSC-derived cardiomyocytes

The hydrazide modified gelatins were tested as coatings with human cardiomyocytes for comparison with our normal culture conditions on native gelatin coating. When replated, the cells recovered their spontaneous beating phenotype in all coating conditions after overnight incubation, indicating the chemical modification did not hinder cardiomyocyte response. However, the focus in **Publication III** was testing the cardiomyocyte aggregates in hydrogel conditions. As cardiomyocyte aggregates can be very tightly packed, the aggregates were treated with a modified enzymatic dissociation protocol to loosen the aggregate, allowing more interaction with the surrounding hydrogel environment but not breaking it down to the single cell level. The cells attached on all the tested hydrogels and cell migration out of the aggregate and into the hydrogel was noted, as the representative examples in Figure 34 show. The protein level expression of the cardiac markers TNNT2 and ACNT2 plus the RNA level expression of MYBPC3 confirms the cardiac nature of these cells, shown in Figure 34 (a).
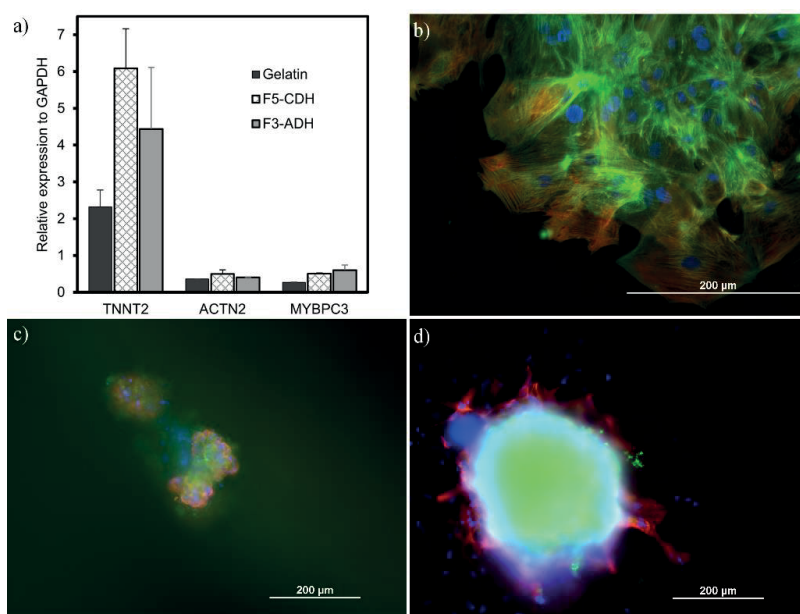
Figure 34. (a) qRT-PCR shows an increase in the cardiac marker gene expressions, most notably on TNNT2, when comparing F3-ADH and F5-CDH to gelatin coating control, relative to house-keeping gene GAPDH. Standard deviations are from 3 biological replicates, each done in technical triplicate. (b), (c) and (d) Immunocytochemical staining of hiPSC-derived cardiomy-ocytes for TNNT2 (red), for ACNT2 (green), and for DAPI (blue). (b) 2D gelatin control, (c) F3-ADH, (d) F5-CDH. The density of the cell aggregate interferes with light penetration, caus-ing blurriness in the image. Scale bar length 200 μm. (from **Publication III**)

The cardiomyocytes recovered their spontaneous beating after overnight culture either on top of or encapsulated inside the hydrogel. This beating behavior is a good indication of the suitability of the material for use in cardiac applications. The cardiomyocytes did not recover their beating in unmod-ified GG or in GG with only a physical mixture of gelatin. The physical mixture of gelatin in GG is

only possible to a small degree because without hydrazone crosslinking and modification the gelatin interferes with bioamine GG crosslinking and causes the formation of a dense white net inside the hydrogel. The spontaneous beating was recorded as phase contrast video, analyzed with digital image correlation based BeatView® software [Ahola et al., 2014], and presented in Table 4. An example of the beating pattern is shown in Figure 16 in **Chapter 4.4.6**. The beating characteristics remained within expected, normal range for both beating frequency and contraction-relaxation duration, and thus all the tested hydrogels are suitable for further cardiac studies.

Table 4. The results of beating analysis of hiPSC-derived cardiomyocytes in gelatin-GG hydrogels, n=4.

Material	2D / 3D	Ratios [mg/mL]	Beating rate [BPM]	Standard deviation	Contraction-relaxation-duration [ms]	Standard deviation
Gelatin coating control		100	35.78	± 20.41	568.60	± 127.10 [a]
GELA-ADH coating	2D	100	42.35	± 6.69	435.50	± 154.02
GELA-CDH coating		100	35.60	± 20.18	662.44	± 268.50 [a]
F1-3-ADH	2D	40:40	36.71	± 17.74	435.25	± 113.70
		40:20	68.04	± 17.01	305.21	± 65.13
	3D	40:40	72.10	± 15.14	264.14	± 41.97
		40:20	52.70	± 47.60	474.59	± 303.62 [a]
F4-6-CDH	2D	60:60	38.63	- [b]	423.74	- [b]
		60:40	37.73	± 2.78 [b]	434.34	± 38.96 [b]
		40:40	41.56	± 5.33	393.14	± 63.67
	3D	60:60	35.77	± 7.00	403.68	± 44.01
		60:40	37.99	± 6.50	452.44	± 32.85
		40:40	33.82	± 3.02	491.88	± 15.65

[a] Major prolongation in contraction-relaxation interval detected in one sample.
[b] Elasticity of hydrogel transferring movement over a long distance interferes with beating analysis, so only one or two aggregates were analyzed successfully.

In the videos, it was possible to see how the cells pulled the hydrogel. First of all, this is proof that the cell aggregate has attached to the hydrogel as it can exert forces on the hydrogel network and deform it. Furthermore, this also shows that the hydrogel is mechanically compliant enough for the cardiac application because a material that is too stiff would not deform under the forces the cells can exert. This is especially important in the encapsulated 3D case, as an aggregate which is connected to its surroundings from all sides would not be able to move if the surrounding hydrogel would not move with it. As the compression measurements in **Chapter 5.3.** show, the hydrazone crosslinked gelatin-GG hydrogels were all mechanically biomimicking with heart tissue at small strains. The most biomimicking composition F5-CDH did not stand out in the cardiomyocyte tests. This was likely due to the other gels being elastic and compliant enough at small strains relevant for cell culture. However, if implanted in an actual heart for clinical TE, higher strains could be relevant and gelatin-CDH gels would be most attractive for initial tests.

6. Discussion

6.1. The need for hydrogels and 3D cell culturing methods

The best universal hydrogel formulation for soft TE or TE as a whole, has yet to be found. Moreover, the field of biomaterials science is constantly developing novel hydrogel designs to cover the needs of biologists and clinicians. A vast number of hydrogel forming polymers have been studied [Chirani et al., 2015] and quite many are also commercially available [Caliari, Burdick, 2016]. In fact, there are so many that it is already impossible to test all the published formulations for a specific cell culture application and even more difficult to follow all the advances in the field. Even just within polysaccharides, the number of published polymer combinations and hydrogel crosslinking strategies for compatibility with various cell types was already in the several hundreds ten years ago [Malafaya et al., 2007]. Moreover, when concentrating on just those hydrogel-containing studies with the aim of treating brain injuries, the number of base hydrogels is just around ten, but the number of published hydrogel combinations is over a hundred in total [Kornev et al., 2018]. It is therefore a relevant question whether more hydrogels are still needed.

When reviewing the literature, however, there are very few commercial TE products on the market and only a few that are currently in the clinical testing phase and being used by a few surgeons [Caliari, Burdick, 2016, Khademhosseini, Langer, 2016, Gomes et al., 2017, Missirlis, Vallet Regi, 2017, Langer, 2017]. Hence, the field of TE is concentrated on finding novel formulations with very little energy being aimed at the actual translation to clinical practice and commercialization. Indeed, when reviewing the published novel hydrogel formulations, the main focus is still on just proving that (A) the polymers crosslink to form a hydrogel and (B) that they are cytocompatible. At the moment, there is far too little progression from this initial stage to the actual use in a TE application and to finally help patients, which is and should be the ultimate goal.

So, when critically comparing **Publications I & III** to the literature, it can be said that we have the same fault of concentrating only on the initial stage of hydrogel development without advancing the development to actual applications. However, we can reject this criticism for a number of reasons. First, the bioamine crosslinked GG developed in **Publication I** provides a simple to use and relatively

cheap model hydrogel for the further development of hydrogel characterization methods, such as the ones developed in **Publications II & IV**, where it has been used. Moreover, because the standards in the field are still rather vague, the development and improvement of material characterization methods specifically relevant for hydrogels is important [ASTM F2900, 2011]. Second, the intended application of neural 3D cell culture is still lacking a scaffold material that would serve to fulfill all the needs, such as guided directional growth. Even though several other hydrogels have also been tested specifically in the application together with hPSC-derived neuronal cells [Ylä-Outinen et al., 2012, Hyysalo et al., 2017, Karvinen et al., 2018, Kornev et al., 2018], the best one for this specific indication has still to be found. The simple functionalization of bioamine-GG by mixing with laminin significantly enhances the cell response, mainly the length and amount of neurite spreading. The results conclusively show that the higher the amount of laminin in the hydrogel, the better the cell response. However, this creates a new problem because the price of laminin is currently too high for continuous and routine use of laminin functionalized bioamine-GG in amounts relevant for the applications of neurobiologists. Thus, the hydrogel formulation found most suitable for the neuronal application is still not in routine use for purely financial reasons. This is another aspect that should be taken into account during the early stages of hydrogel design. Either the final application in clinical TE needs to be vital enough to justify the material costs or cheaper production methods with scale-up possibilities need to be further researched.

However, the cell results shown in **Publication III** offer the promise of a highly usable hydrogel formulation. The elongation of fibroblasts in all the gelatin-GG compositions was already visible at day 3, or even earlier, and the 3D elongation seems to be of higher degree than many of the other recently published hydrogel studies that use fibroblasts for cytocompatibility testing [Gong et al., 2009, Coutinho et al., 2012, H. Shin et al., 2012, López-Cebral et al., 2013, Xu et al., 2018, M. Khan et al., 2018], and the same applies for quantified cell viability [Pacelli et al., 2016]. The feature we have in common with other published studies showing similar cell elongation results as ours is the functionalization of GG with gelatin or RGD [Wen et al., 2014, Koshy et al., 2016, Canadas et al., 2018, George et al., 2018]. Likewise, when using either mouse myoblasts [Ferris et al., 2015] or primary rat cardiomyocytes [Y. S. Zhang et al., 2016, K. Zhu et al., 2017] instead of fibroblasts, a similar improvement of cell response after ECM functionalization is seen. However, even with gelatin, if either the UV exposure during crosslinking or the shear stress during 3D bioprinting is too high, the advantageous effect can be negated, at least in the short term [H. Shin et al., 2012, Melchels et al., 2014, K. Zhu et al., 2017]. Thus, RGD, gelatin, collagen, or another ECM molecule with available cell attachment sites is needed for good cell response. This of course should be an obvious conclusion, but unfortunately, hydrogels are still developed without considering valid attachment sites for cells.

The above considerations lead to the rational design principles of hydrogels, which require a wholesome view of the application area. The design of hydrogels should at least take into consideration

the following points [Brandl et al., 2007, Geckil et al., 2010, Chen, Liu, 2016, Duan, 2017, Darnell, Mooney, 2017]:

1. Biocompatibility of both the polymer itself and the crosslinking strategy. The cells must survive the encapsulation and must have an adequate number of attachment sites to flourish. The cytocompatibility must also include enough attachment sites for the cells.

2. Gelation time and shelf-life of components.

3. Mechanical biomimicry combined with adequate strength to endure the forces in the intended application.

4. Microstructure and porosity suitable for the application, the larger the scaffold, the more important this becomes.

5. Biodegradability or stability depending on the application

6. Scalability of production and price in a range justifiable for the intended application.

7. Suitability to be used with the intended scaffold manufacturing method, for example, 3D-printability or injectability.

8. Transparency in the case of disease modeling, where cells need to be constantly monitored during the culture period.

Many of the methods to measure and quantify the aforementioned properties have been discussed elsewhere in this thesis, but how to conduct the rational design based on previous experiments and the literature? A rising trend in all fields of natural sciences is the use of artificial intelligence (AI) and automatization, both in experiment design as well as in data analysis and interpretation [A. Vasilevich, de Boer, 2018, Lan et al., 2018]. The use of AI-controlled robots to carry out repetitive tasks, such as pipetting multiple closely similar compositions or recording signals from the cells, allows scientists to concentrate on higher level decision-making and the formulation of the most relevant research questions. Making the menial tasks in the screening phase more automatic and increasing high-throughput allows more time for method development and creative work. [A. Vasilevich, de Boer, 2018] The biomedical field is already collecting vast amounts of data and utilizing data mining AI as part of bioinformatics to better understand the complex interplay of biological molecules [Lan et al., 2018]. Combining the materials science data held in libraries in a similar fashion to biological data is lagging behind genomics and other "omics", but the process has begun. Some examples of which are the Materials Genome Project [A. White, 2012, Jain et al., 2016] and the even more specific hydrogel combinatorial library [Vegas et al., 2016]. Screening can also be related to only the material properties, only the chemical properties of biomolecules, or on the cell-biomaterial interaction [Gomes et al., 2017, A. S. Vasilevich et al., 2017, Leijten et al., 2017].

Conducting hydrogel screening in an automatic fashion is one aspect, but the more interesting for rational design is the prediction of material properties. This can also greatly reduce the amount of

screening needed, if accurate predictions already rule out some compositions as being irrelevant. AI and data mining are of course important in the prediction of properties [A. Vasilevich, de Boer, 2018, Lan et al., 2018], but the algorithms behind AI do not always have to be too complex, as shown, for example, by Antoine *et al*. with tunable collagen hydrogels [E. E. Antoine et al., 2015]. The use of multidimensional image texture data for the prediction of hydrogel properties was also suggested in **Publication II**. Combining the analysis of texture properties of **Publication II** with the mechanical properties and neuronal cell culture results of **Publication I** has actually been conducted using regression analysis and mathematical neural network. However, the main conclusion of that study was that more data are needed for a meaningful analysis and prediction of properties. [Koivisto et al., 2018]

6.2. Challenges of mechanical testing

A new, opposing point to our hypothesis raised by the **Publication I** is that neuronal cells seemingly preferred a hydrogel stiffer than that generally reported to be suitable for neural applications. Importantly, however, many of the hydrogel studies where the mechanical properties of the material are studied together with neuronal cell culture use rheology as the characterization method. The shear modulus or storage modulus can sometimes be interpreted as elastic modulus, which should be a compressive or tensile property. This false comparison straight from shear modulus to compressive modulus, naming both of these as elastic moduli, gives a false impression of what exactly is the preferred stiffness for neuronal cells. [Callister, 2003, Flanagan et al., 2002, Levental et al., 2007, Discher et al., 2009, Pogoda et al., 2014, Budday et al., 2017, Antonovaite et al., 2018] So, when specifically comparing the brain compressive modulus, analyzed from engineering stress and strain, our reported modulus of 10 kPa (for rabbit brain) is actually smaller than a literature value of 17-25 kPa (for rat brain) [Karimi, Navidbakhsh, 2014]. Then again, multiaxial compression-shear measurements on actual human brain show a modulus of ~1 kPa with a note that compression yields higher moduli than shear or tension experiments [Budday et al., 2017]. Thus, as stated in **Publication I**, we are still in the correct stiffness range. Finite element simulations of human brain for neurosurgery have even used the same 10 kPa elastic modulus that we reported [Peña et al., 1999, Taylor, Miller, 2004]. Furthermore, the standard deviation between parallel measurements can be ± 5 kPa, both with hydrogels and with tissue samples, so the values should not be checked too rigorously. The small variations or errors can come from multiple sources, such as different measurement speed of viscoelastic material, anisotropy and the direction of testing, anatomical interspecies variations, and so on. Thus, our result of most observed neurite spreading in a 23 kPa hydrogel is not significantly different from the reported literature values [Peña et al., 1999, Taylor, Miller, 2004, Karimi, Navidbakhsh, 2014].

However, the discrepancy between the expected results and our observations resulted in a deeper study of analysis methods and mechanical models of compression testing specifically using bioamine-GG reported in **Publication IV** as well as by Karvinen *et al*. using hydrazone crosslinked HA-GG hydrogels [Karvinen et al., 2017, Karvinen et al., 2019]. First, an attempt to analyze the stiffness as a function of strain and as a second-order elastic constant was done [Brugger, 1964]. This method seems to work well for samples that do not fracture during the compression test, be they hydrogels or soft tissue [Karvinen et al., 2017]. However, when the sample does fracture during the test, it is more difficult to fit the polynomial equation on the stress-strain curve, or the polynomial fitting will arbitrarily change with the inclusion or exclusion of just a single measurement point around the fracture (data not shown). Thus, another method was developed to extract the compressive modulus out of the stress-strain curve. In **Publication IV**, more emphasis is put on the determination of the elastic deformation region, leading to the definition of the two elastic moduli E_1 for toe region and E_2 for the normally considered elastic region. The toe region itself is the initial part of a stress-strain curve that has been treated differently in the analysis in the literature. In simpler analysis, it is suggested to just be disregarded as a non-important nonlinear part of the curve [Bandyopadhyay, Bose, 2013, SFS-EN ISO 604, 2004]. However, as the toe region does biologically represent the phenomena of elastin fiber elongation, the modulus of the toe region has also been previously measured for some scaffolds [Gentleman et al., 2006, Furmanski, Chakravartula, 2011]. Furthermore, many soft tissues have a similarity with GG on the molecular level, GG being a double helix structure and collagen a triple helix. Thus, the three molecular interpretations of response to load, as explained in **Chapter 2.2.4.** Figure 8, are valid for all the samples, GG hydrogels, brain, and heart, studied here. Thus, the response to compression can be called biomimicking even on a molecular scale. [Chandrasekaran, Radha, 1995, H. Kang et al., 2009, Shoulders, Raines, 2009, Elzoghby, 2013] In addition, the barreling effect recorded by 3D-DIC in **Publication IV** can be interpreted as being caused by the molecular scale buckling effect of these semiflexible molecules.

As reviewed in **Chapter 2.2.4.** and reported by others as well, the applied mechanical model will naturally have an effect on the final modulus value [Oyen, 2014, Karimi, Navidbakhsh, 2014]. In **Publication IV**, based on Cauchy stress and Hencky strain [Hencky, 1928, Xiao et al., 2004], we report E_1 = 4.84 kPa and E_2 = 17.67 kPa for our model gel GG 1.10%SPM, while we report engineering stress and strain based modulus E = 22.6 kPa ($\approx E_2$) for the same material in **Publication I**. Based on this, the range in which the elastic modulus of GG 1.10%SPM can be rounded is from 15 to 25 kPa, but a more precise determination can be deemed unfeasible.

Interestingly from the biological point of view, the precise sensitivity of cells with regards to mechanotransduction is unknown. A highly relevant future study could focus on the local elastic modulus in some part of a hydrogel, more in the same range where the cells sense their environment, rather than testing the whole bulk material [Evans, Gentleman, 2014, Pogoda et al., 2014, Ferreira et al.,

2018, Antonovaite et al., 2018]. Measurements comparing macro- and microscale mechanical properties have recently been reported rheologically for a novel amino acid-based hydrogel, but not utilized with cells nor using GG- or gelatin-based hydrogels [U. A. Khan et al., 2018]. Comparisons of nanointendation or atomic force microscopy data with bulk compression testing for the exact same hydrogels and the use of those hydrogels as scaffolds for stem cell differentiation would be the key for both rational hydrogel design as well as for mechanotransduction studies [Galli et al., 2009]. Of course, the choice of applied mechanical model will also be the key in this suggested study as well.

Even though the importance of mechanical properties on the cell culture are evident, the situation with defining and standardizing the hydrogel mechanical testing methods is still lacking [ASTM F2900, 2011, Oyen, 2014, Evans, Gentleman, 2014]. The problem is two-fold. First, different measurement methods and parameters affect the results, as mentioned in **Chapter 2.2.4.** and in **Publication IV**. Second, the terminology used varies in this highly interdisciplinary field. One of the main problems is the various names of modulus used as the simple measure of stiffness. Synonymous or almost synonymous moduli include Young's modulus, elastic modulus, compressive modulus, tangent modulus, and secant modulus, all referring to static or relatively slow tests. Of these, Young's modulus is the most widely used and can refer to both tensile and compressive case as does elastic modulus, while compressive modulus refers only to compression. The tangent and secant moduli can be tensile or compressive because they only define the curve fitting method. Further away are the bulk modulus, which is used for confined compression, and shear modulus, which describes stiffness parallel to the sample surface, not perpendicular to it like tensile and compression moduli. [Callister, 2003] In rheological characterization, the mainly used measures are storage modulus, loss modulus, and complex modulus. [Schramm, 1998] However, the term plateau modulus is also sometimes used for storage and loss moduli in the LVER [U. A. Khan et al., 2018]. Similarly, instantaneous and equilibrium moduli describe dynamic conditions [Roberts et al., 2011]. Unfortunately, the terms elastic modulus and shear modulus are also sometimes used to describe the storage modulus, which is the main source of confusion when interpreting the mechanical testing results of biomaterials. [Normand et al., 2000, Flanagan et al., 2002]

The static measurement of elastic and shear modulus are coupled together via Poisson's ratio, a parameter that defines how the material deforms in the direction perpendicular to the measured deformation. However, in dynamic testing Poisson's ratio links together rheological storage modulus and elastic modulus for dynamic mechanical analysis, not between simple compression and rheology. [Callister, 2003] For both hydrogels and tissues [Normand et al., 2000, Antonovaite et al., 2018], including ionotropically crosslinked GG [J. Tang et al., 1996], Poisson's ratio is often assumed to be 0.5, indicating an isotropic incompressible material. This assumption is based on the incompressibility of water in the swollen hydrogels but might not be accurate due to poroelasticity [Nakamura et al., 2001, Cai et al., 2010]. Likewise, the assumption of material isotropy is more accurate for some

hydrogels than for others, as shown by our index of homogeneity in **Publication II**. However, Poisson's ratio can be also measured, for example, by using poroelasticity theory [Cai et al., 2010], non-linear elasticity theory [Lane et al., 2018], by combining unconfined and confined compression [Moresi, Bruno, 2007], or by 3D-DIC [Palanca et al., 2016, Lane et al., 2018] for a more accurate characterization. The analysis of the Poisson's ratios of our hydrogels is one interesting future step after **Publication IV**. Likewise, the dynamic mechanical response should be analyzed further. Even though the rheology of bioamine-GG hydrogels was briefly analyzed in **Publication I** and a stress relaxation method was proposed in **Publication IV**, similar studies are needed on both the highly cytocompatible gelatin-GG of **Publication III** as well as on control tissue for a comprehensive understanding of the mechanotransduction and mechanical properties of hydrogels.

The main specific problem for hydrogel material development is that they are not yet widely used as bulk, true gels in many commercial applications, and thus the standardization of the testing methods related to these materials is still lacking [Oyen, 2014, Evans, Gentleman, 2014, A. S. Vasilevich et al., 2017]. For example, the ASTM F2900 "Standard Guide for Characterization of Hydrogels used in Regenerative Medicine" combines several relevant standards, but these are either too superficial on details or too specific for a single material type. A middle ground of generalized methods, but under a specific testing category, such as mechanical testing, is still, however, missing. [ASTM F2900, 2011] Another example, the ASTM F2150 "Standard Guide for Characterization and Testing of Biomaterial Scaffolds Used in Tissue-Engineered Medical Products" lists many more specific method-standards, but these standards primarily assume rigid polymers or metals and ceramics as the material groups to be studied, and therefore are not valid in the case of soft hydrogel materials. [ASTM F2150, 2013] Thus, the main standard concerning mechanical testing that is suitable for hydrogels is the ISO 640 "Plastics – Determination of Compressive Properties", which was adhered to for the applicable parts in **Publications I, III**, and **IV**, even though it also assumes a rigid polymer [SFS-EN ISO 604, 2004]. For the scope of this thesis, the standards that are useful specifically for hydrogel biomaterial development are the ones that concern biological evaluation and biocompatibility [SFS-EN ISO 10993-5, 2009, ASTM F2150, 2013].

As has been discussed by others in the literature as well [Oyen, 2014, Yue et al., 2015], the reproducibility of the mechanical characterization of hydrogels between research groups, even for the same formulations, is lacking, and is mainly due to the non-standardized testing and analysis methods employed. The example of how the reported modulus of a simple agar hydrogel can vary over three magnitudes in the literature is a grave reason why more standardization is needed [Oyen, 2014]. This variation is partially the result of comparing different moduli with each other, and highlights why it is important to only compare mechanical testing results with exactly the same setups and parameters. Combining this with the reported variability in the mechanical properties of soft tissue, such as brain and heart [Levental et al., 2007], it was an important decision to include the self-measured properties of rabbit brain and heart tissue in **Publications I** and **III** for a relevant

comparison between the developed hydrogels and the target tissue. Furthermore, as we performed a study on the effects of measurement parameters on material response in **Publication IV**, we also produced a suggested compression measurement protocol for hydrogel studies, presented in **Appendix III**.

Finally, the carrying out of reproducible mechanical testing on both hydrogels and tissues leads back to the rational design [Brandl et al., 2007]. Once the cell requirements for cytocompatibility and mechanotransduction have been defined together with a standardized mechanical testing method, we can start using AI as the next step in rational hydrogel design [D. F. Williams, 2017, Walters, Gentleman, 2015, Oyen, 2014, A. Vasilevich, de Boer, 2018]. An understanding of the mechanical properties is also directly linked to the microstructure of the hydrogel. For example, the reported prediction of collagen scaffold deformation during cell culture helps determine the change in mechanical properties as well as the effect on cells over time [Raub et al., 2010]. Likewise, an interesting aspect would be to find deeper connections between crosslinking strategies and mechanical properties, especially between physical and chemical crosslinking, as both are relevant for our GG [Roberts et al., 2011]. **Publication II** is already aiming towards this, but further studies are needed to find a correlation between mechanical properties and observed microstructure and density variations.

6.3. Defining hydrogel microstructure, mesh size, and porosity

The microstructure of a TE scaffold has multiple roles and is generally one of the quantified properties when developing new scaffolds. As stated in the previous chapter, microstructure and mechanical properties are always linked together. It is therefore very difficult to study only the effect of the microstructure on cells without changing the mechanical properties, even though attempts at this have been made using PAA hydrogels or PDMS films [Pelham, Wang, 1997, A. J. Engler et al., 2004, Trappmann et al., 2012]. If a hydrogel is only used as a 2D substrate with cells cultured on top of it, this can work. However, in 3D encapsulated conditions, the microstructure is changed because of the smaller crosslinking density when producing a less stiff material. Moreover, the number and density of attachment sites for cells likely varies as well when the crosslinking changes, which will affect cell response as well. Then, if a cell has more sites to attach to, does it behave differently than with fewer attachment sites? It is likely that the cell spreading is affected by the ability to form fewer or more focal adhesions. Thus, it is difficult to study mechanotransduction independently of microstructure. [Trappmann et al., 2012, Evans, Gentleman, 2014] It has, however, also been shown with rat smooth muscle cells that substrate stiffness can override the effect of attachment site density over a specific range, this just needs to be verified case-by-case [A. Engler et al., 2004]. Another interesting result with human MSCs in a PEG-based hydrogel has been reported that crosslinking density has a clear effect on differentiation, but it is uncertain whether this is due to stiffness, microstructure, or a combination thereof [Ferreira et al., 2018].

Due to the link between mechanical properties and microstructure, our main approach was to measure and quantify the properties of our newly designed hydrogels and to see if the crosslinking had linearly proportional dependencies on these properties. To study the microstructure of GG hydrogels, the OPT-based methods developed in **Publication II** were highly efficient. The mass transport velocities of different dextran molecules first of all showed that a neutral 20 kDa molecule travels rather quickly and easily through the hydrogel network, while over 150 kDa molecules are hindered significantly more. Then, the 2000 kDa is another step slower in mass transport. The calculated hydrodynamic radius of these molecules are 2.8 nm, 8.0 nm, and 30.8 nm, for the 20 kDa, 150 kDa, and 2000 kDa dextran molecules, respectively [Karvinen et al., 2019]. Thus, we now know that all our tested bioamine-GG hydrogels have a mesh size at least over 2.8 nm. Furthermore, there are also larger openings in the mesh or pores, corresponding to both over 10 nm and over 30 nm sizes. These results are important from the point of nutrient diffusion, as most of them are small molecules and even growth factors are around the 20 kDa size, so we can be sure that the hydrogel network is not preventing nutrients from reaching the cells [Leddy, Guilak, 2003]. However, this mass transport analysis does not take into account the effect of charge and other molecular affinities, as dextrans are neutral, so no reactions between them and GG are expected [Venturoli, Rippe, 2005]. Similar measurements for gelatin-GG hydrogels have not yet been carried out, but they should be conducted in future.

Another important aspect is cell migration, spreading, and growth. The hydrogel network needs, for example, to allow neurite extension and growth through it, as studied in **Publication I**. For cells more prone to migration, the hydrogel should either have big enough pores for the movement or have cell-degradable crosslinks or MMP-sites [Leijten et al., 2017]. Cell movement might be controlled, for example, by a stiffness gradient, such as in durotaxis [Hadden et al., 2017, Nemir, West, 2010], or by a chemical gradient of either bound or diffusing molecules, such as in chemotaxis [D. F. Williams, 2017]. To guide the cell migration and tissue formation, several dynamically changing hydrogel systems have been designed, for example, with controlled network degradation [Leijten et al., 2017, Canadas et al., 2018, Ferreira et al., 2018]. However, in **Publication III**, we did not modify the degradation rate, and only verified that the hydrazone crosslinked gelatin-GG was degradable by collagenase.

The usefulness of transmission OPT in the imaging of hydrogel texture was a very novel finding in **Publication II** because, to the best of our knowledge, we are the only ones using OPT for material characterization purposes. While studying the scaffolds of rigid polymers with μCT or SEM and quantifying their porosity is a standard practice [L. E. Smith et al., 2010, Cengiz et al., 2018], the potential of OPT as a 3D hydrogel characterization method has not previously been fully realized. While our study shows how the different hydrogel formulations can be distinguished from each other via image texture analysis, a more interesting future study would be to combine the analysis of the texture causing density variations with a more thorough crosslinking and biodegradation study. In this way,

we would see the macroscopic, or at least mesoscopic, changes in the microstructure over time. This is comparable to studying the turbidity of hydrogels when formulating them. Indeed, our image texture analysis could be called 3D turbidity analysis [Lau et al., 2000]. Combining the image texture properties with mechanical characterization is another relevant future study that would just need many parallel samples to reach statistically significant results [Koivisto et al., 2018].

Similar imaging studies have been conducted with μCT on the texture of a gelatin-based scaffold [Massai et al., 2014]. However, like all μCT studies on hydrogels, the gels were studied in freeze-dried form and not in the water-swollen state. This is mainly due to the limitations of contrast and resolution to detect a polymer molecular mesh [Massai et al., 2014, Cengiz et al., 2018]. As stated earlier, studying the porosity of a freeze-dried gel makes sense only when the final application will also use freeze-drying as part of the scaffold manufacturing process [Alemán et al., 2009, García-González et al., 2011]. The mixing of gels to be used for studying material properties in wet and dry states is one of the major problems in the field of hydrogel development. It is essential therefore that the final application should always determine how and in which phase the hydrogel material characteristics are studied.

6.4. The future of clinical tissue engineering

Even though the concept of TE was presented already in the 1990s, very few TE-based clinical therapies are in routine use, and the current number of clinical trials using stem cell containing treatments is rather modest [Langer, Vacanti, 1993, Place et al., 2009, Trounson, McDonald, 2015, Cossu et al., 2018]. There are multiple reasons for this slow uptake. One major problem is that TE is not exactly recognized by our current healthcare system and regulatory agencies because the implantation of cells inside a scaffold has a different kind of effect on the patient than only an implant or only a drug would have [D. F. Williams, 2004, SFS-EN ISO 10993-1, 2009, ASTM F2900, 2011]. Another problem is the lack of investments needed for clinical translation due to the challenges in immaterial property rights and patenting [Cossu et al., 2018]. Furthermore, not all studies that have progressed to clinical trials have reached their goals. Common causes of failure include poor survival of the cells, a minor or superficial therapeutic effect, and too high hopes on MSC functionality [Trounson, McDonald, 2015, Madonna et al., 2016]. Even some widely used hydrogel implants without a living cell component have been reported to fail in small but significant numbers in long-term studies. The polymer with the most reported problems is PAA. This polymer seems to have first progressed to wider clinical use in countries with less strict regulations and then progressed to wider use. The use of PAA in plastic surgery for both breast reconstruction and facial soft tissue augmentation has mainly caused problems due to implant migration or breakage under the skin and to a smaller degree due to infections. [Manafi et al., 2010, Shen et al., 2012, Patlazhan et al., 2013] Thus, while the

regulation of true TE is still coming, there is still work and optimization to be done in hydrogel development alone, as discussed in the previous chapters.

Regardless of finding the best hydrogel compositions for each application, a few trends are affecting the outlook of therapeutic clinical TE and guiding the field. One of the most important current trends in the field of materials science is 3D printing, which is also termed general additive manufacturing. In biomedical applications, 3D printing is used for high complexity samples, patient-specific customization, and small production sets [Ngo et al., 2018]. When samples that contain living cells are produced, it is called 3D bioprinting. The development of machines for 3D bioprinting has been rapid and there has already been reported a human-scale TE scaffold printer with combined translation of clinical images into printable files [Gomes et al., 2017]. This was demonstrated to be able to produce bone, cartilage, and skeletal muscle using tissue-specific cells or stem cells. The hydrogel or bioink used was composed of varying concentrations of gelatin, fibrinogen, and HA [H. Kang et al., 2016]. Another example is peripheral nerve regeneration, where a GelMA scaffold with primary neuronal cells and added growth factor release functionality has already been tested in rats [Johnson et al., 2015]. Likewise, in the cardiac field, myocardial tissue, heart valves, and vasculature have already been printed [Duan, 2017]. Compared to above extrusion based 3D printing examples, laser-based printing allows higher contrast and finer details, as has been shown in neural application [Turunen et al., 2017]. Furthermore, when designing biodegradable or otherwise dynamically changing hydrogels, the time-element has even been called 4D printing [Bakarich et al., 2015, Leijten et al., 2017].

As 3D bioprinting is seen as one of the main uses of hydrogels in TE, a lot of research has concentrated on the printability and optimization of novel hydrogel bioinks [Gomes et al., 2017, Paxton et al., 2017]. However, sometimes this 3D printing hype also causes exaggeration to just fit in this category, such as a "hand-held 3D printer", which is essentially a slightly better controlled pipette [Lozano et al., 2015]. Another consequence of the 3D printing hype is that the remarkable ability to produce highly complex shapes is not used. Instead, the printed scaffolds are either just log-house type lines on top of each other or only droplets in a series or pattern. The printing of droplets can of course be useful for HTS in material development. However, printing that results in these simple shapes, and especially with some lower quality 3D printers, could be easily replicated with a pipette in a steady hand. This partial use of the full potential of the technology can be attributed to just the printability being tested and not the final applications. Thus, the field still seems to be stagnating and not demanding that the real potential of the technology be realized. [Gomes et al., 2017] Regardless of the unreached potential, there are also real challenges for 3D printing, which at least include regulatory issues and quality control as well as finding the correct balance between all the relevant material properties together with cytocompatibility [Geckil et al., 2010, Duan, 2017, Ngo et al., 2018].

Another trend in the biomedical field is personalized medicine [Gomes et al., 2017]. The relatively recent iPSC technology is surpassing the use of hESCs in studies aiming for clinical outcome. iPSCs

can be taken from any patient, cultured, and expanded *in vitro* and then transplanted back into the patient. The possibility to use the patient's own cells for regeneration is one of the major advantages of iPSCs because they are autologous, and thus there is no risk of immunorejection [Yamanaka, 2012, Madonna et al., 2016, Cossu et al., 2018]. Furthermore, iPSC technology could be used to produce exactly the cells the patient needs in correct phase of differentiation and combined with 3D bioprinting to produce an implant shape that exactly matches the defect a patient has. [Khademhos-seini, Langer, 2016, Gomes et al., 2017] Additionally, the advances in direct reprogramming from one somatic cell to another, without the intermediary stem cell state, is also progressing fast [S. Zhu et al., 2015]. This could bring down the price and time requirements of current iPSC-based TE ther-apies, which are the main drawbacks at present [Monteiro et al., 2016]. Another solution to ease the laborious iPSC technology for single patient treatment is to not use autologous cells, but instead to collect a library of immunologically matching cells based on human leukocyte antigen type, similar to everyday blood donor types [Monteiro et al., 2016, Cossu et al., 2018].

Other challenges of stem cell-based therapeutic TE include standardization issues, quality control, regulation, and relevant control samples or blind studies. Even the patient selection for first phase clinical trials has recently been recognized as one possibly problematic issue, since co-morbidities and co-medication can have a significant effect on the success of treatment. [Madonna et al., 2016, Cossu et al., 2018] The tendency to start initial tests with more hopeless patient cases can cause a TE implant to fail, even if it would have functioned perfectly on a patient with better overall health [Cossu et al., 2018].

6.5. The future of disease modeling

Personalized medicine and the need for better models are the main driving forces behind the cur-rently rising interest in disease modeling. The numerous possibilities in disease modeling opened up by the invention of iPSC technology was mentioned by Takahashi *et al.* in the first hiPSC study [Takahashi et al., 2007]. Even if genetic alteration makes the implantation of hiPSC back into the patient too risky, the patients can benefit from drug discovery based on cell models of genetic dis-eases with the exact same genetic background as the living patient, combined with the patient's medical records [Penttinen et al., 2015]. In addition, another trending approach is to correct the dis-ease-causing mutation with CRISPR-Cas9 gene editing technology and to compare how the patient-specific cells behave as a corrected, isogenic control cell line in the same conditions [Doudna, Char-pentier, 2014]. Finding drugs via this route is the main point of personalized medicine. As disease modeling is currently in a steadily advancing phase, with almost all somatic cell types being produced *in vitro* from the hiPSC, the reports of *in vitro* recapitulated disease-phenotypes are advancing at the same speed. [Robinton, Daley, 2012, Fang, Eglen, 2017] However, the next steps needed for major future breakthroughs are the transition from 2D culture on the well plate bottom into a biomimicking

3D culture and the transition from single cell studies to organ- and tissue-scale studies. These can better take into account the systemic effects and metabolic pathways because studying a single drug molecule on a single cell can only solve a very limited number of disease cases. [Langley et al., 2016, Fang, Eglen, 2017, Cossu et al., 2018, B. Zhang et al., 2018]

Studying the pathways and better controlling how the molecules of interest reach particular cells is the main point of the microfluidic devices used for organ-on-chip studies. When further combining multiple organs on the same chip, the system can be called body-on-chip or human-on-chip. [Chung et al., 2011, Huh et al., 2011, Nam et al., 2015, B. Zhang et al., 2018] For example, combining endothelial cell membrane with neurons and vasculature could be used to study the barrier properties of the blood-brain-barrier. Likewise, combining hepatocytes via vasculature to other tissue-specific cells, such as cardiomyocytes, could be used to study drug metabolism in the liver and the effect of the metabolites on the final application site. [Langley et al., 2016, B. Zhang et al., 2018] To produce these larger tissue blocks and organoids from single cells, ECM is needed [Shah, Singh, 2017]. There are 3D culture systems, such as the hanging drop method, which do not incorporate an external scaffold but instead rely only on the ECM produced by the cells [Fang, Eglen, 2017]. However, the scale reachable by these methods is limited because the diffusion of nutrients through a dense cell mass is often not sufficient. Thus, a more appealing method is to produce a tissue block with ingrown vasculature, all inside an ECM biomimicking hydrogel scaffold [Ikonen et al., 2013, Fang, Eglen, 2017]. In the ideal organ-on-chip systems, all these culture conditions are controlled and independently changeable by the researcher, so that in addition to just cellular interactions, we can also study, for example, the effect of oxygen concentration or temperature on cell functioning [Katipparambil Rajan et al., 2018, B. Zhang et al., 2018].

Including the cell-cell and cell-ECM interactions into the models will also make them more complex to handle. Here, the rational design principles come into play again, i.e., the complexity should be controlled and too many unknown variables should not be added, which could be seen as one reason for the very slow translation of TE into clinical use [D. F. Williams, 2017]. Even more, the disease model systems should be designed so that the cells not only behave correctly, but that they can also be monitored in various ways throughout the culture period. As many of the current methods to study cells were originally developed with 2D culture in mind, the transitions of the methods simultaneously with the cell culture systems to 3D is on its own a challenging task. [Appel et al., 2013, Nam et al., 2015, Caicedo et al., 2017] For example, when comparing the microscopy methods used in **Publication I** and **Publication III**, it is clear that OPT is a useful method for mesoscale imaging and larger volumes, while confocal microscopy functions very well when the distances are not more than roughly one hundred micrometers [L. E. Smith et al., 2010]. In addition to the rather static immunocytochemistry, the study of the functions of dynamic cells using electrophysiological methods is highly required from a successful disease model [Langley et al., 2016, Wallis et al., 2018]. Out of these, calcium imaging has been done the longest for 3D cultures [O'Connor et al., 2000]. Other

methods commonly used in 2D electrophysiological recordings include patch clamp, microelectrode array, traction force microscopy, nanoscale indentation or probing, and video microscopy, either combining some of these or using them separately [Laurila et al., 2016, Björk et al., 2017, C. Prajapati et al., 2018]. Of these, we only used video recordings for 3D cardiomyocyte cultures in **Publication III**, but the functional studies of 3D neuronal cultures are also coming in the future. Furthermore, for disease models to be actually useful for the pharmaceutical industry, they need to be HTS compatible, as the numbers of drug molecules screened can easily be too high for manual screening [Nam et al., 2015, Mathur et al., 2015, Laurila et al., 2016, Kopljar et al., 2018, Mäkinen et al., 2018].

Once the complexity of combining 3D cell culture systems with microfluidic platforms and measurement methods is solved, yet another aspect to consider will be the maturity of the differentiated cells. There is agreement in both the neural and cardiac fields that differentiated cells need to be in a sufficient maturation state before they can be useful in disease modeling. [Quadrato et al., 2016, Feric, Radisic, 2016, Tan, Ye, 2018] In addition, the cell characterization needs to be accurate enough to distinguish between various cell subtypes and to know what cells are being used [Quadrato et al., 2016, Madonna et al., 2016]. Currently, the differentiated cells, such as the ones used in **Publications I** and **III**, are mature enough to have some spontaneous electrophysiological functions. However, they still do not resemble adult cells, but rather a fetal phenotype, and not extensively screened for subtype [Ylä-Outinen et al., 2012, Vuorenpää et al., 2017]. As many aspects of the cells, such as morphology, electrophysiology, and metabolism, do not fully represent the mature patient cells, the discovered drug effects can also differ between cell studies and clinical studies [Quadrato et al., 2016, Feric, Radisic, 2016]. To solve this problem, multiple stimulation methods have been studied to speed up the cell maturation process, and one of the suggested options is 3D culture and its physical cues, such as mechanotransduction and morphology orientation along a topography [Quadrato et al., 2016, Feric, Radisic, 2016, Tan, Ye, 2018]. This is one of the main reasons why the transition of disease modeling into 3D is so important.

One further trend that is extending from material design to disease modeling is computational disease modeling. Once the amount of data and variables becomes too large to handle manually, the bioinformatics and computational methods come in very handy. They can be used, for example, for the formulation of complex genetic and proteomic pathway analysis and for distinguishing the most important parameter changes. [Nam et al., 2015, A. S. Vasilevich et al., 2017] These methods have already been reported for both the analysis of hiPSC-derived neuronal network maturation [Lenk et al., 2016] as well as for the calcium handling of hiPSC-derived cardiomyocytes [Paci et al., 2018] in the 2D case. Computational modeling is also recognized as one of the key objectives of CiPA for the development of drugs without risks for cardiotoxicity [Wallis et al., 2018]. The obvious next step to advance these models is to apply 3D cell culture data and compare it with 2D culture.

7. Conclusions

The aim of this thesis was to develop and produce hydrogels for 3D cell culturing of neuronal and cardiac cells. Hydrogel biomaterials were developed based on the gellan gum polysaccharide, using both physical and chemical crosslinking strategies. The cytocompatibility of the hydrogel as well as of the crosslinking reaction was verified and functionalization with ECM proteins was deemed necessary for enhanced, positive cell response. The developed hydrogels are compatible with cell encapsulation in 3D inside the hydrogels, with the possible future aim towards disease modeling or clinical therapeutic tissue engineering in soft tissue applications.

The main findings and conclusions of each **Publication** are listed briefly below:

Publication I:

1. The bioamines SPD and SPM are suitable and cytocompatible crosslinkers for GG.

2. The mechanical properties of bioamine crosslinked GG hydrogels are in the relevant range for brain tissue.

3. hPSC-derived neuronal cells survive the crosslinking process and encapsulation inside bioamine-GG hydrogel.

4. Laminin functionalization, even just via simple mixing, is required for the desired neuronal cell response, the neurite spreading. However, too high a laminin concentration is needed for the routine use of the material to be feasible.

Publication II:

1. OPT is both a suitable and a highly valuable method for studying hydrogels. The transmission OPT of plain hydrogels can be used with Haralick's textural features and MDA to distinguish between different hydrogel formulations,

whether physically or chemically crosslinked or whether chemically modified or in the native state.

2. Fluorescent OPT can be used to study mass transport through a hydrogel in macroscopic scale.

3. The movement pattern of fluorescent molecules inside a hydrogel can be used to determine an index of homogeneity, a tool for the characterization of anisotropy.

Publication III:

1. Hydrazone crosslinking, either with ADH or CDH, is a suitable method for the production of gelatin biofunctionalized GG hydrogels.

2. Gelatin-GG hydrogels are much more elastic than the rather brittle bioamine-GG. The compression response of CDH-crosslinked gelatin-GG closely resembles the compression response of heart tissue.

3. Gelatin functionalization greatly enhances the cell response in GG-based gel. Fibroblast cells elongate in 3D and their viability goes up compared with bioamine-GG.

4. The spontaneous, phenotypical beating behavior of hiPSC-derived cardiomyocytes is retained in 3D culture inside gelatin-GG, regardless of the specific hydrazone crosslinking used.

5. The cardiomyocyte beating behavior can be analyzed in detail using the Beat-View® video analysis tool. The beating behavior is not altered by transfer from 2D culture to 3D, and thus this provides a promising platform for the development of disease modeling.

Publication IV:

1. A simple compression testing protocol with detailed, defined parameters was devised and is presented in **Appendix III**.

2. A new bi-phasic material model for the analysis of elastic modulus is presented.

3. 3D-DIC is a suitable method for enhancing the information gained from the compression testing of hydrogels.

References

Ahola, A., Kiviaho, A.L., Larsson, K., Honkanen, M., Aalto-Setälä, K. & Hyttinen, J. 2014, "Video Image-Based Analysis of Single Human Induced Pluripotent Stem Cell Derived Cardiomyocyte Beating Dynamics using Digital Image Correlation", *BioMedical Engineering OnLine,* vol. 13, no. 1, pp. 39-57.

Akopian, V., Andrews, P.W., Beil, S., Benvenisty, N., Brehm, J., Christie, M., Ford, A., Fox, V., Gokhale, P.J., Healy, L., Holm, F., Hovatta, O., Knowles, B.B., Ludwig, T.E., McKay, R.D.G., Miyazaki, T., Nakatsuji, N., Oh, S.K.W., Pera, M.F., Rossant, J., Stacey, G.N. & Suemori, H. 2010, "Comparison of Defined Culture Systems for Feeder Cell Free Propagation of Human Embryonic Stem Cells", *In Vitro Cellular & Developmental Biology - Animal,* vol. 46, no. 3, pp. 247-258.

Alemán, J.V., Chadwick, A.V., He, J., Hess, M., Horie, K., Jones, R.G., Kratochvíl, P., Meisel, I., Mita, I., Moad, G., Penczek, S. & Stepto, R.F.T. 2009, "Definitions of Terms Relating to the Structure and Processing of Sols, Gels, Networks, and Inorganic-Organic Hybrid Materials (IUPAC Recommendations 2007)", *Pure and Applied Chemistry,* vol. 79, pp. 1801-1829.

Antoine, E.E., Vlachos, P.P. & Rylander, M.N. 2015, "Tunable Collagen I Hydrogels for Engineered Physiological Tissue Micro-Environments", *PloS One,* [Online], vol. 10, no. 3, Article ID e0122500.

Antoine, L., Isabelle, D. & Pascale, G. 2012, "Catecholaminergic Polymorphic Ventricular Tachycardia", *Circulation: Arrhythmia and Electrophysiology,* vol. 5, no. 5, pp. 1044-1052.

Antonovaite, N., Beekmans, S.V., Hol, E.M., Wadman, W.J. & Iannuzzi, D. 2018, "Regional Variations in Stiffness in Live Mouse Brain Tissue Determined by Depth-Controlled Indentation Mapping", *Scientific Reports,* vol. 8, no. 1, pp. 12517.

Appel, A.A., Anastasio, M.A., Larson, J.C. & Brey, E.M. 2013, "Imaging Challenges in Biomaterials and Tissue Engineering", *Biomaterials,* vol. 34, no. 28, pp. 6615-6630.

Arslantunali, D., Dursun, T., Yucel, D., Hasirci, N. & Hasirci, V. 2014, "Peripheral Nerve Conduits: Technology Update", *Medical Devices: Evidence and Research,* vol. 7, pp. 405-424.

Asthana, A. & Kisaalita, W.S. 2013, "Biophysical Microenvironment and 3D Culture Physiological Relevance", *Drug Discovery Today,* vol. 18, no. 11–12, pp. 533-540.

ASTM F2150 2013, *Standard Guide for Characterization and Testing of Biomaterial Scaffolds used in Tissue-Engineered Medical Products,* ASTM International, West Conchoken, PA, USA.

ASTM F2900 2011, *Standard Guide for Characterization of Hydrogels used in Regenerative Medicine,* ASTM International, West Conchoken, PA, USA.

ASTM F748 2010, *Standard Practise for Selecting Generic Biological Test Methods for Materials and Devices,* ASTM International, West Conchoken, PA, USA.

Atala, A., Bauer, S.B., Soker, S., Yoo, J.J. & Retik, A.B. 2006, "Tissue-Engineered Autologous Bladders for Patients Needing Cystoplasty", *The Lancet,* vol. 367, no. 9518, pp. 1241-1246.

Aurand, E.R., Lampe, K.J. & Bjugstad, K.B. 2012, "Defining and Designing Polymers and Hydrogels for Neural Tissue Engineering", *Neuroscience Research,* vol. 72, no. 3, pp. 199-213.

Avasthi, S., Srivastava, R.N., Singh, A. & Srivastava, M. 2008, "Stem Cell: Past, Present and Future - A Review Article", *Internet Journal of Medical Update,* vol. 3, no. 1, pp. 22-30.

Axelrod, D., Koppel, D.E., Schlessinger, J., Elson, E. & Webb, W.W. 1976, "Mobility Measurement by Analysis of Fluorescence Photobleaching Recovery Kinetics", *Biophysical Journal,* vol. 16, no. 9, pp. 1055-1069.

Bacelar, A.H., Silva-Correia, J., Oliveira, J.M. & Reis, R.L. 2016, "Recent Progress on Gellan Gum Hydrogels Provided by Functionalization Strategies", *Journal of Materials Chemistry B,* vol. 4, no. 37, pp. 6164-6174.

Bakarich, S.E., Gorkin, R., Panhuis, M.i.h. & Spinks, G.M. 2015, "4D Printing with Mechanically Robust, Thermally Actuating Hydrogels", *Macromolecular Rapid Communications,* vol. 36, no. 12, pp. 1211-1217.

Bandyopadhyay, A. & Bose, S. (eds) 2013, *Characterization of Biomaterials*, Elsevier, [Online Publication].

Basu, A., Wen, Q., Mao, X., Lubensky, T.C., Janmey, P.A. & Yodh, A.G. 2011, "Nonaffine Displacements in Flexible Polymer Networks", *Macromolecules,* vol. 44, no. 6, pp. 1671-1679.

Belay, B., Koivisto, J.T., Vuornos, K., Montonen, T., Koskela, O., Lehti-Polojärvi, M., Miettinen, S., Kellomäki, M., Figueiras, E. & Hyttinen, J. 2018, "Optical Projection Tomography Imaging of Single Cells in 3D Gellan Gum Hydrogel", *IFMBE Proceedings,* vol. 65, pp. 996-999.

Berkowitch J., Charlesby A. & Desreux V. 1957, "Radiation Effects on Aqueous Solutions of Polyvinyl Alcohol", *Journal of Polymer Science,* vol. 25, no. 111, pp. 490-492.

Bhattacharya, M., Malinen, M.M., Lauren, P., Lou, Y., Kuisma, S.W., Kanninen, L., Lille, M., Corlu, A., GuGuen-Guillouzo, C., Ikkala, O., Laukkanen, A., Urtti, A. & Yli-perttula, M. 2012, "Nanofibrillar Cellulose Hydrogel Promotes Three-Dimensional Liver Cell Culture", *Journal of Controlled Release,* vol. 164, no. 3, pp. 291-298.

Biot, M.A. 1941, "General Theory of Three-dimensional Consolidation", *Journal of Applied Physics,* vol. 12, no. 2, pp. 155-164.

Björk, S., Ojala, E.A., Nordström, T., Ahola, A., Liljeström, M., Hyttinen, J., Kankuri, E. & Mervaala, E. 2017, "Evaluation of Optogenetic Electrophysiology Tools in Human Stem Cell-Derived Cardiomyocytes", *Frontiers in Physiology,* vol. 8, no. 884, pp. 1-14.

Bonifacio, M.A., Cometa, S., Cochis, A., Gentile, P., Ferreira, A.M., Azzimonti, B., Procino, G., Ceci, E., Rimondini, L. & De Giglio, E. 2018, "Antibacterial Effectiveness Meets Improved Mechanical Properties: Manuka Honey/Gellan Gum Composite Hydrogels for Cartilage Repair", *Carbohydrate Polymers,* vol. 198, pp. 462-472.

Bonifacio, M.A., Gentile, P., Ferreira, A.M., Cometa, S. & De Giglio, E. 2017, "Insight into Halloysite Nanotubes-Loaded Gellan Gum Hydrogels for Soft Tissue Engineering Applications", *Carbohydrate Polymers,* vol. 163, pp. 280-291.

Brandl, F., Sommer, F. & Goepferich, A. 2007, "Rational Design of Hydrogels for Tissue Engineering: Impact of Physical Factors on Cell Behavior", *Biomaterials,* vol. 28, no. 2, pp. 134-146.

Breslin, S. & O'Driscoll, L. 2013, "Three-Dimensional Cell Culture: The Missing Link in Drug Discovery", *Drug Discovery Today,* vol. 18, no. 5–6, pp. 240-249.

Bruckner, P. 2009, "Suprastructures of Extracellular Matrices: Paradigms of Functions Controlled by Aggregates rather than Molecules", *Cell and Tissue Research,* vol. 339, pp. 7-18.

Brugger, K. 1964, "Thermodynamic Definition of Higher Order Elastic Coefficients", *Physical Review,* vol. 133, no. 6, pp. A1611-A1612.

Budday, S., Sommer, G., Birkl, C., Langkammer, C., Haybaeck, J., Kohnert, J., Bauer, M., Paulsen, F., Steinmann, P., Kuhl, E. & Holzapfel, G.A. 2017, "Mechanical Characterization of Human Brain Tissue", *Acta Biomaterialia,* vol. 48, pp. 319-340.

Buwalda, S.J., Boere, K.W.M., Dijkstra, P.J., Feijen, J., Vermonden, T. & Hennink, W.E. 2014, "Hydrogels in a Historical Perspective: From Simple Networks to Smart Materials", *Journal of Controlled Release,* vol. 190, pp. 254-273.

Caccavo, D. & Lamberti, G. 2017, "PoroViscoElastic Model to Describe Hydrogels' Behavior", *Materials Science and Engineering: C,* vol. 76, pp. 102-113.

Cai, S., Hu, Y., Zhao, X. & Suo, Z. 2010, "Poroelasticity of a Covalently Crosslinked Alginate Hydrogel Under Compression", *Journal of Applied Physics,* vol. 108, no. 11, pp. 113514.

Caicedo, J.C., Cooper, S., Heigwer, F., Warchal, S., Qiu, P., Molnar, C., Vasilevich, A.S., Barry, J.D., Bansal, H.S., Kraus, O., Wawer, M., Paavolainen, L., Herrmann, M.D., Rohban, M., Hung, J., Hennig, H., Concannon, J., Smith, I., Clemons, P.A., Singh, S., Rees, P., Horvath, P., Linington, R.G. & Carpenter, A.E. 2017, "Data-Analysis Strategies for Image-Based Cell Profiling", *Nature Methods,* vol. 14, pp. 849.

Caliari, S.R. & Burdick, J.A. 2016, "A Practical Guide to Hydrogels for Cell Culture", *Nature Methods,* vol. 13, no. 5, pp. 405-415.

Callister, W.D. 2003, *Materials Science and Engineering: An Introduction,* 6th edn, John Wiley & Sons, New York, NY, USA.

Canadas, R.F., Ren, T., Marques, A.P., Oliveira, J.M., Reis, R.L. & Demirci, U. 2018, "Biochemical Gradients to Generate 3D Heterotypic-Like Tissues with Isotropic and Anisotropic Architectures", *Advanced Functional Materials,* vol. 28, pp. 1804148.

Carlfors, J., Edsman, K., Petersson, R. & Jörnving, K. 1998, "Rheological Evaluation of Gelrite® in Situ Gels for Ophthalmic Use", *European Journal of Pharmaceutical Sciences,* vol. 6, no. 2, pp. 113-119.

Carrier, R.L., Papadaki, M., Rupnick, M., Schoen, F.J., Bursac, N., Langer, R., Freed, L.E. & Vunjak-Novakovic, G. 1999, "Cardiac Tissue Engineering: Cell Seeding, Cultivation Parameters, and Tissue Construct Characterization", *Biotechnology and Bioengineering,* vol. 64, no. 5, pp. 580-589.

Carvalho, C., Wrobel, S., Meyer, C., Brandenberger, C., Cengiz, I.F., Lopez-Cebral, R., Silva-Correia, J., Ronchi, G., Reis, R.L., Grothe, C., Oliveira, J.M. & Haastert-Talini, K. 2018, "Gellan Gum-Based Luminal Fillers for Peripheral Nerve Regeneration. an in Vivo Study in the Rat Sciatic Nerve Repair Model", *Biomaterials Science,* vol. 6, pp. 1059-1075.

Cencetti, C., Bellini, D., Longinotti, C., Martinelli, A. & Matricardi, P. 2011, "Preparation and Characterization of a New Gellan Gum and Sulphated Hyaluronic Acid Hydrogel Designed for Epidural Scar Prevention", *Journal of Materials Science: Materials in Medicine,* vol. 22, no. 2, pp. 263-271.

Cengiz, I.F., Oliveira, J.M. & Reis, R.L. 2018, "Micro-CT – a Digital 3D Microstructural Voyage into Scaffolds: A Systematic Review of the Reported Methods and Results", *Biomaterials Research,* vol. 22, no. 26, pp. 1-11.

Cerqueira, M.T., da Silva, L.P., Santos, T., Pirraco, R.P., Correlo, V.M., Reis, R.L. & Marques, A.P. 2014, "Gellan Gum-Hyaluronic Acid Spongy-Like Hydrogels and Cells from Adipose Tissue Synergize Promoting Neoskin Vascularization", *ACS Applied Materials & Interfaces,* vol. 6, no. 22, pp. 19668-19679.

Chandrasekaran, R. & Radha, A. 1995, "Molecular Architectures and Functional Properties of Gellan Gum and Related Polysaccharides", *Trends in Food Science & Technology,* vol. 6, no. 5, pp. 143-148.

Chen, F. & Liu, X. 2016, "Advancing Biomaterials of Human Origin for Tissue Engineering", *Progress in Polymer Science,* vol. 53, pp. 86-168.

Chester, S.A. 2012, "A Constitutive Model for Coupled Fluid Permeation and Large Viscoelastic Deformation in Polymeric Gels", *Soft Matter,* vol. 8, no. 31, pp. 8223-8233.

Chirani, N., Yahia, L., Gritsch, L., Motta, F.L., Chirani, S. & Fare, S. 2015, "History and Applications of Hydrogels", *Journal of Biomedical Sciences,* vol. 4, no. 2.

Choi, M., Kim, J., Lee, W., Lee, Y., Park, K.M., Yang, Y. & Park, K.D. 2017, "Engineered Extracellular Microenvironment with a Tunable Mechanical Property for Controlling Cell Behavior and Cardiomyogenic Fate of Cardiac Stem Cells", *Acta Biomaterialia,* vol. 50, pp. 234-248.

Chung, B.G., Lee, K., Khademhosseini, A. & Lee, S. 2011, "Microfluidic Fabrication of Microengineered Hydrogels and their Application in Tissue Engineering", *Lab on a Chip,* vol. 12, no. 1, pp. 45.

Colatsky, T., Fermini, B., Gintant, G., Pierson, J.B., Sager, P., Sekino, Y., Strauss, D.G. & Stockbridge, N. 2016, "The Comprehensive in Vitro Proarrhythmia Assay (CiPA) Initiative — Update on Progress", *Journal of Pharmacological and Toxicological Methods,* vol. 81, pp. 15-20.

Cossu, G., Birchall, M., Brown, T., De Coppi, P., Culme-Seymour, E., Gibbon, S., Hitchcock, J., Mason, C., Montgomery, J., Morris, S., Muntoni, F., Napier, D., Owji, N., Prasad, A., Round, J., Saprai, P., Stilgoe, J., Thrasher, A. & Wilson, J. 2018, "Lancet Commission: Stem Cells and Regenerative Medicine", *The Lancet,* vol. 391, no. 10123, pp. 883-910.

Coutinho, D.F., Sant, S.V., Shin, H., Oliveira, J.T., Gomes, M.E., Neves, N.M., Khademhosseini, A. & Reis, R.L. 2010, "Modified Gellan Gum Hydrogels with Tunable Physical and Mechanical Properties", *Biomaterials,* vol. 31, no. 29, pp. 7494-7502.

Coutinho, D.F., Sant, S., Shakiba, M., Wang, B., Gomes, M.E., Neves, N.M., Reis, R.L. & Khademhosseini, A. 2012, "Microfabricated Photocrosslinkable Polyelectrolyte-Complex of Chitosan and Methacrylated Gellan Gum", *Journal of Materials Chemistry,* vol. 22, no. 33, pp. 17262-17271.

Coviello, T., Matricardi, P., Marianecci, C. & Alhaique, F. 2007, "Polysaccharide Hydrogels for Modified Release Formulations", *Journal of Controlled Release,* vol. 119, no. 1, pp. 5-24.

Cukierman, E., Pankov, R., Stevens, D.R. & Yamada, K.M. 2001, "Taking Cell-Matrix Adhesions to the Third Dimension", *Science,* vol. 294, no. 5547, pp. 1708-1712.

Dahlmann, J., Krause, A., Möller, L., Kensah, G., Möwes, M., Diekmann, A., Martin, U., Kirschning, A., Gruh, I. & Dräger, G. 2013, "Fully Defined in Situ Cross-Linkable Alginate and Hyaluronic Acid Hydrogels for Myocardial Tissue Engineering", *Biomaterials,* vol. 34, no. 4, pp. 940-951.

Danno, A. 1958, "Gel Formation of Aqueous Solution of Polyvinyl Alcohol Irradiated by Gamma Rays from Cobalt-60", *Journal of the Physical Society of Japan,* vol. 13, no. 7, pp. 722-727.

Darnell, M. & Mooney, D.J. 2017, "Leveraging Advances in Biology to Design Biomaterials", *Nature Materials,* vol. 16, pp. 1178.

Deng, K., He, H., Qiu, J., Lorber, B., Bryson, J.B. & Filbin, M.T. 2009, "Increased Synthesis of Spermidine as a Result of Upregulation of Arginase I Promotes Axonal Regeneration in Culture and in Vivo", *The Journal of Neuroscience,* vol. 29, no. 30, pp. 9545-9552.

Di Franco, S., Amarelli, C., Montalto, A., Loforte, A. & Musumeci, F. 2018, "Biomaterials and Heart Recovery: Cardiac Repair, Regeneration and Healing in the MCS Era: A State of the "heart"", *Journal of Thoracic Disease,* vol. 10, no. 20, pp. 2346-2362.

Discher, D.E., Mooney, D.J. & Zandstra, P.W. 2009, "Growth Factors, Matrices, and Forces Combine and Control Stem Cells", *Science,* vol. 324, no. 5935, pp. 1673-1677.

Dobrynin, A.V. & Carrillo, J.Y. 2011, "Universality in Nonlinear Elasticity of Biological and Polymeric Networks and Gels", *Macromolecules,* vol. 44, no. 1, pp. 140-146.

Doudna, J.A. & Charpentier, E. 2014, "The New Frontier of Genome Engineering with CRISPR-Cas9", *Science,* vol. 346, no. 6213, pp. 1258096-1-1258096-9.

Douglas, T.E.L., Piwowarczyk, W., Pamula, E., Liskova, J., Schaubroeck, D., Leeuwenburgh, S.C.G., Brackman, G., Balcaen, L., Detsch, R., Declercq, H., Cholewa-Kowalska, K., Dokupil, A., Cuijpers, Vincent M. J. I., Vanhaecke, F., Cornelissen, R., Coenye, T., Boccaccini, A.R. & Dubruel, P. 2014, "Injectable Self-Gelling Composites for Bone Tissue Engineering Based on Gellan Gum Hydrogel Enriched with Different Bioglasses", *Biomedical Materials,* vol. 9, no. 4, pp. 045014.

Drury, J.L. & Mooney, D.J. 2003, "Hydrogels for Tissue Engineering: Scaffold Design Variables and Applications", *Biomaterials,* vol. 24, no. 24, pp. 4337-4351.

Duan, B. 2017, "State-of-the-Art Review of 3D Bioprinting for Cardiovascular Tissue Engineering", *Annals of Biomedical Engineering,* vol. 45, no. 1, pp. 195-209.

Duda, R.O., Hart, P.E. & Stork, D.G. 2001, *Pattern Classification,* 2nd edn, Wiley, New York, NY, USA.

Duval, P. & Le Gac, H. 1980, "Does the Permanent Creep-Rate of Polycrystalline Ice Increase with Crystal Size?", *Journal of Glaciology,* vol. 25, no. 91, pp. 151-158.

Eder, A., Vollert, I., Hansen, A. & Eschenhagen, T. 2016, "Human Engineered Heart Tissue as a Model System for Drug Testing", *Advanced Drug Delivery Reviews,* vol. 96, pp. 214-224.

Edmondson, R., Broglie, J.J., Adcock, A.F. & Yang, L. 2014, "Three-Dimensional Cell Culture Systems and their Applications in Drug Discovery and Cell-Based Biosensors", *ASSAY and Drug Development Technologies,* vol. 12, no. 4, pp. 207-218.

Eglen, R.M. & Randle, D.H. 2015, "Drug Discovery Goes Three-Dimensional: Goodbye to Flat High-Throughput Screening?", *ASSAY and Drug Development Technologies,* vol. 13, no. 5, pp. 262-265.

Elzoghby, A.O. 2013, "Gelatin-Based Nanoparticles as Drug and Gene Delivery Systems: Reviewing Three Decades of Research", *Journal of Controlled Release,* vol. 172, no. 3, pp. 1075-1091.

Engler, A.J., Carag-Krieger, C., Johnson, C.P., Raab, M., Tang, H., Speicher, D.W., Sanger, J.W., Sanger, J.M. & Discher, D.E. 2008, "Embryonic Cardiomyocytes Beat Best on a Matrix with Heart-Like Elasticity: Scar-Like Rigidity Inhibits Beating", *Journal of Cell Science,* vol. 121, no. 22, pp. 3794-3802.

Engler, A.J., Griffin, M.A., Sen, S., Bönnemann, C.G., Sweeney, H.L. & Discher, D.E. 2004, "Myotubes Differentiate Optimally on Substrates with Tissue-Like Stiffness: Pathological Implications for Soft Or Stiff Microenvironments", *The Journal of Cell Biology,* vol. 166, no. 6, pp. 877-887.

Engler, A.J., Sen, S., Sweeney, H.L. & Discher, D.E. 2006, "Matrix Elasticity Directs Stem Cell Lineage Specification", *Cell,* vol. 126, no. 4, pp. 677-689.

Engler, A., Bacakova, L., Newman, C., Hategan, A., Griffin, M. & Discher, D. 2004, "Substrate Compliance Versus Ligand Density in Cell on Gel Responses", *Biophysical Journal,* vol. 86, no. 1, pp. 617-628.

Erickson, H. 2009, "Size and Shape of Protein Molecules at the Nanometer Level Determined by Sedimentation, Gel Filtration, and Electron Microscopy", *Biological Procedures Online,* vol. 11, no. 1, pp. 32-51.

Eschenhagen, T., Fink, C., Remmers, U., Scholz, H., Wattchow, J., Weil, J., Zimmermann, W., Dohmen, H.H., Schäfer, H., Bishopric, N., Wakatsuki, T. & Elson, E.L. 1997, "Three-Dimensional Reconstitution of Embryonic Cardiomyocytes in a Collagen Matrix: A New Heart Muscle Model System.", *The FASEB Journal,* vol. 11, no. 8, pp. 683-694.

Eschenhagen, T., Mummery, C. & Knollmann, B.C. 2015, "Modelling Sarcomeric Cardiomyopathies in the Dish: From Human Heart Samples to iPSC Cardiomyocytes", *Cardiovascular Research,* vol. 105, no. 4, pp. 424-438.

Evans, N.D. & Gentleman, E. 2014, "The Role of Material Structure and Mechanical Properties in Cell-Matrix Interactions", *Journal of Materials Chemistry B,* vol. 2, no. 17, pp. 2345-2356.

Fang, Y. & Eglen, R.M. 2017, "Three-Dimensional Cell Cultures in Drug Discovery and Development", *SLAS DISCOVERY: Advancing Life Sciences R&D,* vol. 22, no. 5, pp. 456-472.

Farouz, Y., Chen, Y., Terzic, A. & Menasché, P. 2014, "Concise Review: Growing Hearts in the Right Place: On the Design of Biomimetic Materials for Cardiac Stem Cell Differentiation", *Stem Cells,* vol. 33, pp. 1021-1035.

FDA 2018, *CFR - Code of Federal Regulations Title 21: Part 172 - Food Additives Permitted for Direct Addition to Food for Human Consumption: Sec. 172.665 Gellan Gum.* Food and Drug Administration, Silver Spring, MD, USA.

Feldman, E.L., Boulis, N.M., Hur, J., Johe, K., Rutkove, S.B., Federici, T., Polak, M., Bordeau, J., Sakowski, S.A. & Glass, J.D. 2014, "Intraspinal Neural Stem Cell Transplantation in Amyotrophic Lateral Sclerosis: Phase 1 Trial Outcomes", *Annals of Neurology,* vol. 75, no. 3, pp. 363-373.

Feric, N.T. & Radisic, M. 2016, "Maturing Human Pluripotent Stem Cell-Derived Cardiomyocytes in Human Engineered Cardiac Tissues", *Advanced Drug Delivery Reviews,* vol. 96, pp. 110-134.

Ferreira, S.A., Motwani, M.S., Faull, P.A., Seymour, A.J., Yu, T.T.L., Enayati, M., Taheem, D.K., Salzlechner, C., Haghighi, T., Kania, E.M., Oommen, O.P., Ahmed, T., Loaiza, S., Parzych, K., Dazzi, F., Varghese, O.P., Festy, F., Grigoriadis, A.E., Auner, H.W., Snijders, A.P., Bozec, L. & Gentleman, E. 2018, "Bi-Directional Cell-Pericellular Matrix Interactions Direct Stem Cell Fate", *Nature Communications,* vol. 9, no. 1, pp. 4049.

Ferris, C.J., Stevens, L.R., Gilmore, K.J., Mume, E., Greguric, I., Kirchmajer, D.M., Wallace, G.G. & in het Panhuis, M. 2015, "Peptide Modification of Purified Gellan Gum", *Journal of Materials Chemistry B,* vol. 3, no. 6, pp. 1106-1115.

Ferris, C.J., Gilmore, K.J., Wallace, G.G. & in het Panhuis, M. 2013, "Modified Gellan Gum Hydrogels for Tissue Engineering Applications", *Soft Matter,* vol. 9, no. 14, pp. 3705-3711.

Fialho, A.M., Moreira, L.M., Granja, A.T., Popescu, A.O., Hoffmann, K. & Sá-Correia, I. 2008, "Occurrence, Production, and Applications of Gellan: Current State and Perspectives", *Applied Microbiology and Biotechnology,* vol. 79, no. 6, pp. 889-900.

Figueiras, E., Soto, A.M., Jesus, D., Lehti, M., Koivisto, J.T., Parraga, J.E., Silva-Correia, J., Oliveira, J.M., Reis, R.L., Kellomäki, M. & Hyttinen, J. 2014, "Optical Projection Tomography as a Tool for 3D Imaging of Hydrogels", *Biomedical Optics Express,* vol. 5, no. 10, pp. 3443-3449.

Flanagan, L.A., Ju, Y., Marg, B., Osterfield, M. & Janmey, P.A. 2002, "Neurite Branching on Deformable Substrates", *Neuroreport,* vol. 13, no. 18, pp. 2411-2415.

Flory, P.J. 1985a, "Molecular Theory of Rubber Elasticity", *Polymer Journal,* vol. 17, no. 1, pp. 1-12.

Flory, P.J. 1985b, "Network Topology and the Theory of Rubber Elasticity", *British Polymer Journal,* vol. 17, no. 2, pp. 96-102.

Folkman, J., Haudenschild, C.C. & Zetter, B.R. 1979, "Long-Term Culture of Capillary Endothelial Cells", *Proceedings of the National Academy of Sciences,* vol. 76, no. 10, pp. 5217-5221.

Frigon, R.P., Leypoldt, J.K., Uyeji, S. & Henderson, L.W. 1983, "Disparity between Stokes Radii of Dextrans and Proteins as Determined by Retention Volume in Gel Permeation Chromatography", *Analytical Chemistry,* vol. 55, no. 8, pp. 1349-1354.

Führmann, T., Tam, R.Y., Ballarin, B., Coles, B., Elliott Donaghue, I., van der Kooy, D., Nagy, A., Tator, C.H., Morshead, C.M. & Shoichet, M.S. 2016, "Injectable Hydrogel Promotes Early Survival of Induced Pluripotent Stem Cell-Derived Oligodendrocytes and Attenuates Longterm Teratoma Formation in a Spinal Cord Injury Model", *Biomaterials,* vol. 83, pp. 23-36.

Fujiwara, K., Bai, G. & Kitagawa, T. 1997, "Polyamine-Like Immunoreactivity in Rat Neurons", *Brain Research,* vol. 767, no. 1, pp. 166-171.

Furmanski, J. & Chakravartula, A.M. 2011, "Mechanical Behavior of Structural Tissues" in *Mechanics of Biomaterials - Fundamental Principles for Implant Design*, eds. L.A. Pruitt & A.M. Chakravartula, Cambridge University Press, Cambridge, UK, pp. 129-164.

Galli, M., Comley, K.S.C., Shean, T.A.V. & Oyen, M.L. 2009, "Viscoelastic and Poroelastic Mechanical Characterization of Hydrated Gels", *Journal of Materials Research,* vol. 24, no. 03, pp. 973-979.

García-González, C.A., Alnaief, M. & Smirnova, I. 2011, "Polysaccharide-Based aerogels—Promising Biodegradable Carriers for Drug Delivery Systems", *Carbohydrate Polymers,* vol. 86, no. 4, pp. 1425-1438.

Geckil, H., Xu, F., Zhang, X., Moon, S. & Demirci, U. 2010, "Engineering Hydrogels as Extracellular Matrix Mimics", *Nanomedicine (London, England),* vol. 5, no. 3, pp. 469-484.

Gemeinhart, R.A., Park, H. & Park, K. 2000, "Pore Structure of Superporous Hydrogels", *Polymers for Advanced Technologies,* vol. 11, no. 8, pp. 617-625.

Gentleman, E., Livesay, G.A., Dee, K.C. & Nauman, E.A. 2006, "Development of Ligament-Like Structural Organization and Properties in Cell-Seeded Collagen Scaffolds in Vitro", *Annals of Biomedical Engineering,* vol. 34, no. 5, pp. 726-736.

George, E., Barai, A., Shirke, P., Majumder, A. & Sen, S. 2018, "Engineering Interfacial Migration by Collective Tuning of Adhesion Anisotropy and Stiffness", *Acta Biomaterialia,* vol. 72, pp. 82-93.

Gering, C., Koivisto, J.T., Parraga, J.E. & Kellomäki, M. 2018, "Reproducible Preparation Method of Hydrogels for Cell Culture Applications – Case Study with Spermidine Crosslinked Gellan Gum", *IFMBE Proceedings,* vol. 65, pp. 811-814.

Gomes, M.E., Rodrigues, M., Domingues, R.M.A. & Reis, R.L. 2017, "Tissue Engineering and Regenerative Medicine: New Trends and Directions—A Year in Review", *Tissue Engineering Part B: Reviews,* vol. 23, no. 3, pp. 211-224.

Gómez-Guillén, M.C., Giménez, B., López-Caballero, M.E. & Montero, M.P. 2011, "Functional and Bioactive Properties of Collagen and Gelatin from Alternative Sources: A Review", *Food Hydrocolloids,* vol. 25, no. 8, pp. 1813-1827.

Gong, Y., Wang, C., Lai, R.C., Su, K., Zhang, F. & Wang, D. 2009, "An Improved Injectable Polysaccharide Hydrogel: Modified Gellan Gum for Long-Term Cartilage Regenerationin Vitro", *Journal of Materials Chemistry,* vol. 19, no. 14, pp. 1968-1977.

Gonzalez, R.C. & Woods, R.E. 2008, *Digital Image Processing*, 3rd edn, Prentice Hall, Upper Saddle River, NJ, USA.

Gupta, S. & Markey, M.K. 2005, "Correspondence in Texture Features between Two Mammographic Views", *Medical Physics*, vol. 32, no. 6, pp. 1598-1606.

Hadden, W.J., Young, J.L., Holle, A.W., McFetridge, M.L., Kim, D.Y., Wijesinghe, P., Taylor-Weiner, H., Wen, J.H., Lee, A.R., Bieback, K., Vo, B., Sampson, D.D., Kennedy, B.F., Spatz, J.P., Engler, A.J. & Choi, Y.S. 2017, "Stem Cell Migration and Mechanotransduction on Linear Stiffness Gradient Hydrogels", *Proceedings of the National Academy of Sciences*, vol. 114, no. 22, pp. 5647-5652.

Han, L., Xu, C., Jiang, C., Li, H., Zhang, W., Zhao, Y., Zhang, L., Zhang, Y., Zhao, W. & Yang, B. 2007, "Effects of Polyamines on Apoptosis Induced by Simulated Ischemia/Reperfusion Injury in Cultured Neonatal Rat Cardiomyocytes", *Cell Biology International*, vol. 31, no. 11, pp. 1345-1352.

Haralick, R.M., Shanmuga, K. & Dinstein, I. 1973, "Textural Features for Image Classification", *IEEE Transactions on Systems, Man and Cybernetics*, vol. SMC3, no. 6, pp. 610-621.

Hayflick, L. & Moorhead, P.S. 1961, "The Serial Cultivation of Human Diploid Cell Strains", *Experimental Cell Research*, vol. 25, no. 3, pp. 585-621.

Heidemann, S.R. & Wirtz, D. 2004, "Towards a Regional Approach to Cell Mechanics", *Trends in Cell Biology*, vol. 14, no. 4, pp. 160-166.

Hencky, H. 1931, "The Law of Elasticity for Isotropic and Quasi-Isotropic Substances by Finite Deformations", *Journal of Rheology*, vol. 2, no. 2, pp. 169-176.

Hencky, H. 1928, "Über Die Form Des Elastizitätsgesetzes Bei Ideal Elastischen Stiffen", *Zeitschrift für Technische Physik*, vol. 6, pp. 215-247.

Hennink, W.E. & van Nostrum, C. 2002, "Novel Crosslinking Methods to Design Hydrogels", *Advanced Drug Delivery Reviews*, vol. 54, no. 1, pp. 13-36.

Hoffman, A.F., Simpson, K.J., Horvath, P., Lovitt, C., Silver, S., Easton, E., LaBarbera, D.V., Mendez, M., Rothenberg, M.E., Seldin, J., Wardwell-Swanson, J. & Fennell, M. 2017, "SBI2 HCS/HCA 3D Imaging: Best Practices and Unmet Needs Colloquium", *ASSAY and Drug Development Technologies*, vol. 15, no. 1, pp. 1-7.

Hong, W., Zhao, X. & Suo, Z. 2010, "Large Deformation and Electrochemistry of Polyelectrolyte Gels", *Journal of the Mechanics and Physics of Solids*, vol. 58, no. 4, pp. 558-577.

Hopkins, A.M., DeSimone, E., Chwalek, K. & Kaplan, D.L. 2015, "3D in Vitro Modeling of the Central Nervous System", *Progress in Neurobiology*, vol. 125, pp. 1-25.

Horwitz, E.M., Andreef, M. & Frassoni, F. 2006, "Mesenchymal Stromal Cells", *Current Opinion in Hematology,* vol. 13, no. 6, pp. 419-425.

Hu, Y. & Suo, Z. 2012, "Viscoelasticity and Poroelasticity in Elastomeric Gels", *Acta Mechanica Solida Sinica,* vol. 25, no. 5, pp. 441-458.

Huebsch, N., Gilbert, M. & Healy, K.E. 2005, "Analysis of Sterilization Protocols for Peptide-Modified Hydrogels", *Journal of Biomedical Materials Research Part B: Applied Biomaterials,* vol. 74B, no. 1, pp. 440-447.

Huh, D., Hamilton, G.A. & Ingber, D.E. 2011, "From 3D Cell Culture to Organs-on-Chips", *Trends in Cell Biology,* vol. 21, no. 12, pp. 745-754.

Hyysalo, A., Ristola, M., Joki, T., Honkanen, M., Vippola, M. & Narkilahti, S. 2017, "Aligned Poly(E-Caprolactone) Nanofibers Guide the Orientation and Migration of Human Pluripotent Stem Cell-Derived Neurons, Astrocytes, and Oligodendrocyte Precursor Cells in Vitro", *Macromolecular Bioscience,* vol. 17, no. 7, pp. 1600517.

Ifkovits, J.L. & Burdick, J.A. 2007, "Review: Photopolymerizable and Degradable Biomaterials for Tissue Engineering Applications", *Tissue Engineering,* vol. 13, no. 10, pp. 2369-2385.

Ihalainen, T.O., Aires, L., Herzog, F.A., Schwartlander, R., Moeller, J. & Vogel, V. 2015, "Differential Basal-to-Apical Accessibility of Lamin A/C Epitopes in the Nuclear Lamina Regulated by Changes in Cytoskeletal Tension", *Nature Materials,* vol. 14, no. 12, pp. 1252-1261.

Ikonen, L., Kerkelä, E., Kujala, K., Haaparanta, A.-., Ahola, N., Ellä, V., Poh, T.L., Kellomäki, M. & Aalto-Setälä, K. 2011, "Analysis of Different Natural and Synthetic Biomaterials to Support Cardiomyocyte Growth", *Journal of Clinical and Experimental Cardiology,* vol. S4, no. 002, pp. 1-7.

Ikonen, L., Kerkelä, E., Metselaar, G., Stuart, M.C.A., de Jong, M.R. & Aalto-Setälä, K. 2013, "2D and 3D Self-Assembling Nanofiber Hydrogels for Cardiomyocyte Culture", *BioMed Research International,* vol. 2013, pp. Article ID:285678-1-12.

Ishikiriyama, K., Sakamoto, A., Todoki, M., Tayama, T., Tanaka, K. & Kobayashi, T. 1995, "Pore Size Distribution Measurements of Polymer Hydrogel Membranes for Artificial Kidneys using Differential Scanning Calorimetry", *Thermochimica Acta,* vol. 267, no. 0, pp. 169-180.

Jääskeläinen, P., Heliö, T., Aalto-Setälä, K., Kaartinen, M., Ilveskoski, E., Hämäläinen, L., Melin, J., Nieminen, M.S., Laakso, M., Kuusisto, J., Kervinen, H., Mustonen, J., Juvonen, J., Niemi, M., Uusimaa, P., Huttunen, M., Kotila, M. & Pietilä, M. 2013, "Two Founder Mutations in the Alpha-Tropomyosin and the Cardiac Myosin-Binding Protein C Genes are Common Causes of Hypertrophic Cardiomyopathy in the Finnish Population", *Annals of Medicine,* vol. 45, no. 1, pp. 85-90.

Jain, A., Persson, K.A. & Ceder, G. 2016, "Research Update: The Materials Genome Initiative: Data Sharing and the Impact of Collaborative Ab Initio Databases", *APL Materials,* vol. 4, no. 5, pp. 053102.

Jamshidi, P., Chouhan, G., Williams, R.L., Cox, S.C. & Grover, L.M. 2016, "Modification of Gellan Gum with Nanocrystalline Hydroxyapatite Facilitates Cell Expansion and Spontaneous Osteogenesis", *Biotechnology and Bioengineering,* vol. 113, no. 7, pp. 1568-1576.

Jiang, Y., Chen, J., Deng, C., Suuronen, E.J. & Zhong, Z. 2014, "Click Hydrogels, Microgels and Nanogels: Emerging Platforms for Drug Delivery and Tissue Engineering", *Biomaterials,* vol. 35, no. 18, pp. 4969-4985.

Jochen Birk, U., Darrell, A., Konstantinides, N., Sarasa-Renedo, A. & Ripoll, J. 2011, "Improved Reconstructions and Generalized Filtered Back Projection for Optical Projection Tomography", *Applied Optics,* vol. 50, no. 4, pp. 392-398.

Johnson, B.N., Lancaster, K.Z., Zhen, G., He, J., Gupta, M.K., Kong, Y.L., Engel, E.A., Krick, K.D., Ju, A., Meng, F., Enquist, L.W., Jia, X. & McAlpine, M.C. 2015, "3D Printed Anatomical Nerve Regeneration Pathways", *Advanced Functional Materials,* vol. 25, no. 39, pp. 6205-6217.

Kalia, J. & Raines, R. 2008, "Hydrolytic Stability of Hydrazones and Oximes", *Angewandte Chemie International Edition,* vol. 47, no. 39, pp. 7523-7526.

Kang, H., Wen, Q., Janmey, P.A., Tang, J.X., Conti, E. & MacKintosh, F.C. 2009, "Nonlinear Elasticity of Stiff Filament Networks: Strain Stiffening, Negative Normal Stress, and Filament Alignment in Fibrin Gels", *The Journal of Physical Chemistry B,* vol. 113, no. 12, pp. 3799-3805.

Kang, H., Lee, S.J., Ko, I.K., Kengla, C., Yoo, J.J. & Atala, A. 2016, "A 3D Bioprinting System to Produce Human-Scale Tissue Constructs with Structural Integrity", *Nature Biotechnology,* vol. 34, no. 3, pp. 312-319.

Kang, K.S., Veeder, G.T., Mirrasoul, P.J., Kaneko, T. & Cottrell, I.W. 1982, "Agar-Like Polysaccharide Produced by a *Pseudomonas* Species: Production and Basic Properties", *Applied and Environmental Microbiology,* vol. 43, no. 5, pp. 1086.

Karimi, A. & Navidbakhsh, M. 2014, "An Experimental Study on the Mechanical Properties of Rat Brain Tissue using Different Stress–strain Definitions", *Journal of Materials Science: Materials in Medicine,* vol. 25, no. 7, pp. 1623-1630.

Karvinen, J., Ihalainen, T.O., Calejo, M.T., Jönkkäri, I. & Kellomäki, M. 2019, "Characterization of the Microstructure of Hydrazone Crosslinked Polysaccharide-Based Hydrogels through Rheological and Diffusion Studies", *Materials Science and Engineering: C,* vol. 94, pp. 1056-1066.

Karvinen, J., Joki, T., Ylä-Outinen, L., Koivisto, J.T., Narkilahti, S. & Kellomäki, M. 2018, "Soft Hydrazone Crosslinked Hyaluronan- and Alginate-Based Hydrogels as 3D Supportive Matrices for Human Pluripotent Stem Cell-Derived Neuronal Cells", *Reactive and Functional Polymers,* vol. 124, pp. 29-39.

Karvinen, J., Koivisto, J.T., Jönkkäri, I. & Kellomäki, M. 2017, "The Production of Injectable Hydrazone Crosslinked Gellan Gum-Hyaluronan-Hydrogels with Tunable Mechanical and Physical Properties", *Journal of the Mechanical Behavior of Biomedical Materials,* vol. 71, pp. 383-391.

Katipparambil Rajan, D., Kreutzer, J., Välimäki, H., Pekkanen-Mattila, M., Ahola, A., Skogberg, A., Aalto-Setälä, K., Ihalainen, H., Kallio, P. & Lekkala, J. 2018, "A Portable Live-Cell Imaging System with an Invert-Upright-Convertible Architecture and a Mini-Bioreactor for Long-Term Simultaneous Cell Imaging, Chemical Sensing and Electrophysiological Recording", *IEEE Access,* [Online], vol. 6, no. 99, Article ID 11063-11075.

Kavanagh, G.M. & Ross-Murphy, S.B. 1998, "Rheological Characterisation of Polymer Gels", *Progress in Polymer Science,* vol. 23, no. 3, pp. 533-562.

Kehoe, S., Zhang, X.F. & Boyd, D. 2012, "FDA Approved Guidance Conduits and Wraps for Peripheral Nerve Injury: A Review of Materials and Efficacy", *Injury,* vol. 43, no. 5, pp. 553-572.

Keller, A., Stevens, L., Wallace, G.G. & in het Panhuis, M. 2016, "3D Printed Edible Hydrogel Electrodes", *MRS Advances,* vol. FirstView, pp. 1-6.

Khademhosseini, A. & Langer, R. 2016, "A Decade of Progress in Tissue Engineering", *Nature Protocols,* vol. 11, pp. 1775.

Khan, A.U., Mei, Y.H. & Wilson, T. 1992, "A Proposed Function for Spermine and Spermidine: Protection of Replicating DNA Against Damage by Singlet Oxygen", *Proceedings of the National Academy of Sciences,* vol. 89, no. 23, pp. 11426-11427.

Khan, M., Koivisto, J.T., Hukka, T.I., Hokka, M. & Kellomäki, M. 2018, "Composite Hydrogels using Bioinspired Approach with in Situ Fast Gelation and Self-Healing Ability as Future Injectable Biomaterial", *ACS Applied Materials & Interfaces,* vol. 10, pp. 11950-11960.

Khan, U.A., Oelschlaeger, C., Ali, F.I., Roether, J., willenbacher, N. & Hashmi, I.A. 2018, "Structural, Macro- and Micro-Mechanical Properties of Supramolecular Bi-Component L-Lysine-Sodium Tetraphenyl Borate Based Hydrogels", *Colloids and Surfaces A: Physicochemical and Engineering Aspects,* vol. 546, pp. 366-377.

Kiamehr, M., Viiri, L.E., Vihervaara, T., Koistinen, K.M., Hilvo, M., Ekroos, K., Käkelä, R. & Aalto-Setälä, K. 2017, "Lipidomic Profiling of Patient-Specific Induced Pluripotent Stem Cell-Derived Hepatocyte-Like Cells", *Disease Models & Mechanisms,* .

Kisley, L., Brunetti, R., Tauzin, L.J., Shuang, B., Yi, X., Kirkeminde, A.W., Higgins, D.A., Weiss, S. & Landes, C.F. 2015, "Characterization of Porous Materials by Fluorescence Correlation Spectroscopy Super-Resolution Optical Fluctuation Imaging", *ACS Nano,* vol. 9, no. 9, pp. 9158-9166.

Kitsara, M., Agbulut, O., Kontziampasis, D., Chen, Y. & Menasché, P. 2017, "Fibers for Hearts: A Critical Review on Electrospinning for Cardiac Tissue Engineering", *Acta Biomaterialia,* vol. 48, pp. 20-40.

Kiviaho, A.L., Ahola, A., Larsson, K., Penttinen, K., Swan, H., Pekkanen-Mattila, M., Venäläinen, H., Paavola, K., Hyttinen, J. & Aalto-Setälä, K. 2015, "Distinct Electrophysiological and Mechanical Beating Phenotypes of Long QT Syndrome Type 1-Specific Cardiomyocytes Carrying Different Mutations", *IJC Heart & Vasculature,* vol. 8, pp. 19-31.

Kleinman, H.K. & Martin, G.R. 2005, "Matrigel: Basement Membrane Matrix with Biological Activity", *Seminars in Cancer Biology,* vol. 15, no. 5, pp. 378-386.

Kohane, D.S. & Langer, R. 2010, "Biocompatibility and Drug Delivery Systems", *Chemical Science,* vol. 1, no. 4, pp. 441-446.

Koivisto, J.T., Koskela, O., Montonen, T., Parraga, J.E., Joki, T., Ylä-Outinen, L., Narkilahti, S., Figueiras, E., Hyttinen, J. & Kellomäki, M. 2018, "Texture-Property Relations of Bioamine Crosslinked Gellan Gum Hydrogels", *IFMBE Proceedings,* vol. 65, pp. 189-192.

Koivusalo, L., Karvinen, J., Sorsa, E., Jönkkäri, I., Väliaho, J., Kallio, P., Ilmarinen, T., Miettinen, S., Skottman, H. & Kellomäki, M. 2018, "Hydrazone Crosslinked Hyaluronan-Based Hydrogels for Therapeutic Delivery of Adipose Stem Cells to Treat Corneal Defects", *Materials Science and Engineering: C,* vol. 85, pp. 68-78.

Kolb, H.C., Finn, M.G. & Sharpless, K.B. 2001, "Click Chemistry: Diverse Chemical Function from a Few Good Reactions", *Angewandte Chemie International Edition,* vol. 40, no. 11, pp. 2004-2021.

Koob, T.J. & Hernandez, D.J. 2003, "Mechanical and Thermal Properties of Novel Polymerized NDGA–gelatin Hydrogels", *Biomaterials,* vol. 24, no. 7, pp. 1285-1292.

Kopljar, I., Lu, H.R., Van Ammel, K., Otava, M., Tekle, F., Teisman, A. & Gallacher, D.J. 2018, "Development of a Human iPSC Cardiomyocyte-Based Scoring System for Cardiac Hazard Identification in Early Drug Safety De-Risking", *Stem Cell Reports,* vol. 11, no. 6, pp. 1365-1377.

Kornev, V.A., Grebenik, E.A., Solovieva, A.B., Dmitriev, R.I. & Timashev, P.S. 2018, "Hydrogel-Assisted Neuroregeneration Approaches Towards Brain Injury Therapy: A State-of-the-Art Review", *Computational and Structural Biotechnology Journal,* vol. 16, pp. 488-502.

Koshy, S.T., Desai, R.M., Joly, P., Li, J., Bagrodia, R.K., Lewin, S.A., Joshi, N.S. & Mooney, D.J. 2016, "Click-Crosslinked Injectable Gelatin Hydrogels", *Advanced Healthcare Materials,* vol. 5, no. 5, pp. 541-547.

Kreutzer, J., Ikonen, L., Hirvonen, J., Pekkanen-Mattila, M., Aalto-Setälä, K. & Kallio, P. 2014, "Pneumatic Cell Stretching System for Cardiac Differentiation and Culture", *Medical Engineering and Physics,* vol. 36, no. 4, pp. 496-501.

Ku, D.N., Braddon, L.G. and Wootton, D.M. 1997. US Patent 5,981,826A. *Poly(Vinyl Alcohol) Cryogel.* GA, USA.

Kujala, K., Ahola, A., Pekkanen-Mattila, M., Ikonen, L., Kerkelä, E., Hyttinen, J. & Aalto-Setälä, K. 2012, "Electrical Field Stimulation with a Novel Platform: Effect on Cardiomyocyte Gene Expression but Not on Orientation", *International Journal of Biomedical Science,* vol. 8, no. 2, pp. 109-120.

Kumar, K.K., Aboud, A.A. & Bowman, A.B. 2012, "The Potential of Induced Pluripotent Stem Cells as a Translational Model for Neurotoxicological Risk", *Neurotoxicology,* vol. 33, no. 3, pp. 518-529.

Kuusela, J., Kim, J., Räsänen, E. & Aalto-Setälä, K. 2016, "The Effects of Pharmacological Compounds on Beat Rate Variations in Human Long QT-Syndrome Cardiomyocytes", *Stem Cell Reviews and Reports,* vol. 12, no. 6, pp. 698-707.

Lago, M., da Silva, L.P., Henriques, C., Carvalho, A., Reis, R. & Marques, A. 2018, "Generation of Gellan Gum-Based Adipose-Like Microtissues", *Bioengineering,* vol. 5, no. 3, pp. 52-66.

Lan, K., Wang, D., Fong, S., Liu, L., Wong, K.K.L. & Dey, N. 2018, "A Survey of Data Mining and Deep Learning in Bioinformatics", *Journal of Medical Systems,* vol. 42, no. 8, pp. 139-159.

Lane, B.A., Harmon, K.A., Goodwin, R.L., Yost, M.J., Shazly, T. & Eberth, J.F. 2018, "Constitutive Modeling of Compressible Type-I Collagen Hydrogels", *Medical Engineering & Physics,* vol. 53, pp. 39-48.

Langer, R. & Vacanti, J. 1993, "Tissue Engineering", *Science,* vol. 260, no. 5110, pp. 920-926.

Langer, R. 2017, "Synthetic Tissues", *Molecular Frontiers Journal,* vol. 01, no. 02, pp. 92-98.

Langley, G.R., Adcock, I.M., Busquet, F., Crofton, K.M., Csernok, E., Giese, C., Heinonen, T., Herrmann, K., Hofmann-Apitius, M., Landesmann, B., Marshall, L.J., McIvor, E., Muotri, A.R., Noor, F., Schutte, K., Seidle, T., van de Stolpe, A., Van Esch, H., Willett, C. & Woszczek, G. 2016, "Towards a 21st-Century Roadmap for

Biomedical Research and Drug Discovery: Consensus Report and Recommendations", *Drug Discovery Today,* vol. 22, no. 2, pp. 327-339.

Lao, O., Lu, T.T., Nothnagel, M., Junge, O., Freitag-Wolf, S., Caliebe, A., Balascakova, M., Bertranpetit, J., Bindoff, L.A., Comas, D., Holmlund, G., Kouvatsi, A., Macek, M., Mollet, I., Parson, W., Palo, J., Ploski, R., Sajantila, A., Tagliabracci, A., Gether, U., Werge, T., Rivadeneira, F., Hofman, A., Uitterlinden, A.G., Gieger, C., Wichmann, H., Rüther, A., Schreiber, S., Becker, C., Nürnberg, P., Nelson, M.R., Krawczak, M. & Kayser, M. 2008, "Correlation between Genetic and Geographic Structure in Europe", *Current Biology,* vol. 18, no. 16, pp. 1241-1248.

Lappalainen, R.S., Salomäki, M., Ylä-Outinen, L., Heikkilä, T.J., Hyttinen, J.A.K., Pihlajamäki, H., Suuronen, R., Skottman, H. & Narkilahti, S. 2010, "Similarly Derived and Cultured hESC Lines show Variation in their Developmental Potential Towards Neuronal Cells in Long-Term Culture", *Regenerative Medicine,* vol. 5, no. 5, pp. 749-762.

Lau, M.H., Tang, J. & Paulson, A.T. 2000, "Texture Profile and Turbidity of Gellan/Gelatin Mixed Gels", *Food Research International,* vol. 33, no. 8, pp. 665-671.

Laube, G., Bernstein, H., Wolf, G. & Veh, R.W. 2002, "Differential Distribution of Spermidine/Spermine-Like Immunoreactivity in Neurons of the Adult Rat Brain", *The Journal of Comparative Neurology,* vol. 444, no. 4, pp. 369-386.

Laurila, E., Ahola, A., Hyttinen, J. & Aalto-Setälä, K. 2016, "Methods for in Vitro Functional Analysis of iPSC Derived Cardiomyocytes — Special Focus on Analyzing the Mechanical Beating Behavior", *Biochimica et Biophysica Acta (BBA) - Molecular Cell Research,* vol. 1863, no. 7, Part B, pp. 1864-1872.

Le Gac, H. & Duval, P. 1980, "Constitutive Relations for the Non Elastic Deformation of Polycrystalline Ice" in *Physics and Mechanics of Ice*, ed. P. Tryde, Springer Berlin Heidelberg, Berlin, Heidelberg, pp. 51-59.

Lechler, R.I., Sykes, M., Thomson, A.W. & Turka, L.A. 2005, "Organ Transplantation—how Much of the Promise has been Realized?", *Nature Medicine,* vol. 11, pp. 605-613.

Leddy, H.A. & Guilak, F. 2003, "Site-Specific Molecular Diffusion in Articular Cartilage Measured using Fluorescence Recovery After Photobleaching", *Annals of Biomedical Engineering,* vol. 31, no. 7, pp. 753-760.

Lee, C., Shin, J., Lee, J.S., Byun, E., Ryu, J.H., Um, S.H., Kim, D., Lee, H. & Cho, S. 2013, "Bioinspired, Calcium-Free Alginate Hydrogels with Tunable Physical and Mechanical Properties and Improved Biocompatibility", *Biomacromolecules,* vol. 14, no. 6, pp. 2004-2013.

Leijten, J., Seo, J., Yue, K., Trujillo-de Santiago, G., Tamayol, A., Ruiz-Esparza, G.U., Shin, S.R., Sharifi, R., Noshadi, I., Álvarez, M.M., Zhang, Y.S. & Khademhosseini, A. 2017, "Spatially and Temporally Controlled Hydrogels for Tissue Engineering", *Materials Science and Engineering: R: Reports,* vol. 119, no. Supplement C, pp. 1-35.

Lenk, K., Priwitzer, B., Yla-Outinen, L., Tietz, L.H., Narkilahti, S. & Hyttinen, J.A. 2016, "Simulation of Developing Human Neuronal Cell Networks", *BioMedical Engineering OnLine,* vol. 15, no. 1, pp. 105-016-0226-6.

Levental, I., Georges, P.C. & Janmey, P.A. 2007, "Soft Biological Materials and their Impact on Cell Function", *Soft Matter,* vol. 3, no. 3, pp. 299-306.

Li, J. & Mooney, D.J. 2016, "Designing Hydrogels for Controlled Drug Delivery", *Nature Reviews Materials,* vol. 1, no. 1, pp. 16071.

Lian, X., Zhang, J., Azarin, S.M., Zhu, K., Hazeltine, L.B., Bao, X., Hsiao, C., Kamp, T.J. & Palecek, S.P. 2012, "Directed Cardiomyocyte Differentiation from Human Pluripotent Stem Cells by Modulating Wnt/Î²-Catenin Signaling Under Fully Defined Conditions", *Nature Protocols,* vol. 8, no. 1, pp. 162-175.

Lindvall, O. & Kokaia, Z. 2010, "Stem Cells in Human Neurodegenerative Disorders — Time for Clinical Translation?", *The Journal of Clinical Investigation,* vol. 120, no. 1, pp. 29-40.

Lindvall, O. & Kokaia, Z. 2006, "Stem Cells for the Treatment of Neurological Disorders", *Nature,* vol. 441, pp. 1094.

Liu, S.V. 2008, "iPS Cells: A More Critical Review", *Stem Cells and Development,* vol. 17, no. 3, pp. 391-397.

Livak, K.J. & Schmittgen, T.D. 2001, "Analysis of Relative Gene Expression Data using Real-Time Quantitative PCR and the 2−ΔΔCT Method", *Methods,* vol. 25, no. 4, pp. 402-408.

Loh, Q.L. & Choong, C. 2013, "Three-Dimensional Scaffolds for Tissue Engineering Applications: Role of Porosity and Pore Size", *Tissue Engineering Part B: Reviews,* vol. 19, no. 6, pp. 485-502.

López-Cebral, R., Romero-Caamaño, V., Seijo, B., Alvarez-Lorenzo, C., Martín-Pastor, M., Concheiro, Á, Landin, M. & Sanchez, A. 2014, "Spermidine Cross-Linked Hydrogels as a Controlled Release Biomimetic Approach for Cloxacillin", *Molecular Pharmaceutics,* vol. 11, no. 7, pp. 2358-2371.

López-Cebral, R., Paolicelli, P., Romero-Caamaño, V., Seijo, B., Casadei, M.A. & Sanchez, A. 2013, "Spermidine-Cross-Linked Hydrogels as Novel Potential Platforms for Pharmaceutical Applications", *Journal of Pharmaceutical Sciences,* vol. 102, no. 8, pp. 2632-2643.

Lozano, R., Stevens, L., Thompson, B.C., Gilmore, K.J., Gorkin III, R., Stewart, E.M., in het Panhuis, M., Romero-Ortega, M. & Wallace, G.G. 2015, "3D Printing of Layered Brain-Like Structures using Peptide Modified Gellan Gum Substrates", *Biomaterials,* vol. 67, pp. 264-273.

Lozinsky, V.I., Galaev, I.Y., Plieva, F.M., Savina, I.N., Jungvid, H. & Mattiasson, B. 2003, "Polymeric Cryogels as Promising Materials of Biotechnological Interest", *Trends in Biotechnology,* vol. 21, no. 10, pp. 445-451.

Madonna, R., Van Laake, L.W., Davidson, S.M., Engel, F.B., Hausenloy, D.J., Lecour, S., Leor, J., Perrino, C., Schulz, R., Ytrehus, K., Landmesser, U., Mummery, C.L., Janssens, S., Willerson, J., Eschenhagen, T., Ferdinandy, P. & Sluijter, J.P.G. 2016, "Position Paper of the European Society of Cardiology Working Group Cellular Biology of the Heart: Cell-Based Therapies for Myocardial Repair and Regeneration in Ischemic Heart Disease and Heart Failure", *European Heart Journal,* vol. 37, no. 23, pp. 1789-1798.

Maiti, S., Ranjit, S., Mondol, R., Ray, S. & Sa, B. 2011, "Al^{+3} Ion Cross-Linked and Acetalated Gellan Hydrogel Network Beads for Prolonged Release of Glipizide", *Carbohydrate Polymers,* vol. 85, no. 1, pp. 164-172.

Mäkinen, M.E., Ylä-Outinen, L. & Narkilahti, S. 2018, "GABA and Gap Junctions in the Development of Synchronized Activity in Human Pluripotent Stem Cell-Derived Neural Networks", *Frontiers in Cellular Neuroscience,* vol. 12, pp. 56.

Malafaya, P.B., Silva, G.A. & Reis, R.L. 2007, "Natural–origin Polymers as Carriers and Scaffolds for Biomolecules and Cell Delivery in Tissue Engineering Applications", *Advanced Drug Delivery Reviews,* vol. 59, no. 4–5, pp. 207-233.

Malte, T., Hudson, J.E., Paul, B., Susanne, S., Tim, M., Chang, L.M., Elif, L., Farah, R., Sebastian, Z., Edgar, W., Johannes, R., Mouer, W., Gold, J.D., Izhak, K., Erich, W., Ursula, R., Pieterjan, D., van Laake, L.W., Goumans, M.J., Sara, K., Karl, T., Gerd, H., Couture, L.A., Andreas, U., Linke, W.A., Toshiyuki, A., Benjamin, N., Gordon, K., Lior, G., Wu, J.C. & Zimmermann Wolfram-Hubertus 2017, "Defined Engineered Human Myocardium with Advanced Maturation for Applications in Heart Failure Modeling and Repair", *Circulation,* vol. 135, no. 19, pp. 1832-1847.

Manafi, A., Emami, A., Pooli, A., Habibi, M. & Saidian, L. 2010, "Unacceptable Results with an Accepted Soft Tissue Filler: Polyacrylamide Hydrogel", *Aesthetic Plastic Surgery,* vol. 34, no. 4, pp. 413-422.

Mannhardt, I., Breckwoldt, K., Letuffe-Brenière, D., Schaaf, S., Schulz, H., Neuber, C., Benzin, A., Werner, T., Eder, A., Schulze, T., Klampe, B., Christ, T., Hirt, M., Huebner, N., Moretti, A., Eschenhagen, T. & Hansen, A. 2016, "Human Engineered Heart Tissue: Analysis of Contractile Force", *Stem Cell Reports,* vol. 7, no. 1, pp. 29-42.

Manzini, S., Viiri, L., Marttila, S. & Aalto-Setälä, K. 2015, "A Comparative View on Easy to Deploy Non-Integrating Methods for Patient-Specific iPSC Production", *Stem Cell Reviews and Reports,* , pp. 1-9.

Mao, R., Tang, J. & Swanson, B.G. 2000, "Texture Properties of High and Low Acyl Mixed Gellan Gels", *Carbohydrate Polymers,* vol. 41, no. 4, pp. 331-338.

Mao, Y., Lin, S., Zhao, X. & Anand, L. 2017, "A Large Deformation Viscoelastic Model for Double-Network Hydrogels", *Journal of the Mechanics and Physics of Solids,* vol. 100, pp. 103-130.

Marjamaa, A., Salomaa, V., Newton-Cheh, C., Porthan, K., Reunanen, A., Karanko, H., Jula, A., Lahermo, P., Väänänen, H., Toivonen, L., Swan, H., Viitasalo, M., Nieminen, M.S., Peltonen, L., Oikarinen, L., Palotie, A. & Kontula, K. 2009, "High Prevalence of Four Long QT Syndrome Founder Mutations in the Finnish Population", *Annals of Medicine,* vol. 41, no. 3, pp. 234-240.

Massai, D., Pennella, F., Gentile, P., Gallo, D., Ciardelli, G., Bignardi, C., Audenino, A. & Morbiducci, U. 2014, "Image-Based Three-Dimensional Analysis to Characterize the Texture of Porous Scaffolds", *BioMed Research International,* vol. 2014, pp. 8.

Mathur, A., Loskill, P., Shao, K., Huebsch, N., Hong, S., Marcus, S.G., Marks, N., Mandegar, M., Conklin, B.R., Lee, L.P. & Healy, K.E. 2015, "Human iPSC-Based Cardiac Microphysiological System for Drug Screening Applications", *Scientific Reports,* vol. 5, pp. 8883.

Matricardi, P., Cencetti, C., Ria, R., Alhaique, F. & Coviello, T. 2009, "Preparation and Characterization of Novel Gellan Gum Hydrogels Suitable for Modified Drug Release", *Molecules (Basel, Switzerland),* vol. 14, no. 9, pp. 3376-3391.

Means Jr, K.R., Rinker, B.D., Higgins, J.P., Payne, S.H., Merrell, G.A. & Wilgis, E.F.S. 2016, "A Multicenter, Prospective, Randomized, Pilot Study of Outcomes for Digital Nerve Repair in the Hand using Hollow Conduit Compared with Processed Allograft Nerve", *Hand (New York, USA),* vol. 11, no. 2, pp. 144-151.

Melchels, F.P.W., Dhert, W.J.A., Hutmacher, D.W. & Malda, J. 2014, "Development and Characterisation of a New Bioink for Additive Tissue Manufacturing", *Journal of Materials Chemistry B,* vol. 2, no. 16, pp. 2282-2289.

Menasché, P., Vanneaux, V., Hagège, A., Bel, A., Cholley, B., Parouchev, A., Caccia-puoti, I., Al-Daccak, R., Benhamouda, N., Blons, H., Agbulut, O., Tosca, L., Trouvin, J., Fabreguettes, J., Bellamy, V., Charron, D., Tartour, E., Tachdjian, G., Desnos, M. & Larghero, J. 2018, "Transplantation of Human Embryonic Stem Cell–Derived Cardiovascular Progenitors for Severe Ischemic Left Ventricular Dysfunction", *Journal of the American College of Cardiology,* vol. 71, no. 4, pp. 429-438.

Merryweather, D. & Roach, P. 2017, "The Need for Advanced Three-Dimensional Neural Models and Developing Enabling Technologies", *MRS Communications,* vol. 7, no. 3, pp. 309-319.

Mertens, J., Marchetto, M.C., Bardy, C. & Gage, F.H. 2016, "Evaluating Cell Reprogramming, Differentiation and Conversion Technologies in Neuroscience", *Nature Reviews Neuroscience,* vol. 17, pp. 424.

Milas, M. & Rinaudo, M. 1996, "The Gellan Sol-Gel Transition", *Carbohydrate Polymers,* vol. 30, no. 2–3, pp. 177-184.

Mirsky, I. & Parmley, W.W. 1973, "Assessment of Passive Elastic Stiffness for Isolated Heart Muscle and the Intact Heart", *Circulation Research,* vol. 33, no. 2, pp. 233-243.

Missirlis, Y.F. & Vallet Regi, M.D.N. (eds) 2017, *A Report on the Biomaterials Research Translation in Europe*, European Society of Biomaterials, Athens, Greece.

Mobini, S., Spearman, B.S., Lacko, C.S. & Schmidt, C.E. 2017, "Recent Advances in Strategies for Peripheral Nerve Tissue Engineering", *Current Opinion in Biomedical Engineering,* vol. 4, pp. 134-142.

Molokanova, E., Mercola, M. & Savchenko, A. 2017, "Bringing New Dimensions to Drug Discovery Screening: Impact of Cellular Stimulation Technologies", *Drug Discovery Today,* vol. 22, no. 7, pp. 1045-1055.

Monteiro, J., Yamanaka, S. & Schöler, H. 2016, "iPS Cells 10 Years Later", *Cell,* vol. 166, no. 6, pp. 1356-1359.

Moresi, M. & Bruno, M. 2007, "Characterisation of Alginate Gels using Quasi-Static and Dynamic Methods", *Journal of Food Engineering,* vol. 82, no. 3, pp. 298-309.

Morris, E.R., Nishinari, K. & Rinaudo, M. 2012, "Gelation of Gellan – A Review", *Food Hydrocolloids,* vol. 28, no. 2, pp. 373-411.

Mouser, V.H.M., Melchels, F.P.W., Visser, J., Dhert, W.J.A., Gawlitta, D. & Malda, J. 2016, "Yield Stress Determines Bioprintability of Hydrogels Based on Gelatin-Methacryloyl and Gellan Gum for Cartilage Bioprinting", *Biofabrication,* vol. 8, no. 3, pp. 035003.

Moxon, S.R. & Smith, A.M. 2016, "Controlling the Rheology of Gellan Gum Hydrogels in Cell Culture Conditions", *International Journal of Biological Macromolecules,* vol. 84, pp. 79-86.

Mummery, C.L. 2018, "Perspectives on the use of Human Induced Pluripotent Stem Cell-Derived Cardiomyocytes in Biomedical Research", *Stem Cell Reports,* vol. 11, no. 6, pp. 1306-1311.

Mummery, C.L., Ward-van Oostwaard, D., Doevendans, P., Spijker, R., van den Brink, S., Hassink, R., van der Heyden, M., Opthof, T., Pera, M., de la Riviere, A.B., Passier, R. & Tertoolen, L. 2003, "Differentiation of Human Embryonic Stem Cells to Cardiomyocytes", *Circulation,* vol. 107, no. 21, pp. 2733-2740.

Murphy, W.L., McDevitt, T.C. & Engler, A.J. 2014, "Materials as Stem Cell Regulators", *Nature Materials,* vol. 13, no. 6, pp. 547-557.

Murugan, V. 2009, "Embryonic Stem Cell Research: A Decade of Debate from Bush to Obama", *The Yale Journal of Biology and Medicine,* vol. 82, no. 3, pp. 101-103.

Naahidi, S., Jafari, M., Logan, M., Wang, Y., Yuan, Y., Bae, H., Dixon, B. & Chen, P. 2017, "Biocompatibility of Hydrogel-Based Scaffolds for Tissue Engineering Applications", *Biotechnology Advances,* vol. 35, no. 5, pp. 530-544.

Naghavi, M., Abajobir, A.A., Abbafati, C., Abbas, K.M., Abd-Allah, F., Abera, S.F., Aboyans, V., Adetokunboh, O., Afshin, A., Agrawal, A., Ahmadi, A., Ahmed, M.B., Aichour, A.N., Aichour, M.T.E., Aichour, I., Aiyar, S., Alahdab, F., Al-Aly, Z., Alam, K., Alam, N., Alam, T., Alene, K.A., Al-Eyadhy, A., Ali, S.D., Alizadeh-Navaei, R., Alkaabi, J.M., Alkerwi, A., Alla, F., Allebeck, P., Allen, C., Al-Raddadi, R., Alsharif, U., Altirkawi, K.A., Alvis-Guzman, N., Amare, A.T., Amini, E., Ammar, W., Amoako, Y.A., Anber, N., Andersen, H.H., Andrei, C.L., Androudi, S., Ansari, H., Antonio, C.A.T., Anwari, P., Ärnlöv, J., Arora, M., Artaman, A., Aryal, K.K., Asayesh, H., Asgedom, S.W., Atey, T.M., Avila-Burgos, L., Avokpaho, E.F.G., Awasthi, A., Babalola, T.K., Bacha, U., Balakrishnan, K., Barac, A., Barboza, M.A., Barker-Collo, S.L., Barquera, S., Barregard, L., Barrero, L.H., Baune, B.T., Bedi, N., Beghi, E., Béjot, Y., Bekele, B.B., Bell, M.L., Bennett, J.R., Bensenor, I.M., Berhane, A., Bernabé, E., Betsu, B.D., Beuran, M., Bhatt, S., Biadgilign, S., Bienhoff, K., Bikbov, B., Bisanzio, D., Bourne, R.R.A., Breitborde, N.J.K., Bulto, L.N.B., Bumgarner, B.R., Butt, Z.A., Cahuana-Hurtado, L., Cameron, E., Campuzano, J.C., Car, J., Cárdenas, R., Carrero, J.J., Carter, A., Casey, D.C., Castañeda-Orjuela, C.A., Catalá-López, F., Charlson, F.J., Chibueze, C.E., Chimed-Ochir, O., Chisumpa, V.H.*, et al* 2017, "Global, Regional, and National Age-Sex Specific Mortality for 264 Causes of Death, 1980–2016: A Systematic Analysis for the Global Burden of Disease Study 2016", *The Lancet,* vol. 390, no. 10100, pp. 1151-1210.

Nakamura, K., Shinoda, E. & Tokita, M. 2001, "The Influence of Compression Velocity on Strength and Structure for Gellan Gels", *Food Hydrocolloids,* vol. 15, no. 3, pp. 247-252.

130

Nam, K., Smith, A.S.T., Lone, S., Kwon, S. & Kim, D. 2015, "Biomimetic 3D Tissue Models for Advanced High-Throughput Drug Screening", *Journal of Laboratory Automation,* vol. 20, no. 3, pp. 201-215.

Narkilahti, S., Hovatta, O. & Elovaara, I. 2009, "Kantasolut Multippeliskleroosin Hoidossa", *Duodecim; Lääketieteellinen Aikakauskirja,* vol. 125, no. 9, pp. 965-973.

Narkilahti, S., Ylä-Outinen, L., Sukki, L., Ryynänen, T., Mäkinen, M., Hyysalo, A. and Kreutzer, J. 2016. US Patent 20160312171A1. *A Cell Culturing Platform, a Cell Culture System, and a Method for Modeling Myelination in Vitro.* Finland.

National Institutes of Health 2018, 2018-11-06-last update*, Brain Basics: Life and Death of a Neuron.* Available: https://www.ninds.nih.gov/Disorders/Patient-Caregiver-Education/Life-and-Death-Neuron [2018, 11/27].

Nedelec, J., Grolier, J. & Baba, M. 2006, "Thermoporosimetry: A Powerful Tool to Study the Cross-Linking in Gels Networks", *Journal of Sol-Gel Science and Technology,* vol. 40, no. 2-3, pp. 191-200.

Nemir, S. & West, J. 2010, "Synthetic Materials in the Study of Cell Response to Substrate Rigidity", *Annals of Biomedical Engineering,* vol. 38, no. 1, pp. 2-20.

Ngo, T.D., Kashani, A., Imbalzano, G., Nguyen, K.T.Q. & Hui, D. 2018, "Additive Manufacturing (3D Printing): A Review of Materials, Methods, Applications and Challenges", *Composites Part B: Engineering,* vol. 143, pp. 172-196.

Nimmo, C.M., Owen, S.C. & Shoichet, M.S. 2011, "Diels–Alder Click Cross-Linked Hyaluronic Acid Hydrogels for Tissue Engineering", *Biomacromolecules,* vol. 12, no. 3, pp. 824-830.

Nishinari, K. 1996, "Introduction", *Carbohydrate Polymers,* vol. 30, no. 2–3, pp. 75-76.

Normand, V., Lootens, D.L., Amici, E., Plucknett, K.P. & Aymard, P. 2000, "New Insight into Agarose Gel Mechanical Properties", *Biomacromolecules,* vol. 1, no. 4, pp. 730-738.

Nunes, S.S., Miklas, J.W., Liu, J., Aschar-Sobbi, R., Xiao, Y., Zhang, B., Jiang, J., Masse, S., Gagliardi, M., Hsieh, A., Thavandiran, N., Laflamme, M.A., Nanthakumar, K., Gross, G.J., Backx, P.H., Keller, G. & Radisic, M. 2013, "Biowire: A Platform for Maturation of Human Pluripotent Stem Cell-Derived Cardiomyocytes", *Nature Methods,* vol. 10, no. 8, pp. 781-787.

O'Connor, S.M., Stenger, D.A., Shaffer, K.M., Maric, D., Barker, J.L. & Ma, W. 2000, "Primary Neural Precursor Cell Expansion, Differentiation and Cytosolic Ca2+ Response in Three-Dimensional Collagen Gel", *Journal of Neuroscience Methods,* vol. 102, no. 2, pp. 187-195.

Oelschlaeger, C., Bossler, F. & Willenbacher, N. 2016, "Synthesis, Structural and Micromechanical Properties of 3D Hyaluronic Acid-Based Cryogel Scaffolds", *Biomacromolecules,* vol. 17, no. 2, pp. 580-589.

Ohtsuka, A. & Watanabe, T. 1996, "The Network Structure of Gellan Gum Hydrogels Based on the Structural Parameters by the Analysis of the Restricted Diffusion of Water", *Carbohydrate Polymers,* vol. 30, no. 2–3, pp. 135-140.

Ojala, M. & Aalto-Setälä, K. 2016, "Modeling Hypertrophic Cardiomyopathy with Human Induced Pluripotent Stem Cells" in *Pluripotent Stem Cells - from the Bench to the Clinic*, ed. M. Tomizawa, 1st edn, InTech, London, UK, pp. 227-256.

Ojala, M., Prajapati, C., Pölönen, R., Rajala, K., Pekkanen-Mattila, M., Rasku, J., Larsson, K. & Aalto-Setälä, K. 2016, "Mutation-Specific Phenotypes in hiPSC-Derived Cardiomyocytes Carrying either Myosin-Binding Protein C Or A-Tropomyosin Mutation for Hypertrophic Cardiomyopathy", *Stem Cells International,* vol. 2016, pp. 16.

Okita, K., Matsumura, Y., Sato, Y., Okada, A., Morizane, A., Okamoto, S., Hong, H., Nakagawa, M., Tanabe, K., Tezuka, K., Shibata, T., Kunisada, T., Takahashi, M., Takahashi, J., Saji, H. & Yamanaka, S. 2011, "A More Efficient Method to Generate Integration-Free Human iPS Cells", *Nature Methods,* vol. 8, no. 5, pp. 409-412.

Oliveira, J.T., Martins, L., Picciochi, R., Malafaya, P.B., Sousa, R.A., Neves, N.M., Mano, J.F. & Reis, R.L. 2010, "Gellan Gum: A New Biomaterial for Cartilage Tissue Engineering Applications", *Journal of Biomedical Materials Research Part A,* vol. 93A, no. 3, pp. 852-863.

Oliveira, M.B., Custódio, C.A., Gasperini, L., Reis, R.L. & Mano, J.F. 2016, "Autonomous Osteogenic Differentiation of hASCs Encapsulated in Methacrylated Gellan-Gum Hydrogels", *Acta Biomaterialia,* vol. 41, pp. 119-132.

Olsen, D., Yang, C., Bodo, M., Chang, R., Leigh, S., Baez, J., Carmichael, D., Perälä, M., Hämäläinen, E., Jarvinen, M. & Polarek, J. 2003, "Recombinant Collagen and Gelatin for Drug Delivery", *Advanced Drug Delivery Reviews,* vol. 55, no. 12, pp. 1547-1567.

Ong, C.S., Fukunishi, T., Zhang, H., Huang, C.Y., Nashed, A., Blazeski, A., DiSilvestre, D., Vricella, L., Conte, J., Tung, L., Tomaselli, G.F. & Hibino, N. 2017, "Biomaterial-Free Three-Dimensional Bioprinting of Cardiac Tissue using Human Induced Pluripotent Stem Cell Derived Cardiomyocytes", *Scientific Reports,* vol. 7, no. 1, pp. 4566.

Oommen, O.P., Shujiang, W., Marta, K., Marije, S., Hilborn Jöns & Varghese, O.P. 2013, "Smart Design of Stable Extracellular Matrix Mimetic Hydrogel: Synthesis, Characterization, and in Vitro and in Vivo Evaluation for Tissue Engineering", *Advanced Functional Materials,* vol. 23, no. 10, pp. 1273-1280.

Osmałek, T., Froelich, A. & Tasarek, S. 2014, "Application of Gellan Gum in Pharmacy and Medicine", *International Journal of Pharmaceutics,* vol. 466, no. 1–2, pp. 328-340.

Ossipov, D.A. & Hilborn, J. 2006, "Poly(Vinyl Alcohol)-Based Hydrogels Formed by "Click Chemistry"", *Macromolecules,* vol. 39, no. 5, pp. 1709-1718.

Ossipov, D.A., Piskounova, S., Varghese, O.P. & Hilborn, J. 2010, "Functionalization of Hyaluronic Acid with Chemoselective Groups Via a Disulfide-Based Protection Strategy for in Situ Formation of Mechanically Stable Hydrogels", *Biomacromolecules,* vol. 11, no. 9, pp. 2247-2254.

Oyen, M.L. 2014, "Mechanical Characterisation of Hydrogel Materials", *International Materials Reviews,* vol. 59, no. 1, pp. 44-59.

Oyen, M.L. 2015, "Nanoindentation of Hydrated Materials and Tissues", *Current Opinion in Solid State and Materials Science,* vol. 19, no. 6, pp. 317-323.

Pacelli, S., Paolicelli, P., Moretti, G., Petralito, S., Di Giacomo, S., Vitalone, A. & Casadei, M.A. 2016, "Gellan Gum Methacrylate and Laponite as an Innovative Nanocomposite Hydrogel for Biomedical Applications", *European Polymer Journal,* vol. 77, pp. 114-123.

Paci, M., Pölönen, R., Cori, D., Penttinen, K., Aalto-Setälä, K., Severi, S. & Hyttinen, J. 2018, "Automatic Optimization of an in Silico Model of Human iPSC Derived Cardiomyocytes Recapitulating Calcium Handling Abnormalities", *Frontiers in Physiology,* [Online], vol. 9, , Article ID 709.

Palanca, M., Tozzi, G. & Cristofolini, L. 2016, "The use of Digital Image Correlation in the Biomechanical Area: A Review", *International Biomechanics,* vol. 3, no. 1, pp. 1-21.

Parraga, J.E., Zorzi, G.K., Diebold, Y., Seijo, B. & Sanchez, A. 2014, "Nanoparticles Based on Naturally-Occurring Biopolymers as Versatile Delivery Platforms for Delicate Bioactive Molecules: An Application for Ocular Gene Silencing", *International Journal of Pharmaceutics,* vol. 477, no. 1–2, pp. 12-20.

Pastrana, E. 2010, "Optogenetics: Controlling Cell Function with Light", *Nature Methods,* vol. 8, pp. 24.

Patel, A. & Mequanint, K. 2011, "Hydrogel Biomaterials" in *Biomedical Engineering - Frontiers and Challenges*, ed. R. Fazel-Rezai, InTech, Rijeka, pp. 275-296.

Patlazhan, G., Unukovych, D. & Pshenisnov, K. 2013, "Breast Reconstruction and Treatment Algorithm for Patients with Complications After Polyacrylamide Gel Injections: A 10-Year Experience", *Aesthetic Plastic Surgery,* vol. 37, no. 2, pp. 312-320.

Paxton, N., Smolan, W., Böck, T., Melchels, F., Groll, J. & Jungst, T. 2017, "Proposal to Assess Printability of Bioinks for Extrusion-Based Bioprinting and Evaluation of Rheological Properties Governing Bioprintability", *Biofabrication,* vol. 9, no. 4, pp. 044107.

Pelham, R.J. & Wang, Y. 1997, "Cell Locomotion and Focal Adhesions are Regulated by Substrate flexibility", *Proceedings of the National Academy of Sciences,* vol. 94, no. 25, pp. 13661-13665.

Peña, A., Bolton, M.D., Whitehouse, H. & Pickard, J.D. 1999, "Effects of Brain Ventricular Shape on Periventricular Biomechanics: A Finite-Element Analysis", *Neurosurgery,* vol. 45, no. 1, pp. 107-118.

Penttinen, K., Swan, H., Vanninen, S., Paavola, J., Lahtinen, A.M., Kontula, K. & Aalto-Setala, K. 2015, "Antiarrhythmic Effects of Dantrolene in Patients with Catecholaminergic Polymorphic Ventricular Tachycardia and Replication of the Responses using iPSC Models", *PloS One,* [Online], vol. 10, no. 5, Article ID e0125366.

Peppas, N.A., Hilt, J.Z., Khademhosseini, A. & Langer, R. 2006, "Hydrogels in Biology and Medicine: From Molecular Principles to Bionanotechnology", *Advanced Materials,* vol. 18, no. 11, pp. 1345-1360.

Pereira, D.R., Silva-Correia, J., Caridade, S.G., Oliveira, J.T., Sousa, R.A., Salgado, A.J., Oliveira, J.M., Mano, J.F., Sousa, N. & Reis, R.L. 2011, "Development of Gellan Gum-Based Microparticles/Hydrogel Matrices for Application in the Intervertebral Disc Regeneration", *Tissue Engineering. Part C, Methods,* vol. 17, no. 10, pp. 961-972.

Perugini, V., Guildford, A.L., Silva-Correia, J., Oliveira, J.M., Meikle, S.T., Reis, R.L. & Santin, M. 2018, "Anti-Angiogenic Potential of VEGF Blocker Dendron-Laden Gellan Gum Hydrogels for Tissue Engineering Applications", *Journal of Tissue Engineering and Regenerative Medicine,* vol. 12, pp. 669-678.

Place, E.S., Evans, N.D. & Stevens, M.M. 2009, "Complexity in Biomaterials for Tissue Engineering", *Nature Materials,* vol. 8, pp. 457.

Pogoda, K., Chin, L., Georges, P.C., Byfield, F.J., Bucki, R., Kim, R., Weaver, M., Wells, R.G., Marcinkiewicz, C. & Janmey, P.A. 2014, "Compression Stiffening of Brain and its Effect on Mechanosensing by Glioma Cells", *New Journal of Physics,* [Online], vol. 16, no. 7, Article ID 075002.

Poole, C.A., Brookes, N.H. & Clover, G.M. 1993, "Keratocyte Networks Visualised in the Living Cornea using Vital Dyes", *Journal of Cell Science,* vol. 106, no. 2, pp. 685.

Potjewyd, G., Moxon, S., Wang, T., Domingos, M. & Hooper, N.M. 2018, "Tissue Engineering 3D Neurovascular Units: A Biomaterials and Bioprinting Perspective", *Trends in Biotechnology,* vol. 36, no. 4, pp. 457-472.

Prajapati, C., Pölönen, R. & Aalto-Setälä, K. 2018, "Simultaneous Recordings of Action Potentials and Calcium Transients from Human Induced Pluripotent Stem Cell Derived Cardiomyocytes", *Biology Open,* [Online], vol. 7, no. 7, Article ID bio035030.

Prajapati, V.D., Jani, G.K., Zala, B.S. & Khutliwala, T.A. 2013, "An Insight into the Emerging Exopolysaccharide Gellan Gum as a Novel Polymer", *Carbohydrate Polymers,* vol. 93, no. 2, pp. 670-678.

Quadrato, G., Brown, J. & Arlotta, P. 2016, "The Promises and Challenges of Human Brain Organoids as Models of Neuropsychiatric Disease", *Nature Medicine,* vol. 22, no. 11, pp. 1220-1228.

Rajala, K., Lindroos, B., Hussein, S.M., Lappalainen, R.S., Pekkanen-Mattila, M., Inzunza, J., Rozell, B., Miettinen, S., Narkilahti, S., Kerkelä, E., Aalto-Setälä, K., Otonkoski, T., Suuronen, R., Hovatta, O. & Skottman, H. 2010, "A Defined and Xeno-Free Culture Method Enabling the Establishment of Clinical-Grade Human Embryonic, Induced Pluripotent and Adipose Stem Cells", *PloS One,* [Online], vol. 5, no. 4, Article ID e10246.

Raub, C.B., Putnam, A.J., Tromberg, B.J. & George, S.C. 2010, "Predicting Bulk Mechanical Properties of Cellularized Collagen Gels using Multiphoton Microscopy", *Acta Biomaterialia,* vol. 6, no. 12, pp. 4657-4665.

Reinhardt, P., Glatza, M., Hemmer, K., Tsytsyura, Y., Thiel, C.S., Höing, S., Moritz, S., Parga, J.A., Wagner, L., Bruder, J.M., Wu, G., Schmid, B., Röpke, A., Klingauf, J., Schwamborn, J.C., Gasser, T., Schöler, H.R. & Sterneckert, J. 2013, "Derivation and Expansion using Only Small Molecules of Human Neural Progenitors for Neurodegenerative Disease Modeling", *PLoS One,* [Online], vol. 8, no. 3, Article ID e59252.

Reis, L.A., Chiu, L.L., Wu, J., Feric, N., Laschinger, C., Momen, A., Li, R.K. & Radisic, M. 2015, "Hydrogels with Integrin-Binding Angiopoietin-1-Derived Peptide, QHREDGS, for Treatment of Acute Myocardial Infarction", *Circulation.Heart Failure,* vol. 8, no. 2, pp. 333-341.

Ribas, J., Sadeghi, H., Manbachi, A., Leijten, J., Brinegar, K., Zhang, Y.S., Ferreira, L. & Khademhosseini, A. 2016, "Cardiovascular Organ-on-a-Chip Platforms for Drug Discovery and Development", *Applied In Vitro Toxicology,* vol. 2, no. 2, pp. 82-96.

Rijal, G. & Li, W. 2017, "A Versatile 3D Tissue Matrix Scaffold System for Tumor Modeling and Drug Screening", *Science Advances,* vol. 3, no. 9.

Roberts, J.J., Audrey, E., Ferguson, V.L. & Bryant, S.J. 2011, "Comparative Study of the Viscoelastic Mechanical Behavior of Agarose and Poly(Ethylene Glycol) Hydrogels", *Journal of Biomedical Materials Research Part B: Applied Biomaterials,* vol. 99B, no. 1, pp. 158-169.

Robinton, D.A. & Daley, G.Q. 2012, "The Promise of Induced Pluripotent Stem Cells in Research and Therapy", *Nature,* vol. 481, no. 7381, pp. 295-305.

Roden, D.M. 2004, "Drug-Induced Prolongation of the QT Interval", *New England Journal of Medicine,* vol. 350, no. 10, pp. 1013-1022.

Roshanbinfar, K., Hilborn, J., Varghese, O.P. & Oommen, O.P. 2017, "Injectable and Thermoresponsive Pericardial Matrix Derived Conductive Scaffold for Cardiac Tissue Engineering", *RSC Advances,* vol. 7, no. 51, pp. 31980-31988.

Roylance, D. 2001, *Lecture Material: Engineering Viscoelasticity,* Department of Materials Science and Engineering, Massachusetts Institute of Technology, Cambridge, Massachusetts, USA.

Rutschmann, C., Baumann, S., Cabalzar, J., Luther, K.B. & Hennet, T. 2014, "Recombinant Expression of Hydroxylated Human Collagen in Escherichia Coli", *Applied Microbiology and Biotechnology,* vol. 98, no. 10, pp. 4445-4455.

Saldin, L.T., Cramer, M.C., Velankar, S.S., White, L.J. & Badylak, S.F. 2017, "Extracellular Matrix Hydrogels from Decellularized Tissues: Structure and Function", *Acta Biomaterialia,* vol. 49, no. Supplement C, pp. 1-15.

Santaoja, K. 2014, *Lecture Notes on Continuum Thermodynamics,* Taras, Espoo, Finland.

Sanz-Garcia, A., Oliver-de-la-Cruz, J., Mirabet, V., Gandía, C., Villagrasa, A., Sodupe, E. & Escobedo-Lucea, C. 2015, "Heart Valve Tissue Engineering: How Far is the Bedside from the Bench?", *Expert Reviews in Molecular Medicine,* vol. 17, pp. e16.

Schmidt, C.E. & Leach, J.B. 2003, "Neural Tissue Engineering: Strategies for Repair and Regeneration", *Annual Review of Biomedical Engineering,* vol. 5, no. 1, pp. 293-347.

Schneider, C.A., Rasband, W.S. & Eliceiri, K.W. 2012, "NIH Image to ImageJ: 25 Years of Image Analysis", *Nature Methods,* vol. 9, no. 7, pp. 671-675.

Schramm, G. 1998, *A Practical Approach to Rheology and Rheometry,* 2nd edn, Gebrueder HAAKE GmbH, Karlsruhe, Germany.

Schreier, H., Orteu, J. & Sutton, M.A. 2009, *Image Correlation for Shape, Motion and Deformation Measurements,* Springer US, New York, USA.

Scuderi, G.J. & Butcher, J. 2017, "Naturally Engineered Maturation of Cardiomyocytes", *Frontiers in Cell and Developmental Biology,* vol. 5, no. 50, pp. 1-28.

Sensharma, P., Madhumathi, G., Jayant, R.D. & Jaiswal, A.K. 2017, "Biomaterials and Cells for Neural Tissue Engineering: Current Choices", *Materials Science and Engineering: C,* vol. 77, pp. 1302-1315.

SFS-EN ISO 10993-1 2009, *Biological Evaluation of Medical Devices. Part 1: Evaluation and Testing within a Risk Management Process,* CEN, Finnish Standards Association, Helsinki, Finland.

SFS-EN ISO 10993-5 2009, *Biological Evaluation of Medical Devices. Part 5: Tests for in Vitro Cytotoxicity,* Finnish Standards Association, Helsinki, Finland.

SFS-EN ISO 604 2004, *Plastics. Determination of Compressive Properties,* Suomen Standardoimisliitto SFS & Chemical Industry Federation of Finland.

Shah, S.B. & Singh, A. 2017, "Cellular Self-Assembly and Biomaterials-Based Organoid Models of Development and Diseases", *Acta Biomaterialia,* vol. 53, pp. 29-45.

Sharpe, J., Ahlgren, U., Perry, P., Hill, B., Ross, A., Hecksher-Sørensen, J., Baldock, R. & Davidson, D. 2002, "Optical Projection Tomography as a Tool for 3D Microscopy and Gene Expression Studies", *Science,* vol. 296, no. 5567, pp. 541-545.

Sheehy, S.P., Grosberg, A., Qin, P., Behm, D.J., Ferrier, J.P., Eagleson, M.A., Nesmith, A.P., Krull, D., Falls, J.G., Campbell, P.H., McCain, M.L., Willette, R.N., Hu, E. & Parker, K.K. 2017, "Toward Improved Myocardial Maturity in an Organ-on-Chip Platform with Immature Cardiac Myocytes", *Experimental Biology and Medicine,* vol. 242, no. 17, pp. 1643-1656.

Shen, H., Lv, Y., Xu, J., Hong, X., Zeng, B., Xiao, W. & Zheng, L. 2012, "Complications After Polyacrylamide Hydrogel Injection for Facial Soft-Tissue Augmentation in China: Twenty-Four Cases and their Surgical Management", *Plastic and Reconstructive Surgery,* vol. 130, no. 2, pp. 340e-348e.

Shim, J.L. 1985. US Patent 4,517,216. *Gellan Gum/Gelatin Blends.* N.J., USA.

Shin, H., Olsen, B.D. & Khademhosseini, A. 2012, "The Mechanical Properties and Cytotoxicity of Cell-Laden Double-Network Hydrogels Based on Photocrosslinkable Gelatin and Gellan Gum Biomacromolecules", *Biomaterials,* vol. 33, no. 11, pp. 3143-3152.

Shin, J., Lee, J.S., Lee, C., Park, H., Yang, K., Jin, Y., Ryu, J.H., Hong, K.S., Moon, S., Chung, H., Yang, H.S., Um, S.H., Oh, J., Kim, D., Lee, H. & Cho, S. 2015, "Tissue Adhesive Catechol-Modified Hyaluronic Acid Hydrogel for Effective, Minimally Invasive Cell Therapy", *Advanced Functional Materials,* vol. 25, no. 25, pp. 3814-3824.

Shin, S.R., Jung, S.M., Zalabany, M., Kim, K., Zorlutuna, P., Kim, S.B., Nikkhah, M., Khabiry, M., Azize, M., Kong, J., Wan, K., Palacios, T., Dokmeci, M.R., Bae, H., Tang, X. & Khademhosseini, A. 2013, "Carbon-Nanotube-Embedded Hydrogel Sheets for Engineering Cardiac Constructs and Bioactuators", *ACS Nano,* vol. 7, no. 3, pp. 2369-2380.

Shoulders, M.D. & Raines, R.T. 2009, "Collagen Structure and Stability", *Annual Review of Biochemistry,* vol. 78, no. 1, pp. 929-958.

Shukla, S. & Shukla, A. 2018, "Tunable Antibiotic Delivery from Gellan Hydrogels", *Journal of Materials Chemistry B,* vol. 6, pp. 6444-6458.

Silva, N.A., Cooke, M.J., Tam, R.Y., Sousa, N., Salgado, A.J., Reis, R.L. & Shoichet, M.S. 2012, "The Effects of Peptide Modified Gellan Gum and Olfactory Ensheathing Glia Cells on Neural Stem/Progenitor Cell Fate", *Biomaterials,* vol. 33, no. 27, pp. 6345-6354.

Silva-Correia, J., Miranda-Gonçalves, V., Salgado, A.J., Sousa, N., Oliveira, J.M., Reis, R.M. & Reis, R.L. 2012, "Angiogenic Potential of Gellan-Gum-Based Hydrogels for Application in Nucleus Pulposus Regeneration: In Vivo Study", *Tissue Engineering Part A,* vol. 18, no. 11-12, pp. 1203-1212.

Silva-Correia, J., Oliveira, J.M., Caridade, S.G., Oliveira, J.T., Sousa, R.A., Mano, J.F. & Reis, R.L. 2011, "Gellan Gum-Based Hydrogels for Intervertebral Disc Tissue-Engineering Applications", *Journal of Tissue Engineering and Regenerative Medicine,* vol. 5, no. 6, pp. 97-107.

Simon-Yarza, T., Bataille, I. & Letourneur, D. 2017, "Cardiovascular Bio-Engineering: Current State of the Art", *Journal of Cardiovascular Translational Research,* vol. 10, no. 2, pp. 180-193.

Skip Rocheford, W.E. & Hower, J. 1998, "Rheology in Daily Life – the New Orbitz Drink", *The Society of Rheology 70th Annual Meeting*, ed. S.J. Muller, The Society of Rheology, Monterey, California, USA, 4.-8.10.1998, pp. 8.

Skottman, H. 2010, "Derivation and Characterization of Three New Human Embryonic Stem Cell Lines in Finland", *In Vitro Cellular & Developmental Biology - Animal,* vol. 46, no. 3, pp. 206-209.

Slaughter, B.V., Khurshid, S.S., Fisher, O.Z., Khademhosseini, A. & Peppas, N.A. 2009, "Hydrogels in Regenerative Medicine", *Advanced Materials,* vol. 21, no. 32-33, pp. 3307-3329.

Smith, A.M., Shelton, R.M., Perrie, Y. & Harris, J.J. 2007, "An Initial Evaluation of Gellan Gum as a Material for Tissue Engineering Applications", *Journal of Biomaterials Applications,* vol. 22, no. 3, pp. 241-254.

Smith, L.E., Smallwood, R. & Macneil, S. 2010, "A Comparison of Imaging Methodologies for 3D Tissue Engineering", *Microscopy Research and Technique,* vol. 73, no. 12, pp. 1123-1133.

Sorkio, A.E., Vuorimaa-Laukkanen, E.P., Hakola, H.M., Liang, H., Ujula, T.A., Valle-Delgado, J.J., Österberg, M., Yliperttula, M.L. & Skottman, H. 2015, "Biomimetic Collagen I and IV Double Layer Langmuir–Schaefer Films As microenvironment for Human Pluripotent Stem Cell Derived Retinal Pigment Epithelial Cells", *Biomaterials,* vol. 51, no. 0, pp. 257-269.

Soucy, J.R., Shirzaei Sani, E., Portillo Lara, R., Diaz, D., Dias, F., Weiss, A.S., Koppes, A.N., Koppes, R.A. & Annabi, N. 2018, "Photocrosslinkable Gelatin/Tropoelastin Hydrogel Adhesives for Peripheral Nerve Repair", *Tissue Engineering Part A,* vol. 24, no. 17-18, pp. 1393-1405.

Steimberg, N., Mazzoleni, G., Ciamporcero, E., Ullio, C., Daga, M., Barrera, G. & Pizzimenti, S. 2014, "In Vitro Modeling of Tissue-Specific 3D Microenvironments and Possibile Application to Pediatric Cancer Research", *Journal of Pediatric Oncology,* vol. 2, no. 1, pp. 40-76.

Stevens, L.R., Gilmore, K.J., Wallace, G.G. & in het Panhuis, M. 2016, "Tissue Engineering with Gellan Gum", *Biomaterials Science,* vol. 4, no. 9, pp. 1276-1290.

Storm, C., Pastore, J.J., MacKintosh, F.C., Lubensky, T.C. & Janmey, P.A. 2005, "Nonlinear Elasticity in Biological Gels", *Nature,* vol. 435, no. 7039, pp. 191-194.

Swan, H., Piippo, K., Viitasalo, M., Heikkilä, P., Paavonen, T., Kainulainen, K., Kere, J., Keto, P., Kontula, K. & Toivonen, L. 1999, "Arrhythmic Disorder Mapped to Chromosome 1q42–q43 Causes Malignant Polymorphic Ventricular Tachycardia in Structurally Normal Hearts", *Journal of the American College of Cardiology,* vol. 34, no. 7, pp. 2035-2042.

Szczesniak, A.S. 2002, "Texture is a Sensory Property", *Food Quality and Preference,* vol. 13, no. 4, pp. 215-225.

Takahashi, K., Tanabe, K., Ohnuki, M., Narita, M., Ichisaka, T., Tomoda, K. & Yamanaka, S. 2007, "Induction of Pluripotent Stem Cells from Adult Human Fibroblasts by Defined Factors", *Cell,* vol. 131, no. 5, pp. 861-872.

Takahashi, K. & Yamanaka, S. 2006, "Induction of Pluripotent Stem Cells from Mouse Embryonic and Adult Fibroblast Cultures by Defined Factors", *Cell,* vol. 126, no. 4, pp. 663-676.

Talkhabi, M., Aghdami, N. & Baharvand, H. 2016, "Human Cardiomyocyte Generation from Pluripotent Stem Cells: A State-of-Art", *Life Sciences,* vol. 145, pp. 98-113.

Tan, S.H. & Ye, L. 2018, "Maturation of Pluripotent Stem Cell-Derived Cardiomyocytes: A Critical Step for Drug Development and Cell Therapy", *Journal of Cardiovascular Translational Research,* vol. 11, no. 5, pp. 375-392.

Tang, J., Tung, M.A. & Zeng, Y. 1996, "Compression Strength and Deformation of Gellan Gels Formed with Mono- and Divalent Cations", *Carbohydrate Polymers,* vol. 29, no. 1, pp. 11-16.

Tang, Y., Sun, J., Fan, H. & Zhang, X. 2012, "An Improved Complex Gel of Modified Gellan Gum and Carboxymethyl Chitosan for Chondrocytes Encapsulation", *Carbohydrate Polymers,* vol. 88, no. 1, pp. 46-53.

Tang-Schomer, M., White, J.D., Tien, L.W., Schmitt, L.I., Valentin, T.M., Graziano, D.J., Hopkins, A.M., Omenetto, F.G., Haydon, P.G. & Kaplan, D.L. 2014, "Bioengineered Functional Brain-Like Cortical Tissue", *Proceedings of the National Academy of Sciences of the United States of America,* vol. 111, no. 38, pp. 13811-13816.

Tanodekaew, S., Godward, J., Heatley, F. & Booth, C. 1997, "Gelation of Aqueous Solutions of Diblock Copolymers of Ethylene Oxide and D,L-Lactide", *Macromolecular Chemistry and Physics,* vol. 198, no. 11, pp. 3385-3395.

Taylor, Z. & Miller, K. 2004, "Reassessment of Brain Elasticity for Analysis of Biomechanisms of Hydrocephalus", *Journal of Biomechanics,* vol. 37, no. 8, pp. 1263-1269.

Tezera, L.B., Bielecka, M.K., Chancellor, A., Reichmann, M.T., Shammari, B.A., Brace, P., Batty, A., Tocheva, A., Jogai, S., Marshall, B.G., Tebruegge, M., Jayasinghe, S.N., Mansour, S. & Elkington, P.T. 2017, "Dissection of the Host-Pathogen Interaction in Human Tuberculosis using a Bioengineered 3-Dimensional Model", *eLife,* [Online], vol. 6, , Article ID e21283.

Tirkkonen, L., Halonen, H., Hyttinen, J., Kuokkanen, H., Sievanen, H., Koivisto, A.M., Mannerstrom, B., Sandor, G.K., Suuronen, R., Miettinen, S. & Haimi, S. 2011, "The Effects of Vibration Loading on Adipose Stem Cell Number, Viability and Differentiation Towards Bone-Forming Cells", *Journal of The Royal Society Interface,* vol. 8, pp. 1736-1747.

Toivanen, M., Pelkonen, A., Mäkinen, M., Ylä-Outinen, L., Sukki, L., Kallio, P., Ristola, M. & Narkilahti, S. 2017, "Optimised PDMS Tunnel Devices on MEAs Increase the Probability of Detecting Electrical Activity from Human Stem Cell-Derived Neuronal Networks", *Frontiers in Neuroscience,* vol. 11, pp. 606.

Toivonen, S., Ojala, M., Hyysalo, A., Ilmarinen, T., Rajala, K., Pekkanen-Mattila, M., Äänismaa, R., Lundin, K., Palgi, J., Weltner, J., Trokovic, R., Silvennoinen, O., Skottman, H., Narkilahti, S., Aalto-Setälä, K. & Otonkoski, T. 2013, "Comparative Analysis of Targeted Differentiation of Human Induced Pluripotent Stem Cells (hiP-

SCs) and Human Embryonic Stem Cells Reveals Variability Associated with Incomplete Transgene Silencing in Retrovirally Derived hiPSC Lines", *Stem Cells Translational Medicine,* vol. 2, no. 2, pp. 83-93.

Trappmann, B., Gautrot, J.E., Connelly, J.T., Strange, D.G.T., Li, Y., Oyen, M.L., Cohen Stuart, M.A., Boehm, H., Li, B., Vogel, V., Spatz, J.P., Watt, F.M. & Huck, W.T.S. 2012, "Extracellular-Matrix Tethering Regulates Stem-Cell Fate", *Nature Materials,* vol. 11, no. 7, pp. 642-649.

Trounson, A. & McDonald, C. 2015, "Stem Cell Therapies in Clinical Trials: Progress and Challenges", *Cell Stem Cell,* vol. 17, no. 1, pp. 11-22.

Truong, V.X., Hun, M.L., Li, F., Chidgey, A.P. & Forsythe, J.S. 2016, "In Situ-Forming Click-Crosslinked Gelatin Based Hydrogels for 3D Culture of Thymic Epithelial Cells", *Biomaterials Science,* vol. 4, no. 7, pp. 1123-1131.

Tsaryk, R., Silva-Correia, J., Oliveira, J.M., Unger, R.E., Landes, C., Brochhausen, C., Ghanaati, S., Reis, R.L. & Kirkpatrick, C.J. 2014, "Biological Performance of Cell-Encapsulated Methacrylated Gellan Gum-Based Hydrogels for Nucleus Pulposus Regeneration", *Journal of Tissue Engineering and Regenerative Medicine,* vol. 11, no. 3, pp. 637-648.

Turunen, S., Joki, T., Hiltunen, M.L., Ihalainen, T.O., Narkilahti, S. & Kellomäki, M. 2017, "Direct Laser Writing of Tubular Microtowers for 3D Culture of Human Pluripotent Stem Cell-Derived Neuronal Cells", *ACS Applied Materials & Interfaces,* vol. 9, no. 31, pp. 25717-25730.

Tzatzalos, E., Abilez, O.J., Shukla, P. & Wu, J.C. 2016, "Engineered Heart Tissues and Induced Pluripotent Stem Cells: Macro- and Microstructures for Disease Modeling, Drug Screening, and Translational Studies", *Advanced Drug Delivery Reviews,* vol. 96, pp. 234-244.

van Bemmelen, J.M. 1894, "Das Hydrogel Und Das Krystallinische Hydrat Des Kupferoxyds", *Zeitschrift für Anorganische Chemie,* vol. 5, no. 1, pp. 466-483.

Van Den Bulcke, A.I., Bogdanov, B., De Rooze, N., Schacht, E.H., Cornelissen, M. & Berghmans, H. 2000, "Structural and Rheological Properties of Methacrylamide Modified Gelatin Hydrogels", *Biomacromolecules,* vol. 1, no. 1, pp. 31-38.

van Uden, S., Silva-Correia, J., Oliveira, J.M. & Reis, R.L. 2017, "Current Strategies for Treatment of Intervertebral Disc Degeneration: Substitution and Regeneration Possibilities", *Biomaterials Research,* vol. 21, no. 1, pp. 22.

Van Vlierberghe, S., Dubruel, P. & Schacht, E. 2011, "Biopolymer-Based Hydrogels as Scaffolds for Tissue Engineering Applications: A Review", *Biomacromolecules,* vol. 12, no. 5, pp. 1387-1408.

Vasilevich, A.S., Carlier, A., de Boer, J. & Singh, S. 2017, "How Not to Drown in Data: A Guide for Biomaterial Engineers", *Trends in Biotechnology,* vol. 35, no. 8, pp. 743-755.

Vasilevich, A. & de Boer, J. 2018, "Robot-Scientists Will Lead Tomorrow's Biomaterials Discovery", *Current Opinion in Biomedical Engineering,* vol. 6, pp. 74-80.

Vats, A., Bielby, R., Tolley, N., Nerem, R. & Polak, J. 2005, "Stem Cells", *The Lancet,* vol. 366, no. 9485, pp. 592-602.

Vegas, A.J., Veiseh, O., Doloff, J.C., Ma, M., Tam, H.H., Bratlie, K., Li, J., Bader, A.R., Langan, E., Olejnik, K., Fenton, P., Kang, J.W., Hollister-Locke, J., Bochenek, M.A., Chiu, A., Siebert, S., Tang, K., Jhunjhunwala, S., Aresta-Dasilva, S., Dholakia, N., Thakrar, R., Vietti, T., Chen, M., Cohen, J., Siniakowicz, K., Qi, M., McGarrigle, J., Graham, A.C., Lyle, S., Harlan, D.M., Greiner, D.L., Oberholzer, J., Weir, G.C., Langer, R. & Anderson, D.G. 2016, "Combinatorial Hydrogel Library Enables Identification of Materials that Mitigate the Foreign Body Response in Primates", *Nature Biotechnology,* vol. 34, pp. 345-352.

Venturoli, D. & Rippe, B. 2005, "Ficoll and Dextran Vs. Globular Proteins as Probes for Testing Glomerular Permselectivity: Effects of Molecular Size, Shape, Charge, and Deformability", *American Journal of Physiology-Renal Physiology,* vol. 288, no. 4, pp. F605-F613.

Vert, M., Doi, Y., Hellwich, K., Hess, M., Hodge, P., Kubisa, P., Rinaudo, M. & Schué, F. 2012, "Terminology for Biorelated Polymers and Applications (IUPAC Recommendations 2012)", *Pure and Applied Chemistry,* vol. 84, no. 2, pp. 377-378-410.

Vielreicher, M., Schürmann, S., Detsch, R., Schmidt, M.A., Buttgereit, A., Boccaccini, A. & Friedrich, O. 2013, "Taking a Deep Look: Modern Microscopy Technologies to Optimize the Design and Functionality of Biocompatible Scaffolds for Tissue Engineering in Regenerative Medicine", *Journal of The Royal Society Interface,* [Online], vol. 10, no. 86, Article ID 20130263.

Vilela, C.A., Correia, C., da Silva Morais, A., Santos, T.C., Gertrudes, A.C., Moreira, E.S., Frias, A.M., Learmonth, D.A., Oliveira, P., Oliveira, J.M., Sousa, R.A., Espregueira-Mendes, J.D. & Reis, R.L. 2018, "In Vitro and in Vivo Performance of Methacrylated Gellan Gum Hydrogel Formulations for Cartilage Repair", *Journal of Biomedical Materials Research. Part A,* vol. 106, no. 7, pp. 1987-1996.

Virjula, S., Zhao, F., Leivo, J., Vanhatupa, S., Kreutzer, J., Vaughan, T.J., Honkala, A., Viehrig, M., Mullen, C.A., Kallio, P., McNamara, L.M. & Miettinen, S. 2017, "The Effect of Equiaxial Stretching on the Osteogenic Differentiation and Mechanical Properties of Human Adipose Stem Cells", *Journal of the Mechanical Behavior of Biomedical Materials,* vol. 72, pp. 38-48.

Vogel, V. 2018, "Unraveling the Mechanobiology of Extracellular Matrix", *Annual Review of Physiology,* vol. 80, pp. 353-387.

Vos, T., Abajobir, A.A., Abate, K.H., Abbafati, C., Abbas, K.M., Abd-Allah, F., Abdulkader, R.S., Abdulle, A.M., Abebo, T.A., Abera, S.F., Aboyans, V., Abu-Raddad, L.J., Ackerman, I.N., Adamu, A.A., Adetokunboh, O., Afarideh, M., Afshin, A., Agarwal, S.K., Aggarwal, R., Agrawal, A., Agrawal, S., Ahmadieh, H., Ahmed, M.B., Aichour, M.T.E., Aichour, A.N., Aichour, I., Aiyar, S., Akinyemi, R.O., Akseer, N., Al Lami, F.H., Alahdab, F., Al-Aly, Z., Alam, K., Alam, N., Alam, T., Alasfoor, D., Alene, K.A., Ali, R., Alizadeh-Navaei, R., Alkerwi, A., Alla, F., Allebeck, P., Allen, C., Al-Maskari, F., Al-Raddadi, R., Alsharif, U., Alsowaidi, S., Altirkawi, K.A., Amare, A.T., Amini, E., Ammar, W., Amoako, Y.A., Andersen, H.H., Antonio, C.A.T., Anwari, P., Ärnlöv, J., Artaman, A., Aryal, K.K., Asayesh, H., Asgedom, S.W., Assadi, R., Atey, T.M., Atnafu, N.T., Atre, S.R., Avila-Burgos, L., Avokphako, E.F.G.A., Awasthi, A., Bacha, U., Badawi, A., Balakrishnan, K., Banerjee, A., Bannick, M.S., Barac, A., Barber, R.M., Barker-Collo, S.L., Bärnighausen, T., Barquera, S., Barregard, L., Barrero, L.H., Basu, S., Battista, B., Battle, K.E., Baune, B.T., Bazargan-Hejazi, S., Beardsley, J., Bedi, N., Beghi, E., Béjot, Y., Bekele, B.B., Bell, M.L., Bennett, D.A., Bensenor, I.M., Benson, J., Berhane, A., Berhe, D.F., Bernabé, E., Betsu, B.D., Beuran, M., Beyene, A.S., Bhala, N.*, et al* 2017, "Global, Regional, and National Incidence, Prevalence, and Years Lived with Disability for 328 Diseases and Injuries for 195 Countries, 1990–2016: A Systematic Analysis for the Global Burden of Disease Study 2016", *The Lancet,* vol. 390, no. 10100, pp. 1211-1259.

Vuorenpää, H., Penttinen, K., Heinonen, T., Pekkanen-Mattila, M., Sarkanen, J., Ylikomi, T. & Aalto-Setälä, K. 2017, "Maturation of Human Pluripotent Stem Cell Derived Cardiomyocytes is Improved in Cardiovascular Construct", *Cytotechnology,* vol. 69, no. 5, pp. 785-800.

Wallis, R., Benson, C., Darpo, B., Gintant, G., Kanda, Y., Prasad, K., Strauss, D.G. & Valentin, J. 2018, "CiPA Challenges and Opportunities from a Non-Clinical, Clinical and Regulatory Perspectives. an Overview of the Safety Pharmacology Scientific Discussion", *Journal of Pharmacological and Toxicological Methods,* vol. 93, pp. 15-25.

Walters, N.J. & Gentleman, E. 2015, "Evolving Insights in Cell–matrix Interactions: Elucidating how Non-Soluble Properties of the Extracellular Niche Direct Stem Cell Fate", *Acta Biomaterialia,* vol. 11, pp. 3-16.

Wang, C., Gong, Y., Lin, Y., Shen, J. & Wang, D. 2008, "A Novel Gellan Gel-Based Microcarrier for Anchorage-Dependent Cell Delivery", *Acta Biomaterialia,* vol. 4, no. 5, pp. 1226-1234.

Wang, Q., Mohan, A.C., Oyen, M.L. & Zhao, X. 2014, "Separating Viscoelasticity and Poroelasticity of Gels with Different Length and Time Scales", *Acta Mechanica Sinica,* vol. 30, no. 1, pp. 20-27.

Wang, X. & Hong, W. 2012, "A Visco-Poroelastic Theory for Polymeric Gels", *Proceedings of the Royal Society A: Mathematical, Physical and Engineering Science,* vol. 468, no. 2148, pp. 3824.

Wei, C., Wang, Y., Li, M., Li, H., Lu, X., Shao, H. & Xu, C. 2016, "Spermine Inhibits Endoplasmic Reticulum Stress - Induced Apoptosis: A New Strategy to Prevent Cardiomyocyte Apoptosis", *Cellular Physiology and Biochemistry,* vol. 38, no. 2, pp. 531-544.

Wen, C., Lu, L. & Li, X. 2014, "An Interpenetrating Network Biohydrogel of Gelatin and Gellan Gum by using a Combination of Enzymatic and Ionic Crosslinking Approaches", *Polymer International,* vol. 63, no. 9, pp. 1643-1649.

White, A. 2012, "The Materials Genome Initiative: One Year On", *MRS Bulletin,* vol. 37, no. 8, pp. 715-716.

White, J. & Stelzer, E. 1999, "Photobleaching GFP Reveals Protein Dynamics Inside Live Cells", *Trends in Cell Biology,* vol. 9, no. 2, pp. 61-65.

Wichterle, O. & Lím, D. 1960, "Hydrophilic Gels for Biological Use", *Nature,* vol. 185, pp. 117.

Wikimedia Commons 2010, *, File:Latidos.gif*. Available: https://commons.wikimedia.org/wiki/File:Latidos.gif [2018, 11/30].

Wikimedia Commons 2007, *, File:Maxwell diagram.svg*. Available: https://commons.wikimedia.org/wiki/File:Maxwell_diagram.svg [2019, 01/18].

Williams, C.G., Malik, A.N., Kim, T.K., Manson, P.N. & Elisseeff, J.H. 2005, "Variable Cytocompatibility of Six Cell Lines with Photoinitiators used for Polymerizing Hydrogels and Cell Encapsulation", *Biomaterials,* vol. 26, no. 11, pp. 1211-1218.

Williams, D.F. 2017, "Biocompatibility Pathways: Biomaterials-Induced Sterile Inflammation, Mechanotransduction, and Principles of Biocompatibility Control", *ACS Biomaterials Science & Engineering,* vol. 3, no. 1, pp. 2-35.

Williams, D.F. 2008, "On the Mechanisms of Biocompatibility", *Biomaterials,* vol. 29, no. 20, pp. 2941-2953.

Williams, D.F. 2004, "Benefit and Risk in Tissue Engineering", *Materials Today,* vol. 7, no. 5, pp. 24-29.

Woolf, C.J. & Ma, Q. 2007, "Nociceptors—Noxious Stimulus Detectors", *Neuron,* vol. 55, no. 3, pp. 353-364.

Xi, J., Khalil, M., Shishechian, N., Hannes, T., Pfannkuche, K., Liang, H., Fatima, A., Haustein, M., Suhr, F., Bloch, W., Reppel, M., Saric, T., Wernig, M., Jänisch, R., Brockmeier, K., Hescheler, J. & Pillekamp, F. 2010, "Comparison of Contractile Behavior of Native Murine Ventricular Tissue and Cardiomyocytes Derived from Embryonic Or Induced Pluripotent Stem Cells", *The FASEB Journal,* vol. 24, pp. 2739-2751.

Xiao, H., Bruhns, O.T. & Meyers, A. 2004, "Explicit Dual Stress-Strain and Strain-Stress Relations of Incompressible Isotropic Hyperelastic Solids Via Deviatoric Hencky Strain and Cauchy Stress", *Acta Mechanica,* vol. 168, no. 1, pp. 21-33.

Xu, Z., Li, Z., Jiang, S. & Bratlie, K.M. 2018, "Chemically Modified Gellan Gum Hydrogels with Tunable Properties for use as Tissue Engineering Scaffolds", *ACS Omega,* vol. 3, no. 6, pp. 6998-7007.

Yamanaka, S. 2012, "Induced Pluripotent Stem Cells: Past, Present, and Future", *Cell Stem Cell,* vol. 10, no. 6, pp. 678-684.

Yang, H., Wang, Y., Regenstein, J.M. & Rouse, D.B. 2007, "Nanostructural Characterization of Catfish Skin Gelatin using Atomic Force Microscopy", *Journal of Food Science,* vol. 72, no. 8, pp. C430-C440.

Ylä-Outinen, L., Mariani, C., Skottman, H., Suuronen, R., Harlin, A. & Narkilahti, S. 2010, "Electrospun Poly (L, D-Lactide) Scaffolds Support the Growth of Human Embryonic Stem Cell-Derived Neuronal Cells", *Open Tissue Engineering and Regenerative Medicine Journal,* vol. 3, pp. 1-9.

Ylä-Outinen, L., Joki, T., Varjola, M., Skottman, H. & Narkilahti, S. 2012, "Three-Dimensional Growth Matrix for Human Embryonic Stem Cell-Derived Neuronal Cells", *Journal of Tissue Engineering and Regenerative Medicine,* vol. 8, no. 3, pp. 186-187-194.

Young, J.L. & Engler, A.J. 2011, "Hydrogels with Time-Dependent Material Properties Enhance Cardiomyocyte Differentiation in Vitro", *Biomaterials,* vol. 32, no. 4, pp. 1002-1009.

Yue, K., Trujillo-de Santiago, G., Alvarez, M.M., Tamayol, A., Annabi, N. & Khademhosseini, A. 2015, "Synthesis, Properties, and Biomedical Applications of Gelatin Methacryloyl (GelMA) Hydrogels", *Biomaterials,* vol. 73, pp. 254-271.

Zhang, B., Korolj, A., Lai, B.F.L. & Radisic, M. 2018, "Advances in Organ-on-a-Chip Engineering", *Nature Reviews Materials,* vol. 3, no. 8, pp. 257-278.

Zhang, M., Schulte, J.S., Heinick, A., Piccini, I., Rao, J., Quaranta, R., Zeuschner, D., Malan, D., Kim, K., Röpke, A., Sasse, P., Araúzo-Bravo, M., Seebohm, G., Schöler, H., Fabritz, L., Kirchhof, P., Müller, F.U. & Greber, B. 2015, "Universal

Cardiac Induction of Human Pluripotent Stem Cells in 2D and 3D Formats - Implications for in-Vitro Maturation", *Stem Cells,* vol. 33, no. 5, pp. 1456-1469.

Zhang, S., Holmes, T.C., DiPersio, C.M., Hynes, R.O., Su, X. & Rich, A. 1995, "Self-Complementary Oligopeptide Matrices Support Mammalian Cell Attachment", *Biomaterials,* vol. 16, no. 18, pp. 1385-1393.

Zhang, Y.S., Arneri, A., Bersini, S., Shin, S., Zhu, K., Goli-Malekabadi, Z., Aleman, J., Colosi, C., Busignani, F., Dell'Erba, V., Bishop, C., Shupe, T., Demarchi, D., Moretti, M., Rasponi, M., Dokmeci, M.R., Atala, A. & Khademhosseini, A. 2016, "Bioprinting 3D Microfibrous Scaffolds for Engineering Endothelialized Myocardium and Heart-on-a-Chip", *Biomaterials,* vol. 110, pp. 45-59.

Zhu, K., Shin, S.R., van Kempen, T., Li, Y., Ponraj, V., Nasajpour, A., Mandla, S., Hu, N., Liu, X., Leijten, J., Lin, Y., Hussain, M.A., Zhang, Y.S., Tamayol, A. & Khademhosseini, A. 2017, "Gold Nanocomposite Bioink for Printing 3D Cardiac Constructs", *Advanced Functional Materials,* vol. 27, no. 12, pp. 1605352.

Zhu, S., Wang, H. & Ding, S. 2015, "Reprogramming Fibroblasts Toward Cardiomyocytes, Neural Stem Cells and Hepatocytes by Cell Activation and Signaling-Directed Lineage Conversion", *Nature Protocols,* vol. 10, no. 7, pp. 959-973.

Zimmermann, W. 2018, "Cardiomyocytes Remuscularize the Heart", *Nature Biotechnology,* vol. 36, pp. 592-593.

Appendix I – Additional reagents

Supplementary Table 1. Compositions of buffers for enzymatic dissociation of hiPSC-derived cardiomyocytes and the names of the producers of the reagents.

	1st Low Ca^{2+} (priming)	2nd Enzyme (dissociation)	3rd KB (recovery)	Reagent producer
NaCl	1 M	1 M	-	Honeywell Fluka
CaCl$_2$	-	1 M	-	Sigma-Aldrich
K$_2$HPO$_4$	-	-	1 M	Riedel-de Haën
KCl	1 M	1 M	1 M	Sigma-Aldrich
Na$_2$ATP	-	-	2 mM	Sigma-Aldrich
MgSO$_4$	1 M	1 M	1 M	Sigma-Aldrich
EGTA	-	-	0.1 M	Sigma-Aldrich
Sodium Puryvate	1 M	1 M	0.1 M	Lonza
Creatine	-	-	0.1 M	BioChemica
Taurine	0.1 M	0.1 M	0.1 M	Sigma-Aldrich
Collagenase A	-	1 mg/mL	-	Roche Applied Science
HEPES	1 M	1 M	-	Lonza
Glucose	1 M	1 M	1 M	Sigma-Aldrich

Note 1. Correction to pH 6.9 using NaOH needed for 1st and 2nd buffers and to pH 7.2 using HCl for 3rd buffer.
Note 2. Glucose added to 3rd buffer just before using it to avoid precipitation.
Note 3. Resuspension back to culture medium needs to be gentle and quick to avoid damaging the cardiomyocytes.

Supplementary Table 2. TaqMan assays used in the qRT-PCR protocol.

Gene	Description	Function	TaqMan assay ID
TNNT2	Cardiac type troponin T2	Sarcomeric gene	Hs00165960_m1
ACTN2	α-actinin 2	Sarcomeric gene	Hs00153809_m1
MYBPC3	Myosin binding protein C, cardiac	Sarcomeric gene	Hs00165232_m1
GAPDH	Glyceraldehyde-3-phosphate dehydrogenase	Housekeeping gene	Hs02758991_g1

Appendix II – Neuronal cell quality control

hESC　　　　　　　　hiPSC
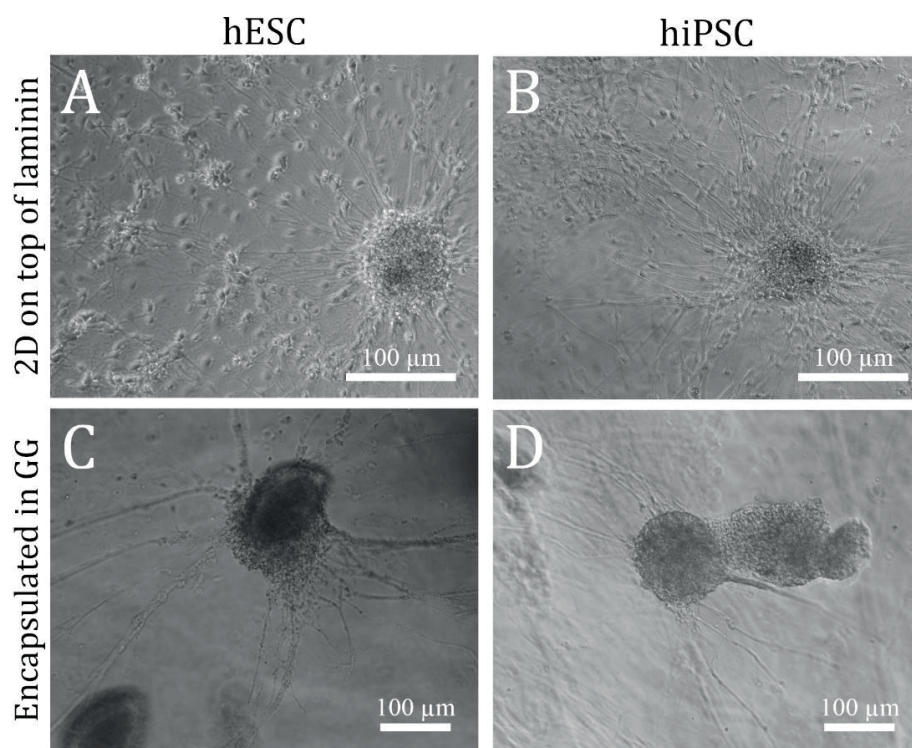
Supplementary Figure 1. Representative phase contrast images of good quality neuronal differentiation and neurite migration (from **Publication I**), (a) & (b) control conditions, (c) & (d) encapsulated in 3D in GG 3.00%SPD with 1% laminin. No difference between hESC and hiPSC origin cell lines.

Appendix III – Hydrogel compression protocol

Here is collected our suggested procedure for hydrogel compression testing based on the findings in **Publication IV**:

1. Choose displacement rate where no leaking of water from the hydrogel is observed in order to negate the poroelasticity effect and to have only viscoelastic material behavior.

2. Sample size should be measured individually for each compression sample due to possible variations in the hydrogel production. Sample height should be low enough to rule out buckling [SFS-EN ISO 604, 2004].

3. Sample slippage can be prevented by adding a small, single-layer piece of wet cellulose wadding paper on both compression plates. This increases friction between the sample and the compression plate and makes the measurement easier. However, this can cause the stress field to be non-uniaxial on the edges of the sample. The paper should be changed between each sample to prevent residue from previous tests reducing the friction and affecting the next measurement.

4. Care should be taken in adjusting the starting point of the measurement to avoid applying an unknown pre-load that can obscure the toe region.

5. Compress over the fracture strain limit to observe the full mechanical behavior range.

6. Data analysis should be done using true stress and true strain instead of engineering stress and engineering strain.

7. The elastic response of hydrogel material is defined using piecewise linear elasticity. The toe region elastic modulus (E_1) and the second elastic modulus (E_2) can be calculated from the stress-strain curve by linear fitting. The strain range of the toe region was calculated by extrapolating the curve tangent of the linear portion of the stress–strain curve to the strain axis. The strain at which the curve crossed the strain axis was taken to be the strain range of the toe region.

ORIGINAL PUBLICATIONS

I

BIOAMINE-CROSSLINKED GELLAN GUM HYDROGEL FOR NEURAL TISSUE ENGINEERING

by

Janne T. Koivisto*, Tiina Joki*, Jenny E. Parraga, Rami Pääkkönen, Laura Ylä-Outinen, Laura Salonen, Ilari Jönkkäri, Marja Peltola, Teemo O. Ihalainen, Susanna Narkilahti, and Minna Kellomäki

Bioamine-crosslinked gellan gum hydrogel for neural tissue engineering

Janne T Koivisto[1,2]*, Tiina Joki[2]*, Jenny E Parraga[1], Rami Pääkkönen[2], Laura Ylä-Outinen[2], Laura Salonen[1], Ilari Jönkkäri[3], Marja Peltola[2], Teemu O Ihalainen[2], Susanna Narkilahti[2]**, Minna Kellomäki[1,2]**

* And ** = writers contributed equally

1 BioMediTech – Biomedical Sciences and Engineering, Tampere University of Technology, Korkeakoulunkatu 3, 33720 Tampere, Finland

2 BioMediTech and Faculty of Medicine and Life Sciences, University of Tampere, Lääkärinkatu 1, 33520 Tampere, Finland

3 Laboratory of Materials Science, Tampere University of Technology, Korkeakoulunkatu 6, 33720 Tampere, Finland

Email: janne.t.koivisto@tut.fi, tiina.joki@uta.fi, susanna.narkilahti@uta.fi, minna.kellomaki@tut.fi

AUTHOR'S ACCEPTED MANUSCRIPT

ABSTRACT:

Neural tissue engineering and 3D *in vitro* tissue modeling require the development of biomaterials that take into account the specified requirements of human neural cells and tissue. In this study, an alternative method of producing biomimetic hydrogels based on gellan gum (GG) was developed by replacing traditional crosslinking methods with the bioamines spermidine and spermine. These bioamines were proven to function as crosslinkers for GG hydrogel at +37°C, allowing for the encapsulation of human neurons. We studied the mechanical and rheological properties of the formed hydrogels, which showed biomimicking properties comparable to naïve rabbit brain tissue under physiologically relevant stress and strain. Human pluripotent stem cell-derived neuronal cells demonstrated good cytocompatibility in the GG-based hydrogels. Moreover, functionalization of GG hydrogels with laminin resulted in cell type-specific behavior: neuronal cell maturation and neurite migration.

1.   Introduction

Tissue engineering (TE) is a field of study that aims to produce tissue-like structures *in vivo* and *in vitro* using a combination of a biomaterial and living cells *[1]*. Thus, TE has combined advances in cell therapy and biomaterials science to stabilize an injury or defect site and deliver cells and molecules to promote the regeneration of damaged tissues *[1; 2]*. Neural TE has emerged as a promising strategy for neural regeneration, both for the central nervous system (CNS) and the peripheral nervous system, which suffer from limited regenerative capacity *[2—4]*. For successful functional neural TE graft, it is important to combine neural tissue mimicking material e.g. a hydrogel and clinically relevant human cell type *[5]*. In addition to therapeutic use in TE, hydrogels as neural scaffolds can also be used for *in vitro* disease modeling, drug testing and developmental biology studies *[5—7]*.

The main requirement for biomaterials intended for TE is biocompatibility *[3; 8; 9]*, defined by the International Union of Pure and Applied Chemistry (IUPAC) as "the ability to be in contact with a living system without producing an adverse effect" *[9]*. Hydrogel biomaterials can fulfill the biocompatibility (systemic scale) and cytocompatibility (cellular scale) requirements *[8]*, and their tunable physical properties can mimic soft tissue, such as CNS *[3—5]*. Thus, while designing hydrogels for TE, important material characteristics to take into account are for example mechanical properties, porosity, permeability and transparency, especially for *in vitro* TE *[4; 10—12]*. Moreover, hydrogels can be further modified to incorporate extracellular matrix (ECM) molecules (such as collagen, fibronectin, and laminin) or peptides to provide anchoring sites for cells and to enhance growth *[3; 4; 11]*.

Gellan gum (GG) is an exopolysaccharide produced by *Sphingomonas elodea* bacteria. This biologically safe polymer has been approved by the Food and Drug Administration (FDA) and the European Medicines Agency (EMA) *[13—15]*, and it has been recently been suggested as a material for scaffold development for TE *[16; 17]*. GG is a deacetylated form of gellan molecule which has a tetrasaccharide repeating structure of β-$_D$-glucose, β-$_D$-glucuronic acid and α-$_L$-rhamnose in a 2:1:1 ratio *[13]*. Like many other polysaccharides, GG is a relatively inert biomaterial *[17]*. To improve cell attachment, GG-based hydrogels have been functionalized with peptides by covalently binding them in the molecule backbone itself *[17; 18]*. GG has been studied for bone *[16; 19]*, cartilage *[20—22]* and

spinal cord *[23—27]* TE applications. In neural applications, GG can support the *in vitro* culture of rodent or human cells (neural stem cells *[18; 28]*, olfactory ensheathing glia cells *[18]*, oligodendrocyte-like cells *[23]*) and has been shown to be biocompatible *in vivo* in a hemisection rat spinal cord injury model *[23]*.

GG hydrogels produced by physical, ionotropic, crosslinking with metallic cations (Ca^{2+}, Mg^{2+}, Na^+, K^+) are primarily mechanically weak *[13; 29]*. Another option is chemical crosslinking using methacrylate derivatives, followed by the addition of a photoinitiator and photocrosslinking with UV-light *[23; 29]*. Disadvantages of these crosslinking methods include cation leakage or exchange, weakening of the mechanical properties of the hydrogel over time *[29; 30]*, phototoxicity of UV-light and chemical reactivity of the photoinitiator *[31—33]*. Chemical crosslinking is often in practice more complicated than ionotropic crosslinking. Bioamines spermine (SPM) and spermidine (SPD) are small cations that have been demonstrated to interact with anionic polymers such as GG *[34—36]*. Crosslinking with bioamines is simple, and a wide crosslinker concentration range can be applied to vary the mechanical properties of GG in a controlled way, so they provide an alternative crosslinking method. SPM and SPD are present in all living cells, and they play important roles in many physiological processes, such as protecting DNA by scavenging oxygen radicals and affecting cell proliferation *[37; 38]* also in neural cells *[39; 40]*.

In this study, we developed GG bioamine hydrogels with mechanical properties that resemble brain tissue. The resulting hydrogels were characterized mechanically and rheologically. The mechanical properties of these hydrogels were compared to naïve rabbit brain tissue by compression testing. Hydrogels with a compressive modulus similar to that of brain tissue were used for the cell studies. Cytocompatibility and cell type-specific behavior were studied *in vitro* using human pluripotent stem cell (hPSC)-derived neuronal cells.

2. Materials & Methods

2.1. Preparation of GG hydrogels

To prepare the hydrogels, GG (Gelzan^{TM}, low acyl, M_w 1 kg/mol), SPD (spermidine trihydrochloride), SPM (spermine tetrahydrochloride) and sucrose were acquired from Sigma-Aldrich (Finland) with the highest level of purity available. A 10% (w/w) sucrose solution in deionized water was used as a solvent for the hydrogel components to reduce osmotic pressure on the cells [5]. The GG solution was prepared at 5 mg/ml. We tested two different crosslinkers (SPD and SPM); both with three different concentrations, the names and details are shown in table 1.

Table 1. Hydrogel compositions used in this study and calculated details of bioamine per GG in the used concentrations.

Hydrogel nomenclature	Bioamine working solution [μM]	Bioamine in hydrogel [w-%]	Bioamine in hydrogel [μM]	Bioamine μmoles / GG [g]	Positive charge / GG [g]
GG 1.10%SPM	1005	1.108	138.7	32.17	128.7
GG 0.60%SPM	502.6	0.5569	69.43	16.08	64.33
GG 0.40%SPM	395.0	0.3984	49.52	11.49	45.95
GG 3.00%SPD	3927	3.101	541.7	125.6	377.0
GG 1.50%SPD	1885	1.513	260.0	60.32	180.0
GG 1.25%SPD	1551	1.248	214.0	49.64	148.9

All solutions were sterile filtered for mechanical and rheological testing with 0.8/0.2 μm Acrodisc® (PALL Corporation, Port Washington, NY, USA) or for cell culture with Whatman FP 30/0.2 CA-s 0.2 μm (Whatman plc, Little Chalfont, UK) syringe filters. The GG solution was heated in a water bath to +60°C for reduced viscosity prior to sterile filtration. All solutions can be stored for up to one month at +4°C.

When preparing hydrogels, the solutions were first heated in a water bath to +37°C. A crosslinker solution of SPM or SPD was mixed with GG at a volume ratio of 4:25 and cast into a suitable mold or directly onto a cell culture plate. When used, laminin (1 mg/ml) was added to the hydrogel just before gelation in the GG solution at 1 v-%, 5 v-% or 10 v-%.

This study follows the ASTM F2900-11 Standard Guide for Characterization of Hydrogels Used in Regenerative Medicine [41]. For initial gelation testing and gelation time estimation, a small glass bottle was used as the mold. Gelation time was estimated with the tube tilt test, as described by

Tanodekaew at al. *[42]*. In brief, after mixing the reagents, the bottle was slowly turned upside down at 30 s time intervals, and the flow of gel was observed. If the solution started to move even slightly once tilting started, it was not tilted further to let the gelation continue. Once the solution did not flow, the gelation was considered complete, and the time was recorded.

2.2. *Mechanical testing*

Compression testing was performed using a BOSE Electroforce Biodynamic 5100 machine equipped with a 225 N load sensor and Wintest 4.1 software (Bose Corporation, Eden Prairie, Minnesota, USA). Samples were cast into a self-made cylindrical mold with an approximate height of 6.5 mm and a diameter of 12.2 mm, and stored overnight before compression testing to ensure the complete gelation before each measurement. Each composition was tested in five parallel samples; the exact dimensions of each sample were measured with calipers before testing. To avoid slippage of samples, the compression plates were covered with a piece of wet cellulose paper to increase friction between the hydrogel and the metal plate. The sample was set in between compression plates so that the upper plate touched the sample, but no pre-stress was used. Unconfined compression was performed with a constant 10 mm/min strain rate, and samples were compressed until 65% strain was reached from the original height. The test was performed in wet conditions at room temperature. After compression, the data were analyzed with MS Excel. According to Hooke's law, $\sigma = E*\varepsilon$, the compressive modulus was calculated from the stress-strain curve as the slope of the elastic region *[43]*. In addition, the fracture strength and fracture strain were recorded as a sudden drop in the stress-strain curve.

To obtain a good reference in terms of the mechanical properties to design hydrogels for neural TE, compression testing was also performed with brain tissue samples. New Zealand white rabbits, age 10 weeks, male, were sacrificed with deep anesthesia, after which the heads were removed and stored in ice for a maximum of 8 hours. The brains were removed from the skulls, and samples containing midbrain, cerebellum or cortex were prepared. The samples were cut with a biopsy punch to the same size and shape as the hydrogel compression samples and stored on ice until compression testing. The test parameters used were the same as those described above. The naïve brain tissues were obtained from animal experiments conducted at Tampere University Medical School, University of Tampere.

2.3.   Rheological testing

Rheological experiments were carried out with a rotational rheometer (Haake RheoStress RS150) equipped with Rheowizard 4.3 software (ThermoHaake, Germany). Parallel plate geometry with 20 mm diameter metal plates was used. All the experiments were conducted at room temperature (~25°C) in the oscillatory mode. In the oscillatory mode the sample is subjected to sinusoidal oscillatory shear strain with amplitude γ_o. In the linear viscoelastic region (LVER) with sufficiently small strain amplitudes the resulting stress will also be sinusoidal of the same frequency with amplitude τ_o and phase angle δ. The complex moduli (G*) represents the rigidity of the sample and in the LVER the following relationship applies:

$$G^* = \frac{\tau_o}{\gamma_o} = \sqrt{\left(G'^2 + G''^2\right)} \tag{1}$$

The storage modulus (G') is the in-phase and loss modulus (G'') the out-of-phase components of the response:

$$G' = \frac{\tau_o}{\gamma_o}\cos\delta \tag{2}$$

$$G'' = \frac{\tau_o}{\gamma_o}\sin\delta \tag{3}$$

The G' represents the elastic and G'' viscous behavior of the sample. The loss factor tan δ is the ratio of the viscous to the elastic portion. *[44]*

The samples for rheological testing were cast in self-made cylindrical molds with height a maximum of 1 mm and 20 mm cross-section diameter. Prior to each measurement, the hydrogels were stored overnight to ensure the complete gelation. During measurement the gap between plates was set to 0.8 mm. All measurements were done in oscillatory shear deformation mode and both amplitude and frequency sweeps were used for all samples. The strain amplitude range for amplitude sweeps was from 0.01 to 5.00 rad (0.1 rad = 1.6 % displacement) with 1 Hz frequency. Six parallel samples were tested with amplitude sweeps and two parallel samples with frequency sweeps. The frequency sweep was done in range from 0.1 to 3.0Hz, with constant 0.1 rad strain amplitude which is in the LVER for all samples.

2.4. Cell culture

hPSCs, both human embryonic stem cells and human-induced pluripotent stem cells were used in this study *[45]*. The used hESC-lines were Regea 08/023 *[46]* and Regea 11/013 *[47]* and the used hiPSC-lines were UTA.04511.WT *[48]*, Hel24.3 and A116 *[49]* (two kind gifts from Prof. Timo Otonkoski, University of Helsinki).

BioMediTech has Pirkanmaa Hospital District's ethical approval to derivate, culture and differentiate hESCs (Skottman, R05116) and permission from the National Authority for Medicolegal Affairs (FIMEA 1426/32/300/05) to conduct human stem cell research. Additionally, approval has been obtained to use hiPSC lines produced by other laboratories for neuronal research (R14023).

2.4.1. Neuronal differentiation

The culture and neuronal differentiation of hPSCs were performed as described previously *[50]*. Briefly, undifferentiated stem cell colonies were mechanically cut into small aggregates and placed in a suspension culture on neural differentiation medium (NDM) containing 1:1 DMEM/F12 (Gibco, Thermo Fisher Scientific, Finland) and Neurobasal medium, 2 mM GlutaMax™, 1 x B27, 1 x N2 (all from Gibco), 20 ng/ml basic fibroblast growth factor (bFGF, R&D Systems, Minneapolis, MN, USA) and 25 U/ml penicillin/streptomycin (Cambrex, Belgium). During suspension culture, the cell aggregates formed round, floating neurospheres. Neurospheres were kept small via mechanical cutting once per week, and 1/3 of the medium was changed three times per week. Cells were kept for 8–17 weeks in the differentiation phase prior to the hydrogel experiments. Cells were under constant monitoring for the quality of differentiation. Only experiments in which cells formed good neuronal cultures in 2D control were included to the analysis (representative images of good quality 2D cultures in supplemental figure 1).

2.4.2. Hydrogel cell culture experiments

For the biological evaluation of the hydrogels, three approaches were taken to study the cell/biomaterial interactions as shown in figure 1. In every case, control cells were plated on laminin-coated cell culture wells (positive control) and on non-coated cell culture wells (negative control). Cell behavior on the studied materials was always compared to that of the controls. Depending on the well

type used, either plastic (Nalge Nunc International, Rochester, NY, USA) or glass bottom (MatTek Corporation, Ashland, MA, USA), the wells were coated either with laminin (10 µg/ml mouse laminin) or poly-L-lysine and laminin (10 µg/ml poly-L-lysine followed by 10 µg/ml mouse laminin), respectively.
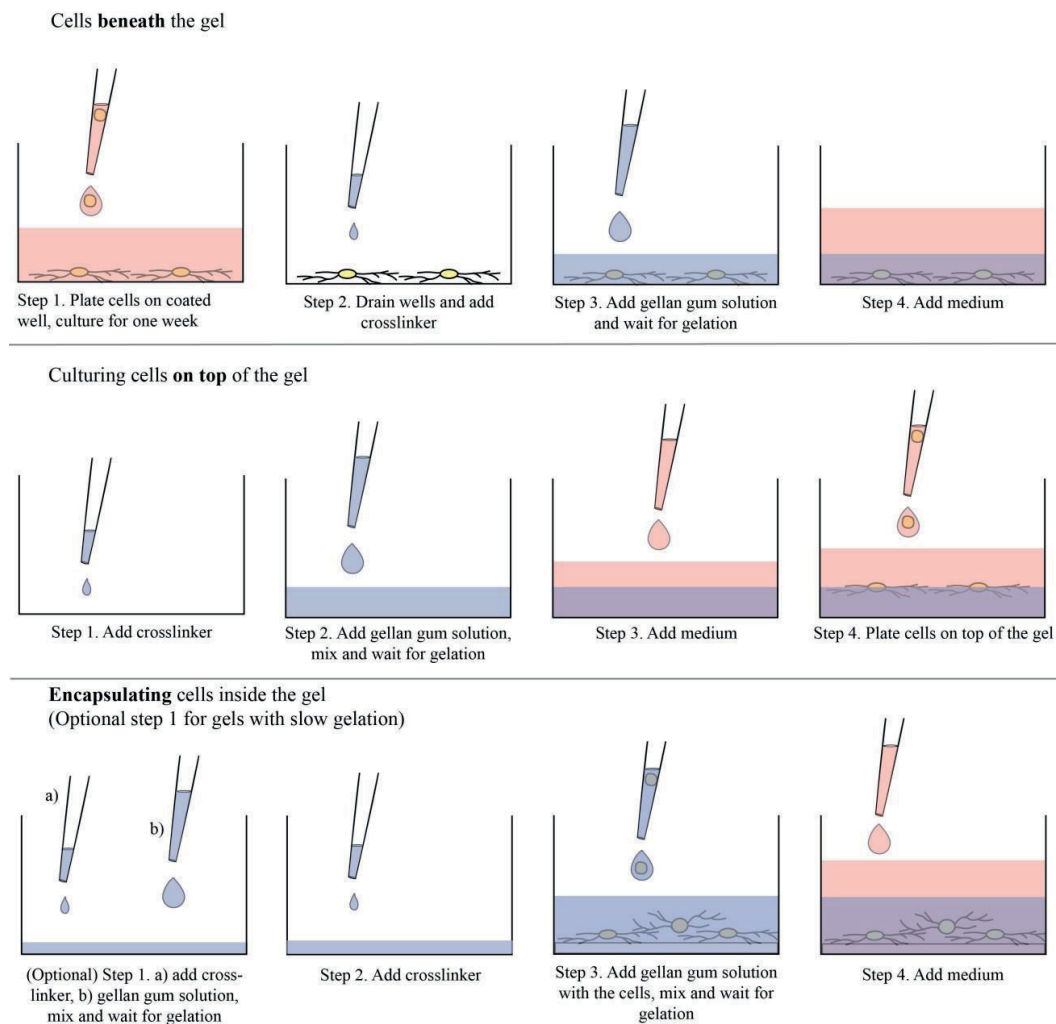
Figure 1. Schematic presentation of plating cells with the hydrogels. All components were kept at 37°C to ensure homogeneous and complete gelation.

Gelation was performed as described in figure 1. A drop of crosslinking agent was added on top of the cell culture, followed by the gentle addition of GG solution, in case of cultures beneath the gel. To avoid disturbing the cells, no additional mixing was performed. For cell encapsulation, the cells were

suspended in GG solution with a minimal amount of medium prior to crosslinking. After complete gelation, medium was gently added on top of the gel. In 3D cell encapsulation studies for gels with slow gelation (all except GG 3.00%SPD), a thin bottom layer of gel was cast beforehand to prevent cell aggregates from sedimenting to the well bottom during gelation.

2.4.3.   Cell plating

Cells were plated either as mechanically cut small cell aggregates or as enzymatically dissociated single cell suspensions prepared using 1X TrypLE Select (Gibco). For the 2D experiments (controls, cells embedded or on top), the plating density was 60,000 cells/cm² or 7–20 small aggregates/cm² (3000-7000 cells/aggregate). The cell density for the 3D experiments (cells encapsulated) was ~3.5 × 10^6 cells/ml of gel, or a corresponding amount of small mechanically cut cell aggregates.

The cells were cultured with the gel for 2 weeks. NDM without bFGF was used during the first week of the experiments. After one week of culture, NDM containing 5 ng/ml bFGF and 4 ng/ml brain-derived neurotrophic factor (BDNF, Prospec Bio, Germany) was used. Half of the medium was changed three times per week using caution to avoid disrupting the gels.

Cells were imaged using a Zeiss AxioVert.A1 microscope and AxioCam ERc 5s camera system or with a Nikon Eclipse TE 2000-S and Nikon Digital Sight DS-Fi1 camera system during the culturing period.

2.5.   Live/dead staining

For viability analysis, the cultures were stained using a LIVE/DEAD® viability/cytotoxicity assay (Molecular probes, Thermo Fisher Scientific). In brief, there are two fluorescent dyes in the kit. Calcein-AM (0.1 µM, $\lambda^{emission}$ = 488 nm) stains intact cells, and ethidium homodimer-1 (0.4 µM, $\lambda^{excitation}$= 568 nm) stains dead cells. After 1 h of incubation at +37°C, the cells were imaged with an Olympus IX51 inverted microscope and an Olympus DP30BW digital camera (Olympus, Finland). The numbers of parallel samples varied between 2 and 4.

2.6.   Immunostaining

We optimized the parameters for immunostaining cells within macroscopic (60-300 μl) hydrogel blocks. In brief, cultures were fixed with 4% paraformaldehyde preheated to +37°C for 30 min. After a brief wash in phosphate buffered saline (PBS), non-specific staining was blocked with 10% normal donkey serum (NDS), 0.1% Triton X-100, and 1% bovine serum albumin (BSA) in PBS for 1 h at room temperature, followed by another wash in 1% NDS, 0.1% Triton X-100, and 1% BSA in PBS. Then, the cells were incubated with a combination of primary antibodies at +4°C for at least 2 days. These antibodies included rabbit anti-microtubule associated protein 2 (MAP-2, 1:400, AB5622, Merck Millipore, Darmstadt, Germany) and rabbit anti-β-tubulin isotype III (β-tub, 1:1000, A01627, GenScript, Piscataway, NJ, USA) in 1% NDS, 0.1% Triton X-100, and 1% BSA in PBS. The samples were washed three times in 1% BSA in PBS (first briefly followed by 2 x 1 hour washes) and then incubated overnight at +4°C with Alexa Fluor 488 conjugated to donkey anti-rabbit antibody (1:400, Life Technologies, A21206) and tetramethylrhodamine isothiocyanate conjugated to phalloidin (TRITC-phalloidin, 0.625 μg/ml, Sigma Aldrich, P1951) in 1% BSA in PBS. The samples were washed three times (first briefly followed by 2 x 1 hour washes) in PBS and then mounted with VECTASHIELD containing 4',6-diamidino-2-phenylindole (DAPI, Vector Laboratories, England). They were then imaged with an Olympus IX51 inverted microscope and an Olympus DP30BW digital camera. Confocal scanning of the samples was performed with a Zeiss LSM 780 mounted into inverted Cell Observer microscope (Carl Zeiss, Jena, Germany) using 10× (NA. 0.45) or 20× (NA. 0.80) air objectives. The samples were scanned through #1.5 glass bottom well plates (MatTek Corporation, Ashland, MA, USA) or through high performance #1.5 coverslips (Carl Zeiss). The confocal data were visualized with the ZEN Black 2012 software (Carl Zeiss) and ImageJ (Version 1.39, U. S. National Institutes of Health, Bethesda, Maryland, USA) *[51; 52]*.

2.7.   Neurite migration

Neurite migration measurements were performed with the ImageJ measure tool. Migration was measured using a straight line from the cell aggregate surface to the visible end of a neuronal process. Each analyzed cell aggregate was measured from 4 longest separately distinguishable neurites. Values of less than 10 µm were considered as representing no migration. The analysis was conducted with at least 2 individual experiments with at least 2 replicative wells. For each studied group, 7 to 16 images were analyzed.

2.8.   Statistical analysis

Due to the non-Gaussian distribution of the data, the nonparametric Kruskal Wallis test and Mann-Whitney U-test were used. A p value of less than 0.05 was considered significant. If more than two groups were compared, the resulting p values were multiplied by the number of comparisons performed (Bonferroni correction).

3.   Results

3.1.   Gel forming and gelation time

GG hydrogels were formed with bioamine weight percentage varying from 0.40% to 1.10% for SPM and from 1.25% to 3.00% for SPD. With these concentrations, the hydrogels were transparent and strong enough to hold their own weight and be handled with tweezers. Higher crosslinker concentrations caused partial gelation of the solutions before they could be mixed uniformly, resulting in high anisotropy with non-transparent (cloudy) areas. Lower crosslinker concentrations formed weak gels that could not support their own weight and were not suitable for 3D cell culture, as the encapsulated cells would sediment to the bottom of gel. The 10 v-% or lower laminin additions did not affect gelation.

The gelation times approximated with tube tilt test are listed in table 2. As seen, the fastest gelation times were just a few seconds, which could cause difficulties in mixing the reagents evenly and cause anisotropic gels. Gelation times over 10 minutes were so slow that during plating the cells could sediment to the bottom of the gel before the gelation is completed. From a practical point of view, a gelation time of 1–5 minutes is optimal, as it is long enough to mix the components uniformly but short enough to keep the cells suspended in the 3D gel and prevent them from sedimenting to the bottom.

Table 2. The gelation times determined by the tube tilt test

Gel composition	1.10%SPM	0.60%SPM	0.40%SPM	3.00%SPD	1.50%SPD	1.25%SPD
Gelation time	1 min	5 min	10 min	5 sec	5 min	10 min

3.2.   Compression testing

The main variable influencing the mechanical properties of hydrogels in this study was the crosslinker concentration. The upper and lower limits of crosslinking were tested along with one concentration between the extremes. The compression testing data were analyzed as stress-strain curves (figure 2), from which the compressive modulus (figure 3) was calculated as the slope of the elastic region. In all GG samples, a distinct fracture point was observed during the test. In contrast, the rabbit brain samples did not have a clear fracture point in the measured displacement but rather a more rubber-like elastic behavior with strong strain stiffening in the end. The GG 0.40%SPM was almost too soft for the load cell, with the force varying during measurement between only 0.01–0.12 N.
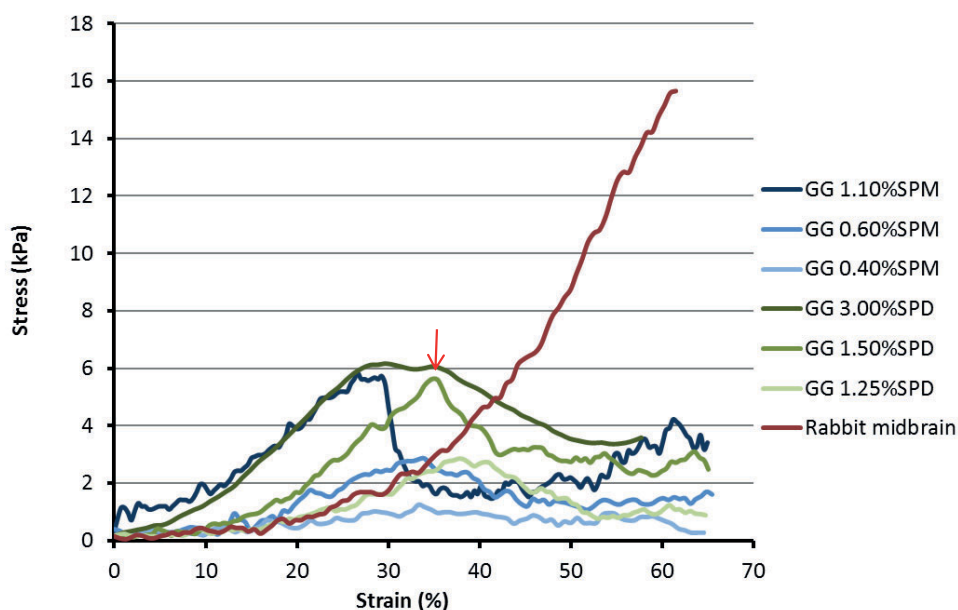
Figure 2. Representative stress-strain curves of GG and brain tissue compression testing. The linear elastic region was determined individually for each sample and ranged from approximately 0.1–0.35 mm/mm strain. As an example, the fracture point of GG 1.50%SPD is marked with a red arrow.

Based on figure 2, it is clear that brain tissue is more ductile than any of the hydrogel samples as it can endure more plastic deformation without fracture than the GG samples. However, the elastic regions at strain of approximately 0.1–0.35 mm/mm of GG 0.60%SPM and GG 1.25%SPM are very similar to those of the brain stress-strain curve, resulting in both cases in a compressive modulus of approximately 10 kPa. The comparison of calculated compressive moduli is shown in figure 3. The strongest compositions, GG 1.10%SPM and GG 3.00%SPD, both have a ~23 kPa modulus, whereas the weakest composition, GG 0.40%SPM, has only a 3.9 kPa modulus. A significant, linear decrease in the compressive modulus is seen with both crosslinkers when lowering the concentration. The addition of laminin did not affect the compressive modulus (data not shown). The part of the stress-strain curve after the fracture point is negligible. The different parts of the rabbit brain, midbrain, cerebellum and cortex, all behaved very similarly throughout the compression testing, with compressive moduli in the 7–10 kPa range.
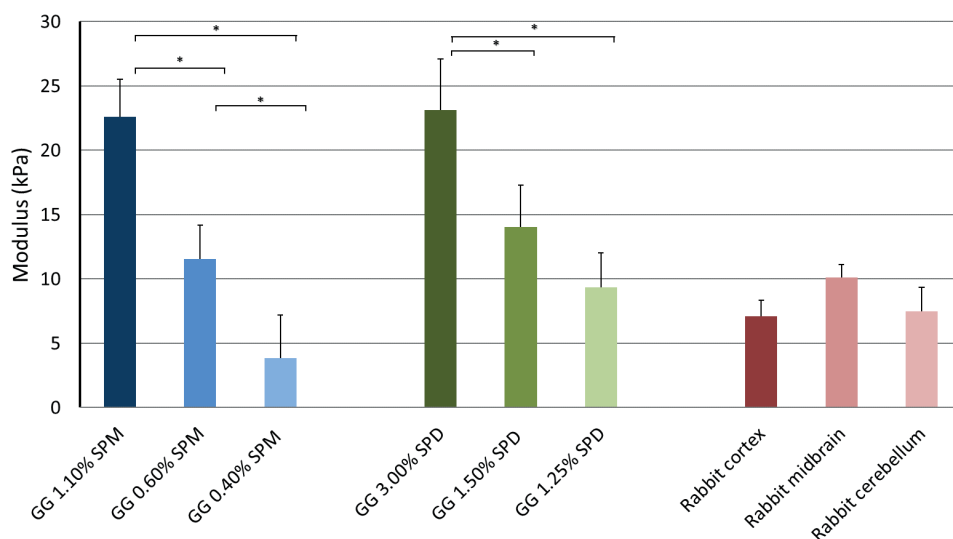
Figure 3. Average compressive moduli of GG bioamine hydrogels and brain tissue samples with error bars showing the standard deviation, n = 5, * = significant at p ≤ 0.05.

The compressive moduli of the hydrogel can be tuned by varying the bioamine concentration, and similar mechanical properties can be achieved with either crosslinker. The compressive moduli of cortex samples were in the same range as the hydrogel moduli with the lowest crosslinker concentrations: GG 0.40%SPM vs. GG 1.25%SPD (p > 0.05). The standard deviation was approximately 2.5–3.5 kPa in all measurements. This result indicates that the calculated moduli less than 5 kPa are not very accurate, being on the lower limit of the compression testing machine load sensor capability. The dependence of the compressive modulus on the crosslinker concentration is linear and within the limits of the standard deviation, as shown in figure 4. SPM has a tetravalent charge, so the rise of the modulus with increasing crosslinker concentration is steeper than that of trivalent SPD.
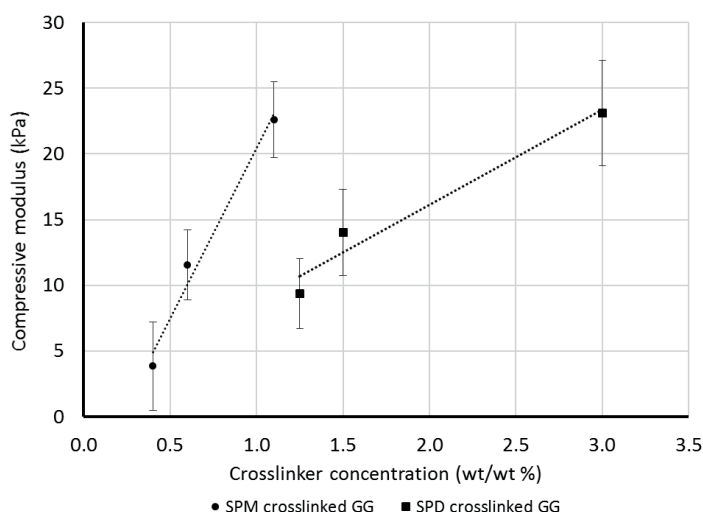
Figure 4. The dependence of the hydrogel compressive modulus on the crosslinker concentration is linear and within the limits of standard deviation as shown by error bars, n = 5. The trend line fit to the average modulus values was determined using MS Excel.

The fracture strength (figure 5) is the ultimate amount of stress a sample can endure, and this value can be critical for load-bearing TE applications even though a cell's mechanotransduction is likely not affected by it. A significant decrease in fracture strength is seen when the crosslinker concentration is lowered. The fracture strain (figure 5) is an indicator of the brittleness of the sample, and the more crosslinker, the more brittle the hydrogel. The brain tissue samples did not have a visible fracture point when compressed to 65% of the original height, but they had a strong strain hardening effect, as shown in figure 2. However, the strain hardening occurred in the plastic deformation region because the deformation was not recoverable (data not shown).
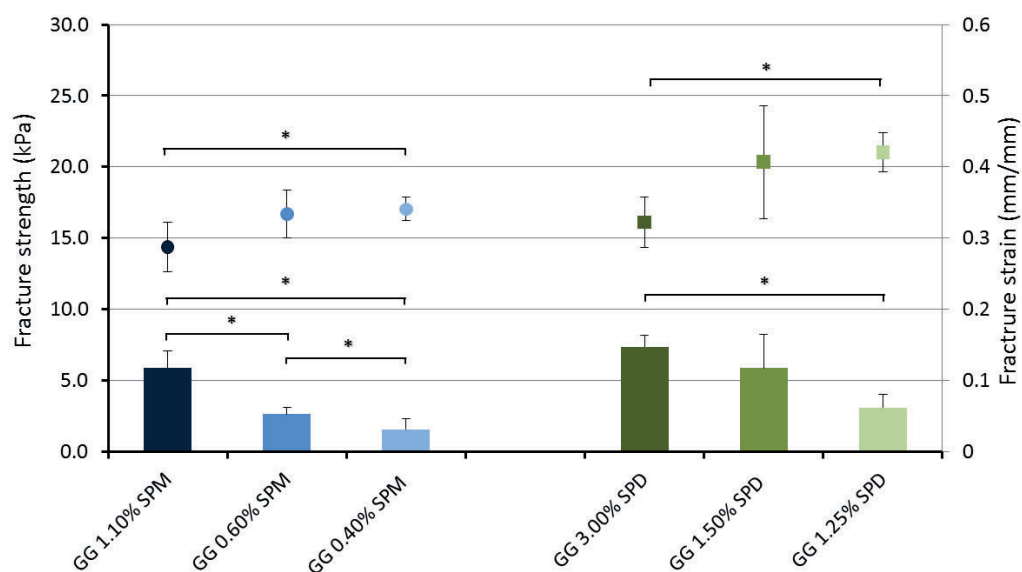
Figure 5. The measured fracture strength is shown on the primary y-axis as bars, and fracture strain is shown on the secondary y-axis as dots. For each hydrogel composition (n = 5), error bars represent standard deviation, * = significant p ≤ 0.05. Brain tissue samples did not have a clear fracture point, so they are excluded from the graph.

3.3.   Rheological testing

The low amplitude strain of the rheological spectrum measured with oscillatory shear amplitude sweep showed a discernible LVER for GG SPM hydrogels, which is used to calculate the complex modulus (figure 6 (d)). At higher strain, a decline due to plastic deformation leads to fracture of the sample at the crossover point of the storage and loss modulus as shown in the figure 6 spectra. All the GG SPM hydrogels have a typical gel-like behavior in the LVER with the storage modulus higher than the loss modulus (G' > G''), which means that elastic behavior dominates over viscous behavior and that the material is more solid than liquid. As shown in figure 6 (a-c) by decrease in the phase angle and tan δ value in LVER, when the crosslinker concentration increases, the solid-like behavior increases. And similar to the compressive modulus, the complex modulus decreased upon lowering the crosslinker concentration.
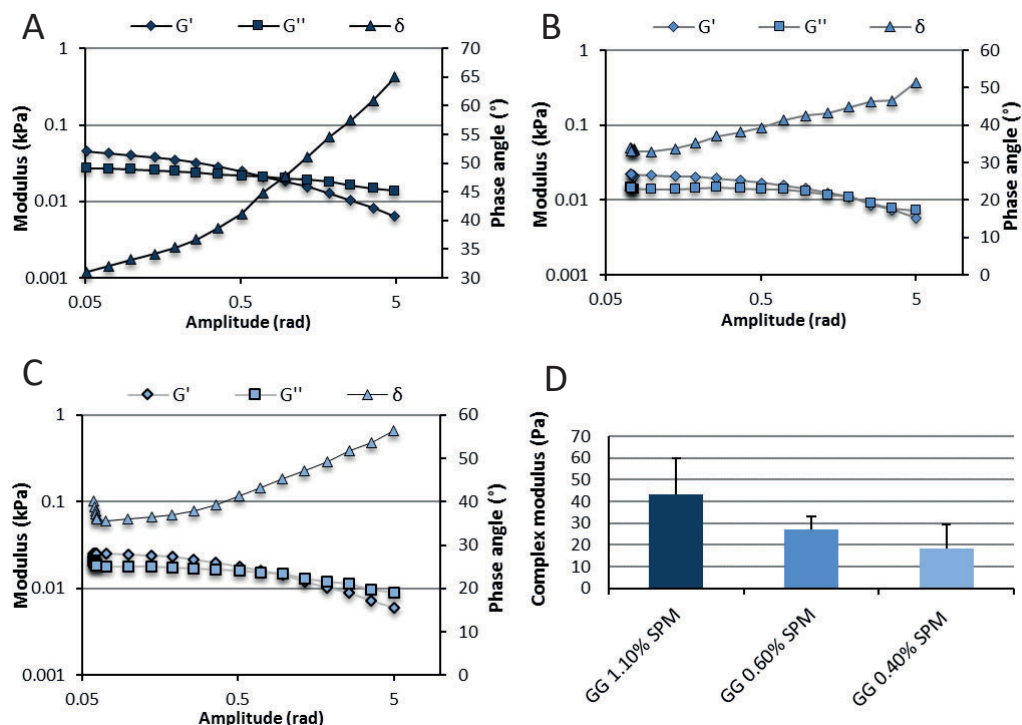
Figure 6. Rotational rheological spectra of (a) GG 1.1%SPM, (b) GG 0.60%SPM and (c) GG 0.40%SPM in amplitude sweep and (d) complex moduli of all GG SPM hydrogels. The LVER exceeds to 0.1 rad amplitude and the gel breaking takes place around 1.0 rad.

Only SPM crosslinked hydrogels displayed distinctive gel-like behavior related to a stable 3D network structure, which was confirmed by a straight line in the frequency sweep (data not shown). The SPD crosslinked gels did not have a discernible LVER, likely due to anisotropy or being too solid for rheology, and thus were not possible to measure with this method. The very quick gelation of SPD crosslinked gels can cause nucleation of crosslinking spots. This nucleation leads to anisotropy of gel network structure and density variations, which are not seen in compression testing.

3.4.   *Neuronal cell cultures beneath the hydrogels*

Neuronal cells were cultured for one week on the plastic dish before casting gel over the cells. The gelation process on top of cultures did not cause any acute cytotoxic effects. During prolonged culture

(up to two weeks) beneath the hydrogel, the neuronal cells remained viable, and neuronal maturation continued similarly as in the positive control cultures without the GG. Culturing beneath the hydrogel did not cause any morphological changes compared to control 2D cultures (figure 7 (a)). In the cell viability analysis, all studied cases had similar degrees of cell viability by visual inspection (figure 7 (b)). Neuronal cultures beneath hydrogel also had similar neuronal protein expression according to immunocytochemical analysis as control cultures without hydrogel (figure 7 (c)). Figure 7 shows the representative images of cultures beneath hydrogel with highest the crosslinker concentration and a 2D positive control. The results were similar at all studied crosslinker concentrations (SPD 3.00%, 1.50%, and 1.25% or SPM 1.10%, 0.60%, and 0.40%, figure 7, data not shown). Thus, SPD and SPM crosslinkers enable the formation of GG hydrogels that are compatible with culturing human neuronal cells. The hydrogel layers (height 2.2–2.8 mm) on top of the neuronal cultures enabled prolonged culturing, implying that the porosity of the formed hydrogels was high enough for nutrient and metabolite exchange.
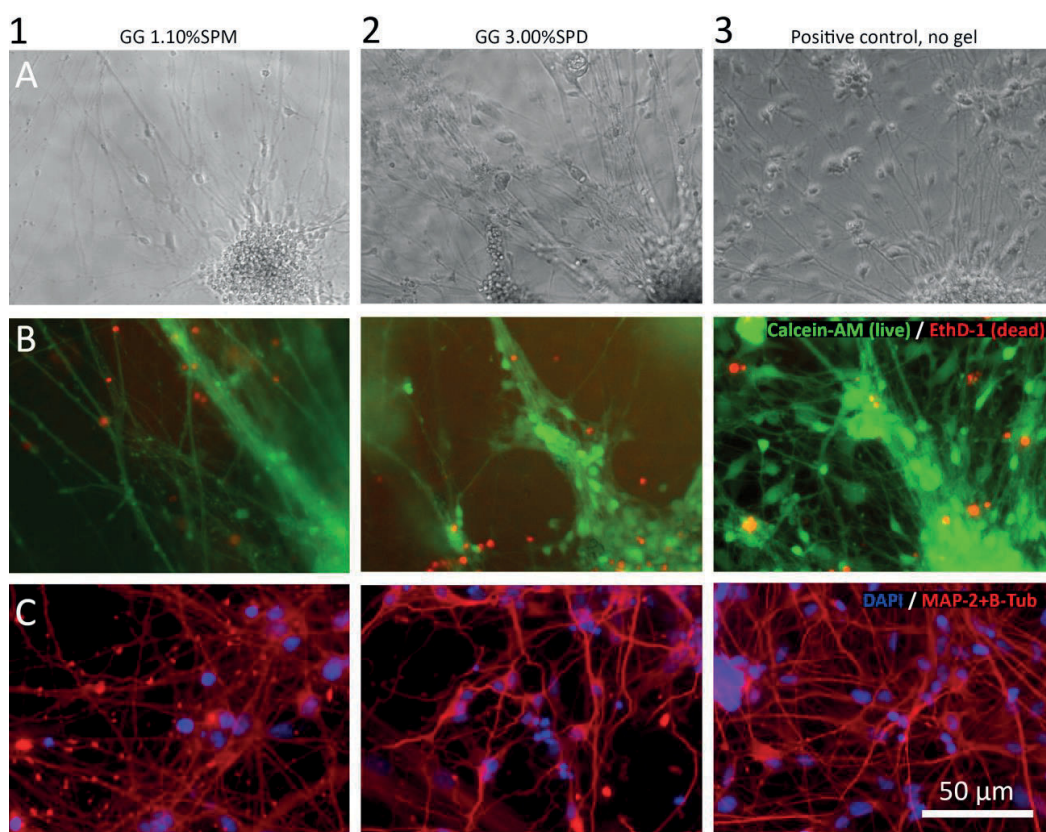
Figure 7. Neuronal cultures beneath the gels. Cells were pre-cultured on a laminin coating for one week, thereafter the gel was cast over the cells and then cultured for 2 additional weeks before analysis. The representative images are shown for the highest crosslinker concentrations, that is, SPM 1.10% (column 1) and SPD 3.00% (column 2) and for the positive 2D control (column 3). Phase contrast images (a), cell viability analysis (b) and immunocytochemistry (c) are shown. Row B: Green = Calcein-AM, live cells, red = EthD-1, dead cells. Row C: Blue = DAPI, Red = MAP-2+B-tub. Scale bar for all images 50 μm.

3.5. Neuronal cell behavior on top of the hydrogels

Neuronal cells remained viable during prolonged culturing (2 weeks) when plated on top of pre-cast hydrogels (success rate 100%, figure 8). For cell type-specific behavior, neurite migration was studied in more detail. Although neuronal cells remained alive on top of all the studied hydrogels, their spreading and migration along the hydrogel surfaces varied within and between groups. Figure 8 shows

a summary of the results. Without any functionalization with laminin, the GG 1.10%SPM and GG 0.60%SPM were the best compositions for supporting neuronal cell spreading (figure 8 (a)). When a low concentration of laminin (1 v-%) was added, the performance of the GG 3.00%SPD hydrogel was superior to any other tested gel composition. (figure 8 (a)). As GG 3.00%SPD with laminin functionalization gave the best results in neuronal cell spreading and migration, functionalization with higher laminin concentrations was further studied.

A

Crosslinker	Crosslinker concentration [w-%]	Compression modulus [kPa]	Functionalization laminin [v-%]	Number of experiments [1]	% of succesful experiments	% of experiments with migration
SPM	1.10 %	22.6	1	5	100 %	20 %
	1.10 %	22.6	-	7	100 %	57 %
	0.60 %	11.5	-	3	100 %	67 %
	0.40 %	2.7	-	3	100 %	33 %
SPD	3.00 %	23.1	1	8	100% *	75% **
	3.00 %	23.1	-	9	100 %	44 %
	1.50 %	11.3	-	2	100 %	50 %
	1.25 %	9.4	-	2	100 %	50 %

[1] Number of replicative wells was at least 2 in all experiments
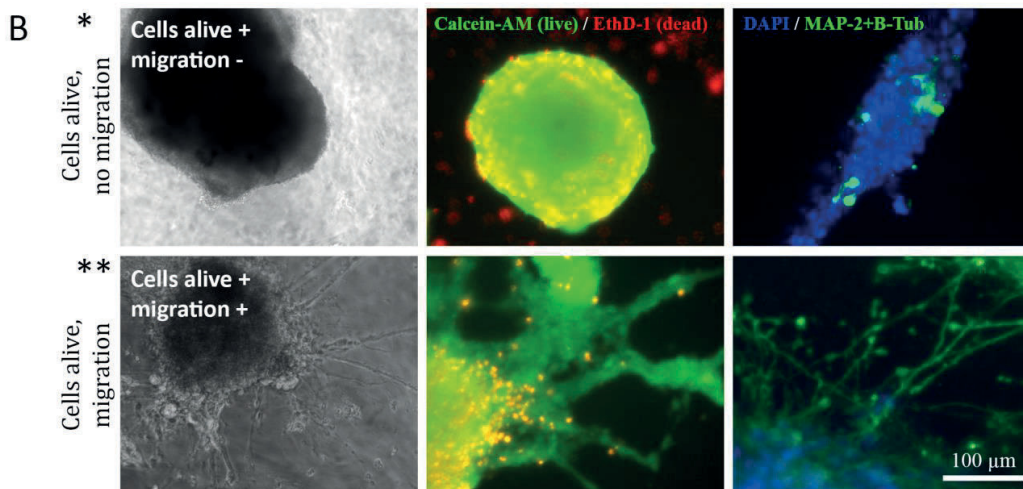
Figure 8. Cell viability and spreading were analyzed on top of GG hydrogel surfaces crosslinked using either SPD (1.25–3.00%) or SPM (0.40–1.10%). With 3.00%SPD and 1.10%SPM, the effects of functionalization with laminin were also tested. All experiments were considered successful, as the cells were alive in all experiments even though neurite outgrowth was not seen in all cases (a). The best neurite migration was seen in 3.00%SPD crosslinked gel with 1% laminin (a**, b**). Representative images of cultures on top of 3.00%SPD crosslinked gel with 1% laminin (b). In some experiments cells

were alive, but no migration was seen (a*, b*), while in other experiments the cells did migrate along

the gel surface (a**, b**). (b) second column: Green = Calcein-AM, live cells, red = EthD-1, dead cells,

(b) third column, Blue: DAPI, Green: MAP-2+B-tub. Scale bar for all images 100 µm.

3.6. Effect of laminin concentration on SPD crosslinked gels

The addition of laminin (5 v-% and 10 v-%) significantly increased neurite migration on top of gel

surfaces during prolonged culturing time (2 weeks). Laminin addition increased both the length of the

neurites (figure 9 (a)) and the number of neurites (figure 9 (b)). The most obvious increase in neurite

migration was seen on top of GG 3.00%SPD, but a similar trend was also observed with 1.5%SPD and

1.25%SPD gels (data not shown).
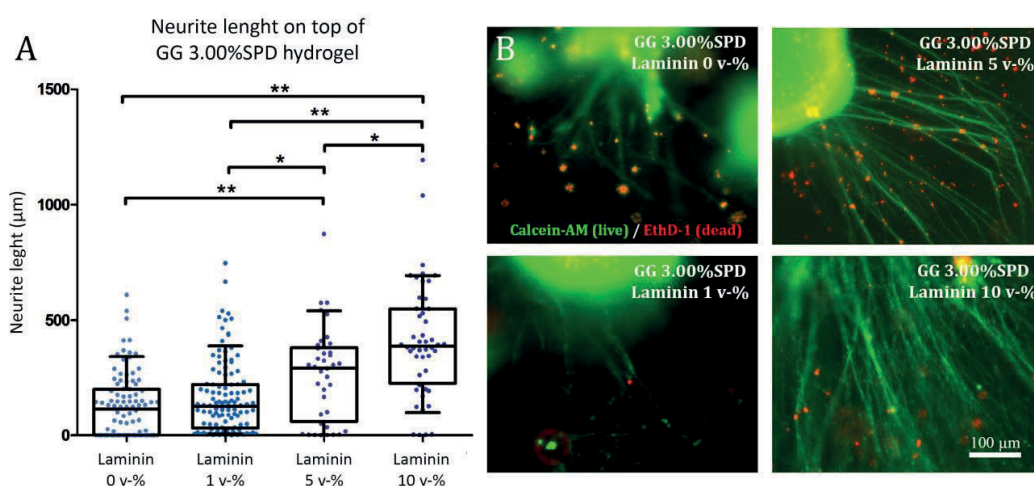
Figure 9. Neurite migration in human derived neuronal cells cultured for 2 weeks on top of GG

hydrogels. Laminin enhances migration in a concentration-dependent manner. Neurite length

distribution in SPD crosslinked gels with different laminin concentrations (a). The box shows 50% of

samples and the median, and the whiskers show 90% of samples. The value of each measured neurite

is shown as a dot in the background. Representative images of neurite migration in each laminin

concentration (b). By visual inspection, the laminin concentration increased the amount of neurite

outgrowth. Green = live cells, red = dead cells. Scale bar 100 µm for all images. *= $p \leq 0.05$, **= $p \leq$

0.0001.

22

3.7.   Neuronal cells encapsulated inside the gel

Neuronal cells were cultured as encapsulated in GG hydrogels for two weeks. Cells remained viable inside all the studied GG bioamine compositions (data not shown). Due to promising neurite migration results obtained from cultures on top of the laminin functionalized GG 3.00%SPD hydrogel, this composition was studied further. Neurite migration was observed in cultures inside the GG 3.00%SPD hydrogel both with and without functionalization with laminin (0–10 v-%). The amount of neurites migrating from the cell aggregates varied from zero to dense outgrowth from aggregate to aggregate (example images of dense outgrowth are presented in figure 10). Neither neurite amount nor neurite length were affected by laminin concentration of hydrogel. Variation observed was also cell line or cell source independent (supplemental figure 1). The neuronal cells cultured encapsulated inside the GG hydrogel formed 3D neuronal network expressing typical neuronal markers (MAP-2 and β-tubulin$_{III}$) co-labelled with phalloidin, (supplemental video 1).
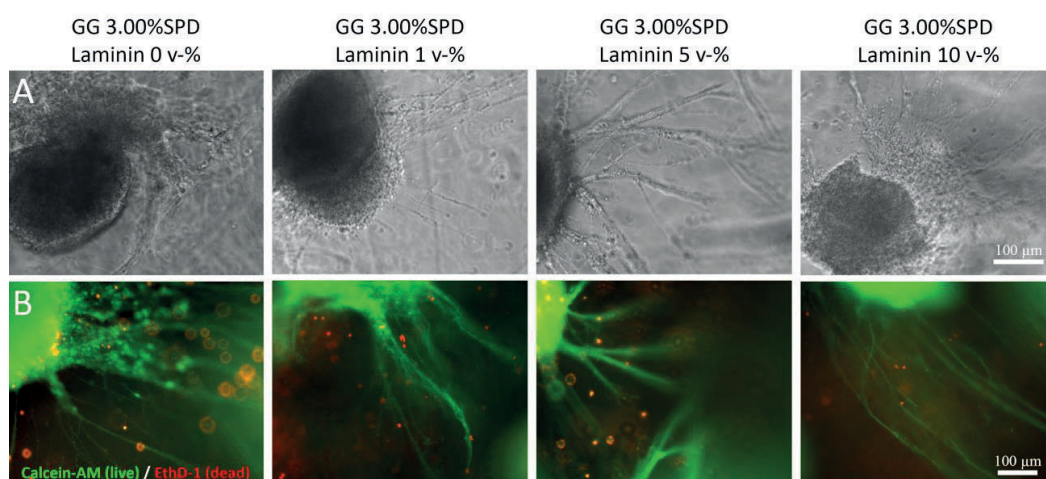
Figure 10. Neuronal cell aggregates cultured for 2 weeks inside the GG 3.00%SPD gel. Phase-contrast images (a) and Live/Dead images of cultures (b). Green = live cells, red = dead cells. Scale bar 100 μm for all images.

4.   Discussion

4.1.   Bioamine crosslinked GG

GG has been approved by the FDA and EMA for food, cosmetic and pharmaceutical applications as a gelling or emulsion agent *[15]*. Taking advantage of the wide usage, GG has been applied for TE with promising results *[15; 27; 28]*.   The common method of physical/ionotropic crosslinking of polysaccharides with metallic cations in order to form hydrogels has some inherent problems: Controlling the crosslinking process and tuning of properties is challenging *[30]*. With this fact in mind, we tested the ability of bioamines for physical crosslinking of GG. The study of alternative ionotropic crosslinking methods using bioamines for anionic polymers in TE is relatively new *[34; 35]* and those studies focused on the development of multicomponent hydrogels for drug delivery applications *[35]*. On the other hand, we have addressed the GG-based bioamine crosslinked hydrogels specifically as a 3D cell culture scaffold for neural TE applications. Other forms of GG have already been studied in spinal cord injury rodent models *[23—27]*, but not with these alternative crosslinking methods. The small cationic bioamine molecules worked efficiently and in a broad range of concentrations, producing stable hydrogels with tuneable mechanical properties.

The definition of a true gel is a material that responds to high stress by fracturing and is self-supporting, whereas a weak gel is a structured fluid that flows under stress *[13]*. The hydrogels we produced were macroscopic and strong enough to keep their shape after casting or even being handled with tweezers, thus they are true gels. For SPM, the lowest concentration that still produced a true gel was 0.40 w-% and for SPD the limit was 1.25 w-%. Lower concentrations produced weak gels that still pass the tube tilt test but flow under stress. When increasing the crosslinker concentration, a non-transparent (cloudy) area is formed inside the gel due to too rapid crosslinking and uneven mixing. This effect corresponds to highly anisotropic hydrogel formation, so the appearance of the cloudy area was considered to indicate the upper limit of the crosslinker concentration. For SPM, this limit was 1.10 w-%, and for SPD, it was 3.00 w-%. These concentration limitations also limit the mechanical properties of produced hydrogels, as they are directly proportional to the crosslinker concentration, as shown in figure 4. The same bioamine crosslinking method could be used as an alternative to many hydrogels

conventionally formed with ionotropic crosslinking, for example, alginate *[30]*, pectin *[13]*, xanthan gum *[13]* and other anionic polysaccharides.

4.2.   Mechanical and rheological properties of GG bioamine hydrogel

One design basis in current TE scaffold development is to produce biomimicking materials with mechanical properties similar to the corresponding tissue *[4; 6; 10—12]*. For the applications requiring higher stiffness (compressive or Young's modulus), such as cartilage TE, suitable GG compositions already exist *[53]*. For lower stiffness applications such as neural TE, however, GG needs to be modified further *[17; 18]*. The comparison of hydrogel properties with tissue properties would be easier if a higher consensus or standardization of the mechanical testing of biomedical samples existed, as also discussed by others *[54; 55]*. The lack of standardization and lack of accepted mathematical models causes high variability and difficulties in interpretation of results between different studies. To overcome this challenge, we included rabbit brain tissue samples and tested them with the same parameters as the hydrogels. According to the measurements, GG 0.40%SPM and GG 1.25%SPD gels with 2.7 and 9.4 kPa modulus, respectively, most closely resembled the compression moduli of rabbit cortical brain samples at 6.3 kPa. These values are slightly higher than those often measured for the brain, with previously reported values being 0.5–3 kPa *[56; 57]*.

The hydrogel's fracture strength and strain are not comparable to brain tissue because no clear fracture point was seen on the brain samples, which underwent only a continuous strain hardening effect. In the biologically relevant deformation range of < 20% strain, the mechanical behavior is similar between bioamine GG and brain. The compression rate, however, has a direct effect on gel fracture due to the visco-elastic recovery, as elegantly shown for GG already before *[58]*. Based on their methodology, we chose the compression rate at a relevant range for our application. In general, our results were in line with those of others *[58]*, showing that higher crosslinker concentration or faster compression rate made GG more brittle (data not shown).

Rotational rheometry was used here as a complementary method to compression testing to gain additional insight into viscoelastic properties of the hydrogels. In addition, rheometry is very sensitive to anisotropy of the measured samples; the rheological spectrum is not continuous if the material is not

isotropic. This effect makes the measurements more laborious to perform, but it can also be used as a quality control for checking the similarity of parallel samples. The measurements show that all the successfully measured samples had a gel-like response *[13; 59]*. In the rheological spectra, the gel storage modulus was always higher than the loss modulus, in both amplitude and frequency sweep, and a fracture was seen under high strain. The rheological spectrum is also in a similar range as previously reported for GG hydrogels *[26]*. The high precision of rotational rheometry revealed the anisotropic nature of SPD crosslinked gels, causing those measurements to fail, but anisotropy was not discerned in compression testing. However, in cell culture, these anisotropies and nanotopographical variations can actually provide better cell anchoring sites than a totally homogenous hydrogel network *[11]*.

4.3.   Suitability of GG as a culturing matrix for human neuronal cells

Cytocompatibility, the cellular scale response, needs to be evaluated with human cells before large-scale systemic biocompatibility testing *[8]*. In this work, we used hPSC-derived neuronal cells *[50]* to study both cytocompability and cell type-specific behavior in developed GGs. Importantly, when aiming for clinical applications, the development of neural TE products requires the usage of human cells already in the preclinical stage *[60]*.

In this study, we used three steps to evaluate the hydrogel performance: 1) culturing cells beneath, 2) on top of or 3) encapsulated inside the hydrogel. This evaluation protocol gives information of cell survival, cell migration, and 3D network formation, but the different approaches should not be directly compared between each other *[5]*. First, performing the crosslinking directly on top of a pre-cultured neuronal network can reveal acute cytotoxicity caused by gel components or gelation during the first days in contact with the material *[5; 61]*. Crosslinking of GG with SPD or SPM did not cause acute (data not shown) or long-term cytotoxicity during 2-week follow-up. This result is in line with previous cytotoxicity studies for GGs *[16; 17; 20; 35]*. Importantly, SPD and SPM at the concentrations used for gelation (213–541 and 49.5–138 μM, respectively) do not cause detrimental effects on neuronal cells. Culturing cells beneath hydrogel can also reveal gel-related effect on cell behavior, e.g., changes in cell fate as described earlier for Matrigel *[61]*. With GG hydrogels, no obvious changes in cell fate were observed, as these cultures developed similarly to control cultures. Successful embedding also

indicates that the porosity of the developed hydrogels was sufficient for medium diffusion and metabolite exchange through the gel block (height: 2.2–2.8 mm) during 2 weeks follow up. In conclusion, bioamine crosslinked GG hydrogels provided a suitable growth environment for human neuronal cells.

To study cell type-specific behavior, we cultured human neuronal cells on top of and encapsulated in GGs. GG hydrogels are considered biologically inert materials *[17]*. According to earlier studies, GG does not *in vitro* support neuronal cell migration on top of gels or as encapsulated without the addition of cell adhesion cues *[18; 28]*. Our experiments using cells on top of gels showed similar results, as some neuronal aggregates remained as spheres without neurite migration as previously described for mouse neural cells *[18]*. Some aggregates, however, had neurite growth along the hydrogel surface. We assume that neurites growing on top of unmodified gel surfaces follow physical cues of the hydrogel. To enhance the cell migration on top of gels, we added the ECM protein laminin by physically mixing it into the GG prior to gelation. This functionalization of GG SPD hydrogels with laminin (5 v-% to 10 v-%) significantly increased neurite migration. A similar positive effect was reported with fibronectin-derived synthetic GRGDS-peptide GG hydrogels *[18]*. Interestingly, functionalization with laminin was not beneficial with SPM crosslinked gels.

Encapsulated human neuronal cells showed a similar level of neurite migration despite functionalization with laminin. Previous studies using neural cells either on top of hydrogels or encapsulated have contradictory results about the benefits of functionalization on growth and migration. For example, functionalization with RGD, IKVAV or YIGSR peptides has shown both favorable and non-meaningful effects in neural cultures *[62; 63]*. This discrepancy could reflect the different microenvironments that cells experience in these cases.

The current paradigm of hydrogel development for TE involves making the mechanical properties mimic the tissue of interest *[4; 10—12]*. For neural cells, a suitable Young's modulus of hydrogel was previously reported between 1–5 kPa *[57; 64; 65]*. Our study revealed a wider, 2.7–22.6 kPa range in compression moduli, enabling neuronal cell growth. At the same time, our measured compression modulus for the rabbit brain samples ranged from 7.1 to 10.1 kPa. These results strongly suggest that

the lack of standardized methods produces high variability in the results, preventing valuable comparisons between studies.

Interestingly, the gels with higher compressive moduli (11.5 to 22.6 kPa) showed the best cell type-specific response for cells grown on top of these hydrogels; even the compressive moduli brain samples were lower (7.1–10.1 kPa). Thus, there is a clear need to determine the actual threshold limits under which cells sense the mechanical properties of the surrounding scaffold and exhibit cell type-specific behavior *[6; 12]*. In other words, the true essence of biomimicking is still unknown. To answer this question, more optimal testing patterns need to be designed specifically for each tissue type. For example, the unconfined compression method measures a bulk hydrogel, whereas locally varying modulus and density, which are measurable with atomic force microscopy (AFM), are likely more important for cells *[11; 12]*. Compression testing should be used only to define the correct range of operations and for screening purposes, not to make specific interpretations. Although they are easier to measure and interpret, the mechanical properties of a bulk hydrogel may not be optimal to predict the cellular level response to the hydrogel.

5.   Conclusions

We conclude that GG hydrogels crosslinked with either SPM or SPD are cytocompatible and provide a compatible 3D scaffold for human neuronal cells. Metallic cations can be replaced by these small bioamines as ionotropic crosslinking agents. The mechanical properties of the GG bioamine hydrogel show a direct proportionality to crosslinker concentration, increasing the predictability of the properties of a certain composition. Mechanically, the GG bioamine hydrogels closely resemble the naïve rabbit brain. Both SPM and SPD crosslinked hydrogels were supporting the migration of neuronal cultures either on top of the hydrogel or as encapsulated inside the hydrogel and from a practical point of view there was no difference in gel handling between the crosslinkers. Neuronal cells grown on top of the SPD crosslinked GG hydrogels clearly benefit from laminin functionalization of the gel in a concentration dependent manner, suggesting that GG itself is too inert material for consistent neurite outgrowth. Based on our results the GG 3.00%SPD hydrogels were the most supportive for 3D neuronal network formation inside the hydrogel, being the most promising gel composition for further studies.

References

[1] Langer R and Vacanti J 1993 Tissue engineering. *Science* **260** pp. 920-926.

[2] Schmidt C E and Leach JB 2003 Neural tissue engineering: Strategies for repair and regeneration. *Annu Rev Biomed Eng* **5** pp. 293-347.

[3] Slaughter B V, Khurshid SS, Fisher OZ, Khademhosseini A and Peppas NA 2009 Hydrogels in regenerative medicine. *Adv Mater* **21** pp. 3307-3329.

[4] Nisbet D R, Crompton KE, Horne MK, Finkelstein DI and Forsythe JS 2008 Neural tissue engineering of the CNS using hydrogels. *J Biomed Mater Res Part B Appl Biomater* **87B** pp. 251-263.

[5] Ylä-Outinen L, Joki T, Varjola M, Skottman H and Narkilahti S 2012 Three-dimensional growth matrix for human embryonic stem cell-derived neuronal cells. *J Tissue Eng Regen Med* **8** pp. 186-187-194.

[6] Asthana A and Kisaalita WS 2013 Biophysical microenvironment and 3D culture physiological relevance. *Drug Discov Today* **18** pp. 533-540.

[7] Annabi N, Tamayol A, Uquillas JA, Akbari M, Bertassoni LE, Cha C, Camci-Unal G, Dokmeci MR, Peppas NA and Khademhosseini A 2014 25th anniversary article: Rational design and applications of hydrogels in regenerative medicine. *Adv Mater* **26** pp. 85-124.

[8] Williams D F 2008 On the mechanisms of biocompatibility. *Biomaterials* **29** pp. 2941-2953.

[9] Vert M, Doi Y, Hellwich K, Hess M, Hodge P, Kubisa P, Rinaudo M and Schué F 2012 Terminology for biorelated polymers and applications (IUPAC recommendations 2012). *Pure Appl Chem* **84** pp. 377-378-410.

[10] Brandl F, Sommer F and Goepferich A 2007 Rational design of hydrogels for tissue engineering: Impact of physical factors on cell behavior. *Biomaterials* **28** pp. 134-146.

[11] Walters N J and Gentleman E 2015 Evolving insights in cell–matrix interactions: Elucidating how non-soluble properties of the extracellular niche direct stem cell fate. *Acta Biomater* **11** pp. 3-16.

[12] Ihalainen T O, Aires L, Herzog FA, Schwartlander R, Moeller J and Vogel V 2015 Differential basal-to-apical accessibility of lamin A/C epitopes in the nuclear lamina regulated by changes in cytoskeletal tension. *Nat Mater* **advance online publication**.

[13] Morris E R, Nishinari K and Rinaudo M 2012 Gelation of gellan – A review. *Food Hydrocoll* **28** pp. 373-411.

[14] CP Kelco. Gellan gum | CP Kelco. 2014. Accessed 12/9, 2014. Available at: http://cpkelco.com/products/gellan-gum/.

[15] Fialho A M, Moreira LM, Granja AT, Popescu AO, Hoffmann K and Sá-Correia I 2008 Occurrence, production, and applications of gellan: Current state and perspectives. *Appl Microbiol Biotechnol* **79** pp. 889-900.

[16] Smith A M, Shelton RM, Perrie Y and Harris JJ 2007 An initial evaluation of gellan gum as a material for tissue engineering applications. *J Biomater Appl* **22** pp. 241-254.

[17] Ferris C J, Gilmore KJ, Wallace GG and in het Panhuis M 2013 Modified gellan gum hydrogels for tissue engineering applications. *Soft Matter* **9** pp. 3705-3711.

[18] Silva N A, Cooke MJ, Tam RY, Sousa N, Salgado AJ, Reis RL and Shoichet MS 2012 The effects of peptide modified gellan gum and olfactory ensheathing glia cells on neural stem/progenitor cell fate. *Biomaterials* **33** pp. 6345-6354.

[19] Barbani N, Guerra G, Cristallini C, Urciuoli P, Avvisati R, Sala A and Rosellini E 2012 Hydroxyapatite/gelatin/gellan sponges as nanocomposite scaffolds for bone reconstruction. *J Mater Sci Mater Med* **23** pp. 51-61.

[20] Oliveira J T, Martins L, Picciochi R, Malafaya PB, Sousa RA, Neves NM, Mano JF and Reis RL 2010 Gellan gum: A new biomaterial for cartilage tissue engineering applications. *J Biomed Mater Res Part A* **93A** pp. 852-863.

[21] Lee H, Fisher S, Kallos MS and Hunter CJ 2011 Optimizing gelling parameters of gellan gum for fibrocartilage tissue engineering. *J Biomed Mater Res Part B Appl Biomater* **98B** pp. 238-245.

[22] Shin H, Olsen BD and Khademhosseini A 2012 The mechanical properties and cytotoxicity of cell-laden double-network hydrogels based on photocrosslinkable gelatin and gellan gum biomacromolecules. *Biomaterials* **33** pp. 3143-3152.

[23] Silva N A, Salgado AJ, Sousa RA, Oliveira JT, Pedro AJ, Leite-Almeida H, Cerqueira R, Almeida A, Mastronardi F, Mano JF, et al 2010 Development and characterization of a novel hybrid tissue engineering--based scaffold for spinal cord injury repair. *Tissue Eng Part A* **16** pp. 45-54.

[24] Pereira D R, Silva-Correia J, Caridade SG, Oliveira JT, Sousa RA, Salgado AJ, Oliveira JM, Mano JF, Sousa N and Reis RL 2011 Development of gellan gum-based microparticles/hydrogel matrices for application in the intervertebral disc regeneration. *Tissue Eng Part C Methods* **17** pp. 961-972.

[25] Silva-Correia J, Oliveira JM, Caridade SG, Oliveira JT, Sousa RA, Mano JF and Reis RL 2011 Gellan gum-based hydrogels for intervertebral disc tissue-engineering applications. *J Tissue Eng Regen Med* **5** pp. e97-e107.

[26] Silva-Correia J, Gloria A, Oliveira MB, Mano JF, Oliveira JM, Ambrosio L and Reis RL 2013 Rheological and mechanical properties of acellular and cell-laden methacrylated gellan gum hydrogels. *J Biomed Mater Res Part A* **101** pp. 3438-3446.

[27] Tsaryk R, Silva-Correia J, Oliveira JM, Unger RE, Landes C, Brochhausen C, Ghanaati S, Reis RL and Kirkpatrick CJ 2014 Biological performance of cell-encapsulated methacrylated gellan gum-based hydrogels for nucleus pulposus regeneration. *J Tissue Eng Regen Med* .

[28] Lozano R, Stevens L, Thompson BC, Gilmore KJ, Gorkin III R, Stewart EM, in het Panhuis M, Romero-Ortega M and Wallace GG 2015 3D printing of layered brain-like structures using peptide modified gellan gum substrates. *Biomaterials* **67** pp. 264-273.

[29] Coutinho D F, Sant SV, Shin H, Oliveira JT, Gomes ME, Neves NM, Khademhosseini A and Reis RL 2010 Modified gellan gum hydrogels with tunable physical and mechanical properties. *Biomaterials* **31** pp. 7494-7502.

[30] Lee C, Shin J, Lee JS, Byun E, Ryu JH, Um SH, Kim D, Lee H and Cho S 2013 Bioinspired, calcium-free alginate hydrogels with tunable physical and mechanical properties and improved biocompatibility. *Biomacromolecules* **14** pp. 2004-2013.

[31] Fedorovich N E, Oudshoorn MH, van Geemen D, Hennink WE, Alblas J and Dhert WJA 2009 The effect of photopolymerization on stem cells embedded in hydrogels. *Biomaterials* **30** pp. 344-353.

[32] Hennink W E and van Nostrum C 2002 Novel crosslinking methods to design hydrogels. *Adv Drug Deliv Rev* **54** pp. 13-36.

[33] Ifkovits J L and Burdick JA 2007 Review: Photopolymerizable and degradable biomaterials for tissue engineering applications. *Tissue Eng* **13** pp. 2369-2385.

[34] Parraga J E, Zorzi GK, Diebold Y, Seijo B and Sanchez A 2014 Nanoparticles based on naturally-occurring biopolymers as versatile delivery platforms for delicate bioactive molecules: An application for ocular gene silencing. *Int J Pharm* **477** pp. 12-20.

[35] López-Cebral R, Paolicelli P, Romero-Caamaño V, Seijo B, Casadei MA and Sanchez A 2013 Spermidine-cross-linked hydrogels as novel potential platforms for pharmaceutical applications. *J Pharm Sci* **102** pp. 2632-2643.

[36] Soto A M, Koivisto JT, Parraga JE, Silva-Correia J, Oliveira JM, Reis RL, Kellomäki M, Hyttinen J and Figueiras E 2016 Optical projection tomography technique for image texture and mass transport studies in hydrogels based on gellan gum. *Langmuir* **32** pp. 5173-5182.

[37] Khan A U, Mei YH and Wilson T 1992 A proposed function for spermine and spermidine: Protection of replicating DNA against damage by singlet oxygen. *Proc Natl Acad Sci* **89** pp. 11426-11427.

[38] Ha H C, Sirisoma NS, Kuppusamy P, Zweier JL, Woster PM and Casero RA,Jr 1998 The natural polyamine spermine functions directly as a free radical scavenger. *Proc Natl Acad Sci U S A* **95** pp. 11140-11145.

[39] Fujiwara K, Bai G and Kitagawa T 1997 Polyamine-like immunoreactivity in rat neurons. *Brain Res* **767** pp. 166-171.

[40] Laube G, Bernstein H, Wolf G and Veh RW 2002 Differential distribution of spermidine/spermine-like immunoreactivity in neurons of the adult rat brain. *J Comp Neurol* **444** pp. 369-386.

[41] ASTM F2900 2011 *Standard Guide for Characterization of Hydrogels used in Regenerative Medicine* (West Conchoken, PA, USA: ASTM International) pp.1-10.

[42] Tanodekaew S, Godward J, Heatley F and Booth C 1997 Gelation of aqueous solutions of diblock copolymers of ethylene oxide and D,L-lactide. *Macromol Chem Phys* **198** pp. 3385-3395.

[43] Callister W D 2003 *Materials Science and Engineering: An Introduction* (New York, NY, USA: John Wiley & Sons) pp.117-120, 480-498.

[44] Schramm G 1998 *A Practical Approach to Rheology and Rheometry* (Karlsruhe, Germany: Gebrueder HAAKE GmbH) pp.119-133.

[45] Rajala K, Lindroos B, Hussein SM, Lappalainen RS, Pekkanen-Mattila M, Inzunza J, Rozell B, Miettinen S, Narkilahti S, Kerkelä E, et al 2010 A defined and xeno-free culture method enabling the establishment of clinical-grade human embryonic, induced pluripotent and adipose stem cells. *PLoS One* **5** pp. e10246.

[46] Skottman H 2010 Derivation and characterization of three new human embryonic stem cell lines in finland. *In Vitro Cell Dev -An* **46** pp. 206-209.

[47] Sorkio A E, Vuorimaa-Laukkanen EP, Hakola HM, Liang H, Ujula TA, Valle-Delgado JJ, Österberg M, Yliperttula ML and Skottman H 2015 Biomimetic collagen I and IV double layer Langmuir–Schaefer films as microenvironment for human pluripotent stem cell derived retinal pigment epithelial cells. *Biomaterials* **51** pp. 257-269.

[48] Ojala M, Prajapati C, Pölönen R, Rajala K, Pekkanen-Mattila M, Rasku J, Larsson K and Aalto-Setälä K 2016 Mutation-specific phenotypes in hiPSC-derived cardiomyocytes carrying either myosin-binding protein C or α-tropomyosin mutation for hypertrophic cardiomyopathy. *Stem Cells Int* **2016** pp. 16.

[49] Toivonen S, Ojala M, Hyysalo A, Ilmarinen T, Rajala K, Pekkanen-Mattila M, Äänismaa R, Lundin K, Palgi J, Weltner J, et al 2013 Comparative analysis of targeted differentiation of human induced pluripotent stem cells (hiPSCs) and human embryonic stem cells reveals variability associated with incomplete transgene silencing in retrovirally derived hiPSC lines. *Stem Cells Transl Med* **2** pp. 83-93.

[50] Lappalainen R S, Salomäki M, Ylä-Outinen L, Heikkilä TJ, Hyttinen JAK, Pihlajamäki H, Suuronen R, Skottman H and Narkilahti S 2010 Similarly derived and cultured hESC lines show variation in their developmental potential towards neuronal cells in long-term culture. *Regener Med* **5** pp. 749-762.

[51] Rasband WS. ImageJ. 2016. Accessed 05/11, 2016. Available at: http://imagej.nih.gov/ij/.

[52] Schneider C A, Rasband WS and Eliceiri KW 2012 NIH image to ImageJ: 25 years of image analysis. *Nat Meth* **9** pp. 671-675.

[53] Oliveira J T, Santos TC, Martins L, Picciochi R, Marques AP, Castro AG, Neves NM, Mano JF and Reis RL 2010 Gellan gum injectable hydrogels for cartilage tissue engineering applications: In vitro studies and preliminary in vivo evaluation. *Tissue Eng Part A* **16** pp. 343-353.

[54] Oyen M L 2014 Mechanical characterisation of hydrogel materials. *Int Mater Rev* **59** pp. 44-59.

[55] Prevost T P, Balakrishnan A, Suresh S and Socrate S 2011 Biomechanics of brain tissue. *Acta Biomater* **7** pp. 83-95.

[56] Laksari K, Shafieian M and Darvish K 2012 Constitutive model for brain tissue under finite compression. *J Biomech* **45** pp. 642-646.

[57] Engler A J, Sen S, Sweeney HL and Discher DE 2006 Matrix elasticity directs stem cell lineage specification. *Cell* **126** pp. 677-689.

[58] Nakamura K, Shinoda E and Tokita M 2001 The influence of compression velocity on strength and structure for gellan gels. *Food Hydrocoll* **15** pp. 247-252.

[59] Kavanagh G M and Ross-Murphy SB 1998 Rheological characterisation of polymer gels. *Prog Polym Sci* **23** pp. 533-562.

[60] Lindvall O and Kokaia Z 2010 Stem cells in human neurodegenerative disorders — time for clinical translation? *J Clin Invest* **120** pp. 29-40.

[61] Thonhoff J R, Lou DI, Jordan PM, Zhao X and Wu P 2008 Compatibility of human fetal neural stem cells with hydrogel biomaterials in vitro. *Brain Res* **1187** pp. 42-51.

[62] Zhang Z, Freitas BC, Qian H, Lux J, Acab A, Trujillo CA, Herai RH, Nguyen Huu VA, Wen JH, Joshi-Barr S, et al 2016 Layered hydrogels accelerate iPSC-derived neuronal maturation and reveal migration defects caused by MeCP2 dysfunction. *Proc Natl Acad Sci* **113** pp. 3185-3190.

[63] Frampton J P, Hynd MR, Shuler ML and Shain W 2011 Fabrication and optimization of alginate hydrogel constructs for use in 3D neural cell culture. *Biomedical Materials* **6** pp. 015002.

[64] Pogoda K, Chin L, Georges PC, Byfield FJ, Bucki R, Kim R, Weaver M, Wells RG, Marcinkiewicz C and Janmey PA 2014 Compression stiffening of brain and its effect on mechanosensing by glioma cells. *New J Phys* **16** pp. 075002.

[65] Palazzolo G, Broguiere N, Cenciarelli O, Dermutz H and Zenobi-Wong M 2015 Ultrasoft alginate hydrogels support long-term three-dimensional functional neuronal networks. *Tissue Eng Part A* **21** pp. 2177-2185.

SUPPORTING INFORMATION
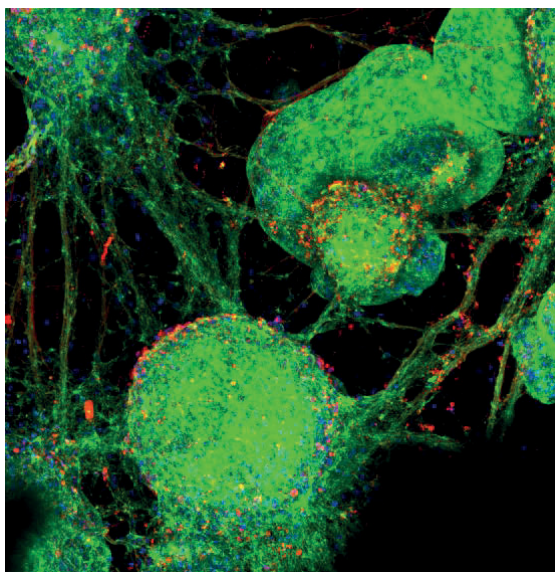
Supplementary video 1. Confocal microscope image of hPSC-derived neuronal cells cultured inside the GG hydrogel. Cells were immunostained against MAP-2+β-tubulin$_{III}$ (green), labelled with phalloidin (red) and DAPI (blue).
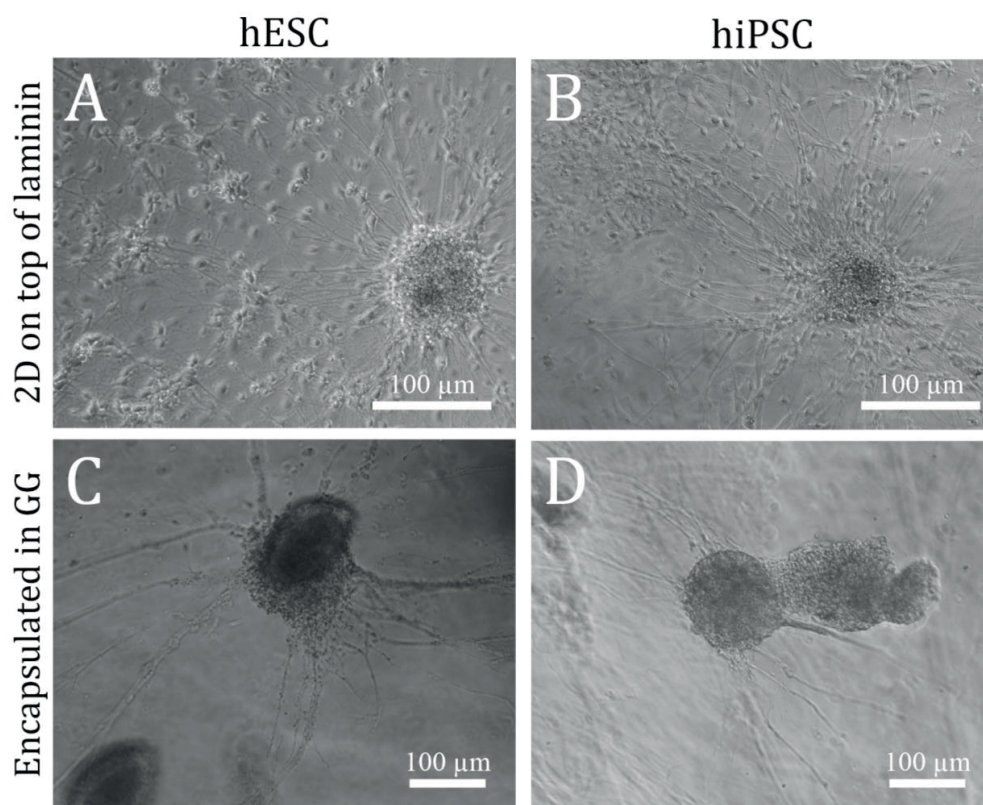
Supplementary figure 1. Phase contrast images of neuronal cultures similarly derived from hESC and hiPSC origin. Representative images of good quality 2D neuronal cultures on top of laminin coated plastic (A, B). Similarly derived neuronal cultures encapsulated inside GG hydrogel (C, D). Scale bars: 100 μm.

II

OPTICAL PROJECTION TOMOGRAPHY TECHNIQUE FOR IMAGE TEXTURE AND MASS TRANSPORT STUDIES IN HYDROGELS BASED ON GELLAN GUM

by

Ana M. Soto, Janne T. Koivisto, Jenny E. Parraga, Joana Silva-Correia, Joaquim M. Oliveira, Rui L. Reis, Minna Kellomäki, Jari Hyttinen, and Edite Figueiras

Optical Projection Tomography Technique for Image Texture and Mass Transport Studies in Hydrogels Based on Gellan Gum

Ana M. Soto,*,[†,‡] Janne T. Koivisto,[‡,§,⊥] Jenny E. Parraga,[‡,§] Joana Silva-Correia,[∥,#] Joaquim M. Oliveira,[∥,#] Rui L. Reis,[∥,#] Minna Kellomäki,[‡,§] Jari Hyttinen,*,[†,‡] and Edite Figueiras[†,‡]

[†]Computational Biophysics and Imaging Group, ELT Department, Tampere University of Technology, 33720 Tampere, Finland

[‡]BioMediTech - Institute of Biosciences and Medical Technology,33720 Tampere, Finland

[§]Biomaterials and Tissue Engineering Group, ELT Department, Tampere University of Technology, 33720 Tampere, Finland

[⊥]Heart Group, BioMediTech, University of Tampere, 33720 Tampere, Finland

[∥]3B's Research Group, Biomaterials, Biodegradables and Biomimetics, University of Minho, Headquarters of the European Institute of Excellence on Tissue Engineering and Regenerative Medicine Barco GMR, 4704-553 Braga, Portugal

[#]ICVS/3B's - PT Government Associate Laboratory, 4710-057 Braga/Guimarães, Portugal

ⓢ *Supporting Information*

ABSTRACT: The microstructure and permeability are crucial factors for the development of hydrogels for tissue engineering, since they influence cell nutrition, penetration, and proliferation. The currently available imaging methods able to characterize hydrogels have many limitations. They often require sample drying and other destructive processing, which can change hydrogel structure, or they have limited imaging penetration depth. In this work, we show for the first time an alternative nondestructive method, based on optical projection tomography (OPT) imaging, to characterize hydrated hydrogels without the need of sample processing. As proof of

concept, we used gellan gum (GG) hydrogels obtained by several cross-linking methods. Transmission mode OPT was used to analyze image microtextures, and emission mode OPT to study mass transport. Differences in hydrogel structure related to different types of cross-linking and between modified and native GG were found through the acquired Haralick's image texture features followed by multiple discriminant analysis (MDA). In mass transport studies, the mobility of FITC-dextran (MW 20, 150, 2000 kDa) was analyzed through the macroscopic hydrogel. The FITC-dextran velocities were found to be inversely proportional to the size of the dextran as expected. Furthermore, the threshold size in which the transport is affected by the hydrogel mesh was found to be 150 kDa (Stokes' radii between 69 and 95 Å). On the other hand, the mass transport study allowed us to define an index of homogeneity to assess the cross-linking distribution, structure inside the hydrogel, and repeatability of hydrogel production. As a conclusion, we showed that the set of OPT imaging based material characterization methods presented here are useful for screening many characteristics of hydrogel compositions in relatively short time in an inexpensive manner, providing tools for improving the process of designing hydrogels for tissue engineering and drugs/cells delivery applications.
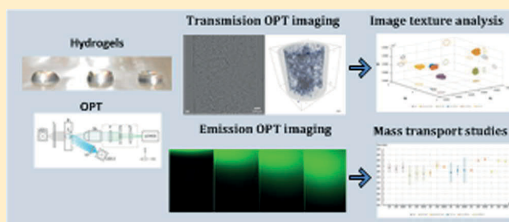
1. INTRODUCTION

Tissue engineering (TE) is an interdisciplinary field which aims to develop technologies able to restore, replace and regenerate damaged tissue or organs.[1] Despite the advances in TE, the current medical treatments are often not optimal, as many of the replaced tissues or prostheses do not function as well as healthy tissue or they can trigger severe immunological response. To overcome many of these problems, new cellular strategies and sophisticated biomaterials are being developed, together with new tools to study their behavior.[1−3]

The main strategy used in TE is to combine a biomaterial scaffold with living cells and bioactive molecules, which together are able to develop a biological process like differentiation and regeneration.[1] To achieve this goal, it is necessary to develop scaffold materials which resemble the natural cellular environment and provide the cells an adequate support for growth.[4] Among the biomaterials, hydrogels have emerged as promising materials for TE due to their structural resemblance to the extracellular matrix (ECM), biocompatibility and tunable properties, such as biodegradability, permeability to nutrients and waste products, injectability and mechanical characteristics.[5−7] Hydrogels are hydrophilic polymeric networks with high content of water which can be obtained from natural sources (i.e., alginate, chitosan, gellan

Table 1. Gellan Gum Hydrogels Fomulations and Preparation Methods

	abbreviation	polymer	cross-linker	final cross-linker concn	cross-linking method
group 1	iGG	low acyl gellan gum 2% w/v	PBS 1×	10% v/v	ionic (physical)
	iGG-MA	methacrylated gellan gum 2% w/v	PBS 1×		ionic (physical)
	photoGG-MA	methacrylated gellan gum 2% w/v	MBF 98% (w/v) + PBS 1×	MBF 0.1% (w/v)	ionic and UV photo-cross-linking (physical and chemical)
group 2	iGG-SPM-H	gellan gum 0.5% w/v	spermine 1.79 mM	0.24 mM	ionic (physical)
	iGG-SPM-L	gellan gum 0.5% w/v	spermine 0.90 mM	0.12 mM	ionic (physical)
	iGG-Ca	gellan gum 0.5% w/v	CaCl$_2$ 10 mM	2.5 mM	ionic (physical)

gum) or synthetic sources (i.e., poly(ethylene oxide) (PEO), poly(vinyl alcohol) (PVA), and poly(acrylic acid) (PAA)).[8]

Hydrogels have been used for several TE applications[9−14] (e.g., cartilage, intervertebral disc (IVD), meniscus, peripheral nerve, and cardiac) as these materials can be processed under mild conditions, making cells and drugs encapsulation a very straightforward process. In spite of the relatively successful clinical application of various engineered tissues using hydrogel scaffolds, one significant challenge associated with the use of hydrogels is the evaluation of their microstructure and permeability, which are critical factors for cell penetration and survival and tissue regeneration. These factors affect the availability, among others, of nutrients and growth factors; in addition, it is known that there is a natural gradient of nutrients and metabolites within the hydrogels.[3,15] Bearing in mind that the success of a TE therapy depends of these features, it is important to evaluate the scaffold capacity to transport these biomolecules.[15,16] Additionally, the determination of the diffusion of drug molecules within the hydrogel is essential for drug delivery applications. Thus, parameters such as polymer network mesh size, porosity and pore interconnectivity are key elements since they are important not only for cell nutrition, but also for cell adhesion, migration and proliferation, differentiation, signaling, and vascular growth.[4,16]

Transport of molecules in hydrogels occurs between the polymer chains in water-filled regions. The movement of the molecules is limited by the polymer network density, the mobility of the polymer chains and the presence of charged groups that potentially could bind biological molecules.[17] Consequently, the movement of molecules is reduced when the cross-linking density increases and the volume fraction of water of the hydrogel decreases.[18]

When developing new hydrogels, the study of porosity and mass transport properties in physiologically relevant conditions is one the most critical design points.[3,19] Conventionally available imaging methods able to characterize hydrated hydrogels have many limitations. They require sample processing or drying, which can change the hydrogel structure (once a hydrogel is dried, the molecular polymer mesh may collapse into thicker walls of pores and therefore the smaller pores are expected to shrink and large ones become even larger), are destructive, or have limited imaging depth penetration. For instance, scanning electron microscopy (SEM) is a destructive method, as it requires sample drying and electrically conductive coating, is limited to the surface of the material with a penetration depth smaller than 200 nm,[20,21] and only gives morphological information on a dried sample surface,[20] which can be different from the wet conditions. On the other hand, X-ray microcomputed tomography (μCT) is able to image the three-dimensional structure of the hydrogels, but it also requires sample drying or contrast agents or both.[20]

Confocal microscopy (CM), two-photon fluorescence microscopy (TPFM), and optical coherence tomography (OCT) offer the possibility of 3D imaging of hydrated hydrogels. However, CM and TPFM are confined to fluorescent signals, require sample labeling or autofluorescence, and they are focused in the microscopic scale (CM and TPFM imaging depth is smaller than 100 μm and 1 mm, respectively). In addition, TPFM can produce thermal damage to the sample.[20,22] OCT is able to generate 3D images but the size of the specimen is limited by the penetration depth of less than 2 mm.[20] In addition, these techniques can be time-consuming and costly.[20]

In this work, we propose an alternative method to characterize hydrogels based on optical projection tomography (OPT). OPT is a nondestructive three-dimensional microscopy technique originally developed by Sharpe et al. in 2002[23] to image the anatomy of embryos and small organs. OPT can be used to image fluorescent (emission mode) and nonfluorescent (transmission mode) specimens embedded in a refractive index matching solution. The ability to image samples in the mesoscopic scale opens the possibility to image complete intact specimens smaller than 10 mm[24] or alive samples.[24,25] However, for opaque specimens, optical clearing of the sample is required for depth imaging. The optical clearing protocols are toxic, making in vivo imaging a challenge for most of the biological samples. On the other hand, due to the transparency of most hydrogels, clearing protocols are not required for OPT imaging.[26]

In the present work, we aim to show for the first time how OPT can offer methods to characterize hydrogel structure and its properties, expanding the preliminary results by Figueiras et al.[27] and Soto and co-workers.[26,28] Here we demonstrate the characterization of gellan-gum-based hydrogels by analyzing image microtextures and mass transport properties. This is done to identify differences between hydrogels structure according to their cross-linking method based on OPT imaging. Specifically, we highlight that OPT is a useful method for imaging transparent hydrogels without the need of labeling, drying, or other sample processing. The use of 3D reconstruction algorithms offers the possibility to estimate/recover the whole 3D volume of hydrated hydrogels. Image texture analysis enables one to perform a comparative study of newly developed gellan gum hydrogel compositions. Finally, we show that OPT offers the possibility to image the transport of molecules through the 3D hydrogel scaffold in real time using OPT in the emission mode.

2. MATERIALS AND METHODS

2.1. Preparation of Hydrogels. In this work, we analyzed two different groups of gellan gum (GG) hydrogels. Table 1 describes the composition and cross-linking method used in each type of hydrogel. The first group includes hydrogels based on natural or methacrylate-

modified GG (GG-MA) prepared by ionic and/or photo-cross-linking method. The second group includes physically cross-linked gellan gum with the bioamine spermine (SPM), at two different concentrations, 0.24 and 0.12 mM, described as iGG-SPM-H and iGG-SPM-L, respectively. In addition, it was used a reference hydrogel cross-linked with calcium ions (iGG-Ca). The first group of hydrogels have been used for intervertebral disc (IVD) tissue engineering applications,[9] and the second group was developed for neural and cardiac cell culture disease modeling applications.[29]

All reagents were purchased from Sigma-Aldrich, unless otherwise specified. All the hydrogel solutions were cast in fluorinated ethylene propylene (FEP) tubes with 2 mm inside diameter (Adtech Polymer Engineering, U.K.) for transmission OPT imaging and in 5 mL polystyrene cuvettes (BRAND UV cuvette, Sigma-Aldrich) for emission OPT imaging.

iGG, iGG-MA, and photoGG-MA with UV photo-cross-linker were prepared as described by Silva-Correia and co-workers.[9,30] The iGG hydrogels were prepared by dissolving low acyl gellan gum (GG) (Gelzan CM) powder in distilled water under constant agitation to obtain a 2% w/v solution. The solution was heated progressively to 90 °C maintaining this temperature for 30 min. Then, the temperature was gradually decreased to 60–65 °C and phosphate-buffered saline (PBS, pH 7.4) was added to a final concentration of 10% v/v in GG solution. The temperature was continuously decreased to 50 °C and poured in the corresponding container. Then, the hydrogels were allowed to cross-link and stabilized by immersion in PBS.

Both iGG-MA and photoGG-MA hydrogels were prepared by using methacrylated gellan gum (GG-MA) solution at 2% (w/v). GG-MA was dissolved in distilled water under vigorous agitation at room temperature until complete and homogeneous dissolution of the powder. For preparing iGG-MA, the solution was cast into its corresponding container and immersed in PBS (pH 7.4) overnight. For preparing photoGG-MA, the photoinitiator methyl benzoylformate (MBF, 98%) was added to the solution to a final concentration of 0.1% (w/v). The gel was transferred to the corresponding container and the hydrogels were obtained by exposure to ultraviolet (UV) light (366 nm; UV lamp Triwood 6/36, Italy). The hydrogels prepared in FEP tubes were exposed for 10 min, whereas the hydrogels prepared in the cuvettes were exposed to UV light for a total period of 40 min, i.e., 10 min for each face of the cuvette. Bioamine based hydrogels, i.e. GG-SPM-H and GG-SPM-L, were prepared using spermine tetrahydochloride (SPM), as cross-linker agent. Briefly, the hydrogel samples were prepared by dissolving GG powder in a deionized water solution of 10% (w/v) sucrose to obtain a concentration of 0.5% w/v. The SPM was dissolved in 10% sucrose and diluted to 1.79 mM (iGG-SPM-H) and 0.90 mM (iGG-SPM-L) concentrations. All solutions were sterile filtered at 60 °C with 0.8/0.2 μm Acrodisc syringe filter, PALL Corporation, before the gelation process. When preparing the gel samples, the solutions were first heated in water bath at 37 °C. SPM and GG were mixed in a volume ratio of 4:25, cast in their corresponding containers and stored overnight at RT before imaging.

Ca-GG hydrogels were prepared in a similar way as previous described for the bioamine-based hydrogels. GG and CaCl₂ (Honeywell Riedel-de Haën, Germany) were dissolved in 10% sucrose at 0.5% w/v and 10 mM, respectively. The solutions were sterile filtered similarly and the GG solution and CaCl₂ solution were heated in a water bath to 37 °C before the gelation process. The solutions were mixed in a volume ratio of 1:3 with final cross-linker concentration of 2.5 mM. The hydrogels were cast in corresponding container and stored overnight at RT before imaging.

2.2. Transmission OPT Imaging for Image Texture Analysis.
An OPT system as previously described[27] with transmission and emission modes was used. A scheme of the system is shown in Figure 1. Five samples of each type of hydrogel were imaged using OPT transmission mode. The hydrogels were prepared into FEP tubes as described above and submerged in water. Projections images were taken around entire 360° at steps of 0.9° resulting in 400 images. The images were taken with a 5x objective, providing a resolution of about 3 μm. The 3D images of the samples visualizing the 3D internal structures we reconstructed from the projection images using back
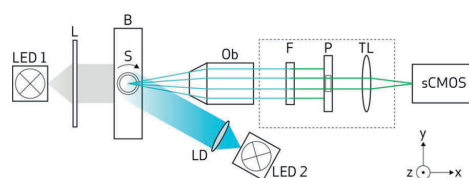
Figure 1. Schematic diagram of the OPT setup: hydrogel samples inserted in FEP tubes are rotated in the rotation stage (S) inside a water bath (B). For brigth field illumination a white light (LED 1) and a telecentric lens (L) are used. For fluorescence illumination, 470 nm wavelength (LED2) collimated with a lens with diffuser (LD) are used. The detection system consist of objective lens (Ob), a band-pass filter (F) used only for fluorescence imaging, a pinhole (P), a tube lens (TL), and a sCMOS camera.

projection algorithm as previously described.[27] Supporting Information Video 1 shows two examples of hydrogels: (a) iGG-SPM-H projections, (b) the reconstruction of (a), (c) photoGG-MA projections, and (d) reconstruction of (c).

2.3. Image Processing and Texture Analysis.
Image texture analysis has been carried out using multiple discriminant analysis (MDA). (Note: Image texture analysis used in this work should not be confused with mechanical texture analysis performed in materials science and food industry.[41]) The analysis was performed to assess and compare the microscopic structures of the hydrogels in the projection images and in their 3D reconstructions using Haralick's textural features[31] in the five samples of each hydrogel type. Preprocessing of the projection images included flat field correction of the illumination nonuniformity created by the white LED (LED1, Figure 1) using 2D polynomial fitting, and removal of the tube from the images by manual segmentation. Histogram equalization was applied to the projections and slices images before performing the textural analysis. The gray level co-occurrence matrix (GLCM), also known as spatial gray level dependence matrix (SGLD), was computed for each image using one and three pixels length at different directions, i.e., 0°, 45°, 90° and 135°, respectively. From the calculated co-occurrence matrix of each image, 13 textural features were computed.[31] Due to the high dimensionality of Haralick's features, MDA was used to reduce dimensionality and find differences between textural features of the hydrogels. MDA is a method to project the feature space onto a lower dimension space in such a way that maximizes the interclass scatter and minimizes the intraclass scatter.[32]

2.4. Emission OPT Imaging for Mass Transport Studies.
The hydrogel samples (~1 mL) for mass transport studies were prepared as described above in 5 mL polystyrene cuvettes. FITC-Dextran (TdB Consultancy AB, Sweden) with different molecular weights, i.e., 20, 150, and 2000 kDa (emission 520 nm, absorbance 493 nm), were used to characterize the transport of molecules. Each FITC-Dextran solution was prepared by dissolving the powder in distilled water at a concentration of 10 mg/mL. Each type of FITC-dextran molecule experiments was replicated five times.

For imaging the mass transport, OPT fluorescent projections were taken always in the same angular position of the sample using the OPT in emission mode as represented in Figure 1. For the fluorescence mode a collimated LED of 470 nm (M470L3, Thorlabs) (LED 2 in Figure 1) was used to excite the samples and a band-pass filter with center wavelength of 520 nm (EO 67–030, Edmund Optics) was added to the detection system (F in Figure 1).

The experiments were performed as follows: (a) the focal plane of the imaging system was placed approximately in the middle plane of the cuvette at the upper part of the hydrogel; (b) 100 μL of solution of one type of molecular weight FITC-dextran was pipetted to the surface of the sample; and (c) projections were acquired each minute for 4 h with an exposure time of 0.04 s. The first image was taken before pipetting the FITC-Dextran (20, 150, or 2000 kDa) on the top of the samples. The imaged area consisted of 3 mm length-square.
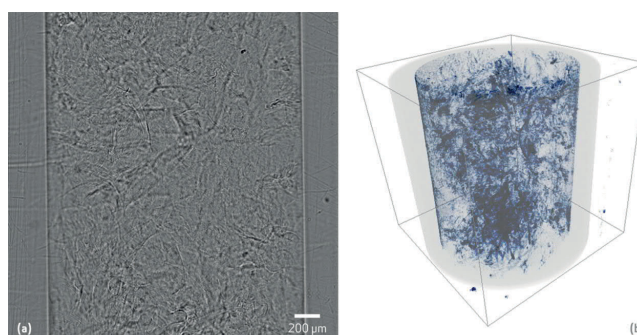
Figure 2. OPT images acquired in transmission mode of a gellan gum hydrogel cross-linked with Ca^{2+}: (a) projection image and (b) 3D reconstruction.

2.5. Mass Transport Image Processing and Analysis. The data was preprocessed by subtracting the background to remove common elements in all images, such as nonuniformity produced by the LED. This was performed by subtracting the first image acquired, before the addition of the FITC−dextran molecules. We devised a new method to assess the homogeneity of the hydrogels by defining an index of homogeneity. The acquired images were first binarized by Otsús method,[33] a heuristic method which iteratively calculates the optimum threshold automatically based on the histogram of the image. This threshold value was calculated for each sample. Thus, when the gray level intensity of the pixel is higher than the calculated threshold, the value of the pixel is converted to 1 (white). By its turn, if the value of the pixel is inferior to that for the calculated threshold, the pixel value is converted to 0 (black). This produces a wavefront descending through the image (see Supporting Information Video 2). We assume that when the binarized signal from FITC-dextran does not travel uniformly, the hydrogel is less homogeneous than when traveling uniformly (see Supporting Information Video 3). The index of homogeneity was defined as the measure of the smoothness of the wavefront descending through the hydrogel. To calculate the index of homogeneity, the gradient in the black and white interface was calculated. The gradient points toward the direction of greatest change in every pixel, thus by analyzing the gradient interface it is possible to determine the flatness of said interface. In this manner, when the interface between black and white pixels is flat, the angle of the gradient vector is 90° (pointing downward in the image). On the contrary, if the interface is not flat, i.e., irregular, its gradient will also be irregular and the angles will be different than 90° (will point in random directions other than downward). Motivated by this behavior, the index of homogeneity is calculated as the ratio between the total number of 90° angles and the total number of angles. When the value of the index is closer to 1, a greater number of 90° angles is present and thus indicates a flat interface. The binary images were also used to analyze the position of the wavefront at different times giving us the velocity of the transport. We calculated the velocities of the wavefront at time ranges of 50 min by polynomial fitting of first degree.

Image processing and analysis of all the experiments was performed using MATLAB. The data normality and homoscedasticity were verified using Shapiro−Wilk and Levene statistics, respectively. The data did not show a normal distribution, so the nonparametric Mann−Whitney U test was used for comparing the differences between groups. Analysis was performed with SPSS v13.0 for Windows (SPSS Inc., Chicago, IL).

3. RESULTS AND DISCUSSION

Several hydrogels were obtained through different cross-linking methods as showed in Table 1. During the preparation, the gelation conditions were controlled to reduce variability between samples. Finally, we obtained hydrogels according to

the previously published information.[9,29,30] SPM cross-linked hydrogels appeared more transparent than the MA hydrogels when imaged with OPT. The observed different optical properties were subsequently studied in more detail by image texture analysis.

3.1. Image Texture Analysis. Two different groups of hydrogels were analyzed: the first group includes hydrogels with different cross-linking methods and the second group includes hydrogels with different physical cross-linking agents and concentrations, as showed in Table 1.

Image texture analysis was performed in the projections acquired with transmission OPT and in the computed reconstructed slices. Figure 2 shows an example of one projection image (Figure 2a) and 3D reconstruction (Figure 2b) of iGG-Ca. The projection image shows the walls of the tube, which were removed for calculating the Haralick's features in both projections and 3D reconstructions.

From the point of view of image processing, texture is the spatial arrangement of pixel intensities.[34] The images/projections acquired by OPT transmission mode shows the contrast caused by transmitted and absorbed light in the sample. This interaction of light with the sample produces spatial variations of intensity in the images, which are known as image texture. By applying filtered back-projection algorithm we reconstructed the 3D volume of the sample to obtain the spatial distribution of the hydrogels structures; see Figure 2b and Supporting Information Video 1. Different spatial characteristics of the internal structure of the samples, such as density variations, created different textures in the images.

Our group previously reported[26,27] the statistical analysis of hydrogel projections and their 3D reconstructions. Kurtosis, a measure of the shape of the probability distribution of the image histogram, and entropy, a measure of the randomness of the pixels' intensities, were calculated from the projections and reconstructed slices. It was observed that kurtosis decreases with the increase of image microstructures while the opposite happened for entropy. However, the information derived from the histograms alone is not enough to characterize the texture of the hydrogels, since it does not give information about the spatial distribution of the pixel intensities.[34] The GLCM is one of the methods used to extract information about the spatial dependence of gray level values and therefore can be used to characterize textures.[34] It should be noted that the use of the GLCM does not describe shape properties, thus this method is
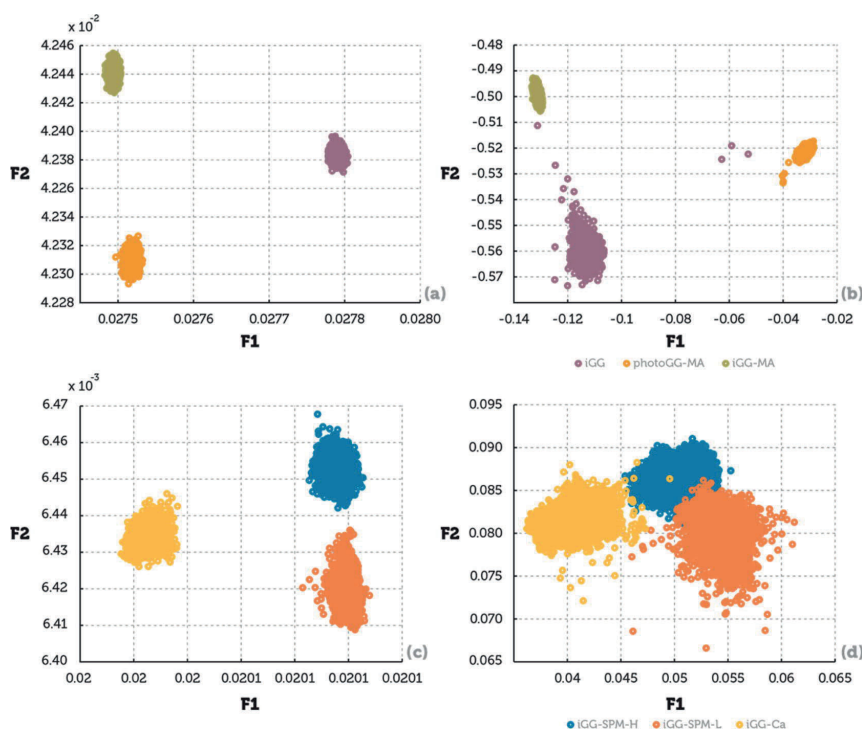
Figure 3. Visualization of the classes projected onto the 2D feature subspaces created by MDA: (a) OPT projection images of hydrogels from group 1; (b) reconstructed slices of hydrogels from group 1; (c) OPT projection images of hydrogels from group 2; and (d) reconstructed slices of hydrogels from group 2. iGG, ionic cross-linked gellan gum; iGG-MA, ionic cross-linked methacrylated gellan gum; photoGG-MA, photo-cross-linked methacrylated gellan gum; iGG-SPM-L, bioamine low cross-linked gellan gum; iGG-SPM-H, bioamine high cross-linked gellan gum; and iGG-Ca, calcium ions cross-linked gellan gum.

more suitable for characterizing microtextures and not for large scale structures.[34]

By analyzing the textural features of the projections and reconstructed images we quantified and compared different hydrogels, Table 1. The textural analysis tool used (Haralick textural features) provides high dimensional data, and in order to better visualize, understand and compare we used MDA to reduce the dimensionality of the feature space. MDA minimize the high dimensionality of this feature space in a manner that best discriminates between different classes (and thus discriminates between different hydrogels), while minimizing the intraclass variations (minimizing the differences within the same hydrogel samples). Thus, MDA selects the combination of textural features that better characterize the hydrogels. If there were not any significant differences between the hydrogels types, MDA would not be able to separate them in different distinct clusters (Figures 3 and 4). Thus, there are discernible differences in the hydrogels image texture, which is related to their internal spatial structure.

Figure 3 shows the results of the MDA of the projections and reconstruction slices of the two hydrogel groups. The high dimensionality of Haralick's features was reduced to two dimensions with two discriminant functions (F1 and F2), which are built as the linear combinations of Haralick's features that contribute most to the separation between hydrogel classes. The features that contribute the most in projections are

Haralick energy, Haralick entropy and Haralick information measure of correlation 1[31] at different pixel lengths and directions, but these image analysis features should not be confused with their counterparts in chemistry. These features are known to be independent of the different gray intensities.[31] On the other hand, the other Haralick's features at the different pixel lengths and directions make a stronger contribution to the discriminant functions built by the MDA for the reconstructed slices. It should be noted that the discriminant functions are different for every case.

The MDA of the hydrogels from group 1, shows three distinguishable clusters in the projection images and reconstructed slices, as can be seen in Figure 3a and b. The projections of the hydrogels with MA modification show that the hydrogels are less transparent suggesting that MA changes their optical properties and in consequence its texture. In addition, photoGG-MA and iGG-MA projection images look similar to the naked eye. However, photoGG-MA hydrogel is cross-linked by covalent bonding and later stabilized by immersion in PBS; thus, these hydrogels are also physically cross-linked by ionic interaction. Thus, it is expected a stronger cross-linking for photoGG-MA, due to the combination of the cross-linking methods, compared to the iGG-MA, which is ionically cross-linked. In addition, the MA-modification in iGG-MA affect the amount of available carboxyl groups and thus has less available cross-linking sites when compared to iGG, which
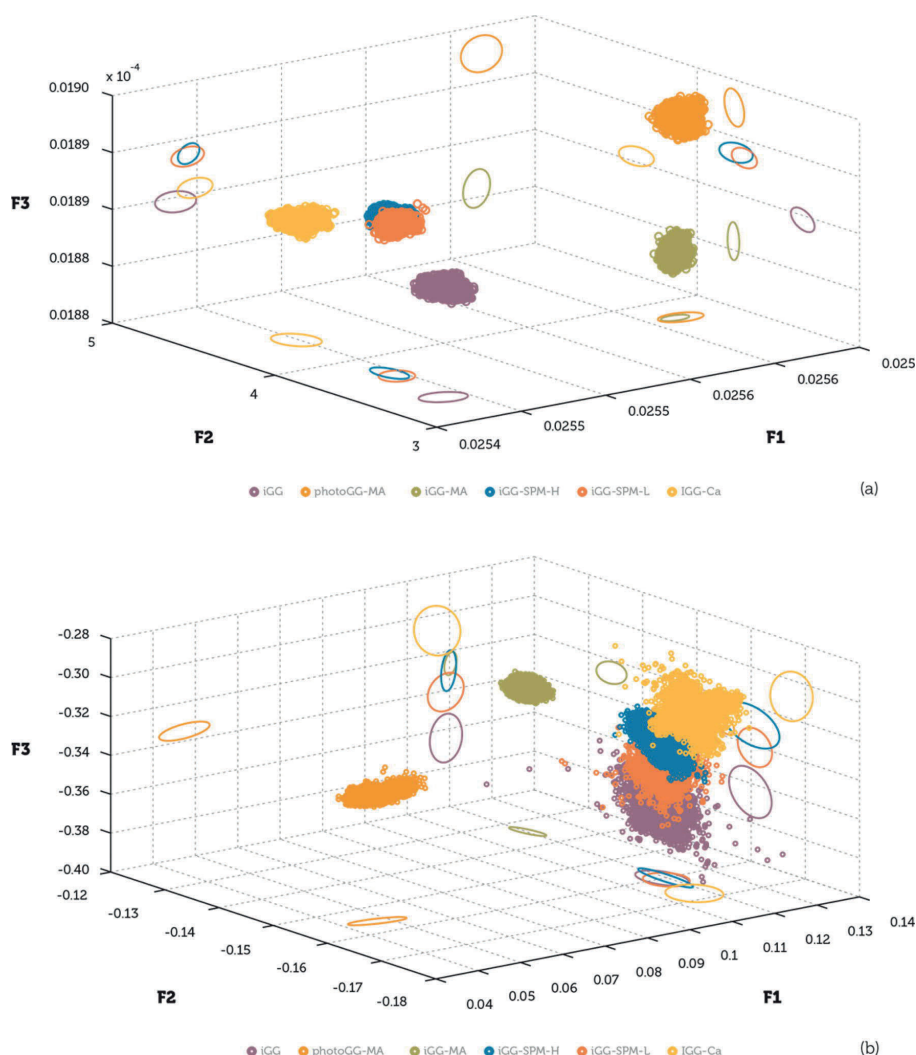
Figure 4. Three-dimensional distributions of the six types of hydrogels projected onto 2D subspaces: (a) projections and (b) reconstructions. iGG, ionic cross-linked gellan gum; iGG-MA, ionic cross-linked methacrylated gellan gum; photoGG-MA, photo-cross-linked methacrylated gellan gum; iGG-SPM-L, bioamine low cross-linked gellan gum; iGG-SPM-H, bioamine high cross-linked gellan gum; and iGG-Ca, calcium ions cross-linked gellan gum.

corresponds to physically cross-linked non modified gellan gum. Therefore, this could cause differences in the cross-linking density and distribution. These differences promote a change in the microstructure of the hydrogel and thus in the image texture of these hydrogels, which are possible to evaluate through the use of OPT and MDA. In addition, in previous studies Silva-Correia et al.[35] have reported that phGG-MA has a storage modulus higher than iGG hydrogels and iGG-MA shows an intermediate behavior; therefore this method can be used to predict some properties of different formulations of hydrogels.

Moreover, image textural analysis can find structural differences between these types of hydrogels. This can be

seen from the results obtained from the reconstructed slices. The reconstruction gives information about the internal structure of the hydrogel; thus, the use of the reconstructed slices enables the possibility to analyze a different dimension than the provided by the projections. MDA results show a clear separation between these groups of hydrogels in the projection images and reconstructed slices, suggesting that OPT can detect cross-linking density, distribution, and method and discriminate between modified and nonmodified GG.

Second group includes physical cross-linking GG hydrogels. In this group, two of the hydrogels are cross-linked by the bioamine spermine (iGG-SPM-H and iGG-SPM-L) and the third is cross-linked by Ca^{2+} cation (iGG-Ca). Polymer
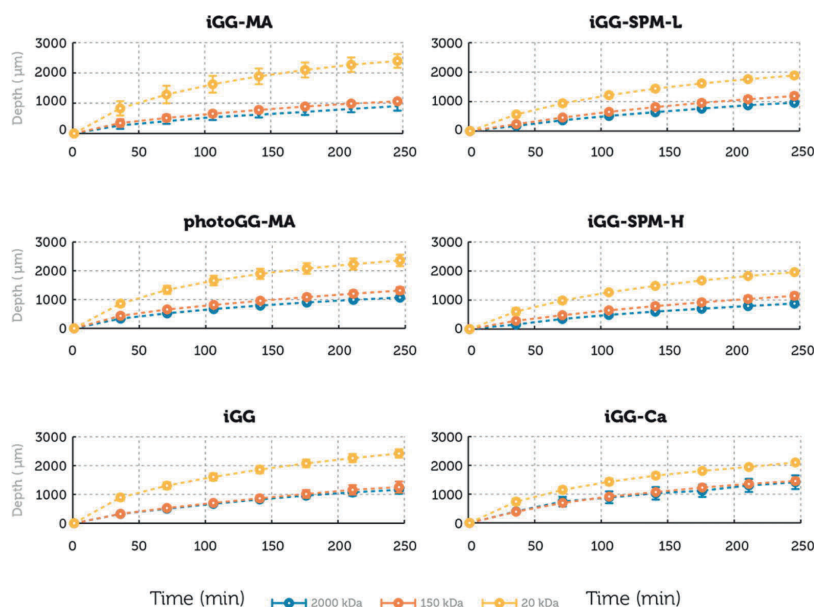
Figure 5. Progression of the frontwave of the binary images. The curves represent the median of the five samples and the vertical bars represent the standard deviation. iGG, ionic cross-linked gellan gum; iGG-MA, ionic cross-linked methacrylated gellan gum; photoGG-MA, photo-cross-linked methacrylated gellan gum; iGG-SPM-L, bioamine low cross-linked gellan gum; iGG-SPM-H, bioamine high cross-linked gellan gum; and iGG-Ca, calcium ions cross-linked gellan gum.

concentration and cross-linking method (physical cross-linking) is the same in this group of hydrogels, however the concentration of cross-linking agent varies.

From MDA results, it can be seen that iGG-SPM-H and iGG-SPM-L clusters are closer in the MDA of the reconstructed slices and in the projection images. Despite the fact that these hydrogels are similar, since the only difference is the cross-linker concentration, it is possible to appreciate that the features clusters are closer but still separated, which indicates small differences between them. From previous studies, Koivisto et al.[29] has found out that iGG-SPM-L has lower young modulus than iGG-SPM-H which is expected from the different cross-linking concentration. On the other hand, there is a clear separation between the hydrogels cross-linked with Ca^{2+} and SPM. The bioamine SPM is a tetravalent salt and $CaCl_2$ is divalent. Therefore, the hydrogels produced by Ca^{2+}-cross-linking are expected to be structurally slightly different from the hydrogels produced with SPM. This result indicates that OPT can also detect structural differences caused by cross-linking concentration, cross-linking density and cross-linking agent, which ultimately affects the hydrogel properties such as mechanical characteristics,

Figure 4 shows the results of the MDA of the two groups of hydrogels together. In this case, we chose to reduce to three dimensions with three discriminant functions (F1, F2, and F3). The different hydrogel classes were projected onto two-dimensional subspaces for better visualization. The functions for the projections and reconstructed slices are built again from similar combination of texture features as described before.

From the MDA of the two groups together (Figure 4) it is possible to observe that the separation between modified gellan gum (GG-MA) and nonmodified GG is evident. The

nonmodified gellan gum hydrogels classes are closer together in both projections and reconstructed slices suggesting that with transmission OPT is possible to detect differences between the types of polymers. Furthermore, the most similar hydrogels (i.e., iGG-SPM-H and iGG-SPM-L) maintain their closeness and separation with the other groups, iGG and iGG-Ca in both the projections and reconstructed slices. The separation between iGG and iGG-Ca groups could be due to the difference in polymer concentration or cross-linking density; however, it is possible to notice that there is an evident difference between these two groups. Finally, iGG-MA and photoGG-MA are much more separated from the nonmodified hydrogel groups, and there is still a separation between these modified gellan gum groups. The results suggest that the cross-linking method has an effect in the final structure of these hydrogels.

The results demonstrate that imaging with transmission OPT together with texture analysis and statistical methods, form a tool that is able to characterize tissue engineering hydrogels during the design and fabrication phases. Moreover, this can be done in a hydrated condition which is closer to the in vivo environment. Transmission OPT allows us to inspect the hydrogel structure not only in one dimension (i.e., the projections images), but also in the third dimension with reconstructed slices, and asses the internal structural changes in the hydrogel due to different compositions. Therefore, we consider that the degree and efficiency of hydrogel cross-linking can be assessed with transmission mode OPT, and this is an important factor when designing hydrogels, since it affects their physical properties and performance.[36] This technique can be used to reduce time and the amount of samples prepared
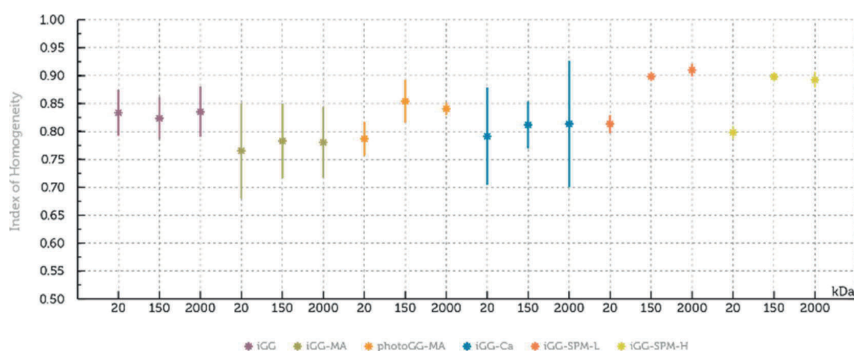
Figure 6. Index of homogeneity. iGG, ionic cross-linked gellan gum; iGG-MA, ionic cross-linked methacrylated gellan gum; photoGG-MA, photo-cross-linked methacrylated gellan gum; iGG-SPM-L, bioamine low cross-linked gellan gum; iGG-SPM-H, bioamine high cross-linked gellan gum; and iGG-Ca, calcium ions cross-linked gellan gum.

during the design of hydrogels and to predict hydrogel suitability for a specific application.

3.2. Mass Transport Studies. Generally, in tissue engineered hydrogel scaffolds, molecules travel though the water filled hydrogel mesh and they rely in passive diffusion since no vasculature exists. Thus, the cross-linking density and inhomogeneity of the cross-linking distribution, size of the porous and porous interconnectivity are some of the factors affecting the transportation of molecules in hydrogels.[37,38] The mobility of differently sized molecules depends on the cross-link density and hydrogel mesh, allowing or restricting their transport.[38] Thus, in this work, mass transport of molecules was studied with emission OPT to examine their mobility through the three-dimensional structure of hydrogels. For this, FITC-dextrans were used with different molecular weights (i.e., 20, 150, and 2000 kDa) as model molecules, comparable to nutrients (glucose, 0.18 kDa), proteins (fibronectin, 550 kDa; TGF-β, 25 kDa; proteoglycans, 2500 kDa), waste , and other metabolites.[39]

The median value of the progression of the wavefront in the binary images corresponding to the FITC-dextran traveling downward through the hydrogel is plotted in Figure 5. The results showed that the 20 kDa FITC-dextran travels faster and deeper through the hydrogel. On the other hand, 150 and 2000 kDa have a similar velocity and do not travel as deep into the gel during the time of the measurement. It was also found that the velocities in all the measurements are not constant. At the beginning the velocities are faster and get slower when going deeper into the hydrogel (see Figure S1 in the Supporting Information). This might be due to the reduction of the dextran concentration on the top of the hydrogel over time as dextran diffuses inside.

Mann–Whitney U test revealed statistically significant ($p <$ 0.05) differences for most of the comparisons between different FITC-dextran molecular weights traveling in the same type of hydrogel, except when comparing 2000 kDa with 150 kDa in iGG-Ca, photoGG-MA, and iGG. From Figure 5, it can be seen that the progression curves are similar for these two molecular weights, and this can be due to 150 kDa has a threshold size which Stokes' radii is between 69 and 95 Å,[40] above which the hydrogel mesh affects the transport, Stokes' radii of 2000 kDa is 270 Å.[40] Furthermore, when comparing the curves for different types of hydrogels with the same FITC-dextran molecular weights, no statistical difference was found for iGG-SPM-L,

iGG-SPM-H, and photoGG-MA. This may be due to the fact that these hydrogels present similar pore size. Large standard deviation is produced by inhomogeneity of the samples and affects the statistical differences. These results are consistent with previous findings. Silva-Correia et al.[35] reported that iGG-MA and photoGG-MA prevented the infiltration of endothelial cells and blood vessels due to their compact structure, which makes these hydrogels good candidates for nucleus pulposus applications. Koivisto et al.[29] studied transportation of molecules on iGG-SPM-L and iGG-SPM-H with Fluorescence recovery after photobleaching (FRAP) technique finding no differences in transportation between these hydrogels.

Figure 6 shows the results of the index of homogeneity with different FITC-dextran molecular weights, for all the hydrogels (the wavefront traveling downward in the binary images is shown in Supporting Information Videos 2 and 3). From the results, it was observed that iGG-SPM-L and iGG-SPM-H are the most homogeneous hydrogels for all the molecules and with smaller standard deviation. The statistical difference of the computed indexes of homogeneity between different FITC-dextrans molecular weights, traveling in the same type of hydrogel and between different types of hydrogels with the same FITC-dextrans molecular weights, was also tested. Statistical differences were found for iGG-SPM-L with different FITC-dextrans molecular weights. There was no statistical differences in the indexes of homogeneity for the progression of 20 kDa molecule in the different types of hydrogels, because the hydrogel mesh does not hinder their mobility considering that their Stokes' radii is between 24 and 45 Å.[40] For the other two FITC-dextrans molecular weights, statistical differences were found between iGG-SPM-L, iGG-Ca, photoGG-MA, and iGG, and between iGG-SPM-H, photoGG-MA, and iGG.

The higher standard deviation and smaller values of homogeneity in iGG-MA hydrogels when compared to iGG can be attributed to the differences in sample preparation. iGG hydrogels are prepared by mixing the solution with PBS, while iGG-MA hydrogels are not mechanically mixed with PBS, but the PBS is slowly poured on top of the GG-MA gel solution for overnight stabilization. This might cause less homogeneous distribution of the ions in the solution, producing inhomogeneous cross-linking distribution. Thus, the method for preparation and time of stabilization can have an impact in the homogeneity of the hydrogel. On the other hand, due to the methacrylation of GG backbone, the amount of available

carboxyl groups for ionic interaction in iGG-MA hydrogels is lower than that in native GG. So the chemical modification of GG can influence the cross-linking process in both iGG-MA and photoGG-MA hydrogels.

Furthermore, the higher standard deviation in iGG-Ca hydrogels, Figure 6, can be attributed to more variability between samples due to the method of preparation and their fast gelation time, i.e., approximately in seconds. iGG-SPM-L and iGG-SPM-H have a longer gelation time which makes the mixing between polymer solution and cross-linker solution more efficient. As a result, the produced hydrogels with this concentration of bioamine are more consistent, which is apparent from the smaller standard deviation presented in Figure 6. Thus, with this method it is also possible to assess the repeatability of the method of preparation.

The results show that the index of homogeneity is useful in studying how freely the molecules can travel through the hydrogels, as well as the cross-linking distribution, which contribute to the homogeneity of the hydrogel structure. Thus, this index can be used as one of the parameters to be correlated to cell response. Even though the mass transport method presented here does not give a precise number for pore size, this technique is able to determine the molecular mobility within the hydrogel, which can be even more relevant for designing tissue engineered hydrogels than just pore size.[21] However, the transport behavior might change when cells produce ECM while the tissue is developing and/or hydrogel is degrading.[37,38] As our method is nondestructive, it presents the possibility to track those changes in transparent hydrogels in the presence of cells and understand the changes during time in mass transport.

4. CONCLUSION

In this work, the capabilities of using optical methods based in OPT technique to analyze material characteristics of hydrated hydrogels were demonstrated. Through visual inspection of hydrogels with OPT it is possible to monitor changes in image texture according to the modifications during the formulation of hydrogels, such as cross-linking concentration or polymer modification.

The usefulness of OPT to characterize mass transport in macroscopic hydrogel scaffold was validated using a model molecule in order to mimic the transport of nutrients and other biomolecules relevant for tissue engineering. Also, an index of homogeneity was defined to evaluate the cross-linking density and distribution. This can be further used to control the efficiency and repeatability of the hydrogel production.

The methods presented here allow the possibility of screening hydrogel compositions. Different groups of hydrogels can be analyzed and compared against a group of hydrogels with known and desired properties. It is expected that with a known cell response to certain hydrogel composition/structure, one can correlate it to the desired features of the newly designed hydrogels. Therefore, with this kind of screening and correlation the amount of cell testing needed can be reduced in the future.

Due to their low cost of components, low time consumption for imaging, and easiness of the method, we believe that OPT system offers good capabilities to develop methods for characterization of hydrogels. The main advantage of OPT is the possibility to characterize hydrogels in the exact same state they will be in the final application, i.e., in the wet form. We showed that the set of OPT imaging based material

characterization methods we developed here are useful for screening many characteristics of hydrogel compositions in relatively short time in an inexpensive manner. The set of methods developed in this work provide new tools for hydrogel development and has potential to impact the design, development, and enhancement of hydrogels for tissue engineering and drug/cell delivery applications.

■ ASSOCIATED CONTENT

Ⓢ Supporting Information

The Supporting Information is available free of charge on the ACS Publications website at DOI: 10.1021/acs.langmuir.6b00554.

> Video 1 shows examples of projections and reconstructions of two different types of hydrogels: (a) shows iGG-SPM-H projections, (b) the reconstruction of (a), (c) photoGG-MA projections, and (d) reconstruction of (c). Video 2 shows the wavefront traveling downward in the binarized images. Video 3 shows an inhomogeneous wavefront in the binarized images. Figure S1 shows FITC-dextran velocities in hydrogels at different time intervals. (ZIP)

■ AUTHOR INFORMATION

Corresponding Authors
*E-mail: ana.sotodelacruz@gmail.com.
*E-mail: jari.hyttinen@tut.fi.

Notes
The authors declare no competing financial interest.

■ ACKNOWLEDGMENTS

■ REFERENCES

(1) Langer, R.; Vacanti, J. P. Tissue Engineering. *Science* **1993**, *260*, 920−926.

(2) Griffith, L. G.; Naughton, G. Tissue Engineering–Current Challenges and Expanding Opportunities. *Science* **2002**, *295*, 1009−1014.

(3) Slaughter, B. V.; Khurshid, S. S.; Fisher, O. Z.; Khademhosseini, A.; Peppas, N. A. Hydrogels in Regenerative Medicine. *Adv. Mater.* **2009**, *21*, 3307−3329.

(4) Geckil, H.; Xu, F.; Zhang, X.; Moon, S.; Demirci, U. Engineering Hydrogels as Extracellular Matrix Mimics. *Nanomedicine (London, U. K.)* **2010**, *5*, 469−484.

(5) Jin, R.; Dijkstra, P. J. Biomedical Applications of Hydrogels Handbook. In *Biomedical Applications of Hydrogels Handbook*; Ottenbrite, R. M., Park, K., Okano, T., Eds.; Springer: New York, 2010; pp 203−225.

(6) Teßmar, J.; Brandl, F.; Göpferich, A. Hydrogels for Tissue Engineering. In *Fundamentals of Tissue Engineering and Regenerative Medicine*; Meyer, U., Handschel, J., Wiesmann, H. P., Meyer, T., Eds.; Springer: Berlin, Heidelberg, **2009**.49510.1007/978-3-540-77755-7_37

(7) Van Vlierberghe, S.; Dubruel, P.; Schacht, E. Biopolymer-Based Hydrogels as Scaffolds for Tissue Engineering Applications: A Review. *Biomacromolecules* **2011**, *12*, 1387−1408.

(8) Drury, J. L.; Mooney, D. J. Hydrogels for Tissue Engineering: Scaffold Design Variables and Applications. *Biomaterials* **2003**, *24*, 4337−4351.

(9) Silva-Correia, J.; Oliveira, J. M.; Caridade, S. G.; Oliveira, J. T.; Sousa, R. A.; Mano, J. F.; Reis, R. L. Gellan Gum-Based Hydrogels for Intervertebral Disc Tissue-Engineering Applications. *J. Tissue Eng. Regener. Med.* **2011**, *5*, e97−e107.

(10) Pereira, D. R.; Silva-Correia, J.; Oliveira, J. M.; Reis, R. L. Hydrogels in Acellular and Cellular Strategies for Intervertebral Disc Regeneration. *J. Tissue Eng. Regener. Med.* **2013**, *7*, 85−98.

(11) Silva-Correia, J.; Pereira, H.; Yan, L. P.; Miranda-Gonçalves, V.; Oliveira, A. L.; Oliveira, J. M.; Reis, R. M.; Espregueira-Mendes, J. D.; Reis, R. L. Advanced Mimetic Materials for Meniscus Tissue Engineering: Targeting Segmental Vascularization. *J. Tissue Eng. Regen. Med.* **2012**, *6*, 8−39.

(12) Pereira, H.; Silva-Correia, J.; Yan, L. P.; Caridade, S. G.; Frias, A. M.; Oliveira, A. L.; Mano, J. F.; Oliveira, J. M.; Espregueira-Mendes, J.; Reis, R. L. Silk-Fibroin/Methacrylated Gellan Gum Hydrogel as an Novel Scaffold for Application in Meniscus Cell-Based Tissue Engineering. *Arthrosc. J. Arthrosc. Relat. Surg.* **2013**, *29*, e53−e55.

(13) Haastert-Talini, K.; Geuna, S.; Dahlin, L. B.; Meyer, C.; Stenberg, L.; Freier, T.; Heimann, C.; Barwig, C.; Pinto, L. F. V; Raimondo, S.; et al. Chitosan Tubes of Varying Degrees of Acetylation for Bridging Peripheral Nerve Defects. *Biomaterials* **2013**, *34*, 9886−9904.

(14) Hunt, J.; Chen, R.; Van Veen, T.; Bryan, N. Hydrogels for Tissue Engineering and Regenerative Medicine. *J. Mater. Chem. B* **2014**, *2*, 5319−5338.

(15) Liu, J.; Hilderink, J.; Groothuis, T. A. M.; Otto, C.; van Blitterswijk, C. A.; de Boer, J. *J. Tissue Eng. Regener. Med.* **2015**, *9*, 952−960.

(16) Stevens, M. M.; George, J. H. Exploring and Engineering the Cell Surface Interface. *Science* **2005**, *310*, 1135−1138.

(17) Amsden, B. Solute Diffusion within Hydrogels. Mechanisms and Models. *Macromolecules* **1998**, *31*, 8382−8395.

(18) Amsden, B. Solute Diffusion in Hydrogels. An Examination of the Retardation Effect. *Polym. Gels Networks* **1998**, *6*, 13−43.

(19) Okay, O. General Properties of Hydrogels. In *Hydrogel Sensors and Actuators*; Gerlach, G., Arndt, K.-F., Eds.; Springer Series on Chemical Sensors and Biosensors; Springer: Berlin, Heidelberg, 2010; Vol. 6, pp 1−14.

(20) Vielreicher, M.; Schürmann, S.; Detsch, R.; Schmidt, M. A.; Buttgereit, A.; Boccaccini, A.; Friedrich, O. Taking a Deep Look: Modern Microscopy Technologies to Optimize the Design and Functionality of Biocompatible Scaffolds for Tissue Engineering in Regenerative Medicine. *J. R. Soc., Interface* **2013**, *10*, 20130263.

(21) Mather, M. L.; Morgan, S. P.; Crowe, J. A. Meeting the Needs of Monitoring in Tissue Engineering. *Regener. Med.* **2007**, *2*, 145−160.

(22) Chalal, M.; Morfin, I.; Vial, J.; Aguilar de Armas, M. A.; San Roman, J. S.; Bolgen, N.; Piskin, E.; Ziane, O.; Casalegno, R. *Macromolecules* **2009**, *42*, 2749−2755.

(23) Sharpe, J.; Ahlgren, U.; Perry, P.; Hill, B.; Ross, A.; Hecksher-Sørensen, J.; Baldock, R.; Davidson, D. Optical Projection Tomography as a Tool for 3D Microscopy and Gene Expression Studies. *Science* **2002**, *296*, 541−545.

(24) Sharpe, J. Optical Projection Tomography as a New Tool for Studying Embryo Anatomy. *J. Anat.* **2003**, *202*, 175−181.

(25) Rieckher, M.; Birk, U. J.; Meyer, H.; Ripoll, J.; Tavernarakis, N. Microscopic Optical Projection Tomography In Vivo. *PLoS One* **2011**, *6*, e18963.

(26) Soto, A. M.; Koivisto, J.; Parraga, J. E.; Silva-Correia, J.; Oliveira, J. M.; Reis, R. L.; Kellomäki, M.; Hyttinen, J.; Figueiras, E. *Optical Projection Tomography as a Tool for Visualizing Hydrogels Microstructures*. In *26th Annual Conference of the European Society for Biomaterials (ESB)*; 2014.

(27) Figueiras, E.; Soto, A. M.; Jesus, D.; Lehti, M.; Koivisto, J.; Parraga, J. E.; Oliveira, J. M.; Reis, R. L.; Kellomäki, M.; Hyttinen, J. Optical Projection Tomography as a Tool for 3D Imaging of Hydrogels. *Biomed. Opt. Express* **2014**, *5*, 3443−3449.

(28) Soto, A. M.; Koivisto, J.; Parraga, J. E.; Hyttinen, J.; Kellomäki, M.; Figueiras, E. *Mass Transport Study with Fluorescent Dextran Molecules in Gellan Gum Hydrogel*. In *27th Annual Conference of the European Society for Biomaterials (ESB)*; 2015.

(29) Koivisto, J.; Teymouri, S.; Parraga, J. E.; Ihalainen, T. O.; Aalto-Setälä, K.; Kellomäki, M. *Development of Bioamine Cross-Linked Gellan Gum Hydrogels as Soft Scaffolds for Neural Tissue Engineering*. In *26th Annual Conference of the European Society for Biomaterials (ESB)*; Liverpool, 2014; pp 39−5.

(30) Silva-Correia, J.; Gloria, A.; Oliveira, M. B.; Mano, J. F.; Oliveira, J. M.; Ambrosio, L.; Reis, R. L. Rheological and Mechanical Properties of Acellular and Cell-Laden Methacrylated Gellan Gum Hydrogels. *J. Biomed. Mater. Res., Part A* **2013**, *101*, 3438−3446.

(31) Haralick, R. M.; Shanmugam, K.; Dinstein, I. Textural Features for Image Classification. *IEEE Trans. Syst. Man. Cybern.* **1973**, *3*, 610.

(32) Duda, R. O.; Hart, P. E.; Stork, D. G. *Pattern Classification*; John Wiley & Sons: New York, 2001.

(33) Gonzalez, R. C.; Woods, R. E. *Digital Image Processing*, 3rd ed.; Prentice Hall: Upper Saddle River, NJ, 2008.

(34) Jain, R.; Kasturi, R.; Schunck, B. G. *Machine Vision*; Munson, E. M., Ed.; McGraw-Hill: New York, 1995.

(35) Silva-Correia, J.; Zavan, B.; Vindigni, V.; Silva, T. H.; Oliveira, J. M.; Abatangelo, G.; Reis, R. L. Biocompatibility Evaluation of Ionic- and Photo-Crosslinked Methacrylated Gellan Gum Hydrogels: In Vitro and In Vivo Study. *Adv. Healthcare Mater.* **2013**, *2*, 568−575.

(36) *ASTM F2900-11, Standard Guide for Characterization of Hydrogels Used in Regenerative Medicine*; ASTM International: West Conshohocken, PA, 2011.

(37) Watkins, A. W.; Anseth, K. S. Investigation of Molecular Transport and Distributions in Poly(ethylene Glycol) Hydrogels with Confocal Laser Scanning Microscopy. *Macromolecules* **2005**, *38*, 1326−1334.

(38) Dhote, V.; Skaalure, S.; Akalp, U.; Roberts, J.; Bryant, S. J.; Vernerey, F. J. On the Role of Hydrogel Structure and Degradation in Controlling the Transport of Cell-Secreted Matrix Molecules for Engineered Cartilage. *J. Mech. Behav. Biomed. Mater.* **2013**, *19*, 61−74.

(39) Leddy, H. A.; Guilak, F. Site-Specific Molecular Diffusion in Articular Cartilage Measured Using Fluorescence Recovery after Photobleaching. *Ann. Biomed. Eng.* **2003**, *31*, 753−760.

(40) FITC-Dextran Fluorescein Isothiocyanate Dextran; http://tdbcons.com/images/pdf/fitcdextran2.pdf.

(41) Szczesniak, A. S. Texture Is a Sensory Property. *Food Qual. Prefer.* **2002**, *13*, 215−225.

Supporting information

Optical projection tomography technique for image texture and mass transport studies in hydrogels based on gellan gum

Ana M. Soto, *,†,‡ Janne T. Koivisto, ‡,§,⊥ Jenny E. Parraga, ‡,§ Joana Silva-Correia, ‖,‡ Joaquim M. Oliveira, ‖,‡ Rui L. Reis, ‖,‡ Minna Kellomäki, ‡,§ Jari Hyttinen, *, †,‡, and Edite Figueiras †,‡

†Computational Biophysics and Imaging Group, ELT Dept., Tampere University of Technology Finland,
‡BioMediTech - Institute of Biosciences and Medical Technology, Finland,
§Biomaterials and Tissue Engineering Group, ELT Dept., Tampere University of Technology Finland,
⊥Heart Group, BioMediTech, University of Tampere, Finland,
‖3B's Research Group, Biomaterials, Biodegradables and Biomimetics, University of Minho, Headquarters of the European Institute of Excellence on Tissue Engineering and Regenerative Medicine Barco GMR, Portugal
‡ICVS/3B's - PT Government Associate Laboratory, Braga/Guimarães, Portugal
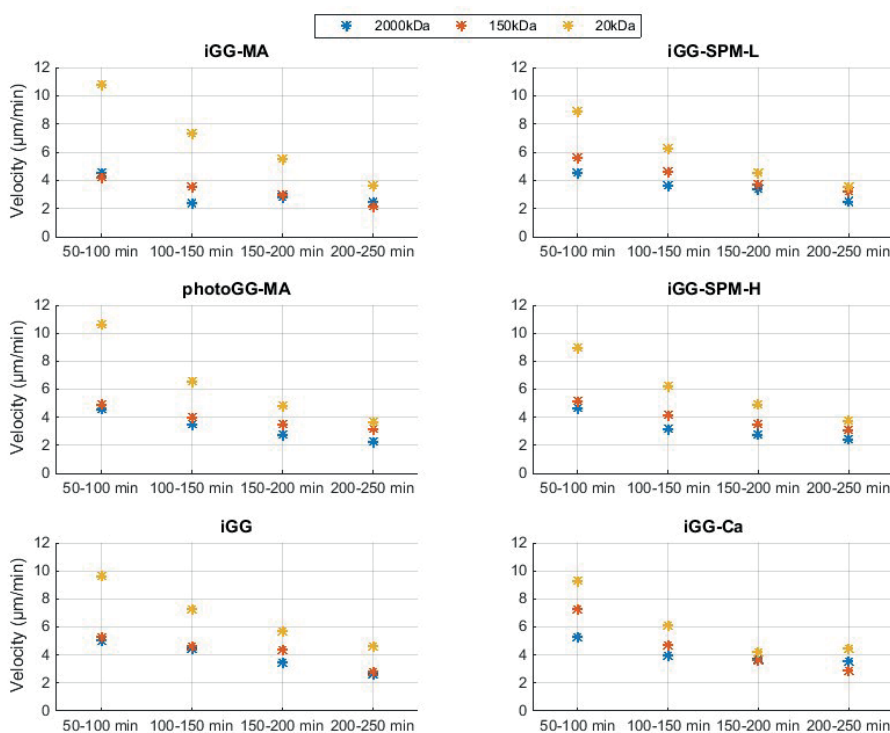
Supplementary Figure 1. Velocities of the wavefront at time intervals of 50 minutes.
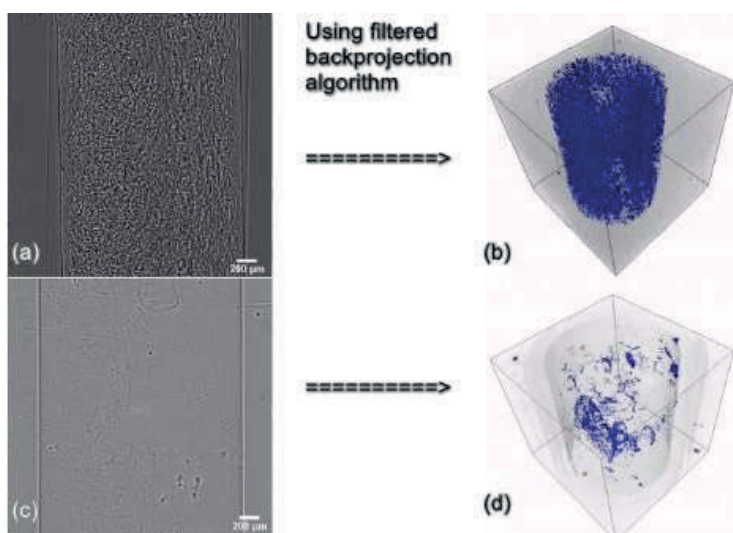
Supplementary Video 2. Representative videos of OPT single projection bright field image and 3D view of the OPT reconstruction using filtered back-projection algorithm. Optical texture pseudo-colored in blue color. (a) & (b) photo-GG-MA hydrogel and (c) & (d) iGG-SPM-H hydrogel.
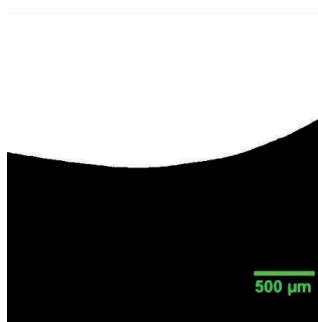
Supplementary Video 2. Binarized wavefront of fluorescent 20 kDa dextran molecule traveling downward through iGG-SPM-H hydrogel. (Still image at 3 seconds time point.)
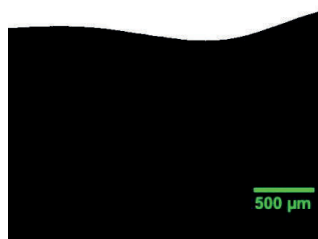
Supplementary Video 2. Binarized wavefront of fluorescent 2000 kDa dextran molecule traveling downward through iGG-SPM-H hydrogel. (Still image at 3 seconds time point.)

III

MECHANICALLY BIOMIMETIC GELATIN-GELLAN GUM HYDROGELS FOR 3D CULTURE OF BEATING HUMAN CARDIOMYOCYTES

by

Janne T. Koivisto, Christine Gering, Jennika Karvinen, Reeja Maria Cherian, Birhanu Belay, Jari Hyttinen, Katriina Aalto-Setälä, Minna Kellomäki, and Jenny Parraga

Mechanically Biomimetic Gelatin−Gellan Gum Hydrogels for 3D Culture of Beating Human Cardiomyocytes

Janne T. Koivisto,*,[†,‡] Christine Gering,[†] Jennika Karvinen,[†] Reeja Maria Cherian,[‡] Birhanu Belay,[§] Jari Hyttinen,[§] Katriina Aalto-Setälä,[‡,‖] Minna Kellomäki,[†] and Jenny Parraga*,[†]

[†]Biomaterials and Tissue Engineering Group, BioMediTech, Faculty of Medicine and Health Technology, Tampere University, 33720 Tampere, Finland

[‡]Heart Group, BioMediTech, Faculty of Medicine and Health Technology and [§]Computational Biophysics and Imaging Group, BioMediTech, Faculty of Medicine and Health Technology, Tampere University, 33520 Tampere, Finland

[‖]Heart Hospital, Tampere University Hospital, 33520 Tampere, Finland

Ⓢ *Supporting Information*

ABSTRACT: To promote the transition of cell cultures from 2D to 3D, hydrogels are needed to biomimic the extracellular matrix (ECM). One potential material for this purpose is gellan gum (GG), a biocompatible and mechanically tunable hydrogel. However, GG alone does not provide attachment sites for cells to thrive in 3D. One option for biofunctionalization is the introduction of gelatin, a derivative of the abundant ECM protein collagen. Unfortunately, gelatin lacks cross-linking moieties, making the production of self-standing hydrogels difficult under physiological conditions. Here, we explore the functionalization of GG with gelatin at biologically relevant concentrations using semiorthogonal, cytocompatible, and facile chemistry based on hydrazone reaction. These hydrogels exhibit mechanical behavior, especially elasticity, which resembles the cardiac tissue. The use of optical projection tomography for 3D cell microscopy demonstrates good cytocompatibility and elongation of human fibroblasts (WI-38). In addition, human-induced pluripotent stem cell-derived cardiomyocytes attach to the hydrogels and recover their spontaneous beating in 24 h culture. Beating is studied using in-house-built phase contrast video analysis software, and it is comparable with the beating of control cardiomyocytes under regular culture conditions. These hydrogels provide a promising platform to transition cardiac tissue engineering and disease modeling from 2D to 3D.

KEYWORDS: hiPSC-derived cardiomyocytes, 3D hydrogel, gelatin, gellan gum, compression testing
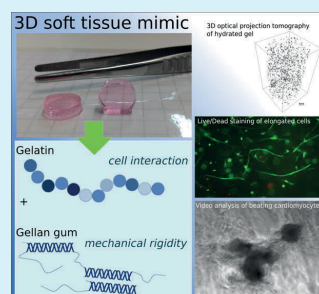
1. INTRODUCTION

The aim of tissue engineering (TE) is to create a new living tissue in vitro using a combination of biomaterial scaffolds, living tissue-specific cells, and biochemical factors.[1] In recent years, there has been a growing interest in the use of in vitro tissue and organoids as components for disease modeling, toxicology, and study of developmental biology.[2−5] In the case of cardiac disease modeling, human-induced pluripotent stem cell (hiPSC)-derived cardiomyocytes have been used to define the electrophysiological behavior of cardiomyocytes affected by specific genetic diseases.[5−8] As part of our earlier work, we reproduced the disease phenotype of genetic catecholaminergic polymorphic ventricular tachycardia in vitro and showed the proof of concept that iPSC-derived cardiomyocytes can reproduce a clinical drug response.[9] Furthermore, since cardiotoxicity is one of the most common causes of the drawbacks associated with many drugs, our group has been working on ways to improve methods for testing drug safety in 2D cardiac models.[10−12] To produce better biomimicking disease and cardiotoxicity models, however, a transition from 2D to 3D is needed to bridge the translational gap in drug discovery from single cell or 2D studies to clinical studies. A 3D disease model enables studying more intercellular interactions compared to 2D models, especially when comparing with single-cell studies.[3,13−15]

Till date, the most relevant cardiac 3D cell culture systems are engineered heart tissues, the so-called Biowire, 3D bioprinted structures, and even 3D printed organs-on-chip.[15−18] All of the above examples use an extracellular matrix (ECM) protein-based hydrogel scaffold, either Matrigel or gelatin methacrylate (GelMA), to support 3D cell culturing. In these studies, the focus is more on cardiomyocyte electrophysiology than on the relationship between the mechanical properties of the material and how cellular mechanotransduction affects the biological response.[19] Thus, more emphasis should be placed on the design and mechanical characterization of these soft biomaterial scaffolds.

To overcome the mechanical challenges of this specific biomedical application, new chemical cross-linking strategies for hydrogel production are needed. Noncovalent interactions have been used to produce hydrogels, mainly with electrostatic and hydrophobic interactions and hydrogen bonding. These hydrogels are usually relatively brittle with a narrow range of mechanical properties.[20,21] On the other hand, covalent cross-linking strategies have the ability to control the cross-linking density and, therefore, the mechanical properties. These strategies can result in higher elasticity, a key feature for the success of soft TE.

The cross-linking design should be chemoselective and efficient and should retain the biocompatibility of the polymer. In addition, gelation under physiological conditions could be beneficial for biomedical applications. Covalent hydrazone cross-linking is known to fulfil these requirements. Indeed, our previous studies have shown the elastic, biomimicking behavior of hydrogels obtained with this chemistry.[22−24]

In this work, we apply hydrazone chemistry to a combination of two well-known biopolymers in TE applications: gelatin and gellan gum (GG). Gelatin is a molecule derived from the abundant ECM protein collagen, and it is routinely used as a coating material in cardiac cell culture applications.[25,26] Gelatin hydrogel scaffolds can be formed by physical cross-linking, namely, thermal gelation. However, the gelation temperature is often below physiological requirements, and thus the use of these hydrogels in native form with cells is limited.[26] On the other hand, GG, a bacterial polysaccharide, is able to form hydrogels with tunable mechanical properties. The relatively bioinert nature of GG, however, does not support cell attachment.[21,27−29] Both GelMA and methacrylated GG (GGMA) have been photo-cross-linked into hydrogels and used to encapsulate cells.[26,30,31] They have even been combined in a double-network hydrogel with relatively good cytocompatibility.[32] However, the main limitations to using this approach for the fabrication of larger 3D tissues or organs is the phototoxicity of ultraviolet (UV) cross-linking and dependence on transparency of the hydrogel components.[33−35]

We have explored the use of these in situ cross-linkable hydrogels as biomimicking scaffolds for 3D cardiac disease modeling. In this study, we use 3D in-house-built microscopy to demonstrate the effects of hydrogel properties on cell morphology.[36] Our results show substantially more elongated fibroblast cells in 3D culture inside these hydrogels and clearly indicate better cytocompatibility than many other published cell results using the same hydrogel components.[32,37] On the basis of our findings, we used these hydrogels in a macroscale 3D culture of hiPSC-derived cardiomyocyte aggregates for the first time. The spontaneous beating behavior of the cardiomyocytes was analyzed with our previously developed motion tracking video analysis software.[11] Furthermore, we demonstrate that this rational hydrogel design supports the transition from 2D to 3D without interfering with the cardiomyocyte behavior and furthers the aim toward in vitro 3D hiPSC-derived cardiac disease modeling and drug screening.

2. EXPERIMENTAL SECTION

2.1. Materials. Gelatin A from porcine skin, GG (Gelzan CM Gelrite, M_w 1000 g mol^{-1}), spermidine trihydrochloride (SPD), sucrose, adipic dihydrazide (ADH), carbodihydrazide (CDH), dimethyl sulfoxide (DMSO), ethylene glycol, 1-ethyl-3-[3-(dimethy-lamino)-propyl]-carbodiimide (EDC), hydroxylamine hydrochloride, N-hydroxybenztotriazole (HOBt), 4-hydroxybenzaldehyde, deuterium oxide (99.9 atom % D, contains 0.05 wt % 3-(trimethylsilyl)-propionic-2,2,3,3-d4 acid, sodium salt), hydrochloric acid (HCl), sodium hydroxide (NaOH), sodium chloride (NaCl), and sodium periodate (NaIO$_4$) were purchased from Sigma-Aldrich (St. Louis, MO, USA). Dialysis membrane (Spectra/Por 12−14 kDa) was purchased from Spectrum Laboratories (Rancho Dominguez, CA, USA).

2.2. Preparation of ADH-Modified Gelatin (Gelatin-ADH). First, 300 mg of gelatin was dissolved in 100 mL of water, and 3.92 g (0.225 M) of ADH was added to this solution. The pH of the reaction mixture was adjusted to 6.8. Then, 576 mg (0.03 M) of EDC and 405 mg (0.03 M) of HOBt were dissolved in 3 mL of DMSO/water (1.5:1 v/v) and added to the reaction mixture drop by drop, while keeping the pH at 6.8 with 0.1 M NaOH and 0.1 M HCl during the mixture addition and for another 4 h. Then, the reaction was continued for another 20 h. The pH was adjusted to 7, and gelatin-ADH was exhaustively dialyzed against water for 2 d. Then, NaCl was added to produce a 7% (w/v) solution, and the product was precipitated in cold ethanol (4 vol equiv). Then, the product was dissolved in water and dialyzed against water for 2 days. Finally, the solution was lyophilized through a molecular weight cutoff 12−14 kDa dialysis membrane followed by freeze-drying.

2.3. Preparation of CDH-Modified Gelatin (Gelatin-CDH). First, 300 mg of gelatin was dissolved in 100 mL of water, and 3.6 g (0.4 M) of CDH was added to this solution. The pH of the reaction mixture was adjusted to 4.7 with 0.5 M HCl. Then, 575 mg (0.03 M) of EDC and 405 mg (0.03 M) of HOBt were dissolved in 3 mL of DMSO/water (1.5:1 v/v) and added to the reaction mixture drop by drop, while keeping the pH at 6.8 with 0.1 M NaOH and 0.1 M HCl during the mixture addition and for another 4 h. Then, the reaction was kept for another 20 h. Gelatin-CDH was exhaustively dialyzed against water for 2 days. Additional purification was carried out as described above followed by freeze-drying.

2.4. Preparation of Oxidized GG (GG-CHO). GG was modified by NaIO$_4$ oxidation according to the method previously reported by our group to produce GG-CHO at the modification degree of 25%.[22]

2.5. Polymer Characterization. To confirm the presence of hydrazide functionality, 20 mg of gelatin-ADH or gelatin-CDH was treated with 10 mL of 4-hydroxybenzaldehyde (20 mg mL^{-1}) in distilled water for 24 h at room temperature. The product was dialyzed and lyophilized as described above and analyzed by nuclear magnetic resonance (NMR) spectroscopy. All experiments were measured with a Jeol JNM-ECZR 500 MHz NMR spectrometer (Tokyo, Japan). The samples (5 mg) were dissolved in deuterium oxide (600 μL) containing an internal standard (0.05 wt % 3-(trimethylsilyl)-propionic-2,2,3,3-d4 acid, sodium salt). The samples were measured at 40 °C. The relative substitution was calculated by comparing the integral of the lysine amino acid peak at δ 3.0 ppm to the aromatic proton peak of 4-hydroxybenzaldehyde at δ 7.6 ppm. The presence of aldehyde groups in GG-CHO was qualitatively evaluated using Fourier transform infrared (FTIR) spectroscopy. FTIR-spectra from the GG-CHO polymer was measured on a PerkinElmer Spectrum One attenuated total reflection−FTIR spectrometer (Waltham, MA, USA) in the spectral range of 400−4000 cm^{-1}.

2.6. Hydrogel Preparation and Characterization. Modified gelatins and GG-CHO solutions were prepared separately by dissolving each polymer in an aqueous solution of 10% (w/w) sucrose or in Dulbecco's modified eagle medium (DMEM), as shown in Table 1. Before the hydrogel preparation, the gelatin polymer solutions were filtered using a Whatman FP 30/0.2 CA-S sterile filter (Thermo Fisher Scientific, MA, USA) at 37 °C, and the GG solutions were filtered using a Sterivex-GP 0.22 μm Millipore Express (polyethersulfone) sterile filter (Merck Millipore, MA, USA) at 60 °C. The solutions were kept at 37 °C, and then equal volumes (1:1) of the solutions were mixed for a few seconds by pipetting. The F7-SPD bioamine-GG compositions were prepared as stated previously[21]

Table 1. Formulation of Hydrazone Cross-Linked Hydrogels Based on Gelatin and GG

formulation code	components	concentration [mg mL^{-1}]	gelation medium	
			10% sucrose	DMEM/F-12 or PBS
F1-ADH	gelatin-ADH	40	+	
	GG-CHO	40		
F2-ADH	gelatin-ADH	40	+	
	GG-CHO	30		
F3-ADH	gelatin-ADH	40	+	
	GG-CHO	20		
F4-CDH	gelatin-CDH	60		+
	GG-CHO	60		
F5-CDH	gelatin-CDH	60		+
	GG-CHO	40		
F6-CDH	gelatin-CDH	40		+
	GG-CHO	40		
F7-SPD	unmodified GG	5	+	
	SPD	0.5	+	

with 1.5 wt % of SPD cross-linker per GG and used as the negative control.

2.7. In Vitro Hydrogel Degradation. For in vitro degradation tests, 500 μL of hydrogels were formed in Eppendorf tubes. A solution of 10 U mL^{-1} of collagenase II (Sigma-Aldrich, St. Louis, MO, USA) was added to the tubes, and aliquots were collected at the indicated time points and refreshed with fresh enzyme solution. The fluorescamine (Sigma-Aldrich, St. Louis, MO, USA) test was used to determine the presence of gelatin in the collected samples using a QuantaMaster PTI spectrofluorometer (Photon Technology International, Inc., Lawrenceville, NJ, USA) (excitation 390 nm, emission 465 nm).

2.8. Mechanical Characterization. Hydrogel samples were prepared in custom-made polydimethylsiloxane (PDMS) molds with a diameter of 12 mm and a height of 6 mm and tested at the earliest 2 h after gelation. PDMS was fabricated from the SYLGARD 184 base polymer and a curing agent (10:1, w/w, SYLGARD 184, Dow Corning, USA), acquired from Ellsworth Adhesives AB (Sweden). Mechanical testing was performed, as we have previously described in detail, using a BOSE ElectroForce BioDynamic 5100 machine equipped with a 225 N load sensor and Wintest 4.1 software (Bose Corporation, Eden Prairie, MN, USA).[21] Unconfined compression was performed with a constant 10 mm min^{-1} strain rate until 75% strain of the original height was reached. The fracture point was seen as a clear drop in the stress−strain curve.

To obtain a relevant reference for our hydrogel's biomimicry of the tissue, we used the compression testing data from fresh heart tissues of New Zealand white rabbits, based on our previous results.[22] The compression samples were cut from both the left and right heart ventricle, compressed in the direction perpendicular to the beating direction, and pooled together. The rabbit tissues were obtained from animal experiments conducted at the Tampere University Medical School.

Statistical analysis of the mechanical testing data was performed by SPSS Version 25.0 (IBM SPSS Statistics for Windows, NY, USA). The data were presented as mean ± standard deviation. One-way analysis of variance was performed with a confidence level of 95%. P values less than 0.05 were considered as statistically significant. Pair comparisons of data were done with the Tukey post-hoc test to identify significant differences between the hydrogel formulations.

2.9. Fibroblast Hydrogel Cell Culture. The commercial human lung fibroblasts (WI-38, Culture Collections, Public Health England, United Kingdom) were cultured and expanded in Nunc T75 culture flasks (Thermo Fisher Scientific, USA) with DMEM/Ham's Nutrient Mixture F-12 (F-12 1:1; Thermo Fisher Scientific, USA) supplemented with 10% fetal bovine serum (FBS; South American

Origin, Biosera, Finland) and 50 U mL^{-1} penicillin/streptomycin (Pen/Strep; Thermo Fisher Scientific, USA). For cytocompatibility testing, fibroblasts were detached from the culture flask via trypsin (Lonza, Basel, Switzerland) treatment and then counted and plated with 30 000 cells cm^{-2} under 2D conditions and with 300 000 cells mL^{-1} under 3D conditions. To test the cytocompatibility of the modified gelatin, separate cell culture wells were dip-coated with gelatin-ADH or gelatin-CDH (40 mg mL^{-1}) with 1 h incubation at 37 °C.

Hydrogel cell cultures were conducted both on top of the hydrogel (2D) and encapsulated inside the hydrogel (3D), with all hydrogel compositions listed in Table 1. In the 2D experiment, the hydrogel was cast in the well plate 20 min before the cells were plated on top. In the 3D experiment, 30 μL of cell suspension was mixed with gelatin-ADH or gelatin-CDH and GG-CHO simultaneously during gelation to form a total of 330 μL of hydrogel. Cell culture medium was applied on top of the samples after ∼20 min of gelation time. Unmodified gelatin coating was used as a control in all cell experiments. All coating and hydrogel cell tests were done on a Greiner CELLSTAR 48-multiwell plate (Sigma-Aldrich).

After 3 and 7 days of culturing, the samples were stained with a Live/Dead (Thermo Fisher Scientific, USA) cell viability kit. The fluorescent calcein-AM (at 0.2 μM) stains intact cells green, and ethidium homodimer-1 (at 1.0 μM) stains dead cells red. After 1 h of incubation at room temperature with a rocker, the cells were imaged with an Olympus IX51 inverted microscope and an Olympus DP30BW digital camera (Olympus, Finland). Staining concentrations were double that recommended by the kit instructions to allow for faster diffusion under 3D hydrogel conditions. During wide-field microscopy, the 3D position in the middle of the hydrogel was verified by using the 2D cell control at the well-plate bottom as a reference point and changing the focus distance accordingly.

The cell numbers were quantified using ImageJ (Version 1.39, US National Institutes of Health, Bethesda, MD, USA)[38] particle counting algorithm based on at least three parallel Live/Dead stained images taken with 4× magnification from all studied conditions. Fibroblast viability percentage was calculated from the detected live and dead cell area according to the following equation

$$\text{Viability \%} = \frac{\text{area of live cells}}{\text{area of live cells} + \text{area of dead cells}}$$

$$= \frac{\sum_{i=1}^{n} L_i}{\sum_{i=1}^{n} D_i + L_i}$$

2.10. Optical Projection Tomography Imaging. An in-house built optical projection tomography (OPT) system in transmission mode was used for imaging cells encapsulated in the hydrogel to visualize the 3D morphology of fibroblasts under selected hydrogel conditions.[36,39] Cell cultures were prepared in fluorinated ethylene propylene tubes with water matching the refractive index and submerged inside a cuvette filled with water for imaging. All OPT samples were imaged after 7 days of culture. A white light-emitting diode source (Edmund, USA) was used to illuminate the sample. The transmitted light was detected by a 5× infinity-corrected objective (Edmund, USA) with a numerical aperture of 0.14 and imaged with a sCMOS camera (ORCA-Flash 4.0, Hamamatsu, Japan). The sample was rotated 360° while a total of 400 projection images were captured at 0.9° intervals. 3D reconstruction was computed in MATLAB from projection images using standard filtered back-projection algorithm.[36] Visualization in 3D was done in Avizo software (Thermo Fisher Scientific, Waltham, MA, USA).

2.11. Cardiomyocyte Differentiation. The Ethics Committee of Pirkanmaa Hospital District gave approval to conduct research on hiPSC lines (Aalto-Setälä R08070). The hiPSC line UTA.04602.WT was cultured and characterized at the stem cell state, as previously described.[40] The cardiomyocyte differentiation was done by modulating Wnt signaling with small molecules, according to the protocol published by Lian et al. 2012.[41] In short, differentiation was initiated by plating 700 000 hiPSCs/well in a Nunc 12-multiwell plate (Thermo Fisher Scientific, USA) in feeder-free condition on Geltrex-
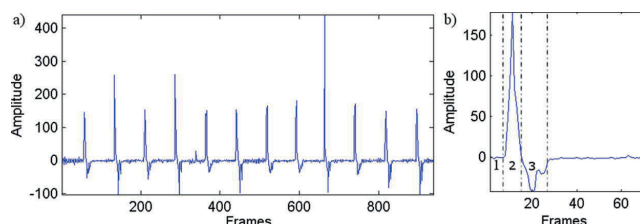
Figure 1. Beating pattern of cardiomyocyte aggregate in F4-CDH hydrogel as an example of the BeatView analysis. This is the same aggregate as in Video S8. Graph (a) shows regular beating rhythm; (b) shows the breakdown of a single beat into relaxed state (1) and contracting (2) and relaxing (3) movements.
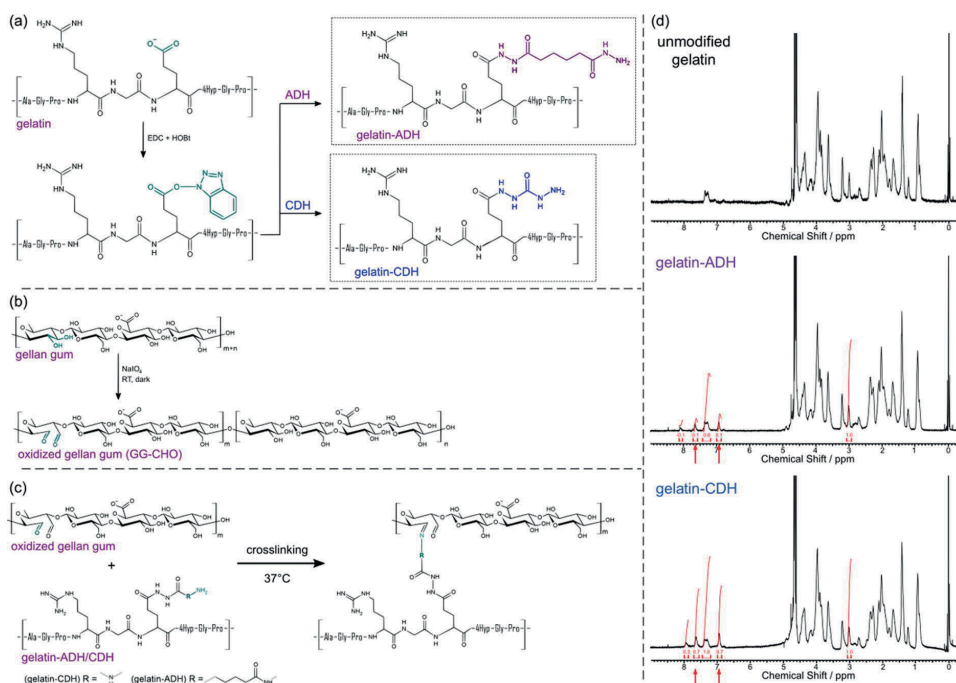
Figure 2. (a) Chemical modification of gelatin carboxylic groups with hydrazide molecules ADH (provides 10-atom bridge) and CDH (provides 5-atom bridge). (b) Periodate oxidation of vicinal diols in GG. (c) Hydrazone cross-linking reaction between gelatin-ADH/CDH and GG-CHO. (d) ^{1}H NMR-spectra of nonmodified gelatin, gelatin-ADH, and gelatin-CDH modifications. The arrows highlight the appearance of aromatic protons in gelatin-ADH and gelatin-CDH spectra after the coupling reaction of CDH and ADH with 4-hydroxybelzandehyde. Chemical modification was successful based on the appearance of extra peaks.

coating (Thermo Fisher Scientific, USA) in mTeSR1 medium (STEMCELL Technologies, Canada) supplemented with 50 U mL^{-1} Pen/Strep for 4 days. Ten days after initiation, the medium was changed to RPMI (Thermo Fisher Scientific, USA) supplemented with B27($-$insulin) (Thermo Fisher Scientific, USA) and 50 U mL^{-1} Pen/Strep. During this time, on day one, 8 μM CHIR99021 (REPROCELL, United Kingdom) was applied to the cells. After 24 h, CHIR99021 was removed. On day3, 5 μM IWP-4 (R&D Bio-Techne, USA) was added for 48 h. From day 10 onwards, B27($-$insulin) was changed to B27($+$insulin) (Thermo Fisher Scientific, USA), and the cells were cultured in this medium until they were used for the hydrogel experiments.

2.12. Cardiomyocyte Hydrogel Cell Culture. After differentiation, beating cardiomyocyte areas were cut with a scalpel under a microscope and collected. Then, the aggregates were partially dissociated to loosen the cell-to-cell bonds inside the aggregate and to better allow the attachment on the hydrogel. Dissociation was modified from the study of Ahola et al. 2014.[11] The enzymatic dissociation buffers were applied to the cells incubated at 37 °C: First buffer for 45 min, second buffer for 15 min, and third buffer for 10 min, but no mechanical dissociation was done. The gentle dissociation treatment loosens the cardiomyocyte aggregate and makes it more susceptible to attach on to the hydrogel surface. Four aggregates were plated per well with all coating and hydrogel preparations (2D and 3D), as described above for fibroblasts. Cells were cultured with KnockOut-DMEM medium (Thermo Fisher Scientific, USA) supplemented with 20% FBS, 1% nonessential amino acids (Cambrex, NJ, USA), 2 mM GlutaMAX (Thermo Fisher Scientific, USA), and 50 U mL^{-1} Pen/Strep. The medium was changed every 3 days, always 1 day before analysis, and the cells were cultured for 7 days maximum.

2.13. Analysis of Cardiomyocyte Hydrogel Cell Culture. The cardiomyocyte cultures were primarily analyzed by phase contrast microscopy using a Nikon Eclipse TS100 (Nikon Corporation, Japan) microscope with a Nikon accessory heating plate, and monochrome 8-bit videos were acquired with an Optika DIGI-12 (Optika Microscopes, Italy) camera. The video recording of beating cardiomyocytes was done with the same setup using 60 frames per second, recording for 30 s. The beating is temperature sensitive, and our measurement setup has been previously verified to be at 37 °C inside the well plate.[42] The videos were analyzed with BeatView software.[11] Figure 1 shows a representative beating pattern of a cardiomyocyte aggregate.

Additionally, the cardiac nature of the differentiated cardiomyocytes was verified using real time polymerase chain reaction (RT-PCR), qPCR, and immunocytochemical staining. For PCR, the total RNA from the cardiomyocyte aggregates in the hydrogel was isolated using the Qiagen RNeasy kit (Qiagen, Germany) after 2 weeks in culture. For the RNA extraction, the culture medium was removed, and the hydrogel was washed in phosphate-buffered saline (PBS) briefly three times. The cardiomyocyte aggregates in the hydrogel were cut with a scalpel under a microscope and collected in a microcentrifuge tube. The hydrogel surrounding the cluster was partially digested by adding 100 μL of pronase solution (stock 10 mg mL^{-1} in water, Sigma-Aldrich, St. Louis, MO, USA) and incubated at 37 °C for 5 min with mild shaking. The digested hydrogel solution was then added directly to the RNeasy lysis buffer and homogenized, and RNA was extracted according to the manufacturer's instructions. DNase I-treated total RNA was reverse-transcribed using a high capacity cDNA reverse transcription kit (Applied Biosystems, Foster City, CA, USA). The cDNA was amplified by the TaqMan Universal Master Mix (Applied Biosystems) using the BioRad CFX384 real-time PCR detection system. Samples were analyzed in triplicates, and glyceraldehyde 3-phosphate dehydrogenase (GAPDH) was used for normalization of expression levels of individual genes, which was calculated by the $\Delta\Delta C_T$ method.[43] TaqMan assays used in the qPCR protocol are presented in Table S1.

Immunocytochemical staining was done with the previously reported, optimized protocol for 3D cell culture.[21] In brief, cultures were fixed with 4% paraformaldehyde for 30 min. After a brief wash in PBS, nonspecific staining was blocked with 10% normal donkey serum (NDS), 0.1% Triton X-100, and 1% bovine serum albumin (BSA) (all from Sigma-Aldrich, St. Louis, MO, USA) in PBS for 1 h in room temperature, followed by another wash in 1% NDS, 0.1% Triton X-100, and 1% BSA in PBS. Then, a combination of primary antibodies, troponin T (1:1750) from goat and α-actinin (1:1250) from mouse, dissolved in 1% NDS, 0.1% Triton X-100, and 1% BSA in PBS, was applied to the cells and incubated at 4 °C for 2 days. The samples were washed three times in 1% PBS (first 5 min, followed by 2 × 1 h) and then incubated for 2 days at 4 °C with Alexa Fluor 488 conjugated to donkey anti-mouse (1:800) and Alexa Fluor 568 conjugated to donkey anti-goat (1:800) in 1% BSA in PBS. The samples were washed three times (first 5 min, followed by 2 × 1 h) in PBS. As the last step, 4′,6-diamidino-2-phenylindole (DAPI) for nuclei staining was applied at 1:2000 concentration in 1% PBS, and the samples were stored light-protected at 4 °C. The cells were imaged with an Olympus IX51 inverted microscope and an Olympus DP30BW digital camera (Olympus, Finland) similar to Live/Dead stained fibroblasts.

3. RESULTS AND DISCUSSION

3.1. Modification of Biopolymers. To form hydrazone cross-links between GG and gelatin, we hypothesized that hydrazide groups could be introduced to the gelatin backbone to form cross-links with the aldehyde groups generated in the GG molecule (Figure 2). Our results show that the carboxylic group present in the gelatin molecule can be modified with ADH or CDH, and the modifications were confirmed by ^{1}H NMR spectroscopy (Figure 2). The spectra of gelatin-ADH

and gelatin-CDH after the derivatization with 4-hydroxybenzaldehyde shows the appearance of protons at δ 6.9 ppm and δ 7.6 ppm, compared with unmodified gelatin, and indicates the presence of hydrazide groups available for the cross-linking process. The integrated intensity of these protons was much higher for gelatin-CDH (0.7) than for gelatin-ADH (0.1). In addition, the peak at δ 7.3 ppm, corresponding to phenylalanine amino acid, increased in gelatin-CDH (1.0) compared with gelatin-ADH (0.6) because of the contribution of the aromatic group in 4-hydroxybenzaldehyde. As a reference, we used the amino acid lysine with a signal at δ 3.0 ppm. The degree of modification of gelatin-CDH was slightly higher than that of gelatin-ADH. This was likely due to the formation of bonds between two molecules of gelatin generating an adduct.[44] On the other hand, GG was modified through periodate oxidation (GG-CHO), and the presence of aldehyde groups was corroborated by FTIR, where a typical aldehyde shoulder was detected at 1733 cm^{-1}, as shown in Figure S1.[22]

3.2. Gelatin-GG Hydrogel Preparation. Hydrazide-modified gelatins and oxidized GG (GG-CHO) form hydrazone bonds that are capable of creating a hydrogel under physiological conditions without any external energy, cross-linkers, or catalysis. To obtain self-standing hydrogels with adequate mechanical properties, several volume ratios and polymer concentrations were tested. The detailed hydrogel formulations obtained and studied in this work are described in Table 1 in the Experimental Section. Briefly, formulations of F1–F3-ADH are composed of gelatin-ADH and GG-CHO, and formulations of F4–F6-CDH are composed of gelatin-CDH and GG-CHO. In general, poor gelation was shown by concentrations below 20 mg mL^{-1} (2%) of gelatin-ADH and 30 mg mL^{-1} (3%) gelatin-CDH. Forming the gels with components of equal concentration, the volume ratio 1:1 yielded the best gelation. When the ratio was changed by increasing the volume of the gelatin component, the gels became very weak. The maximum amount of gelatin required to produce a true hydrogel was 60% w/w in polymer weight, which was achieved with gelatin-CDH because of the higher modification degree compared with gelatin-ADH. The gelatin-ADH or gelatin-CDH with GG-CHO components form a sticky and true gel within seconds. Complete gelation is reached within 5 min for F1–F3-ADH and within 10 min for F4–F6-CDH.

Cross-linking of GG with calcium ions and PBS or DMEM to make covalently cross-linked hydrogels that are mechanically robust has been extensively explored.[27] However, these cross-linking methods lack cytocompatibility. Here, with the inclusion of gelatin, it is expected that the cell interaction with the material will improve significantly because of the natural cell adhesion motifs (e.g., RGD) and the matrix metalloproteinase-mediated degradability present in gelatin.[45] The simplicity of this cross-linking method provides the opportunity to control the mechanical properties, for example, by adjusting the ratio or concentration of the polymers in the system.

Our approach simplifies hydrogel formation relative to other gelatin cross-linking schemes because it does not require high ion concentrations, varying temperature during gelation, or UV light and enables gelation under mild, physiological conditions.[31,46,47] In general, we can state that our hydrogel production method using simple casting is an easier and biologically safer way to produce 3D culture substrates for cardiomyocytes than many of the other published methods.
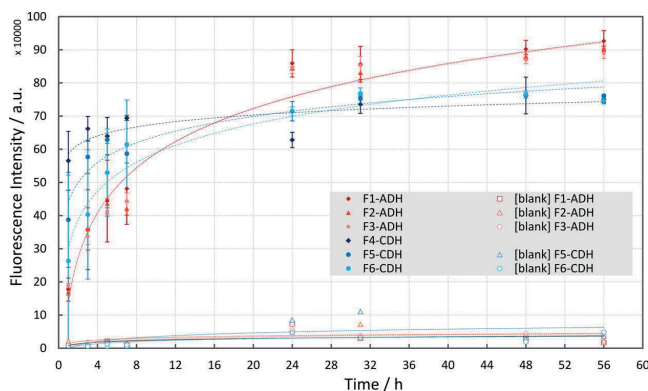
Figure 3. Degradation profiles of the tested hydrogels incubated with collagenase for 56 h. Values represent the mean and standard deviation. Sigmoidal curve fits were applied to the data.

For example, even though the layer-by-layer technique described by Amano et al. 2016 produces well-controlled 3D structures, it requires longer fabrication times per sample.[48] Moreover, the Biowire method by Nunes et al. 2013 requires a special, custom-made mold to retain the weak hydrogel until the cells produce their own ECM, and even more complex molds are required for the microphysiological system reported by Mathur et al. 2015.[16,49] In contrast, our self-supporting hydrogel can be cast, or even injected, in many different shapes for 3D cell encapsulation. Moreover, it could replace the Matrigel or GelMA used in the aforementioned 3D cardiomyocyte culture systems.[16,48,49] For future cardiac drug-screening studies, however, a high throughput study setup suitable for our gelatin-GG hydrogel would be cell-encapsulating droplets that can be studied optically and electrophysiologically, as suggested by Oliveira et al. 2016.[50]

3.3. In Vitro Hydrogel Degradation. To evaluate the degradation profile, the hydrogels were incubated at 37 °C in collagenase (10 U mL^{-1}) solution for 56 h, and sample aliquots were periodically taken. The presence of gelatin was evaluated by fluorescence. Figure 3 shows the degradation profiles of the hydrogels. The concentrations used for the ADH or CDH formulations did not show any significant differences within either chemistry type, but the degradation rate of CDH hydrogels showed a clear difference when compared with ADH hydrogels. As expected, the degradation rate decreased with F4–F6-CDH hydrogels, whereas the different degradation observed between the hydrogels based on CDH or ADH may be attributed to an increased number of cross-links (covalent and ionic) in F4–F6-CDH. Compared with the previously developed gelatin-based hydrogels exposed to similar concentrations of collagenase, our CDH gelatin-based hydrogels showed better resistant to collagenase, albeit they have been shown to be less resistant than GelMA-based hydrogels.[51,52] This lack of resistance is due to the higher cross-linking density of GelMA, which is not always beneficial for nutrient diffusion and cell spreading.

3.4. Mechanical Properties of Hydrogels. Mechanical characterization of these hydrogels was carried out as uniaxial compression testing at a compression rate of 10 mm min^{-1} under ambient conditions. The sticky characteristic of the specimens meant that they had to be cut out from their PDMS

molds, and their difficult handling likely decreased the repeatability of some of the specimens.

As fresh, healthy human heart tissue is not easily available for mechanical testing, many different mammalian tissues have been used in the literature for the determination of the mechanical properties of the tissue, and we chose to use rabbit heart as the reference as it was readily available.[53−55] Figure 4 shows the representative stress−strain curves of the measured gelatin-GG hydrogel compositions and compares them with the fresh rabbit heart muscle.[22] All samples were initially very easily deformed, but the strain-hardening behavior of gelatin-CDH-based hydrogels and rabbit heart is remarkably similar and occurs at the same strain values of over 40%. The gelatin-ADH-based hydrogel's strain hardening effect is smaller and occurs at even higher strains than with gelatin-CDH-based hydrogels. Because the chemical modification does not affect the groups available for ionotropic cross-linking in GG, extra cross-linking was expected to occur in gelatin-CDH-based hydrogels as they were produced in DMEM/F-12.

The gelatin-ADH-based hydrogels had a fracture strength of 23 to 27 kPa, whereas F6-CDH had a fracture strength of 97 kPa and F5-CDH of even over 300 kPa, as can be seen in Figure 4. All tested compositions exhibited fracture between 60 and 75% strains, indicating high elasticity. For both modifications, the highest strength hydrogel was the composition with an uneven amount of gelatin to GG-CHO (F2-ADH and F5-CDH). This indicates that not all cross-linking points are used in compositions with even concentrations of both components; thus additional cross-linking occurs with the increase of hydrazide groups. Meanwhile, the increase in GG-CHO enhances the stability of the hydrogels but also makes the hydrogels slightly more brittle.

In the literature, the mechanical properties of hydrogels are too often intermixed, and the exact same parameters are not compared. For example, in the case of viscoelastic materials, different compression rates affect the material response, and in consequence, elastic regions are being defined differently.[20,56] Thus, we only compared our results with previous results from unconfined compression at 10 mm min^{-1} strain rate. When comparing the current gelatin-GG hydrogels with our previously published bioamine-GG, hyaluronic acid-GG hydrazone, and plain hyaluronic acid hydrazone hydrogels, the gelatin-ADH-based hydrogels more closely resemble the
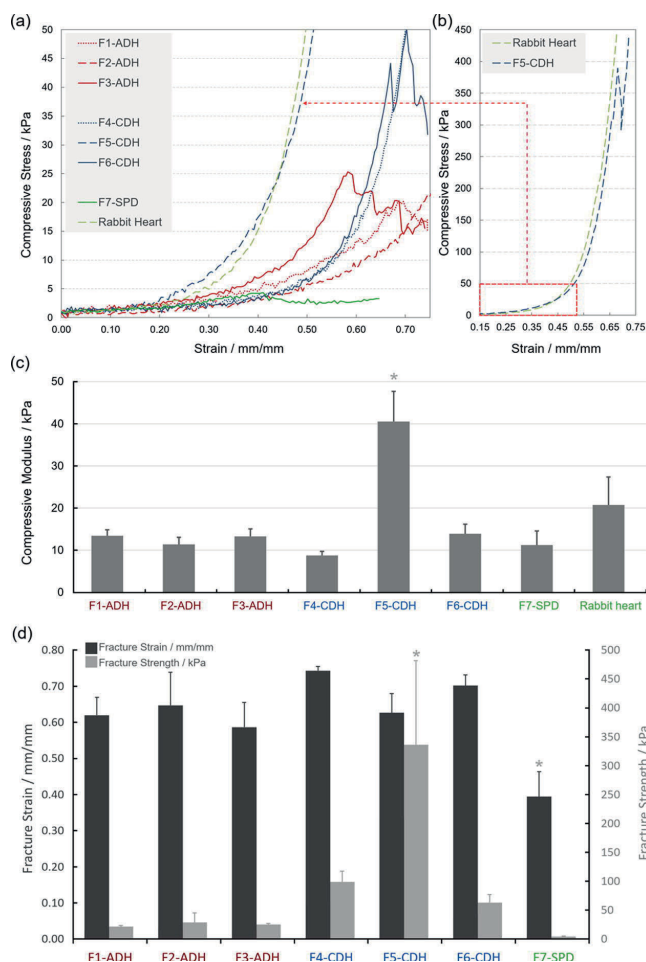
Figure 4. Representative stress−strain curves of the different hydrogel compositions and the rabbit heart tissue. (a) All representative curves with stress range 0 to 40 kPa. (b) Extended graph with the stress scale up to 450 kPa to highlight the similarities between F5-CDH and rabbit heart tissue. (c) Compressive moduli of the hydrogels compared to the rabbit heart. (d) Fracture strain and strength measured by compression testing. The y-axis on the left and the dark gray bars show the fracture strain relative to the original sample height. The y-axis on the right and the light gray bars show the fracture strength. In (c) and (d), $n = 5$; * = significantly different from other formulations at $p < 0.05$.

hyaluronic acid-based hydrogels.[21−23] The bioamine-GG, such as F7-SPD, is rather brittle in comparison to any hydrazone cross-linked hydrogels, with fracture occurring already at 35% strain. The cross-linking chemistry in all of these materials is the same and consistently produces similar mechanical behavior. This shows that the exact biopolymer concentration has only a minor effect on the mechanical behavior, whereas the chemistry used (ADH or CDH) determines the mechanical properties. At the same polymer concentration, F6-CDH is stronger than F3-ADH. However, F5-CDH has more than a 10-fold increase in fracture strength and a 2-fold increase in compressive modulus, compared to other CDH formulations, and thus substantially higher strain-hardening behavior while still being very elastic and compliant until 40% strain.

One clear effect of changing to hydrazone cross-linking from our previous ionotropic bioamine cross-linking of GG was the change in the compression behavior from being rather brittle to highly elastic. This change in compression behavior was accompanied by an increase in the fracture strength.[21] In cardiac TE, the mechanical properties of the growth substrate affect the spontaneous beating of cardiomyocytes.[57,58] In the case of a very rigid polystyrene substrate, the standard 2D well plate, the upper part of the cell is free to move, allowing for the unconstrained beating of the cell.[11] For 3D matrices, however, the cell is in contact with the surrounding scaffold material in all directions. As a result, the constant spontaneous beating of the cell while encapsulated could be prevented, if the hydrogel is not elastic and compliant enough, whereas a biomimicking hydrogel could support cell differentiation and further maturation.[57,58]
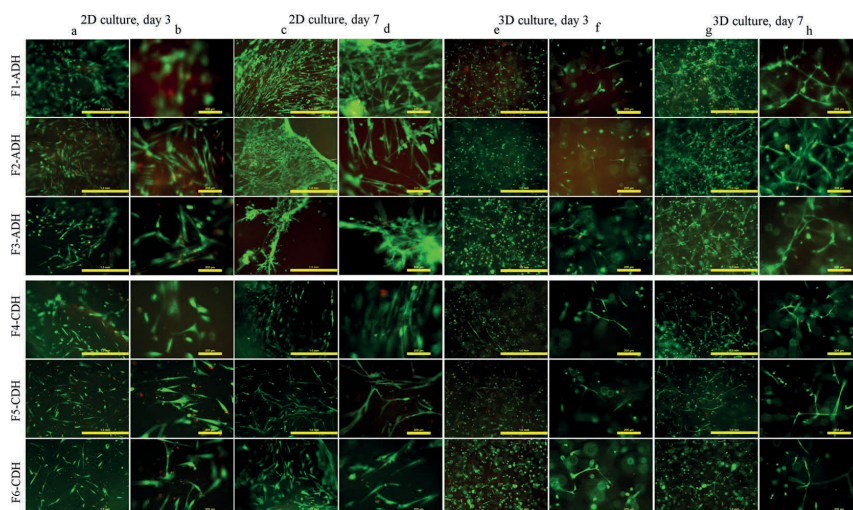
Figure 5. Representative images of Live/Dead stained fibroblast cell cultures in all tested hydrogel formulations and both 2D and 3D culture conditions at the 3-day and 7-day time points. The 3D cultures were imaged in the middle of the hydrogel. Green indicates live cells and red indicates dead cells. Rows (a), (c), (e), and (g) are with lower magnification, and the scale bar length is 1000 μm; rows (b), (d), (f), and (h) are with higher magnification with a scale bar length of 200 μm.
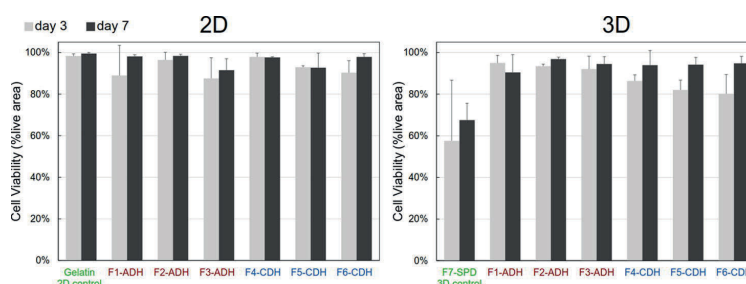
Figure 6. Measured fibroblast viability percentage based on amount of live cells compared to amount of all cells, 4× magnification images. Error bars represent mean values ± standard deviation, $n \geq 3$.

One of the earliest reports about increasing hydrogel strength by blending GG with gelatin is from US patent 4 517 216.[46] However, the patent is aimed at food applications and requires heating the components to 80 °C, which clearly exceeds the range suitable for cell encapsulation applications.[46] More suitable gelatin-GG hydrogels for cell encapsulation have been presented by Shin et al. 2012 and Melchels et al. 2014, both using GelMA that requires UV cross-linking. Both groups show a significant increase in the hydrogel fracture strength by the addition of GG to GelMA.[32,59] Shin et al. also describe a similar elasticity and strain hardening effect as shown for our hydrogels in Figure 4.[32] When compressed alone, GelMA has higher fracture strength and strain than our strongest hydrogels, whereas GGMA alone is clearly more brittle and has lower fracture strength than our hydrogels.[31,32,37,60] By combining GelMA and GGMA into a double-network GelMA-GGMA hydrogel with double the polymer concentration of ours, the fracture strength and strain are increased even further.[32] Wen et al. 2014 present another double-network hydrogel composed of GG and gelatin that utilizes enzymatic cross-linking instead of UV.[61] They report tensile, but not

compressive, mechanical test results, and the measured values of fracture strength and strain are in the same range as ours, if tested without the initiation of a double network by Ca^{2+} addition. With the double network, their highest concentrations produced higher strength and elasticity than ours.[61]

3.5. Cell Culture Studies. *3.5.1. Hydrazide-Modified Gelatin Cytocompatibility.* First, native and modified gelatins (gelatin-ADH and gelatin-CDH) were used as coating at 40 mg mL^{-1} for seeding human lung fibroblast WI-38 cells to test the cytocompatibility. The WI-38 cell line was chosen for this purpose based on ISO 10993-5:2009 standard (Biological Evaluation of Medical Devices. Part 5: Tests for In Vitro Cytotoxicity) as a well-known, general purpose human cell line for initial biomaterial screening.[62] The results showed that the modifications did not alter the gelatin's inherent ability for cell attachment and proliferation. The cells attached and showed an elongated morphology after overnight culture under all gelatin-coating conditions (data not shown). In a prolonged culture, the cells became confluent in a week (Figure S2).

3.5.2. Hydrogel Cell Culture of Fibroblasts. After successful cytocompatibility tests with gelatin modifications, the fibro-
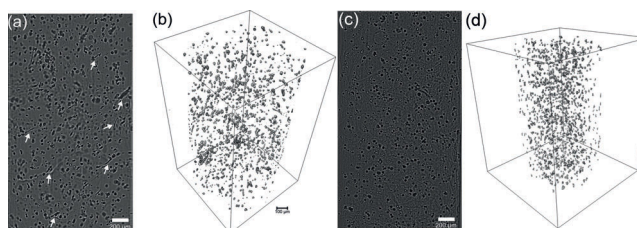
Figure 7. Bright-field OPT visualization of fibroblast cell culture under 3D hydrogel condition. (a) Single projection image of F3-ADH hydrogel, with highly elongated cells highlighted with arrows, (b) 3D reconstruction of the previous giving a view of the whole sample, (c) single projection image of negative control F7-SPD hydrogel, and (d) 3D reconstruction of the previous.

blasts were cultured on top of the hydrazone cross-linked hydrogels listed in Table 1 to study cell attachment and elongation. The fibroblasts were also encapsulated in the same hydrogels to study the cytocompatibility of the cross-linking reaction as well as viability and elongation under 3D conditions. Since gelatin has integrin binding sites and enzymatic cleavage sites, we hypothesized that the cells encapsulated in the hydrogels would be able to elongate in 3D. The initial cell response was examined after 3 days of culture and prolonged culture on day 7. Live/Dead staining was used to visually assess the viability and morphology of the fibroblasts, as shown in Figures 5 and 6. The negative control F7-SPD is shown in Figure S2. On day 3, the cells were already highly elongated and even more so at day 7.

As can be seen in Figure 5, the fibroblast cells are predominantly alive under all tested conditions and at both time points (day 3 and day 7). First, this indicates that the chemical modification is not harmful to the cells and that the cross-linking reaction is efficient and does not leave too many unreacted aldehyde groups to affect cell viability after gelation. A few dead cells were present on day 3, but the number of live cells was much higher, as seen from the viability in Figure 6 being between 80 and 95% for all hydrazone cross-linked hydrogels. Although the initial cell numbers were the same, the cultures seemed more confluent on day 7, indicating cell proliferation. Second, the cells exhibited a high degree of elongation in all directions in 3D under all tested conditions. However, a normal widefield microscope does not convey the status of the cells in a large hydrogel sample but rather gives a snapshot of the culture at a certain position. A holistic view of the sample is critical when evaluating the quality of tissue development.[63] Therefore, we use OPT to visualize several cellular features in a label-free 3D system.[39] Here, we emphasized morphology and elongation as parameters of cytocompatibility (Figure 7 and Videos S1 and S2). Moreover, both the shape and distribution of the cells throughout the hydrogel can be viewed from various angles as shown in Video S1. As can be seen with the F3-ADH hydrogel, a good proportion of the cells are elongated and uniformly distributed in 3D, indicating hydrogel homogeneity in composition and good diffusion of nutrient throughout.

As the cell morphology was well visible in the Live/Dead images, an additional phalloidin or immunocytochemical cytoskeleton staining was deemed unnecessary. The F4-6-CDH hydrogels seemed to have more elongated cells at the earlier time point, and even longer spindlelike cells were seen at the later time point compared with the F1-3-ADH hydrogels. This highly elongated cell morphology is typical for these WI-38 fibroblasts under 2D culture conditions on cell

culture plastic.[64] Under 3D culture conditions and in normal cytocompatibility testing, this high degree of elongation is rarely seen. In fact, none of the gelatin-GG studies discussed in Section 2.4 report similar elongation as observed here.[32,59,61] Elongation has been previously reported with mouse fibroblasts in the click-chemistry cross-linkable gelatin hydrogel,[51] and moderate polarization of human adipose stem cells has been reported in the GG-based hydrogel, if collagen is added.[50] Qualitatively estimating the amount of elongation shown in Figure 5 is magnitudes higher compared with either of those studies.[50,51] The elongation of human fibroblast cells on top of a GG microsphere surface modified with gelatin has been previously reported by Wang et al. 2008.[65] However, they did not encapsulate the cells inside the gel microspheres because of the complexity of the cross-linking process. In summary, we have achieved a higher degree of elongation and viability of human fibroblast cells in the encapsulated condition than has been previously reported. Thus, our GELA-GG hydrogel presents an exciting step toward 3D tissue development.

3.5.3. Hydrogel Cell Culture of Cardiomyocytes. Encouraged by the fibroblast results, we studied hiPSC-derived cardiomyocyte aggregates with the hydrogels. In our group, native gelatin coating is routinely used to culture these cells. Here, we compared the modified gelatin coatings and found that the cardiomyocytes recovered their spontaneously beating phenotype after overnight culture and continued the beating as long as they were cultured. As the beating was observed, there was no need for Live/Dead staining of the cardiomyocytes.

As no difference was observed between the compositions in the fibroblast culture, we chose to use the highest and lowest ADH-formulations and all CDH-formulations, as listed in Table 1. Phase contrast microscopy showed spreading and migration of the cells from the cardiomyocyte aggregates plated on top of the hydrogel, as seen in Figure 8. The cardiac nature of the differentiated cells was verified by qPCR after 2 weeks in culture and by immunocytochemical staining after 1 week in culture, as shown in Figure 9. The expression of TNNT2 and ACTN2 on the protein level and the expression of these same markers plus MYBPC3 on the RNA level confirms the cardiac nature of our hiPSC-derived cells. The qPCR result in Figure 9a especially shows increased expression of TNNT2 in the 3D hydrogel culture compared to the 2D control, indicating positive cell response. Similarly, Figure 9d shows spreading of TNNT2 positive cells from the cell aggregate into the hydrogel.

The cardiomyocytes were also beating spontaneously under all tested conditions both on top of and encapsulated inside the hydrogels, as can be seen in Videos S6–S10. This
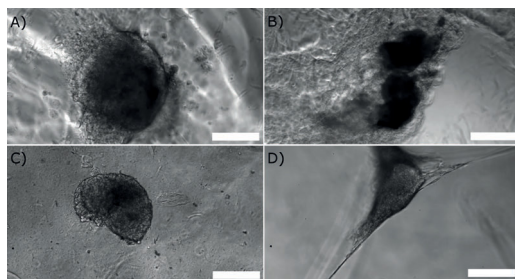
Figure 8. Microscope images of hiPSC-derived cardiomyocyte aggregates cultured under hydrogel conditions: (a) F1-ADH, (b) F3-ADH, (c) F4-CDH, and (d) F5-CDH. The scale bar length is 200 μm.

spontaneous beating is a strong indication of a positive cell response to the culture environment.

The recorded phase contrast videos of cardiomyocyte beating were analyzed with BeatView software that has already been successfully used for hiPSC-derived cardiomyocyte disease modeling in 2D.[11,40] The aggregate beating was not affected by the change of environment from a 2D natural gelatin coated surface to a chemically modified gelatin coating or by being on top of or encapsulated inside the gelatin-GG hydrogel, as shown in Table 2. Cardiomyocytes cultured in the negative control F7-SPD hydrogel did not seem to attach on the hydrogel. They looked worse than in gelatin-GG conditions and did not beat. In the hydrogel culture condition Videos S6−S10, it can be seen how the beating aggregate pulls the hydrogel with it. This observation confirms that suitable elasticity is required of the encapsulating hydrogel, otherwise the cells would be unable to manipulate their surroundings and

would be entrapped inside a too rigid hydrogel network; see Videos S6−S11. In the case of two individually beating aggregates in close proximity, this transfer of movement via the hydrogel can be detrimental for the analyzability of the beating. The main beating parameters are shown in Table 2. The beating rate shows how many beats per minute (BPM) are recorded, and the contraction-relaxation duration is the length of a single beat (milliseconds). Between the contractions, the cell is at rest.

The beating behavior observed here is typical for hiPSC-derived cardiomyocytes produced with this differentiation method.[66] The beating frequency remained at ∼30 to 70 BPM, regardless of whether the aggregate was cultured on the standard unmodified gelatin coating, on the modified gelatin coating, on top of the hydrogels, or encapsulated inside the hydrogels. Culturing cardiomyocytes in the 3D-engineered heart tissue has been shown to cause their electrophysiology to have a higher resemblance to the real situation in the body.[15] However, the method uses a very weak hydrogel substrate based on Matrigel and relies on the cell's ECM production during the differentiation.[15] Our hydrogel, on the other hand, is strong enough to be handled with tweezers. Subsequently, we can use cells differentiated with any method and move them to hydrogel culture once they start beating, and they recover the beating already after 24 h. The previously discussed Biowire method is a relevant option for cardiomyocyte 3D culture. The method is, however, impeded by the mechanical weakness of Matrigel and greatly constrained by the mold shape.[16] Both of these methods would benefit from replacing the Matrigel-based substrate with our cardiomimetic gelatin-GG hydrogel.

One hurdle to overcome when developing 3D disease modeling is the maturation of hiPSC-derived cardiomyocytes.[67] It has been demonstrated that current differentiation
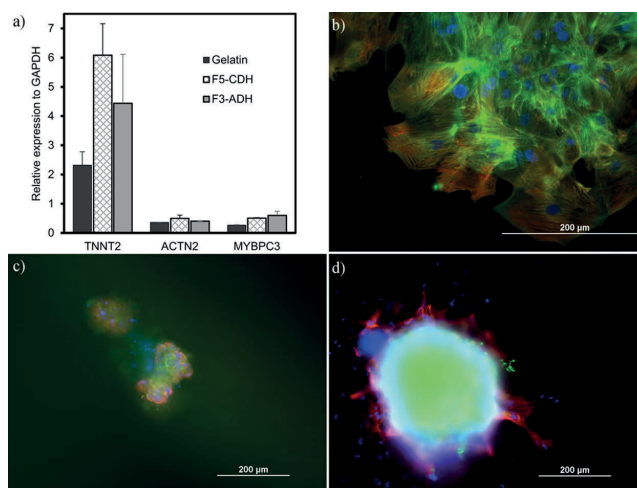
Figure 9. (a) Quantitative RT-PCR validation of cardiac specific genes expressed in hiPSC-derived cardiomyocytes cultured in the gelatin coating control, F5-CDH and F3-ADH. Shown are the expression levels of cardiac type troponin T2 (TNNT2), α-actinin 2 (ACTN2), and Myosin binding protein C (MYBPC3), relative to the housekeeping gene GAPDH. Standard deviations are from three biological replicates, each done in technical triplicate in qPCR. (b−d) Immunocytochemical staining of hiPSC-derived cardiomyocytes using red for TNNT2, green for ACTN2, and blue for DAPI. (b) 2D control on gelatin coating. (c) Aggregate 3D culture in F3-ADH. (d) Aggregate 3D culture in F5-CDH. The density of cell aggregate in F5-CDH slightly prevents antibody and fluorescent light penetration, causing blurriness in the image.

Table 2. Contraction-Relaxation Durations and Beating Frequencies of the hiPSC-Derived Cardiomyocyte Aggregates Under All Tested Conditions, Analyzed with BeatView Software; $n = 4$

material	2D/3D	ratio[c] [mg mL^{-1}]	beating rate [BPM]	standard deviation	contraction−relaxation duration [ms]	standard deviation
gelatin coating control	2D	100:0	35.78	±20.41	568.60	±127.10[a]
GELA-ADH coating		100:0	42.35	±6.69	435.50	±154.02
GELA-CDH coating		100:0	35.60	±20.18	662.44	±268.50[a]
F7-SPD	3D	0:100	0		0	
F1−3-ADH	2D	40:40	36.71	±17.74	435.25	±113.70
		40:20	68.04	±17.01	305.21	±65.13
	3D	40:40	72.10	±15.14	264.14	±41.97
		40:20	52.70	±47.60	474.59	±303.62[a]
F4−6-CDH	2D	60:60	38.63	[b]	423.74	[b]
		60:40	37.73	±2.78[b]	434.34	±38.96[b]
		40:40	41.56	±5.33	393.14	±63.67
	3D	60:60	35.77	±7.00	403.68	±44.01
		60:40	37.99	±6.50	452.44	±32.85
		40:40	33.82	±3.02	491.88	±15.65

[a]Major prolongation in contraction−relaxation interval detected in one sample. [b]Elasticity of hydrogel transferring movement over a long distance interferes with the beating analysis; so only one or two aggregates were analyzed successfully. [c]Ratio of gelatin to GG.

protocols produce cardiomyocytes that resemble the fetal human heart in gene expression as well as on the structural and functional level.[67,68] There is a multitude of strategies that are aimed at maturing cardiomyocytes. These range from mechanical and electrical stimulations to simply longer culture times.[67] However, the physical cues from the ECM are one potential strategy that we would like to further explore in future. The correct stiffness of the culture substrate as well as its topography can provide cues that can aid the maturation process.[48,67−69] As proven by compression testing (Figure 4), our hydrogels have a biomimicking elasticity that is comparable with the heart tissue. These hydrogels are a promising tool for testing cardiomyocyte maturation. Even though gelatin-ADH-GG hydrogels had a significantly lower strain-hardening effect than gelatin-CDH-GG hydrogels, the beating and mechanotransduction of the cells occur at lower strains and thus make all hydrogel compositions equally promising in this regard.

4. CONCLUSIONS

The current trend in the development of disease models is toward transitioning from 2D cultures to the more biomimicking 3D cultures. This opens up possibilities for studying more tissuelike cellular interactions instead of only studying individual cells. We conclude that the hydrogels based on gelatin-ADH-GG and gelatin-CDH-GG presented in this study are suitable candidates for cardiac TE and 3D cardiac disease modeling. Hydrazide modification of gelatin and oxidation of GG facilitate spontaneous covalent bonding between the polymers. This aids the rapid gelation with homogeneous cross-link distribution under mild conditions suitable for the 3D encapsulation of cells. The stress−strain behavior of hydrogels based on gelatin-CDH very closely resembles the ex vivo heart tissue. The hydrogels enable cell attachment, spreading, and elongation in the encapsulated 3D culture, demonstrated first with human fibroblasts. The hiPSC-derived cardiomyocyte aggregates exhibit normal phenotypical beating behavior when plated on top of or encapsulated inside the hydrogel. On top of the hydrogel, the cardiomyocyte aggregates attached, and cell spreading and migration out of the aggregate were observed. The beating can then be quantitatively analyzed from simple phase contrast microscopy

videos with BeatView software, as shown here. The beating analysis shows that cells retain their normal beating characteristics when moved from differentiation in 2D culture to 3D hydrogel culture. No significant biological difference was noticed between the formulations based on gelatin-ADH and gelatin-CDH. Overall, the results suggest the suitability of these gelatin-GG hydrogels with tunable properties for 3D soft tissue modeling and specifically to develop cardiac disease models.

■ ASSOCIATED CONTENT

⑤ Supporting Information

The Supporting Information is available free of charge on the ACS Publications website at DOI: 10.1021/acsami.8b22343.

> FTIR spectra of GG-CHO compared to unmodified GG; Live/Dead micrographs of fibroblast grown on gelatin-ADH, gelatin-CDH, and unmodified gelatin coatings as well as negative control 3D fibroblast cell culture in F7-SPD composition; and table of the used TaqMan assays for qRT-PCR (PDF)
>
> Reconstruction of bright-field OPT imaging of cultured fibroblasts encapsulated in GELA-ADH-GG 40:20 hydrogel (MPG)
>
> Reconstruction of bright-field OPT imaging of cultured fibroblasts encapsulated in the negative control SPD cross-linked GG hydrogel (MPG)
>
> Beating hiPSC-derived cardiomyocytes on control gelatin coating (AVI)
>
> Beating hiPSC-derived cardiomyocytes on gelatin-ADH coating (AVI)
>
> Beating hiPSC-derived cardiomyocytes on gelatin-CDH coating (AVI)
>
> Beating hiPSC-derived cardiomyocytes in F1-ADH hydrogel culture conditions (AVI)
>
> Beating hiPSC-derived cardiomyocytes in F3-ADH hydrogel culture conditions (AVI)
>
> Beating hiPSC-derived cardiomyocytes in F4-CDH hydrogel culture conditions (AVI)
>
> Beating hiPSC-derived cardiomyocytes in F5-CDH hydrogel culture conditions (AVI)
>
> Beating hiPSC-derived cardiomyocytes in F6-CDH hydrogel culture conditions (AVI)

Nonbeating hiPSC-derived cardiomyocytes in negative control F7-SPD hydrogel culture conditions (AVI)

AUTHOR INFORMATION

Corresponding Authors

*E-mail: janne.t.koivisto@tuni.fi (J.T.K.).

*E-mail: jenny.parraga@tuni.fi (J.P.).

ORCID

Janne T. Koivisto: 0000-0002-7904-4780

Jari Hyttinen: 0000-0003-1850-3055

Notes

The authors declare no competing financial interest.

REFERENCES

(1) Langer, R.; Vacanti, J. Tissue Engineering. *Science* 1993, *260*, 920−926.

(2) Asthana, A.; Kisaalita, W. S. Biophysical Microenvironment and 3D Culture Physiological Relevance. *Drug Discovery Today* 2013, *18*, 533−540.

(3) Langley, G. R.; Adcock, I. M.; Busquet, F.; Crofton, K. M.; Csernok, E.; Giese, C.; Heinonen, T.; Herrmann, K.; Hofmann-Apitius, M.; Landesmann, B.; Marshall, L. J.; McIvor, E.; Muotri, A. R.; Noor, F.; Schutte, K.; Seidle, T.; van de Stolpe, A.; Van Esch, H.; Willett, C.; Woszczek, G. Towards a 21st-century roadmap for biomedical research and drug discovery: consensus report and recommendations. *Drug Discov. Today* 2017, *22*, 327−339.

(4) Akopian, V.; Andrews, P. W.; Beil, S.; Benvenisty, N.; Brehm, J.; Christie, M.; Ford, A.; Fox, V.; Gokhale, P. J.; Healy, L.; Holm, F.; Hovatta, O.; Knowles, B. B.; Ludwig, T. E.; McKay, R. D. G.; Miyazaki, T.; Nakatsuji, N.; Oh, S. K. W.; Pera, M. F.; Rossant, J.; Stacey, G. N.; Suemori, H. Comparison of defined culture systems for feeder cell free propagation of human embryonic stem cells. *In Vitro Cell. Dev. Biol.: Anim.* 2010, *46*, 247−258.

(5) Lu, H. R.; Whittaker, R.; Price, J. H.; Vega, R.; Pfeiffer, E. R.; Cerignoli, F.; Towart, R.; Gallacher, D. J. High Throughput Measurement of Ca++Dynamics in Human Stem Cell-Derived Cardiomyocytes by Kinetic Image Cytometry: A Cardiac Risk Assessment Characterization Using a Large Panel of Cardioactive and Inactive Compounds. *Toxicol. Sci.* 2015, *148*, 503−516.

(6) Robertson, C.; Tran, D. D.; George, S. C. Concise Review: Maturation Phases of Human Pluripotent Stem Cell-Derived Cardiomyocytes. *Stem Cells* 2013, *31*, 829−837.

(7) Ojala, M.; Aalto-Setälä, K. Modeling Hypertrophic Cardiomyopathy with Human Induced Pluripotent Stem Cells. In *Pluripotent Stem Cells—from the Bench to the Clinic*; Tomizawa, M., Ed.; InTech: London, U.K., 2016; pp 227−256.

(8) Liang, P.; Lan, F.; Lee, A. S.; Gong, T.; Sanchez-Freire, V.; Wang, Y.; Diecke, S.; Sallam, K.; Knowles, J. W.; Wang, P. J.; Nguyen, P. K.; Bers, D. M.; Robbins, R. C.; Wu, J. C. Drug Screening Using a Library of Human Induced Pluripotent Stem Cell-Derived Cardiomyocytes Reveals Disease-Specific Patterns of Cardiotoxicity. *Circulation* 2013, *127*, 1677−1691.

(9) Penttinen, K.; Swan, H.; Vanninen, S.; Paavola, J.; Lahtinen, A. M.; Kontula, K.; Aalto-Setälä, K. Correction: Antiarrhythmic Effects of Dantrolene in Patients with Catecholaminergic Polymorphic Ventricular Tachycardia and Replication of the Responses Using iPSC Models. *PLoS One* 2015, *10*, No. e0134746.

(10) Roden, D. M. Drug-Induced Prolongation of the QT Interval. *N. Engl. J. Med.* 2004, *350*, 1013−1022.

(11) Ahola, A.; Kiviaho, A. L.; Larsson, K.; Honkanen, M.; Aalto-Setälä, K.; Hyttinen, J. Video Image-Based Analysis of Single Human Induced Pluripotent Stem Cell Derived Cardiomyocyte Beating Dynamics using Digital Image Correlation. *Biomed. Eng. Online* 2014, *13*, 39−57.

(12) Kuusela, J.; Kujala, V. J.; Kiviaho, A.; Ojala, M.; Swan, H.; Kontula, K.; Aalto-Setälä, K. Effects of Cardioactive Drugs on Human Induced Pluripotent Stem Cell Derived Long QT Syndrome Cardiomyocytes. *Springerplus* 2016, *5*, 234.

(13) Ribas, J.; Sadeghi, H.; Manbachi, A.; Leijten, J.; Brinegar, K.; Zhang, Y. S.; Ferreira, L.; Khademhosseini, A. Cardiovascular Organ-on-a-Chip Platforms for Drug Discovery and Development. *Appl. In Vitro Toxicol.* 2016, *2*, 82−96.

(14) Gomes, M. E.; Rodrigues, M. T.; Domingues, R. M. A.; Reis, R. L. Tissue Engineering and Regenerative Medicine: New Trends and Directions-A Year in Review. *Tissue Eng., Part B* 2017, *23*, 211−224.

(15) Eder, A.; Vollert, I.; Hansen, A.; Eschenhagen, T. Human Engineered Heart Tissue as a Model System for Drug Testing. *Adv. Drug Delivery Rev.* 2016, *96*, 214−224.

(16) Nunes, S. S.; Miklas, J. W.; Liu, J.; Aschar-Sobbi, R.; Xiao, Y.; Zhang, B.; Jiang, J.; Massé, S.; Gagliardi, M.; Hsieh, A.; Thavandiran, N.; Laflamme, M. A.; Nanthakumar, K.; Gross, G. J.; Backx, P. H.; Keller, G.; Radisic, M. Biowire: a platform for maturation of human pluripotent stem cell-derived cardiomyocytes. *Nat. Methods* 2013, *10*, 781−787.

(17) Zhu, K.; Shin, S. R.; van Kempen, T.; Li, Y.-C.; Ponraj, V.; Nasajpour, A.; Mandla, S.; Hu, N.; Liu, X.; Leijten, J.; Lin, Y.-D.; Hussain, M. A.; Zhang, Y. S.; Tamayol, A.; Khademhosseini, A. Gold Nanocomposite Bioink for Printing 3D Cardiac Constructs. *Adv. Funct. Mater.* 2017, *27*, 1605352.

(18) Zhang, Y. S.; Arneri, A.; Bersini, S.; Shin, S.-R.; Zhu, K.; Goli-Malekabadi, Z.; Aleman, J.; Colosi, C.; Busignani, F.; Dell'Erba, V.; Bishop, C.; Shupe, T.; Demarchi, D.; Moretti, M.; Rasponi, M.; Dokmeci, M. R.; Atala, A.; Khademhosseini, A. Bioprinting 3D Microfibrous Scaffolds for Engineering Endothelialized Myocardium and Heart-on-a-Chip. *Biomaterials* 2016, *110*, 45−59.

(19) Walters, N. J.; Gentleman, E. Evolving insights in cell-matrix interactions: Elucidating how non-soluble properties of the extracellular niche direct stem cell fate. *Acta Biomater.* 2015, *11*, 3−16.

(20) Nakamura, K.; Shinoda, E.; Tokita, M. The Influence of Compression Velocity on Strength and Structure for Gellan Gels. *Food Hydrocoll.* 2001, *15*, 247−252.

(21) Koivisto, J. T.; Joki, T.; Parraga, J. E.; Pääkkönen, R.; Ylä-Outinen, L.; Salonen, L.; Jönkkäri, I.; Peltola, M.; Ihalainen, T. O.; Narkilahti, S.; Kellomäki, M. Bioamine-Crosslinked Gellan Gum Hydrogel for Neural Tissue Engineering. *Biomed. Mater.* 2017, *12*, 025014.

(22) Karvinen, J.; Koivisto, J. T.; Jönkkäri, I.; Kellomäki, M. The Production of Injectable Hydrazone Crosslinked Gellan Gum-Hyaluronan-Hydrogels with Tunable Mechanical and Physical Properties. *J. Mech. Behav. Biomed. Mater.* **2017**, *71*, 383−391.

(23) Koivusalo, L.; Karvinen, J.; Sorsa, E.; Jönkkäri, I.; Väliaho, J.; Kallio, P.; Ilmarinen, T.; Miettinen, S.; Skottman, H.; Kellomäki, M. Hydrazone Crosslinked Hyaluronan-Based Hydrogels for Therapeutic Delivery of Adipose Stem Cells to Treat Corneal Defects. *Mater. Sci. Eng., C* **2018**, *85*, 68−78.

(24) Karvinen, J.; Joki, T.; Ylä-Outinen, L.; Koivisto, J. T.; Narkilahti, S.; Kellomäki, M. Soft Hydrazone Crosslinked Hyaluronan- and Alginate-Based Hydrogels as 3D Supportive Matrices for Human Pluripotent Stem Cell-Derived Neuronal Cells. *React. Funct. Polym.* **2018**, *124*, 29−39.

(25) Dubruel, P.; Unger, R.; Van Vlierberghe, S.; Cnudde, V.; Jacobs, P. J. S.; Schacht, E.; Kirkpatrick, C. J. Porous Gelatin Hydrogels: 2. In Vitro Cell Interaction Study. *Biomacromolecules* **2007**, *8*, 338−344.

(26) Van Den Bulcke, A. I.; Bogdanov, B.; De Rooze, N.; Schacht, E. H.; Cornelissen, M.; Berghmans, H. Structural and Rheological Properties of Methacrylamide Modified Gelatin Hydrogels. *Biomacromolecules* **2000**, *1*, 31−38.

(27) Bacelar, A. H.; Silva-Correia, J.; Oliveira, J. M.; Reis, R. L. Recent progress in gellan gum hydrogels provided by functionalization strategies. *J. Mater. Chem. B* **2016**, *4*, 6164−6174.

(28) Ferris, C. J.; Stevens, L. R.; Gilmore, K. J.; Mume, E.; Greguric, I.; Kirchmajer, D. M.; Wallace, G. G.; in het Panhuis, M. Peptide Modification of Purified Gellan Gum. *J. Mater. Chem. B* **2015**, *3*, 1106−1115.

(29) da Silva, L. P.; Jha, A. K.; Correlo, V. M.; Marques, A. P.; Reis, R. L.; Healy, K. E. Gellan Gum Hydrogels with Enzyme-Sensitive Biodegradation and Endothelial Cell Biorecognition Sites. *Adv. Healthcare Mater.* **2018**, *7*, 1700686.

(30) Silva-Correia, J.; Gloria, A.; Oliveira, M. B.; Mano, J. F.; Oliveira, J. M.; Ambrosio, L.; Reis, R. L. Rheological and Mechanical Properties of Acellular and Cell-Laden Methacrylated Gellan Gum Hydrogels. *J. Biomed. Mater. Res., Part A* **2013**, *101*, 3438−3446.

(31) Yue, K.; Trujillo-de Santiago, G.; Alvarez, M. M.; Tamayol, A.; Annabi, N.; Khademhosseini, A. Synthesis, Properties, and Biomedical Applications of Gelatin Methacryloyl (GelMA) Hydrogels. *Biomaterials* **2015**, *73*, 254−271.

(32) Shin, H.; Olsen, B. D.; Khademhosseini, A. The Mechanical Properties and Cytotoxicity of Cell-Laden Double-Network Hydrogels Based on Photocrosslinkable Gelatin and Gellan Gum Biomacromolecules. *Biomaterials* **2012**, *33*, 3143−3152.

(33) Fedorovich, N. E.; Oudshoorn, M. H.; van Geemen, D.; Hennink, W. E.; Alblas, J.; Dhert, W. J. A. The Effect of Photopolymerization on Stem Cells Embedded in Hydrogels. *Biomaterials* **2009**, *30*, 344−353.

(34) Williams, C. G.; Malik, A. N.; Kim, T. K.; Manson, P. N.; Elisseeff, J. H. Variable Cytocompatibility of Six Cell Lines with Photoinitiators used for Polymerizing Hydrogels and Cell Encapsulation. *Biomaterials* **2005**, *26*, 1211−1218.

(35) Mironi-Harpaz, I.; Wang, D. Y.; Venkatraman, S.; Seliktar, D. Photopolymerization of Cell-Encapsulating Hydrogels: Crosslinking Efficiency Versus Cytotoxicity. *Acta Biomater.* **2012**, *8*, 1838−1848.

(36) Figueiras, E.; Soto, A. M.; Jesus, D.; Lehti, M.; Koivisto, J.; Parraga, J. E.; Silva-Correia, J.; Oliveira, J. M.; Reis, R. L.; Kellomäki, M.; Hyttinen, J. Optical Projection Tomography as a Tool for 3D Imaging of Hydrogels. *Biomed. Opt. Express* **2014**, *5*, 3443−3449.

(37) Coutinho, D. F.; Sant, S. V.; Shin, H.; Oliveira, J. T.; Gomes, M. E.; Neves, N. M.; Khademhosseini, A.; Reis, R. L. Modified Gellan Gum Hydrogels with Tunable Physical and Mechanical Properties. *Biomaterials* **2010**, *31*, 7494−7502.

(38) Schneider, C. A.; Rasband, W. S.; Eliceiri, K. W. NIH Image to ImageJ: 25 Years of Image Analysis. *Nat. Methods* **2012**, *9*, 671−675.

(39) Belay, B.; Koivisto, J. T.; Vuornos, K.; Montonen, T.; Koskela, O.; Lehti-Polojärvi, M.; Miettinen, S.; Kellomäki, M.; Figueiras, E.; Hyttinen, J. Optical Projection Tomography Imaging of Single Cells

in 3D Gellan Gum Hydrogel. In *EMBEC & NBC 2017: Joint Conference of the European Medical and Biological Engineering Conference (EMBEC) and the Nordic-Baltic Conference on Biomedical Engineering and Medical Physics (NBC), Tampere, Finland, June 2017*; Eskola, H., Väisänen, O., Viik, J., Hyttinen, J., Eds.; Springer Singapore: Singapore, 2018; pp 996−999.

(40) Kiviaho, A. L.; Ahola, A.; Larsson, K.; Penttinen, K.; Swan, H.; Pekkanen-Mattila, M.; Venäläinen, H.; Paavola, K.; Hyttinen, J.; Aalto-Setälä, K. Distinct Electrophysiological and Mechanical Beating Phenotypes of Long QT Syndrome Type 1-Specific Cardiomyocytes Carrying Different Mutations. *Int. J. Cardiol. Heart Vasc.* **2015**, *8*, 19−31.

(41) Lian, X.; Zhang, J.; Azarin, S. M.; Zhu, K.; Hazeltine, L. B.; Bao, X.; Hsiao, C.; Kamp, T. J.; Palecek, S. P. Directed cardiomyocyte differentiation from human pluripotent stem cells by modulating Wnt/β-catenin signaling under fully defined conditions. *Nat. Protoc.* **2012**, *8*, 162−175.

(42) Laurila, E.; Ahola, A.; Hyttinen, J.; Aalto-Setälä, K. Methods for in vitro functional analysis of iPSC derived cardiomyocytes - Special focus on analyzing the mechanical beating behavior. *Biochim. Biophys. Acta, Mol. Cell Res.* **2016**, *1863*, 1864−1872.

(43) Livak, K. J.; Schmittgen, T. D. Analysis of Relative Gene Expression Data Using Real-Time Quantitative PCR and the 2−$\Delta\Delta$CT Method. *Methods* **2001**, *25*, 402−408.

(44) Prestwich, G. D.; Marecak, D. M.; Marecek, J. F.; Vercruysse, K. P.; Ziebell, M. R. Controlled Chemical Modification of Hyaluronic Acid: Synthesis, Applications, and Biodegradation of Hydrazide Derivatives. *J. Controlled Release* **1998**, *53*, 93−103.

(45) Vandooren, J.; Van den Steen, P. E.; Opdenakker, G. Biochemistry and Molecular Biology of Gelatinase B Or Matrix Metalloproteinase-9 (MMP-9): The Next Decade. *Crit. Rev. Biochem. Mol. Biol.* **2013**, *48*, 222−272.

(46) Shim, J. L. N. J.. U.S. Patent 4,517,216. Gellan gum/gelatin blends, 1985.

(47) Kozlov, P. V.; Burdygina, G. I. The Structure and Properties of Solid Gelatin and the Principles of their Modification. *Polymer* **1983**, *24*, 651−666.

(48) Amano, Y.; Nishiguchi, A.; Matsusaki, M.; Iseoka, H.; Miyagawa, S.; Sawa, Y.; Seo, M.; Yamaguchi, T.; Akashi, M. Development of Vascularized iPSC Derived 3D-Cardiomyocyte Tissues by Filtration Layer-by-Layer Technique and their Application for Pharmaceutical Assays. *Acta Biomater.* **2016**, *33*, 110−121.

(49) Mathur, A.; Loskill, P.; Shao, K.; Huebsch, N.; Hong, S.; Marcus, S. G.; Marks, N.; Mandegar, M.; Conklin, B. R.; Lee, L. P.; Healy, K. E. Human iPSC-Based Cardiac Microphysiological System for Drug Screening Applications. *Sci. Rep.* **2015**, *5*, 8883.

(50) Oliveira, M. B.; Custódio, C. A.; Gasperini, L.; Reis, R. L.; Mano, J. F. Autonomous Osteogenic Differentiation of hASCs Encapsulated in Methacrylated Gellan-Gum Hydrogels. *Acta Biomater.* **2016**, *41*, 119−132.

(51) Koshy, S. T.; Desai, R. M.; Joly, P.; Li, J.; Bagrodia, R. K.; Lewin, S. A.; Joshi, N. S.; Mooney, D. J. Click-Crosslinked Injectable Gelatin Hydrogels. *Adv. Healthcare Mater.* **2016**, *5*, 541−547.

(52) Zhao, X.; Lang, Q.; Yildirimer, L.; Lin, Z. Y.; Cui, W.; Annabi, N.; Ng, K. W.; Dokmeci, M. R.; Ghaemmaghami, A. M.; Khademhosseini, A. Photocrosslinkable Gelatin Hydrogel for Epidermal Tissue Engineering. *Adv. Healthcare Mater.* **2016**, *5*, 108−118.

(53) Mirsky, I.; Parmley, W. W. Assessment of Passive Elastic Stiffness for Isolated Heart Muscle and the Intact Heart. *Circ. Res.* **1973**, *33*, 233−243.

(54) Levental, I.; Georges, P. C.; Janmey, P. A. Soft Biological Materials and their Impact on Cell Function. *Soft Matter* **2007**, *3*, 299−306.

(55) Neal, R. A.; Jean, A.; Park, H.; Wu, P. B.; Hsiao, J.; Engelmayr, G. C., Jr.; Langer, R.; Freed, L. E. Three-Dimensional Elastomeric Scaffolds Designed with Cardiac-Mimetic Structural and Mechanical Features. *Tissue Eng., Part A* **2013**, *19*, 793−807.

　　　　　　　　　　　　　　　　　　　　　　　　Research Article

(56) Oyen, M. L. Mechanical Characterisation of Hydrogel Materials. *Int. Mater. Rev.* **2014**, *59*, 44−59.

(57) Bashir, B.; Iyer, R. K.; Chen Wen, L. K.; Ruogang, Z.; Sider, K. L.; Morakot, L.; Simmons, C. A.; Milica, R. Influence of Substrate Stiffness on the Phenotype of Heart Cells. *Biotechnol. Bioeng.* **2010**, *105*, 1148−1160.

(58) Engler, A. J.; Carag-Krieger, C.; Johnson, C. P.; Raab, M.; Tang, H.-Y.; Speicher, D. W.; Sanger, J. W.; Sanger, J. M.; Discher, D. E. Embryonic Cardiomyocytes Beat Best on a Matrix with Heart-Like Elasticity: Scar-Like Rigidity Inhibits Beating. *J. Cell Sci.* **2008**, *121*, 3794−3802.

(59) Melchels, F. P. W.; Dhert, W. J. A.; Hutmacher, D. W.; Malda, J. Development and Characterisation of a New Bioink for Additive Tissue Manufacturing. *J. Mater. Chem. B* **2014**, *2*, 2282−2289.

(60) Nichol, J. W.; Koshy, S. T.; Bae, H.; Hwang, C. M.; Yamanlar, S.; Khademhosseini, A. Cell-Laden Microengineered Gelatin Methacrylate Hydrogels. *Biomaterials* **2010**, *31*, 5536−5544.

(61) Wen, C.; Lu, L.; Li, X. An Interpenetrating Network Biohydrogel of Gelatin and Gellan Gum by using a Combination of Enzymatic and Ionic Crosslinking Approaches. *Polym. Int.* **2014**, *63*, 1643−1649.

(62) *SFS-EN ISO 10993-5 Biological Evaluation of Medical Devices. Part 5: Tests for in Vitro Cytotoxicity*; Finnish Standards Association: Helsinki, Finland, 2009.

(63) Appel, A. A.; Anastasio, M. A.; Larson, J. C.; Brey, E. M. Imaging Challenges in Biomaterials and Tissue Engineering. *Biomaterials* **2013**, *34*, 6615−6630.

(64) Hayflick, L.; Moorhead, P. S. The Serial Cultivation of Human Diploid Cell Strains. *Exp. Cell Res.* **1961**, *25*, 585−621.

(65) Wang, C.; Gong, Y.; Lin, Y.; Shen, J.; Wang, D.-A. A Novel Gellan Gel-Based Microcarrier for Anchorage-Dependent Cell Delivery. *Acta Biomater.* **2008**, *4*, 1226−1234.

(66) Vuorenpää, H.; Penttinen, K.; Heinonen, T.; Pekkanen-Mattila, M.; Sarkanen, J.-R.; Ylikomi, T.; Aalto-Setälä, K. Maturation of Human Pluripotent Stem Cell Derived Cardiomyocytes is Improved in Cardiovascular Construct. *Cytotechnology* **2017**, *69*, 785−800.

(67) Tan, S. H.; Ye, L. Maturation of Pluripotent Stem Cell-Derived Cardiomyocytes: a Critical Step for Drug Development and Cell Therapy. *J Cardiovasc Transl Res* **2018**, *11*, 375−392.

(68) Tzatzalos, E.; Abilez, O. J.; Shukla, P.; Wu, J. C. Engineered Heart Tissues and Induced Pluripotent Stem Cells: Macro- and Microstructures for Disease Modeling, Drug Screening, and Translational Studies. *Adv. Drug Delivery Rev.* **2016**, *96*, 234−244.

(69) Besser, R. R.; Ishahak, M.; Mayo, V.; Carbonero, D.; Claure, I.; Agarwal, A. Engineered Microenvironments for Maturation of Stem Cell Derived Cardiac Myocytes. *Theranostics* **2018**, *8*, 124−140.

Supporting Information

Mechanically Biomimetic Gelatin-Gellan Gum Hydrogels for 3D Culture of Beating Human Cardiomyocytes

Janne T. Koivisto[1, 2]*, Christine Gering[1], Jennika Karvinen[1], Reeja Maria Cherian[2], Birhanu Belay[3], Jari Hyttinen[3], Katriina Aalto-Setälä[2,4], Minna Kellomäki[1], Jenny Parraga[1]*

[1] Biomaterials and Tissue Engineering Group, Faculty of Medicine and Health Technology, Tampere University, 33720 Tampere, Finland.

[2] Heart Group, Faculty of Medicine and Health Technology, Tampere University, 33520 Tampere, Finland

[3] Computational Biophysics and Imaging Group, Faculty of Medicine and Health Technology, Tampere University, 33520 Tampere, Finland

[4] Heart Hospital, Tampere University Hospital, 33520 Tampere, Finland

*Corresponding authors: janne.t.koivisto@tuni.fi, jenny.parraga@tuni.fi

Supporting Information

Supporting Information is available from the journal website or from the author.
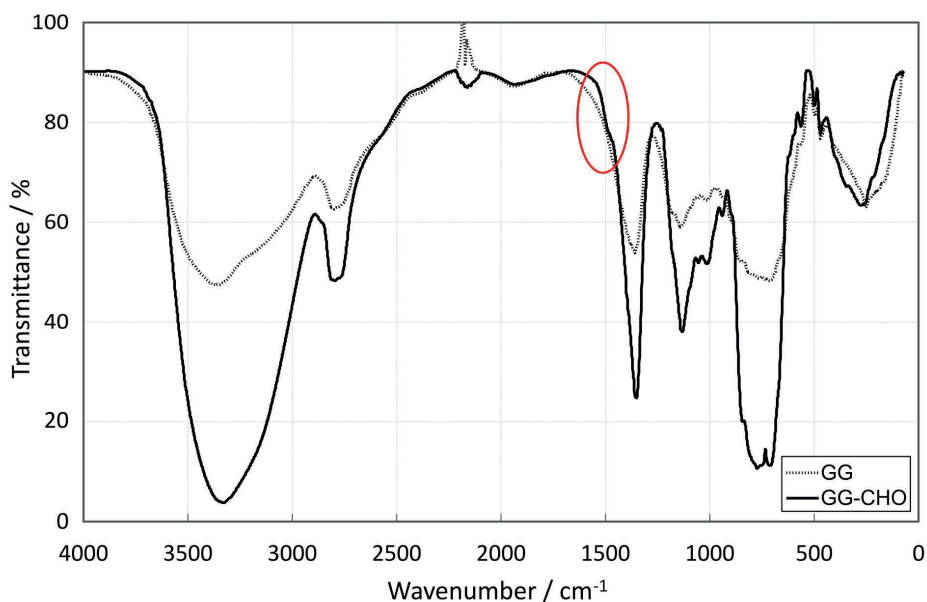
Figure S1. FTIR spectra of GG-CHO compared with unmodified GG.
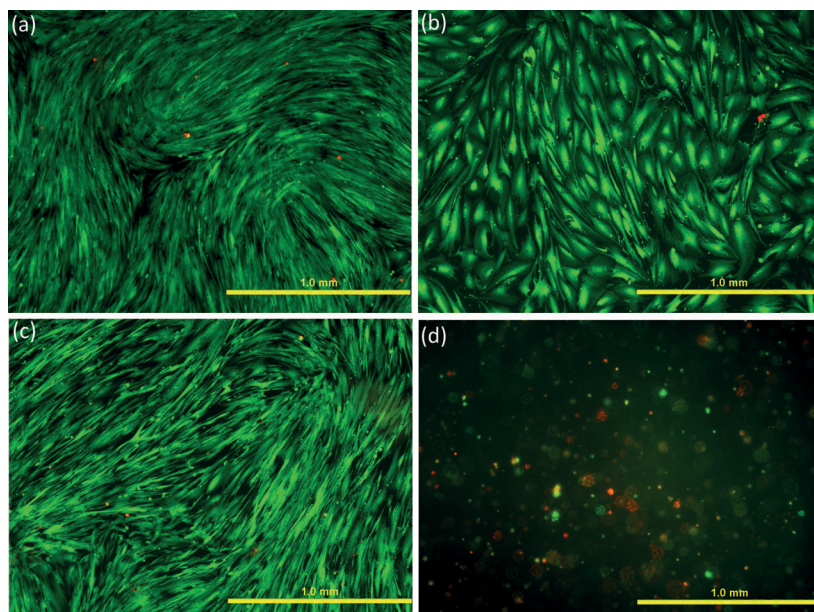
Figure S2. Live/Dead® stained confluent fibroblast cell culture on each tested gelatin coating after one week: a) native gelatin, b) gelatin-ADH, c) gelatin-CDH; d) 3D negative control F7-SPD hydrogel. Scale bar length 1.0 mm.
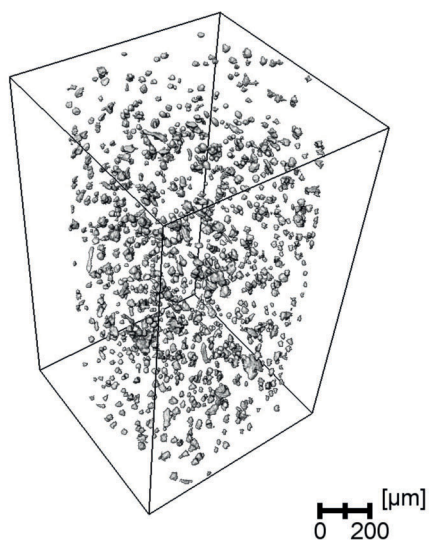
Video S1. Reconstruction of bright field OPT imaging of fibroblasts cultured encapsulated in GELA-ADH-GG 40:20 hydrogel. The 3D view reveals how well elongated the fibroblasts are inside the hydrogel.
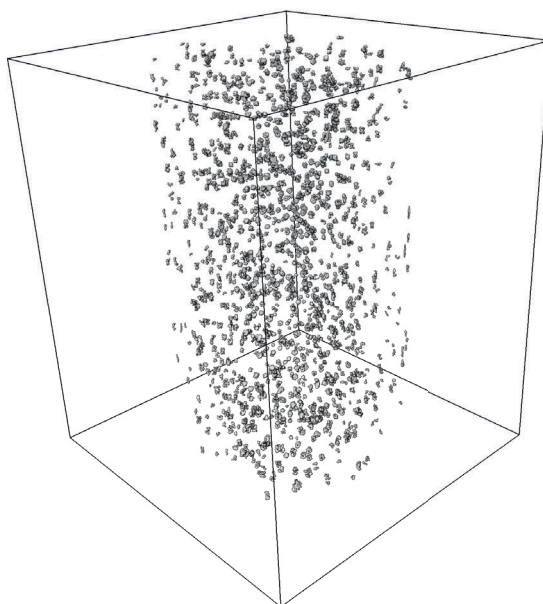
Video S2. Reconstruction of bright field OPT imaging of fibroblasts cultured encapsulated in the negative control SPD crosslinked GG hydrogel. The 3D view reveals poorer elongation when compared to gelatin-GG culture.
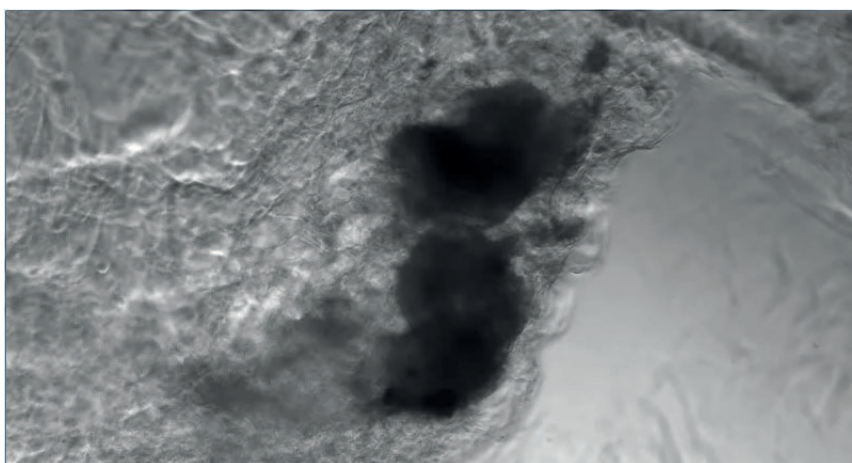
Video S3. Beating hiPSC-derived cardiomyocytes on control gelatin coating.
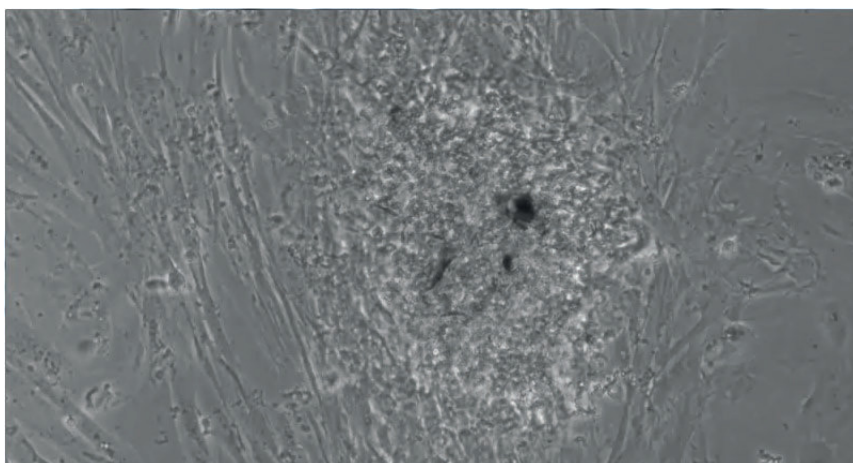
Video S4. Beating hiPSC-derived cardiomyocytes on gelatin-ADH coating.
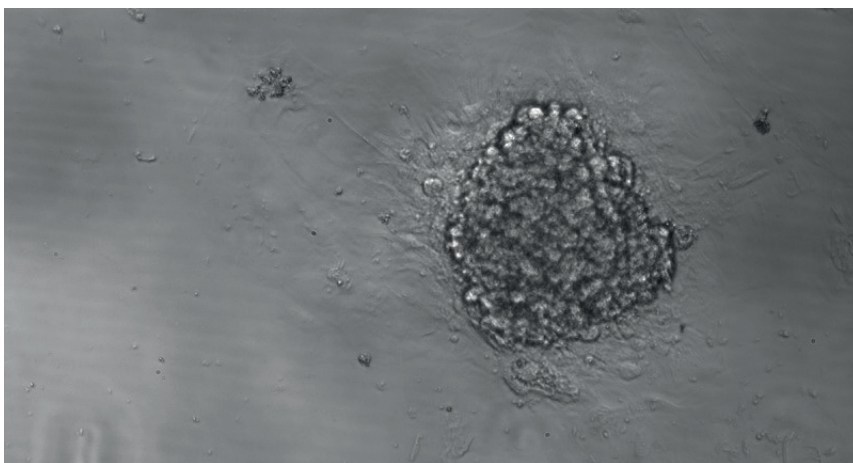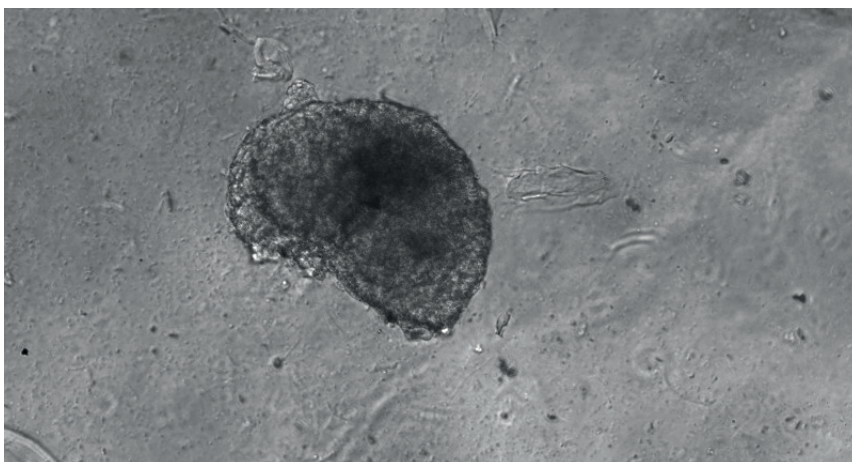

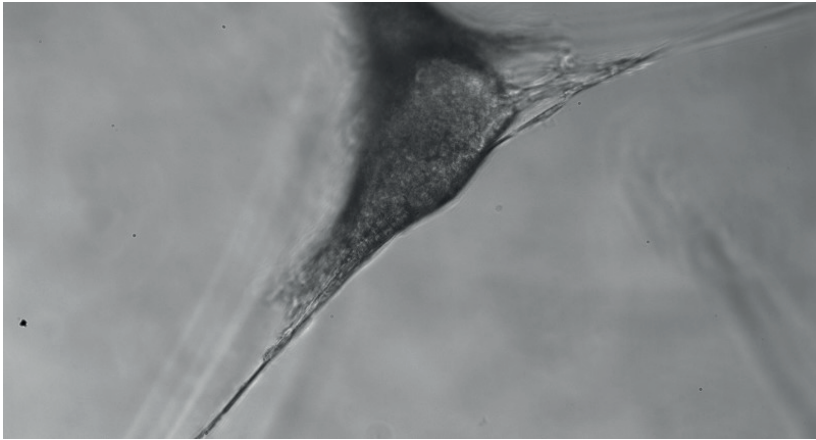**Video S5.** Beating hiPSC-derived cardiomyocytes on gelatin-CDH coating.
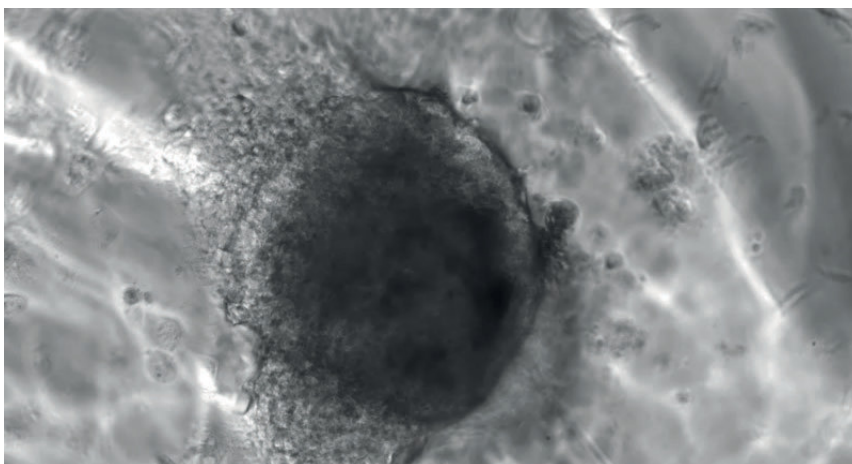
Video S6. Beating hiPSC-derived cardiomyocytes in F1-ADH hydrogel culture conditions.
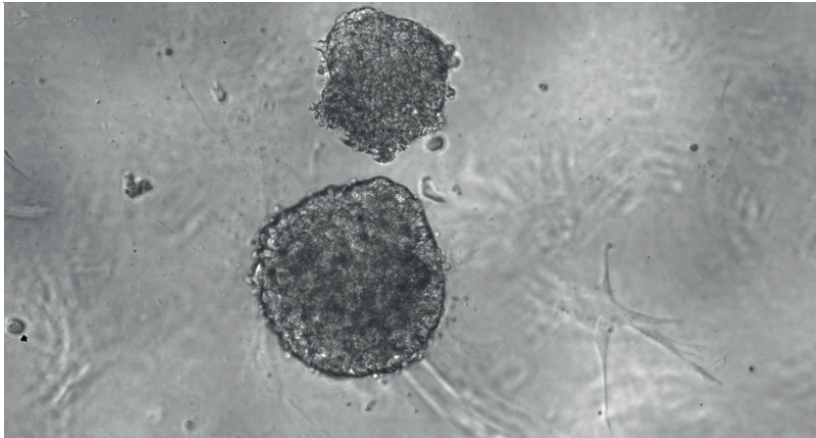

Video S7. Beating hiPSC-derived cardiomyocytes in F3-ADH hydrogel culture conditions.
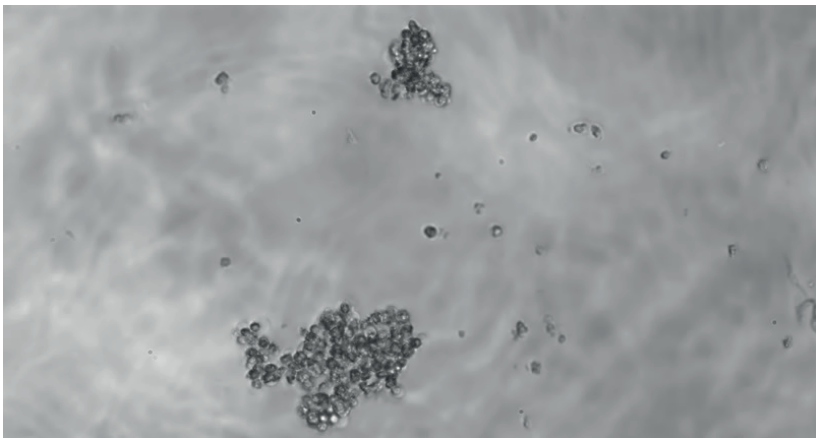

Video S8. Beating hiPSC-derived cardiomyocytes in F4-CDH hydrogel culture conditions.

Video S9. Beating hiPSC-derived cardiomyocytes in F5-CDH hydrogel culture conditions.

Video S10. Beating hiPSC-derived cardiomyocytes in F6-CDH hydrogel culture conditions.

Video S11. Non-beating hiPSC-derived cardiomyocytes in negative control F7-SPD hydrogel culture conditions.

Table S1. TaqMan assays used in the qRT-PCR protocol.

Gene	Description	Function	TaqMan assay ID
TNNT2	Cardiac type troponin T2	Sarcomeric gene	Hs00165960_m1
ACTN2	α-actinin 2	Sarcomeric gene	Hs00153809_m1
MYBPC3	Myosin binding protein C, cardiac	Sarcomeric gene	Hs00165232_m1
GAPDH	Glyceraldehyde-3-phosphate dehydrogenase	Housekeeping gene	Hs02758991_g1

IV

**CHARACTERIZATION OF COMPRESSIVE BEHAVIOR OF
BIOAMINE CROSSLINKED GELLAN GUM HYDROGEL**

by

Jairan Nafar Dastgerdi*, Janne T. Koivisto*, Kari Santaoja, Olli Orell, Mikko
Kanerva, and Minna Kellomäki